5-2011

A FINITE ELEMENT MODEL FOR COUPLED DEFORMATION-FLOW ANALYSIS OF UNSATURATED SOIL-STRUCTURE SYSTEMS AND ITS VALIDATION

Hadakopan Krishnapillai
Clemson University, kkrishn@clemson.edu

A FINITE ELEMENT MODEL FOR COUPLED DEFORMATION-FLOW ANALYSIS OF UNSATURATED SOIL-STRUCTURE SYSTEMS AND ITS VALIDATION

A Dissertation
Presented to
the Graduate School of
Clemson University

In Partial Fulfillment
of the Requirements for the Degree
Doctor of Philosophy
Civil Engineering

---

by
Hadakopan Krishnapillai
May 2011

Accepted by:
Dr. Nadarajah Ravichandran, Committee Chair
Dr. Ronald D. Andrus
Dr. C. Hsein Juang
Dr. Abdul A. Khan

ABSTRACT

The unsaturated soil mechanics is one of the emerging fields that require extensive studies to understand its behavior under various loading and environmental conditions. Unsaturated soil consists of three bulk phases: solid, liquid and gas and three interfaces: solid-liquid, liquid-gas and gas-solid. It is generally accepted that the interaction among various bulk phases and interfaces has to be taken into account in the characterization of unsaturated soils. The behavior of soil-structure systems is complex and the complexity further increases when the structure is located in unsaturated soil. Numerical methods such as the finite element method are ideally suited for elucidating such complex behavior of unsaturated soil-structure systems.

In recent years, various forms of finite element formulations and numerical tools have been developed for studying the behavior of unsaturated soils. Among these, TeraDysac, a framework based finite element software developed by Ravichandran and Muraleetharan is found to be an effective tool for analyzing soil-structure interaction in a fully coupled manner. This software consists of two decoupled codes: dysac and udysac. dysac is for the analysis of saturated soil-pile system and udysac is for the analysis of unsaturated soil-pile system. The original udysac code has simplified (reduced formulation) and complete finite element formulations. Although the complete formulation represents the real condition more closely, it is highly nonlinear and cannot be used for solving practical problems within a reasonable amount of computational time.

On the other hand, the simplified formulation is computationally efficient and numerically stable. However, because the relative accelerations and relative velocities of

both water and air phases are neglected at the governing equation level, its applicability to solve coupled mechanical-flow problems, is limited. Also the damping matrix does not naturally appear at the governing equation level, resulting in predicting unreasonably high accelerations.

In this research, the simplified formulation is improved by incorporating a viscous damping model. The improved simplified formulation seems to predict the unsaturated soil-pile interaction response reasonably well, compared to the simplified formulation. As a major development, *a partially reduced finite element formulation for coupled deformation-flow analysis* of unsaturated soil-structure systems is developed and implemented in TeraDysac. Soil-Water Characteristic Curve (SWCC), which represents the moisture-suction variation of unsaturated soils, is one of the constitutive models necessary for numerical modeling of unsaturated soil systems. In this research, limitations of commonly used SWCC models such as the Brooks and Corey, van Genuchten, and Fredlund and Xing models are extensively analyzed and limitations/disadvantages are identified. Based on this and also to avoid the identified limitations, two new SWCC models are developed and presented in this dissertation. The capability of the new SWCC models in fitting the measured data of different types of soil is investigated. The comparisons show that the new models are effective and can be used to fit the experimental data well over the entire range of degree of saturation. The numerical stability and the performance of the new models in finite element simulations are investigated by implementing these models within TeraDysac and simulating both static and dynamic problems. These studies showed that the new models are numerically

stable and effective in calculating the moisture-suction variation in finite element simulations.

Permeability coefficients of fluids occupying the pore space of unsaturated soils greatly influence the deformation and flow behaviors of unsaturated soils. The permeability coefficient varies with degree of saturation or volumetric water content of the unsaturated soils. The other properties that affect the permeability coefficient are void ratio and particle/pore size distribution. Accurate evaluation of the *permeability-degree of saturation* or *permeability-suction* relationship is very important to study the coupled deformation-flow behaviors of unsaturated soils using numerical tools. However, experimental studies of coupled deformation-flow problems such as slope failure after rainfall, and contaminant transport will be time consuming and may require advanced equipments. As a result, experimental studies will not be an effective choice.

The properties which affect the permeability coefficients also affect the soil water characteristic of unsaturated soils. Therefore, soil water characteristic curve models can be effectively used to calculate permeability-degree of saturation or permeability-suction variation. In this research, a simple mathematical equation is developed using the model parameters of S-R SWCC models for determining the permeability-suction variation. The predictive capability of the permeability model is verified by comparing with experimental data of eight different soils found in the literature. This proposed model is capable of predicting the relative permeability of water in unsaturated soil over a wide range of degrees of saturation.

An effective coupled deformation-flow analysis finite element model for unsaturated soils, should consist of the following elements: (1) governing equations and corresponding *finite element formulation* that represent the physical phenomena of unsaturated soils more closely and capable of calculating deformation-flow characteristics in a fully coupled manner, (2) realistic and accurate *constitutive model* that represents the stress-strain behavior of unsaturated soil skeleton, (3) *soil-water characteristic curve* (*SWCC*) *model* that represents the moisture-suction relationship in unsaturated soils, and (4) *permeability model* that represents the flow of fluids in unsaturated soils.

Upon successful completion of a finite element model development, the model must be validated against experimental measurements before using it as a viable tool. In this research, the finite element model is validated against experimental data obtained from a series of centrifuge tests; conducted at the University of Boulder, Colorado. The comparison of the numerical simulation results and the centrifuge measurements shows that the accuracy of the coupled deformation-flow analysis finite element model can be considered to be adequate for both elastoplastic and elastic simulations. Based on this research study, it can be concluded that the coupled deformation-flow analysis finite element model, which is implemented in TeraDysac, can be effectively used to analyze the elastic and elastoplastic behavior of unsaturated soils and soil-structure systems.

DEDICATION

This dissertation is dedicated to those who have dedicated their lives to the pursuit of social justice and human rights.

ACKNOWLEDGMENTS

I would like to first acknowledge my advisor Dr. Nadarajah Ravichandran, for his precious guidance and support throughout my graduate life at Clemson. His research style and enthusiasm was a model for me to improve my research skills. His expertise in numerical tool development and modeling helped me a lot to complete this research successfully. I would also like to extend my sincere thanks to my research committee members Dr. Ronald D. Andrus, Dr. C. Hsein Juang, and Dr. Abdul A. Khan for their valuable advice and support. I am also grateful to Dr. John S. McCartney from the University of Colorado at Boulder for sharing his experimental skills and knowledge to complete the centrifuge modeling program successfully. I would also like to give my recognition to all civil engineering department staff at Clemson University, especially to Ms. Kristin Baker for her valuable advice and help. I would also like to give heartfelt thanks to my family for their love and moral support. I am also indebted to all my friends who were part of my graduate life at Clemson University.

TABLE OF CONTENTS

TITLE PAGE i

ABSTRACT ii

DEDICATION vi

ACKNOWLEDGMENTS vii

TABLE OF CONTENTS viii

LIST OF FIGURES xi

LIST OF TABLES xx

CHAPTER

1. INTRODUCTION 1

    Background of the Study 1
    Design of the Research Study 6
    Dissertation Organization 13

2. LITERATURE REVIEW 15

    Characteristics of Unsaturated Soils 15
    Constitutive Modeling of Unsaturated Soils 19
    Characteristics of Unsaturated Soil-Structure Systems and Influencing Factors 22
    Summary of Soil-Structure Interaction Studies and Related Research Outcomes 23

3. REPRESENTING THE CHARACTERISTICS OF UNSATURATED SOILS IN MATHEMATICAL EQUATIONS AND SOLVING 28

    Developing the Governing Equations 28
    Solving the Governing Equations 32
    TeraDysac Software 42

4. UNDERSTANDING THE INFLUENCE OF DEGREE OF SATURATION ON THE BEHAVIOR OF UNSATURATED SOILS 43

    Introduction 43

Simulation Study 44
Results and Discussion 49
Summary of the Study 73

5. UNDERSTANDING THE INFLUENCE OF DEGREE OF SATURATION ON THE BEHAVIOR OF SOIL-PILE SYSTEMS 74

Introduction 74
Simulation Study 76
Results and Discussion 79
Summary of the Study 83

6. IMPROVING THE PERFORMANCE OF THE SIMPLIFIED FINITE ELEMENT FORMULATION 85

Introduction 85
Importance of Incorporating an External Damping Model 86
Rayleigh Damping Model 87
Incorporating the Rayleigh Damping Model with the Simplified Formulation and Performance Analysis 88
Results and Discussion 93
Summary of the Study 104

7. SWCCS OF UNSATURATED SOILS AND THE DEVELOPMENT OF NEW MODELS 105

Introduction 105
Factors Influencing the SWCC/ Moisture-Suction Variation 106
Popular SWCC Models of Unsaturated Soils 108
Limitations and Issues of the Popular SWCC Models 116
Development of a New SWCC Model (S-R-1 Model) 117
Dependency of Fitting Parameters in the S-R-1 and the other SWCC Models 133
A New SWCC Model with Independent Fitting Parameters (S-R-2 Model) 134
Another Form of the S-R-2 Model with Reduced Number of Fitting Parameters 143
Improving the Performance of Popular SWCC Models and Comparisons 146
Summary of the Study 153

8. PERMEABILITY MODELS OF UNSATURATED SOILS AND THE DEVELOPMENT OF A NEW MODEL 155

Introduction 155

Popular Permeability Models/Functions of Unsaturated Soils 157
Development of a New Permeability Model for Unsaturated Soils 161
Predictive Capability of the Proposed Permeability Model 163
Summary of the Study 175

9. FINITE ELEMENT MODEL FOR COUPLED DEFORMATION-FLOW ANALYSIS OF UNSATURATED SOILS 176

Introduction 176
Example Analysis 1: Flow through Unsaturated Embankment 179
Results and Discussion 181
Example Analysis 2: Coupled Deformation-Flow Analysis of Unsaturated SPI 186
Results and Discussion 188
Summary of the Study 193

10. VALIDATION OF THE COUPLED DEFORMATION-FLOW ANALYSIS FINITE ELEMENT MODEL 195

Classical Procedure of Centrifuge Modeling of SPI Problems 195
A New Centrifuge Modeling Scheme for Unsaturated SPI Modeling 197
Physical Modeling of Soil-Pile Interaction Using the Classical and the New Scheme 200
Numerical Modeling and Comparison with Centrifuge Data 227
Summary of the Study 237

11. SUMMARY, CONCLUSIONS, AND RECOMMENDATIONS 238

Summary and Conclusions 238
Recommendations for Future Research 242

REFERENCES 243

LIST OF FIGURES

1.1 Element of unsaturated soil with significant phases 1

1.2 Typical foundation design procedure 7

1.3 Soil-structure systems with various loading and environmental conditions 9

2.1 Unsaturated soil elements with forces generated by pore fluids 18

3.1 A representative element for rigorous volume averaging technique 29

3.2 The accuracy of the results vs. size of the REV 29

3.3 Motions in unsaturated soil system 30

3.4 Primary nodal and element variables for the complete formulation 34

3.5 Primary nodal variables for the partially reduced formulation 35

3.6 Primary nodal variables for the simplified/ reduced formulation 38

4.1 Calibration of SWCC for Minco silt 46

4.2 Calibration of SWCC for Speswhite kaolin 46

4.3 Degree of saturation related parameter Vs. Degree of saturation 48

4.4 Asymmetric four element mesh (all dimensions are in meters) 49

4.5 Vertical displacement time history (nodes N2, N3 and N6) 50

4.6 Comparison of element fields for Minco silt ($E= 1.2 \times 10^5$ kPa) and Speswhite kaolin ($E = 3 \times 10^4$ kPa) 51

4.7 Comparison of element fields for Speswhite kaolin with $\nu = 0.2, 0.3$ 54

4.8 Comparison of element fields for Minco silt (E = 1.2 x 10^2 kPa) and Speswhite kaolin (E = 3 x 10^2 kPa) 56

4.9 Comparison of element fields for stiff and soft Speswhite kaolin..... 57

4.10 Comparison of element fields with and without suction effect 59

4.11 2D finite element mesh of the embankment (175 quadrilateral elements) 60

4.12 Base motion acceleration time history (El Centro, 1940)..... 61

4.13 Comparison of element and nodal fields for Minco silt 62

4.14 Comparison of element and nodal fields for Minco silt with smaller E (E = 1.2 x 10^2 kPa)..... 64

4.15 Comparison of element and fields for Speswhite kaolin 66

4.16 Comparison of element and nodal fields for Speswhite kaolin with smaller E (E = 3.0 x 102 kPa)..... 67

4.17 Comparison of element fields with and without matric suction effect for Minco silt (left side) and Speswhite kaolin (right side) 69

4.18 The 3D finite element mesh of the embankment (1925 brick elements)..... 70

4.19 Comparison of 2D and 3D analysis results for both silt and clay..... 72

5.1 The 2D finite element mesh for the example problem 77

5.2 Time history of applied base motion acceleration..... 77

5.3 Comparison of horizontal displacement histories..... 81

5.4 Comparison of spectral accelerations 82

5.5 Time history of incremental suction in elements E130 and E137 83

6.1 Finite element mesh for the TeraDysac simulation 90

6.2 Finite element mesh for the PLAXIS simulation 90

6.3 El Centro earthquake (1940) acceleration time history 93

6.4 Comparison of Simplified, Improved Simplified, and Plaxis predictions 95

6.5 Effect of Rayleigh damping parameter □ on the spectral accelerations 97

6.6 Effect of Rayleigh damping parameter n on the spectral accelerations 98

6.7 Kobe earthquake (1995) acceleration time history 99

6.8 Effect of soil stiffness and fundamental period of soil deposit on the spectral accelerations 100

6.9 Comparison of spectral accelerations predicted with elastic and elastoplastic constitutive models 103

7.1 Typical SWCC with different regions of saturation 107

7.2 Role of fitting parameters in the B-C model 109

7.3 Role of fitting parameters in the van Genuchten model 111

7.4 Role of fitting parameters in the F-X model 113

7.5 Role of Cr in the F-X model 114

7.6 Role of the B when the F-X model is used with factor C1(ψ) 115

7.7 Role of the B when the F-X model is used with factor C2(ψ) 115

7.8 Role of the fitting parameters in the S-R-1 model 120

7.9 SWCC data of various soils fitted with the S-R-1 model 122

7.10 SWCC data of various soils fitted with all four SWCC models 124

7.11 SWCC data of Speswhite kaolin fitted with all four SWCC models 127

7.12 SWCC data of Speswhite kaolin fitted with all four SWCC models 127

7.13 FE mesh and the loading history for the problem #1, (a) Asymmetric four element mesh (all dimensions are in meters), (b) Loading 128

7.14 Consolidation simulations with 70% initial degree of saturation 129

7.15 The 2D finite element mesh of unsaturated compacted embankment 130

7.16 The acceleration-time history of applied base motion 130

7.17 Embankment simulations with 10% initial degree of saturation 131

7.18 Simulations with 10%, 70% degrees of saturation using the S-R-1 model 133

7.19 Role of the fitting parameter a in the S-R-2 model 136

7.20 Role of the fitting parameter n in the S-R-2 model 136

7.21 Role of the fitting parameter m in the S-R-2 model 137

7.22 Role of the fitting parameter Nr in the S-R-2 model 138

7.23 SWCC data of various soils fitted with the S-R-2 model 140

7.24 Simulations using the S-R-2 and other popular models 142

7.25 Role of the fitting parameter m in the S-R-3 model 144

7.26 SWCC data of various soils fitted with the S-R-3 model 145

7.27 B-C and I-B-C SWCCs for Columbia sandy loam 147

7.28 B-C and I-B-C SWCCs for Madrid clay sand 148

7.29 B-C and I-B-C SWCCs for Arlington soil 148

7.30 B-C and I-B-C SWCCs for Indian head till 148

7.31 v-G and I-v-G SWCCs for Columbia sandy loam 150

7.32 v-G and I-v-G SWCCs for Madrid clay sand 150

7.33 v-G and I-v-G SWCCs for Arlington soil 150

7.34 v-G and I-v-G SWCCs for Indian head till 151

7.35 F-X and I-F-X SWCCs for Columbia sandy loam 152

7.36 F-X and I-F-X SWCCs for Madrid clay sand 152

7.37 F-X and I-F-X SWCCs for Arlington soil 152

7.38 F-X and I-F-X SWCCs for Indian head till 153

8.1 Calibrated SWCCs and calculated permeability functions for Superstition sand (experimental data - Richards 1952) 166

8.2 Calibrated SWCCs and calculated permeability functions for Lakeland sand (experimental data - Elzeftawy and Cartwright 1981) 167

8.3 Calibrated SWCCs and calculated permeability functions for Columbia sandy loam (experimental data - Brooks & Corey 1964) 168

8.4 Calibrated SWCCs and calculated permeability functions for Touchet silt loam (GE3) (experimental data - Brooks & Corey 1964) 169

8.5 Calibrated SWCCs and calculated permeability functions for Silt loam (experimental data - Reisenauer 1963) 170

8.6 Calibrated SWCCs and calculated permeability functions for Guelph loam (experimental data - Elrick & Bowmann 1964) 172

8.7 Calibrated SWCCs and calculated permeability functions for Yolo light clay (experimental data - Moore 1939) 173

8.8 Calibrated SWCCs and calculated permeability functions for Speswhite kaolin (experimental data - Peroni et al. 2003) 174

9.1 The availability of the u-p-p formulation in the user-interface of TeraDysac 177

9.2 Availability of the S-R-2 SWCC model in the user-interface of TeraDysac 177

9.3 Availability of the nodal liquid pressure boundary condition in TeraDysac 178

9.4 The 2D finite element mesh of the compacted embankment 179

9.5 History of applied pore liquid pressure (applied along BCD, Figure 10.4) 180

9.6 Calibrated S-R-2 model and the fitting parameters for Speswhite kaolin 181

9.7 Time history of predicted incremental pore liquid pressure 182

9.8 Time history of predicted incremental degree of saturation 183

9.9 Contour plots of predicted degree of saturation at different simulation times 184

9.10 Contour plots of predicted pore liquid pressure at different simulation times 185

9.11 Finite element mesh for the TeraDysac simulation 186

9.12 The acceleration-time history of applied base motion 186

9.13 Comparison of predicted spectral accelerations and the base acceleration 190

9.14 Comparison of the predicted horizontal displacement-time histories 191

9.15 Comparison of predicted incremental suction-time histories 193

10.1 A figure explaining the proposed scheme 198

10.2 Plan and section views of the physical model (dimensions are in cm) 200

10.3 The container with drainage tube system 201

10.4 The container with the drainage layer 201

10.5 Instrumentation layout of the physical model (dimensions are in cm) 202

10.6 Some of the important steps of model construction; (a) pluviation, (b) leveling process, and (c) supporting the piles and instrumentation 204

10.7 The hydraulic actuator and static loading unit 205

10.8 A layout showing the drainage system and the model in centrifuge flight 206

10.9 Acceleration-time history of the applied motion 207

10.10 Results measured without SPI influence at pile tip level 209

10.11 Results measured with SPI influence at pile tip level 209

10.12 Comparison of results measured with and without SPI influence, at pile tip level, at dry condition 209

10.13 Comparison of results measured with and without SPI influence, at pile tip level, at saturated condition 210

10.14 Results measured without SPI influence at surface level 210

10.15 Results measured with SPI influence at surface level 210

10.16 Comparison of results measured with and without SPI influence, at surface level, at dry condition 211

10.17 Comparison of results measured with and without SPI influence, at surface level, at saturated condition 211

10.18 Comparison of settlement and horizontal displacement measured at dry and saturated conditions 213

10.19 The nozzle system with equally distributed tubing 214

10.20 A layout showing the drainage system and the model at the centrifuge flight .. 215

10.21 The model with plastic cover 216

10.22 A display of moisture sensor readings 217

10.23 The time history of applied acceleration 217

10.24 Results measured without SPI influence at pile tip level 220

10.25 Results measured with SPI influence at pile tip level 221

10.26 Comparison of results measured (at pile tip level) with and without the SPI influence, at 10% degree of saturation 222

10.27 Comparison of results measured (at pile tip level) with and without the SPI influence, at 15% degree of saturation 223

10.28 Comparison of results measured (at surface level) without SPI influence at 10% and 15% degrees of saturation 224

10.29 Comparison of results measured (at surface level) with SPI influence at 10% and 15% degrees of saturation 225

10.30 Comparison of results measured (at surface level) with and without SPI influence, at 10% degree of saturation 226

10.31 Comparison of results measured (at surface level) with and without SPI influence, at 15% degree of saturation 227

10.32 The finite element mesh used for the TeraDysac simulation 228

10.33 SWCC of Ottawa sand fitted with S-R-2 SWCC model 230

10.34 Time history of applied base motion 231

10.35 Comparison of elastoplastic simulation and experimental results (spectral accelerations) 232

10.36 Comparison of elastoplastic simulation and experimental results (displacement) 234

10.37 The time history of applied base motion..... 235

10.38 Comparison of elastic simulation results and centrifuge measurements 237

LIST OF TABLES

1.1 Commonly used centrifuge scaling factors 5

4.1 Linear elastic model parameters for Minco silt and Speswhite kaolin 45

4.2 Degree of saturation related parameter Vs. Degree of saturation 48

5.1 Material properties and model parameters of Minco silt 78

5.2 Suction related parameters of Minco silt 79

5.3 Properties of structural elements 79

6.1 Linear elastic model parameters and soil properties of Minco silt 92

6.2 Linear elastic model parameters for structural elements 92

6.3 Bounding surface based elastoplastic model parameters for the Minco silt 102

6.4 Suction related elastoplastic model parameters for Minco silt 102

7.1 Properties of the selected soils and calibrated SWCC model parameters 121

7.2 Linear elastic model parameters for Minco silt and Speswhite kaolin 126

8.1 Properties of the selected soils 164

9.1 Linear elastic model parameters for Speswhite kaolin 180

9.2 Bounding surface based elastoplastic model parameters for the Minco silt 187

9.3 Suction related elastoplastic model parameters of Minco silt 188

9.4 Linear elastic model parameters of structural elements 188

10.1 Coordinates of WCs' location 203

10.2 Coordinates of PPTs' location 203

10.3 Coordinates of accelerometers' location..... 203

10.4 Coordinates of LVDTs' location 203

10.5 Summary of model preparation procedure 204

10.6 Bounding surface based elastoplastic model parameters for Ottawa sand 229

10.7 Suction related elastoplastic model parameters 229

10.8 Linear elastic model parameters for the structural elements 230

10.9 Linear elastic model parameters and soil properties for Ottawa sand 235

CHAPTER ONE

INTRODUCTION

Background of the Study

Mechanics of Unsaturated Soils and Its Significances

Most civil engineering constructions start at the ground surface, which is often unsaturated and many structures never extend to the saturated layer or water table. Unsaturated soil consists of three bulk phases: solid, liquid and gas and three interfaces: solid-liquid, liquid-gas and gas-solid (Figure 1.1). The behavior of the unsaturated porous system is governed not only by the behavior of the bulk phases and interfaces but also by the interaction between bulk phases and interfaces (Fredlund and Rahardjo, 1993). Therefore the interaction among various bulk phases and interfaces has to be taken into account in the characterization of unsaturated soils. The behavior of bulk phases and interfaces can vary when the amount of liquid (degree of saturation) present within the voids varies.

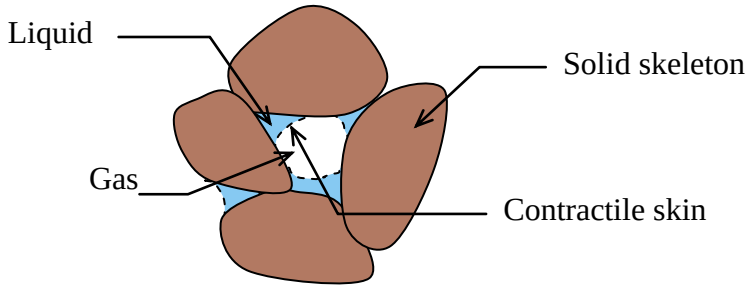

Figure 1.1 Element of unsaturated soil with significant phases

Presence of the liquid phase with negative pore water pressure and compressible air phase (Fredlund 1999) are unique characteristics of unsaturated soils. Variation in water

potential due to deformation and flow, significantly influences the behavior of unsaturated soils.

Coupling of Deformation and Flow Characteristics of Unsaturated Soils

Significant numbers of geotechnical engineering problems in day to day life are associated with deformation and flow behaviors of unsaturated soils. These problems include contaminant transport, wetting induced collapse/settlement, slope failures after extended period of rainfall, failures related to seepage, and shrinking and swelling issues in problematic soils.

Permeability coefficients of fluids occupying the pore space of unsaturated soils have great influence not only on the flow behavior but also on the deformation behavior. Similarly the permeability coefficient can be indirectly affected by both deformation of the solid skeleton and flow of pore fluids. For example, a reduction in void volume will increase the degree of saturation. Increase in degree of saturation will increase the coefficient of permeability of the water phase. Therefore, the deformation and the flow characteristics are inter-related and need to be considered in a coupled manner.

The wetting and drying process which implies whether the water is flowing out or into the soil, is a significant factor affecting the responses of unsaturated soils. In saturated soils, the water phase exists in a bulk form. Due to the bulk arrangement, the pore water produces both tangential and normal compressive stresses to the solid particles at inter-particle contacts. In unsaturated soils, the meniscus form of the water phase provides only normal tensile stresses (negative pore water pressure) and it provides additional stability to the contacts. During a wetting process, the increase of pore water

pressure might cause swelling. Also a reduction in inter-particle attractive force might cause particle slippage and it will result in a volumetric compression. The resultant magnitude of these two opposite volume change behaviors and the duration of these processes depend on many factors. The structure of the particle arrangement, cementing characteristic of the soil and the nature of bonding are the main factors influencing the process. The confining stress, density, water content or the degree of saturation at the time of compaction, clay content (Lawton et al. 1991), and the physico-chemical properties of the soil (e.g. Matyas & Radhakrishna, 1968, Jennings & Burland, 1962) can also be considered as some other influencing factors.

Recent studies show that the wetting process can induce a collapse in particle arrangement and it might cause problems like embankment settlement (Miller et al. 2001). Also this collapse can be a slow or fast process (few minutes to many years) and the magnitude can vary from 1% to 10% or sometime even more than that (Lawton et al., 1991).

Investigating the Characteristics of Unsaturated Soils & Soil-Structure Systems

Centrifuge Modeling

The dynamics of unsaturated soil-structure interaction is an emerging field which requires utilization of numerical and experimental methods. Advanced physical modeling techniques such as geotechnical centrifuge modeling is commonly used to gain better insights into such complex behavior. Centrifuge procedure and test setup for testing saturated soils and saturated soil-structure systems are well established. However a well

established centrifuge procedure to study the behavior of unsaturated soils or unsaturated soil-structure systems is not available in the literature.

The centrifuge experimental method was introduced by Bucky (1931) and Pokrovsky (1932) in the field of geotechnical engineering. Afterward, a large number of geotechnical centrifuge facilities have been installed in many research institutes in the U.S and all over the world. Even though it is costly and time consuming, it is now very popular for Geotechnical researches.

Using the centrifuge technique, the behavior of geotechnical or other civil engineering structures can be investigated using an identical physical model. In order to produce identical self-weight stresses in the model and the prototype, the gravitational acceleration in the model will be increased using the centrifuge facility. Therefore, the stresses experienced in the physical model will be same as the stresses in the prototype. These identical stresses enable the model to behave similar to the prototype. In geotechnical modeling, centrifuge technique can be effectively used to investigate the behavior of complex problems such as soil-structure interaction, settlement of embankments, stability of slopes and retaining structures, and earthquake-induced liquefaction. The accuracy of numerical tools can also be verified using centrifuge test data.

One of the important steps in centrifuge model design is scaling the prototype parameters to corresponding model parameters. It is generally accepted that all the prototype parameters should be scaled so that it enables identical stresses in the model and prototype. Basically, all the linear dimensions should be scaled by a factor of 1/N, if

the gravitational force in the physical model is to be increased by a factor of N. The scaling factors for some of the basic parameters are summarized in Table 1.1.

Table 1.1 Commonly used centrifuge scaling factors

Parameter	Scaling Factor (Prototype/Model)
Linear dimensions	N/1
Microscopic length	1
Time (dynamic)	N/1
Time (consolidation)	N 2/1
Acceleration, Gravity	1/N
Force	N 2/1
Fluid interfacial tension	1
Stress, Pressure, Strain	1/1
Flexural rigidity	N 4/1
Frequency (dynamic)	1/N
Pore fluid velocity	1/N
Hydraulic conductivity	1/N
Porosity, density, viscosity	1

Using centrifuge modeling, behavior of soil-structure systems in saturated soils is excessively studied by various researchers. For example, Chang and Kutter (1989), Cafe (1991), Leung and Ko (1993), Rashidi (1994), Honda et al. (1994), Liu and Dobry (1995), Abdoun et al. (1997), Horikoshi et al. (1997), Michael et al. (1998), Wang et al. (1998), Wilson (1998), Bruno and Randolph (1999), Ross et al. (1999), Scott et al. (2007), Anirban (2008), Lenart et al. (2009), and Shideh et al. (2010).

Numerical Modeling

A verified and calibrated numerical model can be effectively used for investigating the response of complex systems subjected to various loading and boundary conditions. It

can also be used for identifying parameters that affect a particular response. This study is intended to develop, verify and calibrate a coupled finite element model for unsaturated soil-structure systems and to use it to understand the behavior of unsaturated soil-pile systems. Even though significant improvements in numerical techniques have been made in last two decades, the coupling of deformation and flow behaviors still needs extensive studies.

Design of the Research Study

Motivations of the Study

Importance of Soil-Structure Interaction (SSI) Analysis

The dynamic structural systems subjected to earthquake loads are typically studied in an uncoupled manner, that is without taking into account the interaction between the supporting soil and the structure. In this approach, the free-field response of soil deposit for a given earthquake will be predicted (1^{st} step as shown in Figure 1.2). In the 2^{nd} step the dynamic behavior of structure will be analyzed by applying the predicted free-field response, assuming the base of the structure is fixed. In the 3^{rd} step, a possible maximum moment (M_{max}) and shear force (F_{max}) on the foundation will be calculated using the acceleration design response spectra (ADRS) of the predicted free-field response. And then the foundation will be designed or the capacity of the designed foundation will be checked using the calculated M_{max} and F_{max}. However presence of structural components will significantly affects the response of soil-structure systems and the usage of free-field response will usually give under estimations. Therefore, it is very important to analyze the behavior of coupled soil-structure systems and take necessary measures in design.

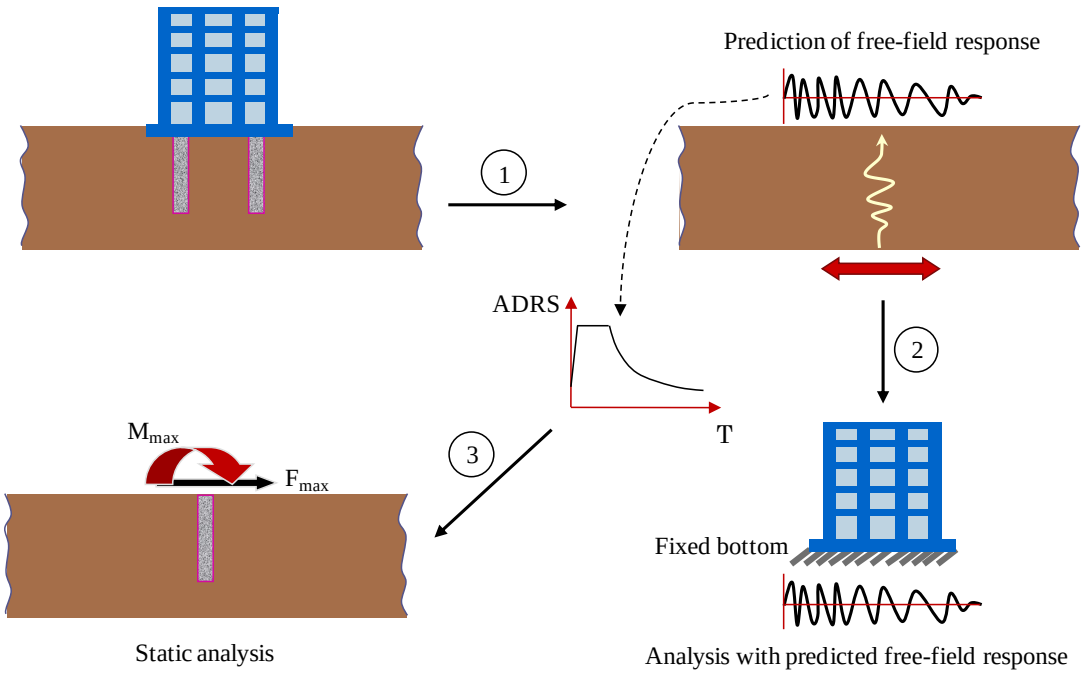

Figure 1.2 Typical foundation design procedure

Importance of Coupled Deformation-Flow Analysis of Unsaturated SSI and the Need for Numerical Simulations

Large numbers of geotechnical problems in day-to-day life involve the deformation of soil skeleton and flow of fluids through the pore space between soil particles. These problems include contaminant transport and settlement issues, wetting induced collapse, slope failures after extended period of rainfall, seepage related failures, and shrinking and swelling of problematic fine grained soil due to moisture content changes. The behavior of solid skeleton and other bulk phases, which govern the deformation behavior, will be greatly influenced by the variation in degree of saturation, i.e. flow of water. Therefore most of the geotechnical problems are significantly associated with both deformation and flow characteristics. The classical saturated soil mechanics theories fall well short in capturing phenomena associated with flow of fluids in unsaturated soils. Therefore, better

understanding of coupled deformation-flow behavior of unsaturated soils is required for safe, economical construction of geotechnical structures.

The Need for a Numerical Tool

Typically, structures are designed considering critical loading conditions and appropriate safety factors. For the critical condition, strength of the material will be considered at its lowest value, and the external load will be considered at its highest value while being in worst environmental condition. The strength of the soil is affected by amount of fluids presents in the pore space i.e. degree of saturation. Due to seasonal variation, amount of water presents in pore space will vary and it will show a discrepancy in the strength of the soil. In addition, the seasonal variation will naturally create the soil profile with different degree of saturation. As a result, the presence of soil layers with different degree of saturation will affect the behavior of soil-structure systems. In addition, gaps might be formed at the soil-structure interfaces due to the dryness and volume change characteristic in dry seasons. The gaps can also be formed due to an adjacent disturbing loading such as earthquake or blasting. Depending on the location and the environmental condition, these gaps might cause the system to become weak. For example, during a rainfall or surface flow, the soil-structure interface could be filled with water and it can lead to a wetting induced collapse. In this way, the effects of climate changes and seasonal variations can create a worst condition than the design condition.

Investigating the effects of seasonal variations and related problems will be complex. Specifically, experimental methods will be very complicated and very costly and time consuming. However, numerical simulations such as finite element simulation can be

effectively used to study the behavior of such complicated mechanism. Therefore development of a finite element model to analyze the coupled deformation-flow behavior of unsaturated soil-structure systems will be definitely useful. Such a finite element model will help to study the behavior of unsaturated soil-structure systems by taking the effects of various loading and environmental conditions into account.

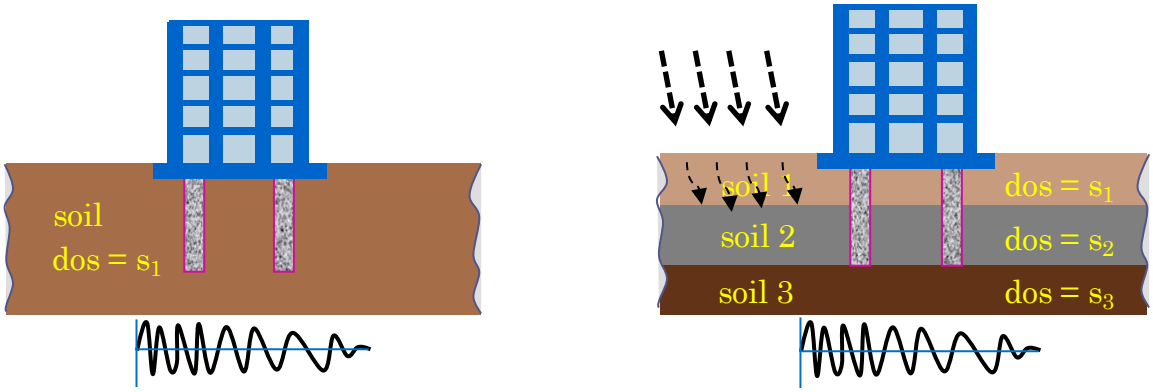

Figure 1.3 Soil-structure systems with various loading and environmental conditions

Essential Elements of an Effective Deformation-Flow Analysis Finite Element Model of Unsaturated Soil-Structure Systems

An effective deformation-flow analysis finite element model of unsaturated soil-structure systems should consist of the following elements. (1) *A Finite Element Formulation* which accurately represents the physical phenomena and capable of calculating the coupled deformation-flow behavior of unsaturated soil-structure systems, (2) Effective *Constitutive Models* to calculate/model the stress-strain relationship of unsaturated soils, (3) Effective *Soil-Water Characteristic Curve* (*SWCC*) *Models* to calculate/model the moisture-suction relationship of unsaturated soils, and (4) *Permeability Models* to calculate/model the permeability-suction relationship of unsaturated soils. Another important element of an effective finite element model is

validation. The predictions of the finite element model will not be broadly accepted if the accuracy of the model is not validated against experimental measurements. Therefore, the accuracy of the finite element model should be validated.

Methodology Outline

The focus of this study is to develop a coupled deformation-flow analysis finite element model for unsaturated soil-structure systems, implement it into a framework based finite element software called TeraDysac, and validate it against centrifuge experimental results. The development of a coupled deformation-flow analysis finite element model of unsaturated soil-structure systems requires in-depth understanding of the fundamental of unsaturated soils mechanics and unsaturated soil-structure systems subjected to static and dynamics loads. Therefore in-depth literature review on related topics is carried out and the findings are presented in this dissertation. In addition, to understand the effect of degree of saturation on the undrained behavior of unsaturated soils and unsaturated soil-pile systems, extensive numerical studies were performed using a simplified finite element formulation of TeraDysac software. Based on the outcomes of the literature reviews and the simulation studies, the simplified formulation is updated with latest research suggestions such as improving the performance by incorporating an external damping model. Subsequently, the dynamic response of unsaturated soil-pile systems at various degree of saturation is investigated using the improved simplified formulation.

The outcomes of the literature reviews and the simulation studies gave a platform to identify the key elements that are necessary to develop an effective deformation-flow

finite element model. It also helped to understand the features and limitations of available models, which can be used for the development of the finite element model. With these in-depth understandings and experiences, a deformation-flow analysis finite element model which consists of (1) *A partially reduced finite element formulation,* (2) *new soil-water characteristic curve models,* and (3) *a new relative permeability model* is developed and implemented in TeraDysac. The features of the newly developed soil-water characteristic curve models and relative permeability model are comprehensively presented in this dissertation.

To improve the performance of the deformation-flow analysis finite element model, nodal pore pressure boundary condition is implemented in TeraDysac. Once the implementation phase is completed, the ability of the model to simulate (1) flow through unsaturated soils and (2) coupled deformation-flow behavior of unsaturated soil-structure systems is investigated through sample simulations. Predictions of any numerical tool will not be broadly accepted if the accuracy of the model is not validated. Therefore, to validate the accuracy of the implemented deformation-flow analysis finite element model, dynamic response of unsaturated soil-pile systems is examined using centrifuge modeling and the results are compared with the prediction of numerical simulations.

Objectives and Hypothesis

Objectives

This research study is carried out with wide range of objectives. However, it can be stated that this study is basically intended to expand the simulation capabilities and features of TeraDysac software by implementing a coupled deformation-flow analysis

finite element model. It can be further illustrated in detail as follows: Developing a fully coupled finite element model for coupled deformation-flow analysis of unsaturated soil-structure systems and validating its accuracy is the aim of this study. This aim could be achieved through the following key objectives: (i) developing and implementing a finite element formulation which accurately represents the physical phenomena and capable of calculating the coupled deformation-flow behavior of unsaturated soil-structure systems, (ii) developing and implementing effective soil-water characteristic curve and relative permeability models for unsaturated soils. The other objectives of this study are; (i) to perform a wide range of numerical simulations to study the characteristics of unsaturated soils and unsaturated soil-structure systems, and understand the influence of suction on the behavior of unsaturated soils and soil-pile systems, (ii) to perform a wide range of centrifuge tests to study the dynamic behavior of unsaturated soil-pile systems and use the centrifuge data to validate the finite element model.

Hypothesis

Soil is composed of discrete particles. However, in this research, it is assumed that the continuum theory is applicable for soils. It is also assumed that all the phases are continuous, although the water phase may no longer be continuous at low degree of saturation. Similarly, at high degree of saturation the air phase might become discontinuous. Due to temperature and pressure variations, the phases of the soil might change one to another i.e. *solid to liquid* or *liquid to solid*, and *liquid to gas* or *gas to liquid*. However, it is assumed that there is no phase change occurs during an analysis. In addition, the soil is considered as homogenous material in this study.

Contribution of the Study

A validated finite element model for analyzing the coupled deformation-flow behavior of unsaturated soil-structure systems is developed. Geotechnical centrifuge test setup and procedure is developed, and preliminary test data on the static and dynamic behavior of piles supported by unsaturated soil is obtained the first time. Furthermore, analytical models to represent the moisture-suction relation and relative permeability of water in unsaturated soil are developed and implemented in the in-house finite element software.

Dissertation Organization

Characteristics of unsaturated soils and its constitutive modeling, along with relevant literature study are presented in Chapter 2 of the dissertation. Detailed description about stress state variables, effective stress concept, consideration of two-stress state variables, and the characteristics of suction is presented in this chapter. This chapter also includes the characteristics of unsaturated soil-structure interaction responses and summery of relevant literature study. Chapter 3 of this dissertation gives an overview about governing equations of unsaturated soils, finite element formulations and solving methods. An introduction to the TeraDysac software is also presented in Chapter 3. Following two chapters describe the details of two important simulation studies. Chapter 4 is about the influence of degree of saturation on the deformation behavior of unsaturated soils. The study presented in Chapter 5 is carried out to understand the influence of degree of saturation on the deformation behavior of unsaturated soil-pile systems. Chapter 6 provides the details of an improved simplified finite element formulation, which can be

used effectively to study the dynamic behavior of unsaturated soil-pile systems. To improve the performance of the coupled deformation-flow analysis finite element model, two soil-water characteristic curve models and a relative permeability model of unsaturated soils were developed. The details of these models are presented in Chapter 7 and Chapter 8, respectively. Chapter 9 presents the details of the coupled deformation-flow analysis finite element model and its implementation in TeraDysac. This chapter also presents the details of two example simulations, which are carried out to analyze the capability of the implemented deformation-flow analysis finite element model. To validate the accuracy of the deformation-flow analysis finite element model, centrifuge tests were conducted and measured results are compared with the predictions of the finite element model. The details about the centrifuge and the numerical modeling studies and the validation of the finite element model are presented in Chapter 10. The summary and conclusion of this study are presented in the next chapter. The references are provided at the end of the dissertation

.

CHAPTER TWO

LITERATURE REVIEW

Characteristics of Unsaturated Soils

Stress State Variables

The effective stress, the total stress minus the pore water pressure, is the single stress state variable that governs the shear strength and volume change characteristics of saturated soil. Thus the effective stress concept for saturated soil is well defined and accepted. However, the concept of effective stress for unsaturated soil is not well defined. A single stress state variable concept introduced in the early development of unsaturated soil mechanics seems to fail to completely characterize the unsaturated soil. Identifying appropriate stress state variable or a set of variables for unsaturated soils is an ongoing research. In contrast to saturated soil, the shear strength and volume change behaviors of unsaturated soil is relatively complicated due to complex geometric arrangement of bulk phases, and presence of compressible air phase and air-water interface. The air-water interface is commonly known as contractile skin and it maintains the pressure balance between the water and air phase. The pressure difference between the water and air phase, known as matric suction influences the shear strength of unsaturated soils. The constitutive relationship for the solid skeleton, which is one of the most important element in numerical modeling, requires appropriate stress state variable to accurately relate the stress to the strain or vice versa. This chapter presents detailed literature review on stress state variables, constitutive models that uses various stress state variables and

soil-structure interaction studies using various stress state variables and constitutive models.

Effective Stress Concept for Unsaturated Soils

The effective stress concept proposed by Terzaghi (Terzaghi, 1936) for fully saturated soils was extended to unsaturated soils by various researchers in various forms (Biot, 1941; Bishop, 1959; Aitchison, 1965; Aitchison et al., 1973). Among those various propositions, Bishop's (1959) equation which incorporates the total stress, pore air pressure and pore water pressure (Equation 2.1) gained widespread reference.

$$\boldsymbol{\sigma}' = (\boldsymbol{\sigma} - p^g\mathbf{I}) + \chi(p^g - p^l)\mathbf{I} \tag{2.1}$$

where $\boldsymbol{\sigma}'$ is the effective stress tensor, $\boldsymbol{\sigma}$ is the total stress tensor, p^l is pore liquid pressure, p^g is pore gas pressure, $\mathbf{I}$ is the unit tensor and χ is a parameter related to degree of saturation. The magnitude of the parameter χ varies from one to zero when the degree of saturation changes from 100% to fully dry condition. Additionally the parameter χ also slightly varies with soil type and stress history.

The Concept of Two-Stress State Variables

Matyas and Radhakrishna (1968) introduced the concept of state parameters in describing the volume change behavior of unsaturated soils. Volume change was presented as a three-dimensional surface with respect to the state parameters, $(\boldsymbol{\sigma} - p^g\mathbf{I})$ and $(p^g - p^l)$. Barden et al., (1969) also suggested that the volume change of unsaturated soils can be analyzed in terms of two stress-state variables, i.e. $(\boldsymbol{\sigma} - p^g\mathbf{I})$ and $(p^g - p^l)$. Fredlund and Morgenstern (1977) suggested that any of the three combinations: net

normal stress $(\boldsymbol{\sigma} - p^g \mathbf{I})$, matric suction $(p^g - p^l)$, and $(\boldsymbol{\sigma} - \mathbf{I}\, p^l)$ can be used to analyze unsaturated soils. Fredlund (1978) suggested that net stress $(\boldsymbol{\sigma} - p^g \mathbf{I})$ and matric suction $(p^g - p^l)$ are the most advantageous combinations. Even though the two-stress state variable concept has gained widespread reference in the recent years, the effective stress concept proposed by Bishop (1959) still remains popular, because of its simplicity and widespread application. And also a recent study (Muraleetharan and Liu, 2009) shows that the suction can be changed not only due to the flow of water but also due to the deformation of the solid skeleton. The stress-strain behavior of the solid skeleton can be modeled using an elastic or elastoplastic constitutive model.

Suction in Unsaturated Soils

The suction is an important parameter in unsaturated soils. As discussed above, it is one of the widely accepted stress state variables. Also the suction significantly influences the deformation and flow behavior of unsaturated soils. The primary component of the suction is matric suction, which can be defined as the difference between pore air pressure and pore water pressure. The ion concentration of pore fluids might produce an additional suction which is also known as osmotic suction. The total is addition of both matric suction and osmotic suction (Equation 2.2). Usually the osmotic suction is very small compared to the matric suction and it will not change due to deformation or loading. Therefore changes in soil suction can be considered as the changes in the matric suction $(p^g - p^l)$. In this study the term suction is used to represent the matric suction.

$$\psi = (p^g - p^l) + \pi \qquad (2.2)$$

where ψ is the total suction, (p^g - p^l) is matric suction, and π is osmotic suction. Generally the pore gas pressure p^g will be equal to the atmospheric pressure, because it is assumed that the air voids are inter-connected and also connected to the atmosphere. Therefore pore water pressure in unsaturated soils will be always negative.

The suction is directly related to the water potential of the soil. In the past, many researchers conducted experiments to understand the moisture-suction relationship and key influencing factors. All those studies confirmed an inverse proportional relationship between the degree of saturation and the suction. This variation can be explained with a simple meniscus theory. An infinitesimally small element of unsaturated soils along with the meniscus is shown in Figure 2.1. Considering the equilibrium of the element, a relationship between the matric suction and the radius of meniscus (Equation 2.3) can be derived (Fisher, 1926). When the degree of saturation or the volumetric water content increases, the radius of the meniscus R_s (see Figure 2.1) will increase and it will reduce the matric suction.

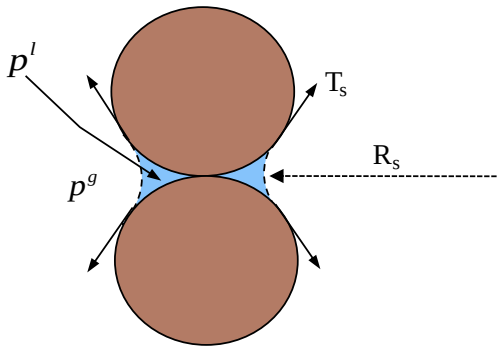

Figure 2.1 Unsaturated soil elements with forces generated by pore fluids

$$\left(p^g - p^l\right) = \frac{2T_s}{R_s} \tag{2.3}$$

where (p^g - p^l) is matric suction, T_s is surface tension or the meniscus force, and R_s is radius of the meniscus.

Constitutive Modeling of Unsaturated Soils

Stress-Strain Relationship

The deformation or the stress-strain behavior of the solid skeleton can be modeled using an elastic or elastoplastic constitutive model. The elastic models are simple and usually these models require a few number of model parameters such as Young's modulus and Poisson ratio. The linear elastic models can be effectively used with small deformation problems in which the maximum strain is within the linear portion of the stress-strain behavior of the soil. Finite element simulation with elastic models is relatively faster than that of elastoplastic models due to lesser number of calculations and local iterations. However, the linear elastic models cannot predict the true stress-strain behavior of soils since the soil is truly elastoplastic material in the practical range of strains. Therefore, an elastoplastic model needs to be used to represent the stress-strain behavior of soils.

There are numerous constitutive models available in the literature for saturated soils. However, only a few models are available for unsaturated soils. The bounding surface model for saturated soil was originally developed by Dafalias and Herrman (1986). This was later modified by Muraleetharan and Nedunuri (1998) for unsaturated soils, by incorporating the suction related behavior such as loading collapse (L-C curve) proposed by Alonso et al. (1990) and Wheeler and Sivakumar (1995). The model for unsaturated soils uses two widely accepted stress state variables of unsaturated soils: net stress and

suction. When the suction is zero, the bounding surface of both saturated and unsaturated soils will be identical and when the suction increases, the bounding surface will expand.

The elasto-plastic model proposed by Alonso et al. (1990) is widely referred as Barcelona-Basic Model (BBM) and it is a very popular model in unsaturated modeling. In this model, isotropic normal compression lines were assumed to have different gradients and intercepts when the value of suction is different. The key feature of this model is the addition of L-C yield curve with the capability to calculate plastic compression during an isotropic loading or wetting process. The BBM model will reflect the modified cam-clay model when the suction is zero, i.e. at fully saturated condition. The BBM model is primarily proposed for low or moderate plasticity fine-grained soils. Based on the BBM model, another similar model was proposed by Wheeler and Sivakumar (1995). In order to improve the flexibility and make the model more realistic, the following simplifications were made by Wheeler and Sivakumar (1995). For different values of suction, the normal compression lines were fitted based on experimental data. In the BBM model, the critical state line in the *q-p* plane is assumed to shift proportionally with suction, whereas in the model proposed by Wheeler and Sivakumar (1995), the shift is related to the suction through a mathematical function. Alonso et al., (1999) presented a modified form of the BBM model. The modified model is capable of calculating the stress-strain behavior of expansive unsaturated soils, whereas the BM model is not very effective.

Moisture-Suction and Permeability-Suction Relationships

To formulate the actual response of unsaturated soils, it is important to model the moisture-suction relation and permeability-suction variation accurately in addition to the stress-strain relationship. The moisture-suction relation is being modeled/calculated using Soil-Water Characteristic Curves (SWCC) models. The soil-water characteristic curve is a relationship between the amount of water present in the soil and the suction. The amount of water present in the soil can be expressed in terms of degree of saturation, volumetric water content, or gravimetric water content. Gardner (1956), Brooks and Corey (1964), Brutsaert (1966), van Genuchten (1980), McKee and Bumb (1987), Kosugi (1994) and Fredlund and Xing (1994) are some of the SWCC models found in the literature. Extensive studies were carried out to understand the applicability and accuracy of popular soil-water characteristic curves and it is comprehensively presented in Chapter 7. The permeability-suction variation is usually calculated using soil-water characteristic curves. The models which are used to calculate the permeability-suction variation is widely referred as permeability functions, for example Fredlund et al. (1994) permeability function. In-depth details about permeability-suction variation and calculating it from the soil-water characteristic curves are illustrated in Chapter 8.

Characteristics of Unsaturated Soil-Structure Systems and Influencing Factors

Pile foundations are an integral part of many civil engineering structures such as highway bridges, wharves, towers, and other tall buildings, with the structural load transferred to the supporting soil through the foundation. The dynamic behavior of superstructure is greatly influenced by the characteristics of the supporting soil. Therefore, a safe and economical design of the foundation requires in-depth understanding of the interaction between the structure and the supporting soil. The acceleration design response spectrum, which is calculated without considering the presence of pile foundation, is widely used for designs. However, research studies show that the presence of structure significantly alters the soil-structure system responses.

Numerous numerical (Cubrinovski et al., 2001; Han, 2001; Chang et al., 2001; and Amin et al., 2001) and physical experimental (Finn and Gohl, 1987; Chang and Kutter, 1989; Café, 1991; Rashidi, 1994; Honda et al., 1994; Liu & Dobry, 1995; Abdoun et al., 1997; Horihoshi et al., 1997; Wang et al., 1998; Wilson, 1998) studies have been carried out in the past to understand the behavior of soil-structure interaction and to identify the factors that influence the load carrying capacity under various soil, loading and boundary conditions. It should be noted that a few numerical studies and experimental studies have been conducted on unsaturated soil-pile response (Georgiadis et al., 2003). The results show that the soil-structure interaction is important for the design of safe and economical structure and revealed that the response of soil-structure system can be affected by *degree of saturation* (Georgiadis et al., 2003), *soil type and density* (Wilson, 1998), *strength of the soil* (Cubrinovski et al., 2001), *pile installation method* (Abdoun et al., 1997),

support condition at pile base (Han, 2001), *strength of soil-structure interface* (Chang et al., 2001), *loading type and loading rate* (Tokida et al., 1992), *excess pore pressure ratio* (Liu and Dobry, 1995; Tokida et al., 1992), *displacement history* (Wilson, 1998), and *adjacent buildings* (Amin et al., 2001).

Summary of Soil-Structure Interaction Studies and Related Research Outcomes

The influence of partial saturation on the axial capacity of a pile was studied by Georgiadis et al. (2003), in which they determined that the load capacity (ultimate pile load) increases as the degree of saturation decreases. The analysis also showed an excessive settlement due to collapse exhibited by the unsaturated soil under the tip of the pile. This settlement is perhaps attributed to wetting-induced collapse behavior of unsaturated soils (Miller et al., 2001). It is important to note that this settlement could not be recognized with saturated finite element analysis (Georgiadis et al., 2003). Therefore, the effect of partial saturation on the soil-pile system behavior should be investigated under various loading and environmental conditions. Unsaturated soil-structure interaction analysis is relatively a new area, and thus many example studies are not available in the literature. However, results of saturated soil-structure interaction analysis can be used as a base to further investigate the response of unsaturated soil-structure interaction analysis. Some of the important results of saturated soil-structure interaction analysis would be significant for unsaturated soil-structure interaction analysis and are described below.

In dynamic analyses with numerical tools, usually the bottom of the structures is assumed to be fixed. However, it might show some flexible characteristic (Martel 1940,

Tanabashi and Ishizaki 1953) in real situations and therefore the period of actual dynamic behavior of the structure will be slightly higher than the numerical predictions. The destructions due to earthquakes at Carcas (1967) and Gediz, Turkey (1970), pointed out the effect of surrounding soils on the dynamic period of structures. This effect should be taken into account in a dynamic soil-structures interaction analysis and design procedures (Dowrick, 1977)

The behavior of soil-structures systems with dynamic loading was also studied by Kobayashi et al. (1991), Yan et al. (1991), and Dou and Byrne (1996). Also the analyses with static lateral loading were studied by Crouse et al. (1993), Brown et al. (1988), Ochaoa and O'Neill (1989), and Dunnavant and O'Niell (1989). These studies were carried out for wide range of soil types using numerical tools and advanced experimental testing methods such as full scale testing and centrifuge testing.

The effect of soil-structure interaction on the response of adjacent buildings was investigated by Amin et al. (2001) using SASSI and ABAQUS software. Three adjacent buildings of U.S. Department of Energy, the Savannah River site, SC were considered for this study. Among these buildings, two of them were very large compared to the other one. Peak accelerations and seismic loads were computed using both software and compared. The studies show that the effects of adjacent buildings on the response of large structures were insignificant. However, the predicted forces at the base of the smaller building were slightly increased due to the presence of adjacent buildings. So the presence of larger buildings affects the behavior of adjacent smaller buildings.

A coupled soil-pile-superstructure interaction response was studied by Han (2001) using SAP2000. The analysis was performed with both fixed and flexible pile bases. The superstructure was modeled with finite element method and the soil-pile interaction behavior was taken into account by representing the soil with springs and dashpots. The DYNAN and DYNA4 programs were used to compute the stiffness of the pile foundation and the damping coefficients. The effects of the fixed and flexible bases were recognized on the vertical response of the superstructure, but it was insignificant on the predicted horizontal response.

Effect of Kobe earthquake in 1995 on a storage tank and the response of the tank with damaged pile foundations are investigated by Cubrinovski et al. (2001). The tank was supported by 0.45 m diameter and 23 m long concrete hollow piles. The surface soil layer was a gravelly soil deposit for 13.6 m depth and below that it was silty sand. An important point to note is, few years before the earthquake incident, the site was improved by constructing sand piles to a depth of 15 m. And presence of sandy soils might have increased liquefaction-induced damages during the earthquake. A 2-D finite element analysis was carried out to analyze the soil-pile-tank system behavior. To evaluate the effectiveness of the sand pile improvement, the analysis was performed with both improved and unimproved conditions. The results show that the ground improvement significantly reduced the displacements and bending moments of the piles.

A soil-foundation-pier system interaction behavior was studied by Yang et al. (2001) using ABAQUS software through 2-D and 3-D nonlinear finite element analyses. The predicted results were also compared with centrifuge experimental measurements. The

results from both studies show that the pile inclusion significantly influences the system behavior. Another study by Richards (1993) showed that the response of shallow foundation will be significantly affected by the behavior of subsoil and soil-foundation interface. It also showed that the bearing capacity of shallow foundation decreases due to subsoil inertial forces and shear transferring at the soil- foundation interface.

During the Hyogo-ken earthquake in 1995, pile foundations of a five-story building were damaged and caused settlement to the building. Also the site experienced a liquefaction-induced lateral deformation. The failure of the above incident was investigated by Uzuoka et al. (2001) through a 3-D soil-pile-superstructure interaction analysis. The free-field response was predicted and compared with field measurements. The predicted failure mechanism showed that the structure was tilted in the directions of foundation failure.

The effect of soil-structure interaction on the response of buildings is expected to be higher in buildings with multiple basement floors. The response of such a building which has three basement floors and multiple stories was studied by Wartman et al. (2001) using FLUSH computer software. The interaction effects were investigated by comparing the predicted free field response with the response of the building base. The response spectral values of the predicted horizontal acceleration at the base of the structure were 35% higher than the free field response. This study also showed that the effect of soil-structure interaction was insignificant in the vertical response.

Dynamic response of an underground structure was studied by Takemiya et al. (2001) using a 2-D finite element analysis. Predicted results showed that the presence of

such underground structures will significantly influence the response of the surrounding soils. The predicted results were also compared with results of another soil deformation analysis. The dynamic load on the structure was predicted using a 1-D wave propagation analysis and the SSI analysis was carried out using the predicted dynamic loading.

The dynamic response of a bridge caisson was studied by Chang et al. (2001). 2-D and 3-D finite element models of pier W3 of the west spans of the San Francisco-Oakland bay bridge was simulated using SASSI finite element tool. In addition to the dynamic response, the analysis was also focused on the effects of soil movements such as yielding, gapping, slippage, sliding and uplifting. The predicted stresses exceeded the static stresses along the soil-caisson interfaces and it might form gaps or uplifting issues. 2-D linear and nonlinear analyses were performed using FLAC software and in this study, interface element was considered at the soil-caisson interface to evaluate the effect of SSI more realistically. Possibility of gap formation and sliding issues along the soil-caisson interfaces was recognized in this study. It also showed that the weak soil-caisson interface significantly reduced the forces and the bending moments in the caisson.

CHAPTER THREE

REPRESENTING THE CHARACTERISTICS OF UNSATURATED SOILS IN MATHEMATICAL EQUATIONS AND SOLVING

Developing the Governing Equations

The mathematical equations governing the behavior of soils are usually derived based on physical laws such as mass balance equations, linear and angular momentum balance equations, and the thermodynamic laws (first and second). In order to write the balance equations of unsaturated soils, a reasonable representative element has to be considered, and that element should be large enough to represent the unsaturated soil condition with all the significant phases. However it should be small enough to provide adequate accuracy. Therefore, rigorous volume averaging technique is being widely used to identify macroscopic quantities that represent microscopic quantities. In this method, a Representative Elementary Volume (REV) is considered to represent the volume spanned of the solid phase. For unsaturated soils, a representative element for rigorous volume averaging technique should represent all three phases (for example see Figure 3.1). The accuracy of the results directly depends on the size of the REV, and the accuracy vs. size of the REV is shown in Figure 3.2.

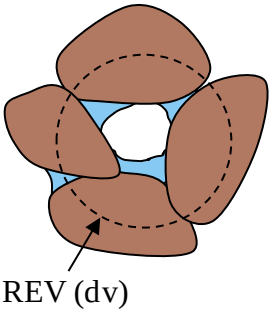

Figure 3.1 A representative element for rigorous volume averaging technique

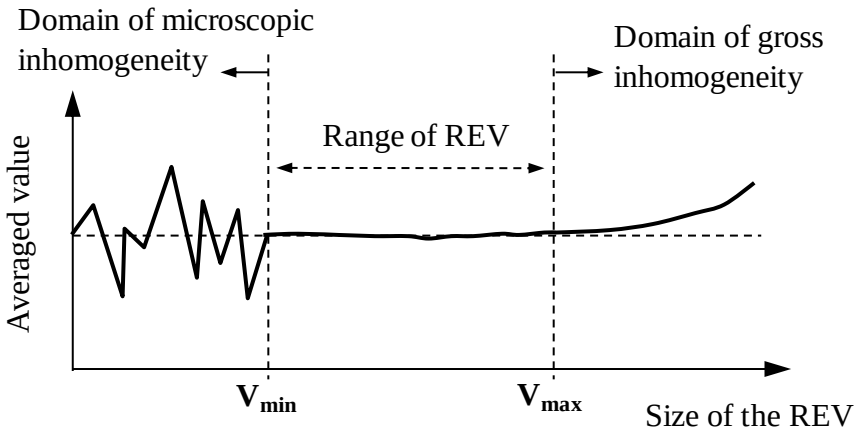

Figure 3.2 The accuracy of the results vs. size of the REV

The motion of the REV is taken into account by considering the coordinate of the material ($\mathbf{X}$) and time (t), and it is denoted as $\phi^s(\mathbf{X},t)$ in Figure 3.3. The fluids movement is considered in this derivation procedure. The fluids may flow out from the REV of the reference configuration and occupy a volume spanned by a different reference configuration. Similarly, the fluids that occupy the voids in a different reference configuration can move into the current configuration which is being considered. Therefore, the net fluid flow across the REV has to be taken into account when deriving the mass balance equations of the REV.

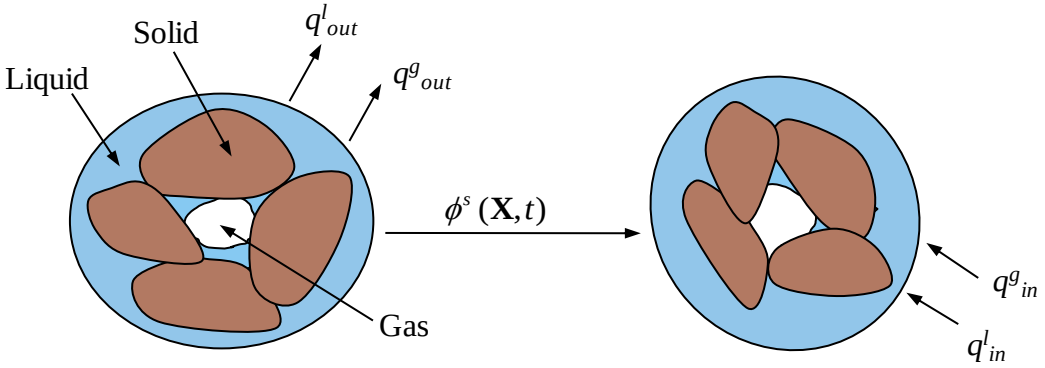

Figure 3.3 Motions in unsaturated soil system

$$\bar{\alpha}(\mathbf{x},t)=\frac{1}{\delta V}\int_{\delta V}\alpha(\mathbf{x},t)dV$$

$$n^{\alpha}(\mathbf{x},t)=\frac{\delta v^{\alpha}}{\delta v}$$

Unsaturated soil behavior is significantly influenced by the suction which is directly related to the water potential of unsaturated soils. Therefore, to analyze the coupled deformation-flow behavior of unsaturated soils, a constitutive equation, which relates the amount of water potential and suction have to be established and it should be incorporated in the governing equation. The volume fraction of the liquid phase is considered as a function of suction and volumetric strain of the solid skeleton (Wei, 2001; Wei and Muraleetharan 2002a; Schrefler et al., 1990).

$$n^l = n^l(S,\varepsilon_v)$$

Mass Balance Equation

The mass balance equation for the solid phase is derived by assuming the solid phase as incompressible.

$$-\dot{n}+(1-n)\mathrm{div}\left(\mathbf{v}^s\right)=0 \tag{3.1}$$

where n is the porosity of the unsaturated soil system and $\mathbf{v}^s$ is the velocity vector of the solid phase. By incorporating the mass balance equation of the solid phase into the mass balance equation for the liquid and the gas phases, following equation can be derived for the mass balance of the liquid phase (Equation 3.2) and gas phase (Equation 3.3).

$$\left(\frac{\partial n^l}{\partial \varepsilon_v}\right)\dot{u}^s_{i,i}+n^l\dot{u}^l_{i,i}+\left(\frac{n^l}{\Gamma^l}-\frac{\partial n^l}{\partial S}\right)\dot{p}^l+\left(\frac{\partial n^l}{\partial S}\right)\dot{p}^g=0 \tag{3.2}$$

$$\left(1-n-\frac{\partial n^l}{\partial \varepsilon_v}\right)\dot{u}^s_{i,i}+n^g\,\dot{u}^g_{i,i}+\left(\frac{\partial n^l}{\partial S}\right)\dot{p}^l+\left(\frac{n^g}{\Gamma^g}-\frac{\partial n^l}{\partial S}\right)\dot{p}^g=0 \tag{3.3}$$

where u is the displacement of the solid phase, u^l is the displacement of the liquid phase, Γ^l is the bulk modulus of the liquid phase. u^g is the displacement of the gas phase, and Γ^g is the bulk modulus of the gas phase.

Linear Momentum Balance Equation

Motion of the unsaturated soil system can be described using momentum balance equations for the solid-fluid mixture, liquid phase and the gas phase. The momentum balance equations of the fluids are essentially same as the generalized Darcy's law.

For the Mixture:

$$n^s\rho^s\ddot{u}^s_j+n^l\rho^l\ddot{u}^l_j+n^g\rho^g\ddot{u}^g_j-\sigma_{ij,i}-\rho g_j=0 \tag{3.4}$$

For the Liquid:

$$\rho^l\ddot{u}^l_j-\left(\hat{k}^l_{ij}\,n^l\right)\dot{u}^s_i+\left(\hat{k}^l_{ij}\,n^l\right)\dot{u}^l_i+\left(\delta_{ij}p^l\right)_{,i}-\rho^l g_j=0 \tag{3.5}$$

For the Gas:

$$\rho^g \ddot{u}_j^g - \left(\hat{k}_{ij}^g n^g\right)\dot{u}_i^s + \left(\hat{k}_{ij}^g n^g\right)\dot{u}_i^g + \left(\delta_{ij} p^g\right)_{,i} - \rho^g g_j = 0 \tag{3.6}$$

where σ_{ij} is the total stress tensor, g_j is the gravitational acceleration vector, $\hat{k}_{ij}^l$ is the inverted permeability tensor of the liquid phase (i.e., in 1-D $\hat{k} = 1/k$, where k = coefficient of permeability of liquid). $\hat{k}_{ij}^g$ is the inverted permeability tensor of the gas phase, and δ_{ij} is the Kronecker delta.

The complete set of governing equations of unsaturated soils is given in Equations 4.2 through 4.6. These equations consist of two mass balance equations and three momentum balance equations, which have the following five unknowns: solid displacement, liquid displacement, gas displacement, liquid pressure and gas pressure.

Solving the Governing Equations

In order to model the behavior of unsaturated soil-structure systems, the representative mathematical equations have to be solved. However, it is impossible to find closed form solutions for these complex equations. Therefore, a numerical technique has to be employed to find approximate solutions for such complex problems. Among the current numerical techniques, finite element method is the most powerful and widely used method in the field of geotechnical engineering.

Depending on the problem domain, the system of equations can be simplified by neglecting certain terms if those terms are insignificant, so that the solutions can be found through relatively simplified procedure. Certain terms in the governing equations (Equations 3.2 through 3.6) cannot be taken into account for some of the geotechnical

problems; therefore those terms can be neglected in the solution procedure. For example, relative movement of fluids should not be considered for undrained analysis. The degree of simplification also depends on the nodal unknowns of selected finite element formulations.

Different Types of Finite Element Formulations

By simplifying these five equations at various levels (Ravichandran and Muraleetharan, 2009), three different types of finite element formulations can be obtained. These formulations may include the following: (i) complete formulation (u-u-u formulation), (ii) partially reduced formulation (u-p-p formulation), and (iii) Simplified/Reduced formulation (u formulation).

Complete Formulation

The complete formulation was first solved for unsaturated soils by Ravichandran and Muraleetharan (2009). The complete formulation takes both relative acceleration and relative velocities in the calculation. This formulation is computationally very intense and numerically unstable (Ravichandran and Muraleetharan, 2009), therefore, not suitable for large simulations at this time. The displacement of all three phases (u_i, U_i^l, and U_i^g) are considered as primary nodal unknowns and also the pore liquid and pore gas pressures (p^l, p^g) are considered as element variables (see Figure 3.4). The system of equations can be simplified further without loss of accuracy by eliminating the liquid and gas pressures in the momentum balance equations using the mass balance equations. This formulation is comparable to the displacement formulation or irreducible form for saturated soils used

by various researchers (Wei, 2001; Muraleetharan et al, 1994; Zienkiewicz and Shiomi, 1984).

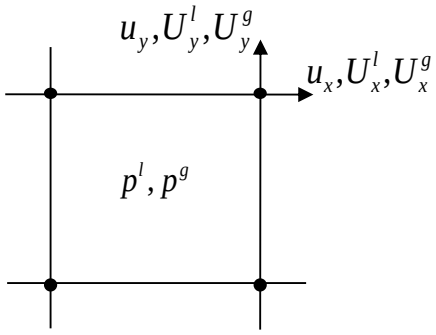

Figure 3.4 Primary nodal and element variables for the complete formulation

The final set of equations for the complete formulation is summarized below.

$$n^s \rho^s \ddot{u}_j + n^l \rho^l \ddot{U}_j^l + n^g \rho^g \ddot{U}_j^g - \sigma_{ij,i} - \rho b_j = 0 \tag{3.7}$$

$$\rho^l \ddot{U}_j^l - \left(\hat{k}_{ij}^l n^l\right)\dot{u}_i + \left(\hat{k}_{ij}^l n^l\right)\dot{U}_i^l + \mu^{11}\, u_{i,ij} + \mu^{12} U_{i,ij}^l + \mu^{13} U_{i,ij}^g - \rho^l b_j = 0 \tag{3.8}$$

$$\rho^g \ddot{U}_j^g - \left(\hat{k}_{ij}^g n^g\right)\dot{u}_i + \left(\hat{k}_{ij}^g n^g\right)\dot{U}_i^g + \mu^{21}\, u_{i,ij} + \mu^{22} U_{i,ij}^l + \mu^{23} U_{i,ij}^g - \rho^g b_j = 0 \tag{3.9}$$

where $\mu^{11}, \mu^{12}, \mu^{13}, \mu^{21}, \mu^{22}$, and μ^{23} are functions of a_{12}, a_{12}, a_{21}, a_{22}, b_{11}, b_{12}, b_{21}, and b_{22}.

$$a_{11} = \left(\frac{n^l}{\Gamma^l} - \frac{\partial n^l}{\partial S}\right), a_{12} = \left(\frac{\partial n^l}{\partial S}\right), b_{11} = \left(\frac{\partial n^l}{\partial \varepsilon_v}\right),\ b_{12} = n^l$$

$$a_{21} = \left(\frac{\partial n^l}{\partial S}\right), a_{22} = \left(\frac{n^g}{\Gamma^g} - \frac{\partial n^l}{\partial S}\right), b_{21} = \left(1 - n - \frac{\partial n^l}{\partial \varepsilon_v}\right) \text{ and } b_{22} = \left(n^g\right)$$

The liquid and gas pressures can be calculated using the following equations.

$$p^l = \mu^{11}\, u_{k,k} + \mu^{12} U_{k,k}^l + + \mu^{13} U_{k,k}^g \tag{3.10}$$

$$p^g = \mu^{21} u_{k,k} + \mu^{22} U_{k,k}^l + \mu^{23} U_{k,k}^g \tag{3.11}$$

Partially Reduced Formulation

In this formulation, the relative accelerations of the liquid and gas phases are neglected, but relative velocities are considered. A detailed description of this formulation can be found in Wei (2001). In the special discretization of the above governing equations, the liquid pressure and gas pressure are considered as nodal unknowns in addition to the solid displacement and it is another major difference in this formulation. Figure 3.5 shows the four-node quadrilateral element with primary nodal unknowns at a node. Same order of interpolation function is used for both displacement and pressure fields. Although such formulation violates the well known Babuska-Brezzi condition (Brezzi and Fortin, 1991), the applicability of this technique is justified in unsaturated soils. Because of the high compressibility of the gas phase, the volumetric element locking that occurs in incompressible materials does not exist in unsaturated soils. However, in order to solve saturated soil problems, this type of element has been successfully used with special consideration of volume change terms to avoid element locking (Herrmann and Mish, 1983). The partially reduced formulation has been used by Schrefler et al. (1990), Muraleetharan and Wei (1999b) and Wei (2001).

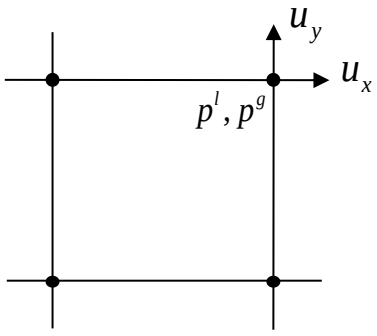

Figure 3.5 Primary nodal variables for the partially reduced formulation

Conservation laws for the liquid and gas:

$$\left(n^l + \frac{\partial n^l}{\partial \varepsilon_v}\right)\dot{u}^s_{i,i} + \left(\frac{n^l}{\Gamma^l} - \frac{\partial n^l}{\partial S}\right)\dot{p}^l + \left(\frac{\partial n^l}{\partial S}\right)\dot{p}^g + \dot{\bar{U}}^l_{i,i} = 0 \tag{3.12}$$

$$\left(1 - n^l - \frac{\partial n^l}{\partial \varepsilon_v}\right)\dot{u}^s_{i,i} + \left(\frac{\partial n^l}{\partial S}\right)\dot{p}^l + \left(\frac{n^g}{\Gamma^g} - \frac{\partial n^l}{\partial S}\right)\dot{p}^g + \dot{\bar{U}}^g_{i,i} = 0 \tag{3.13}$$

Linear momentum balance equation for the mixture, liquid and gas:

$$\rho \ddot{u}^s_i - \sigma_{ij,j} - \rho g_i = 0 \tag{3.14}$$

$$\dot{U}_i{}^l = -\left(\frac{K_{ij}\, K_r{}^l}{\mu^l}\right)\left(p_{,j}{}^l - \rho^l g_j + \rho^l \ddot{u}^s_j\right) \tag{3.15}$$

$$\dot{U}_i{}^g = -\left(\frac{K_{ij}\, K_r{}^g}{\mu^g}\right)\left(p_{,j}{}^g - \rho^g g_j + \rho^g \ddot{u}^s_j\right) \tag{3.16}$$

where n is the porosity, and u^s is the displacement of the solid phase, p^l, p^g are nodal liquid and gas pressure, respectively. Γ^l, Γ^g are bulk moduli of the liquid and gas phases, respectively. K_{ij} is saturated permeability, $K_r{}^l, K_r{}^g$ are the relative permeability of liquid and gas, respectively. μ^l, μ^g are viscosity of liquid, gas phases, respectively, and ρ^l, ρ^g, ρ are mass density of the liquid phase, gas phase and the mixture, respectively.

The velocity terms in the conservation laws of the liquid and gas phases (Equations 3.12 and 3.13) can be eliminated using the momentum balance equations of the liquid and gas phases (Equations 3.15 and 3.16). The final set of governing equations in terms of solid displacement, liquid pressure and gas pressure is given below.

$$\rho \ddot{u}^s_i - \sigma_{ij,j} - \rho g_i = 0$$

$$\left(n^l + \frac{\partial n^l}{\partial \varepsilon_v}\right)\dot{u}^s_{i,i} + \left(\frac{n^l}{\Gamma^l} - \frac{\partial n^l}{\partial S}\right)\dot{p}^l + \left(\frac{\partial n^l}{\partial S}\right)\dot{p}^g + \left(\frac{K_{ij}\,K_r{}^l}{\mu^l}\right)\left(p_{,j}{}^l - \rho^l g_j + \rho^l \ddot{u}^s_j\right) = 0$$

$$\left(1 - n^l - \frac{\partial n^l}{\partial \varepsilon_v}\right)\dot{u}^s_{i,i} + \left(\frac{\partial n^l}{\partial S}\right)\dot{p}^l + \left(\frac{n^g}{\Gamma^g} - \frac{\partial n^l}{\partial S}\right)\dot{p}^g + \left(\frac{K_{ij}\,K_r{}^g}{\mu^g}\right)\left(p_{,j}{}^g - \rho^g g_j + \rho^g \ddot{u}^s_j\right) = 0$$

Reduced Formulation

The permeability coefficient of the liquid and gas phases are very low for unsaturated soils compared to saturated soils. During an earthquake or when it is subjected to a dynamics loading, the unsaturated soils can be assumed to behave under undrained condition. To simulate such undrained conditions, the governing equations described in the previous section can be simplified by neglecting the relative movement of pore fluids (both accelerations and velocities). This system of equations will consist of momentum balance equation for the mixture and mass balance equations for the liquid and gas phases. In this case, the momentum balance equation will be solved considering the solid displacements (see Figure 3.6) as the primary nodal unknowns. Even though the relative movement of fluids is neglected, pore liquid and pore gas pressures can be computed using mass balance equations. In this formulation, any changes in matric suction (pore liquid pressure and pore gas pressure) and degree of saturation are directly related to the deformation of the solid skeleton and not to the flow of the fluids since this formulation simulate the undrained behavior of the unsaturated soils. Simplified formulation is computationally very efficient and its predictions were proved to be comparable with predictions of *complete* and *partially reduced formulations* for selected problems with elastoplastic constitutive model (Ravichandran and Muraleetharan, 2009).

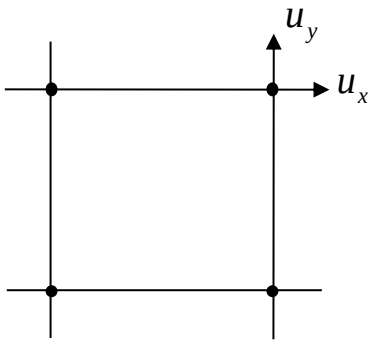

Figure 3.6 Primary nodal variables for the simplified/ reduced formulation

The final set of equations for the reduced formulation is summarized below.

$$\rho \ddot{u}_j - \sigma_{ij,i} - \rho g_j = 0$$

$$\left(n^l + \frac{\partial n^l}{\partial \varepsilon_v} \right) \dot{u}_{i,i} + \left(\frac{n^l}{\Gamma^l} - \frac{\partial n^l}{\partial S} \right) \dot{p}^l + \left(\frac{\partial n^l}{\partial S} \right) \dot{p}^g = 0$$

$$\left(1 - n^l - \frac{\partial n^l}{\partial \varepsilon_v} \right) \dot{u}_{i,i} + \left(\frac{\partial n^l}{\partial S} \right) \dot{p}^l + \left(\frac{n^g}{\Gamma^g} - \frac{\partial n^l}{\partial S} \right) \dot{p}^g = 0$$

Corresponding finite element equations for the reduced formulations are derived using four-node quadrilateral isoparametric elements with linear interpolation functions. The major advantage of the simplified formulation is computational efficiency. To further increase the computational efficiency, the element matrices and vectors are evaluated using a novel uniform gradient element formulation (single point integration for 4 node quadrilateral elements) with hourglass control scheme for computational efficiency (Ravichandran and Muraleetharan, 2009).

Time Integration Procedure

Time integration of the spatially discretized governing equations is one of the important steps in numerical analysis of dynamic problems for achieving accurate results

and saving computational effort through low number of iterations. In many dynamic problems, only low-frequency modes are of interest, since the major contribution to the overall behavior comes from low frequency modes. Furthermore, in dynamic analysis using finite element methods, some of the high frequency modes are due to the spatial discretization of the problem domain rather than due to the real behavior of the material. Hence, it is desirable to have a time integration algorithm, which poses some form of numerical dissipation, to damp out any spurious participation of high frequency modes.

The Newmark's family of time integration methods (Newmark, 1959) is widely used in the dynamic analysis of geotechnical engineering problems. The amount of dissipation can be controlled by a parameter other than time step. The Newmark's method is unconditionally stable for linear problems when the parameters, β and γ associated with the method, are selected such that $\gamma \geq 0.5$ and $\beta \geq 0.25(\gamma + 0.5)^2$. The amount of dissipation, for a fixed time step can be increased by increasing γ. The disadvantage of Newmark's method is that it has second order accuracy in linear problems only when $\gamma = 0.5$ and $\beta = 0.25$, which constraints the controlling of the numerical dissipation of higher frequency modes. For other values of β and γ, the method has only first order accuracy.

Hilber, Hughes and Taylor (1977) improved Newmark's method by incorporating an additional parameter α. This method has a second order accuracy and unconditional stable in linear problems when the parameters α, β and γ are selected such that

$-1/3 \le \alpha \le 0$, $\gamma = 0.5(1-2\alpha)$ and $\beta \ge 0.25(1-\alpha^2)$. The numerical dissipation is increased by increasing the absolute value of α.

For nonlinear problems, when an algorithm is used in a consistent linear manner some of the conditions derived for linear problems are applicable to the nonlinear problems to a certain extent (Hughes and Pister, 1978). For example, the necessary and sufficient stability conditions derived for the linear problems become only the necessary condition for stability in nonlinear problems (Hughes, 1983). In this research, the Hilber-Hughes-Taylor α-method together with a predictor corrector algorithm proposed by Hughes and Pister (1978) is used to integrate the spatially discretized nonlinear governing equations in the time domain. Muraleetharan et al. (1994) used a similar algorithm to study dynamics of saturated soils.

The spatially discrete governing equations can be written in matrix form as

$$\mathbf{M}\mathbf{a} + \mathbf{C}\mathbf{v} + \mathbf{K}_p\mathbf{d} + \mathbf{p} = \mathbf{f} \tag{3.17}$$

where $\mathbf{M}$ is the mass matrix, $\mathbf{C}$ is the damping matrix, $\mathbf{K}_p$ is the pore fluid stiffness, $\mathbf{p}$ is the internal force vector, $\mathbf{f}$ is the external force vector, $\mathbf{a}$ is the nodal acceleration vector, $\mathbf{v}$ is the nodal velocity vector and $\mathbf{d}$ is the nodal displacement vectors.

Equation E4.17 can be rewritten as follows using the Hilber-Hughes-Taylor α-method

$$\mathbf{M}\mathbf{a}_{n+1} + (1+\alpha)\mathbf{C}\mathbf{v}_{n+1} - \alpha\mathbf{C}\mathbf{v}_n + (1+\alpha)\mathbf{K}_p\mathbf{d}_{n+1} - \alpha\mathbf{K}_p\mathbf{d}_n + (1+\alpha)\mathbf{p}_{n+1} - \alpha\mathbf{p}_n = (1+\alpha)\mathbf{f}_{n+1} - \alpha\mathbf{f}_n$$

where

$$\mathbf{v}_{n+1} = \mathbf{v}_n + \Delta t\left[(1-\gamma)\mathbf{a}_n + \gamma\,\mathbf{a}_{n+1}\right],$$

$$\mathbf{d}_{n+1} = \mathbf{d}_n + \Delta t\,\mathbf{v}_n + \Delta t^2\left[(0.5-\beta)\mathbf{a}_n + \beta\,\mathbf{a}_{n+1}\right],$$

where n is the time step and $\Delta t = t_{n+1} - t_n$

The fully discretized (in space and time) governing equations can be written in the following form.

$$\mathbf{M}^{\mathrm{i}}_{\mathrm{eff}}\,\Delta\mathbf{a}^{i+1} = \mathbf{f}^{\mathrm{i}}_{\mathrm{eff}} \tag{3.18}$$

where i is the iteration counter and $\mathbf{M}_{\mathrm{eff}}$ is the effective stiffness and given by:

$$\mathbf{M}_{\mathrm{eff}} = \mathbf{M} + \left[(1+\alpha)\gamma\,\Delta t\right]\mathbf{C} + \left[(1+\alpha)\beta\,\Delta t^2\right]\mathbf{K}_p + \left[(1+\alpha)\beta\,\Delta t^2\right]\mathbf{K}_T^i$$

where $\mathbf{K}_T$ is the global tangent stiffness matrix given by $\mathbf{K}_T = \dfrac{\partial \mathbf{p}_{n+1}}{\partial \mathbf{d}_{n+1}}$ and $\mathbf{f}_{\mathrm{eff}}$ is the effective force vector and given by:

$$\mathbf{f}^{\mathrm{i}}_{\mathrm{eff}} = (1+\alpha)\mathbf{f}_{n+1} - \alpha\,\mathbf{f}_n - \mathbf{M}\,\mathbf{a}^{\mathrm{i}}_{n+1} - (1+\alpha)\mathbf{C}\,\mathbf{v}^{\mathrm{i}}_{n+1} + \alpha\,\mathbf{C}\,\mathbf{v}_n - (1+\alpha)\mathbf{K}_p\,\mathbf{d}^{\mathrm{i}}_{n+1} + \alpha\,\mathbf{K}_p\,\mathbf{d}_n - (1+\alpha)\mathbf{p}^{i}_{n+1} + \alpha\,\mathbf{p}_n$$

The incremental acceleration is calculated by solving the Equation 4.18 and these acceleration increments are used to calculate the acceleration, velocity, and displacement for the next iteration as follows.

$$a^{i+1}_{n+1} = a^{i}_{n+1} + \Delta a^{i+1}$$

$$v^{i+1}_{n+1} = v^{i}_{n+1} + \gamma\,a^{i+1}_{n+1}\Delta t$$

$$d^{i+1}_{n+1} = d^{i}_{n+1} + \beta\,a^{i+1}_{n+1}\Delta t^2$$

The convergence of the solution can be verified for the acceleration norm as follows.

$$\frac{\left\|\Delta \mathbf{a}^{i+1}\right\|}{\left\|\mathbf{a}_{n+1}^{i+1}\right\|} \leq \varepsilon$$

The finite element formulations and the time integration procedure should be implemented within a finite element framework, which can be used to simulate the behavior of unsaturated soils and soil-structure systems. A brief description of the finite element framework, which will be used in this study, is given in the next section.

TeraDysac Software

TeraDysac is a finite element software (Ravichandran 2005, Muraleetharan et al, 2003), developed to simulate the behavior of geotechnical structures with both unsaturated and saturated soils. In contrast to conventional code development procedure in civil engineering research practice, TeraDysac is developed within a finite element framework (Anatech Corp, 2001) which made the resulting software similar to commercially available software in terms of user interface and other input and output services. Even though TeraDysac is capable of simulating problems with both unsaturated and saturated soils, the piece of code for unsaturated soil is currently decoupled from the piece of code for saturated soils, i.e., problems with full range of degree of saturation (from 0 to 100%) cannot be simulated using a single code. However, modifications are being undertaken to incorporate the general theory. The finite element formulations of unsaturated soils and the time integration procedure, which are presented in the previous section, are implemented into the piece of code for unsaturated soil.

CHAPTER FOUR

UNDERSTANDING THE INFLUENCE OF DEGREE OF SATURATION ON THE BEHAVIOR OF UNSATURATED SOILS

Introduction

The behavior of saturated and dry soils has been well studied in the past several decades. The study of unsaturated soil behavior is, however, a relatively new field. Because of short duration of loading, response of Geotechnical structures subjected to earthquake loadings can be analyzed by assuming an undrained condition i.e. without taking the flow of liquids into account. However the deformation of solid skeleton might affect the water potential and the variation in water potential might considerably influence the overall responses of the geotechnical systems with unsaturated soils. Since the water potential is directly related to the suction of the soil, it is also essential to investigate the influence of degree of saturation/suction on the deformation behavior of unsaturated soils.

Because of the uniqueness of unsaturated soils and the influence of suction, geotechnical structures designed with the knowledge of saturated and/or dry soils may not perform adequately when the soil is in unsaturated conditions. Therefore, construction of safe and economical structures requires extensive study of unsaturated soil behavior. Acquiring further insights into the behavior of the unsaturated soil can be effectively done through numerical simulations. Therefore, to investigate the undrained behavior of unsaturated soils and the influence of degree of saturation and suction, a wide

range of numerical simulations were carried out and the details are presented below. These analyses reveal that the suction significantly influences the deformation behavior of clayey soils. In silty soils, the influence of suction is insignificant for selected problems; however it cannot be neglected if the silt is relatively soft.

Simulation Study

In this study, the reduced/simplified finite element formulation of TeraDysac together with the Bishop's effective stress equation is used to study the behavior of unsaturated silt and clay under various loading conditions. The influence of the suction with various initial degree of saturation is also investigated. The numerical analyses were carried out with three different problems: (i) a 2D asymmetric four element problem subjected to a vertical quasi-static loading, (ii) a 2D problem of a compacted embankment subjected to base motion acceleration, and (iii) a 3D problem of the compacted embankment subjected to base motion acceleration. Two different types of soils, Minco silt and Speswhite kaolin, were used to study the behavior of unsaturated silty soil and clayey soil, respectively.

Material Models and Model Parameters

To avoid further complications when using elastoplastic constitutive models, the stress-strain behavior of the soil skeleton is modeled using linear elastic material model. Linear elastic model parameters used for the Minco silt and the Speswhite kaolin are listed in Table 4.1. To further study the role of suction, the analyses were repeated with relatively softer materials (Young's modulus of $1.2x10^2$ kPa for Minco silt, $3.0x10^2$ kPa for Speswhite Kaolin). i.e., based on the Bishop's effective stress equation, the

contribution of the suction induced stresses in the overall responses can be increased by reducing the contribution of strain induced stresses (by reducing the stiffness/Young's modulus).

Table 4.1 Linear elastic model parameters for Minco silt and Speswhite kaolin

Properties			Value	
			Minco silt	Speswhite kaolin
Solid grain density		Mg/m^3	2.67	2.62
Liquid density		Mg/m^3	1.0	1.0
Gas density	$x10^{-3}$	Mg/m^3	2.1	2.1
Bulk modulus of liquid	$x10^6$	kPa	2.2	2.2
Bulk modulus of gas		kPa	101.325	101.325
Young's Modulus	$x10^5$	kPa	1.2	0.3
Poisson's ratio			0.3	0.2

The moisture-suction relationship of the Minco silt and the Speswhite kaolin is modeled using the Brooks and Corey SWCC model (Brooks and Corey, 1964). The SWCC model parameters for the Minco silt and Speswhite kaolin were calibrated using experimental data presented by Ananthanathan (2003) and Sivakumar (1993), respectively. The model parameters were adjusted until the model curve matches with the experimental curve. The calibrated SWCC curves together with the model parameters for the Minco silt (***a*** = 2.35 kPa, ***n*** = 0.68) and Speswhite kaolin (***a*** = 14 kPa, ***n*** = 0.182) are shown in Figure 4.1 and Figure 4.2, respectively.

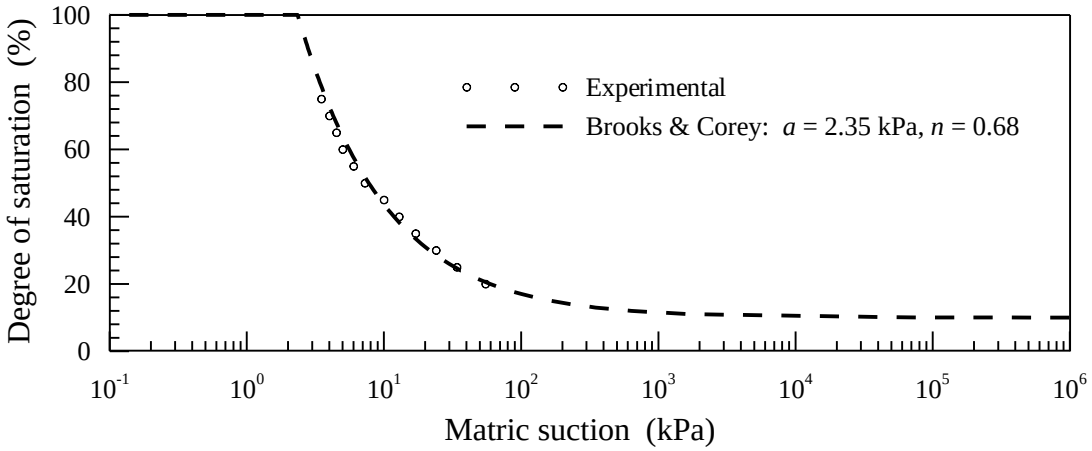

Figure 4.1 Calibration of SWCC for Minco silt

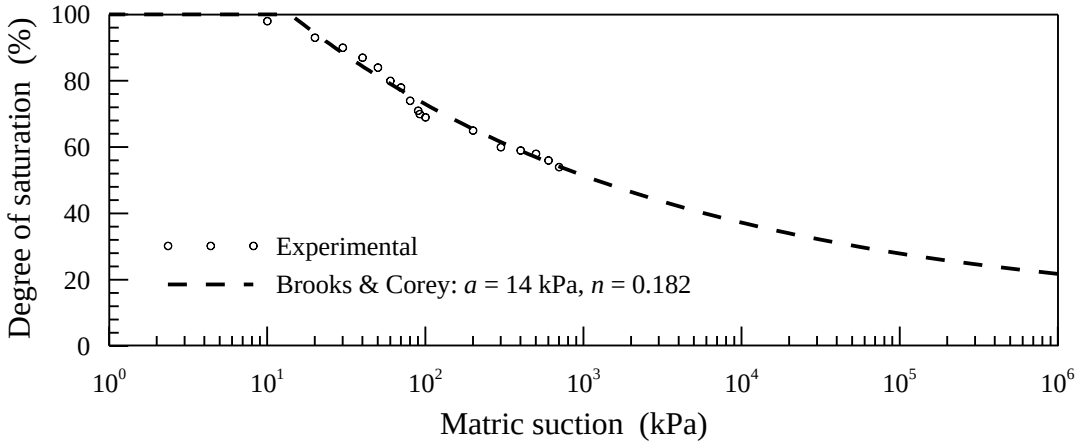

Figure 4.2 Calibration of SWCC for Speswhite kaolin

Calibration of Bishop's Degree of Saturation Related Parameter (χ)

The degree of saturation of unsaturated soils will be a variable for any static or dynamic analysis especially when the soil is subjected to a volume change. So the Bishop's degree of saturation related parameter will not be constant throughout any numerical analysis and there is an intention to establish a mathematical relationship between the degree of saturation and the corresponding related parameters

The parameter χ is directly related to the degree of saturation and it can also be varied slightly with soil type and stress history (Fredlund and Rahardjo, 1993). The experimental prediction of χ - degree of saturation relationship obtained by Fredlund and Rahardjo (1993) can be used in this study without significant error. Because, the actual values of χ for silt and clay at a given degree of saturation might be slightly smaller than the experimental values obtained by Fredlund and Rahardjo (1993) but it will never be higher. In addition, it is reasonable to assume that a small difference in the predicted χ will not affect the suction related component significantly in undrained analysis as the change in matric suction will be relatively small. So it is reasonable to use the experimental prediction of χ - degree of saturation relationship obtained by Fredlund and Rahardjo (1993) to establish a mathematical equation for this study.

It was complicated to develop a single equation for the entire range of degree of saturation to fit the experimental results obtained by Fredlund and Rahardjo (1993). So, two second order equations (Equations 4.1 and 4.2) are established to harmonize the entire experimental results. The first equation is applicable when the degree of saturation is less than 65% and the second equation is applicable when the degree of saturation is greater or equal to 65%. The predicted values using equations (Equations 4.1 and 4.2) well harmonize with the experimental data obtained by Fredlund and Rahardjo (1993) as shown in Figure 4.3 and in the Table 4.2.

$$\chi = -1.8678(S - 0.7819)^2 + 0.8325 \qquad if \quad S < 0.65 \tag{4.1}$$

$$\chi = -0.476(S - 1.425)^2 + 1.086 \qquad if \quad S \geq 0.65 \tag{4.2}$$

where the χ is the degree of saturation related parameter and S is the degree of saturation of the soil.

Table 4.2 Degree of saturation related parameter Vs. Degree of saturation

Degree of saturation (S)	Degree of saturation related parameter (χ)	
	Experimental	Calibrated
0.20	0.20	0.20
0.30	0.41	0.40
0.40	0.56	0.56
0.50	0.68	0.68
0.60	0.76	0.77
0.65	0.80	0.80
0.70	0.83	0.84
0.80	0.90	0.90
0.90	0.95	0.95
1.00	1.00	1.00

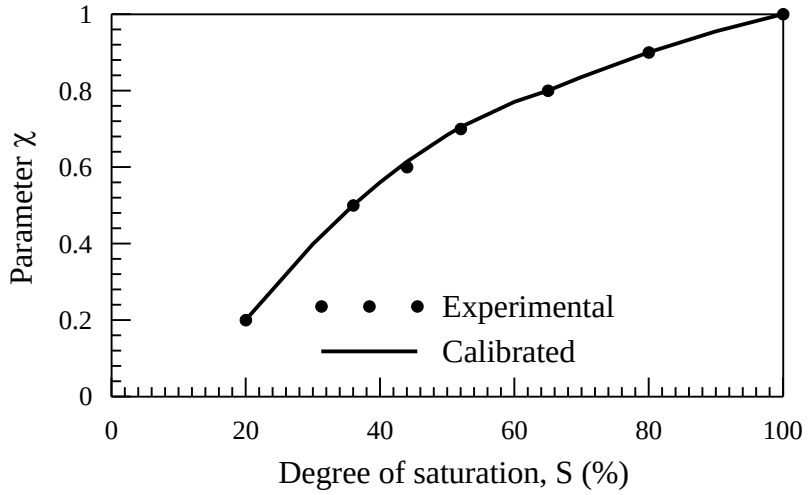

Figure 4.3 Degree of saturation related parameter Vs. Degree of saturation

Results and Discussion

Three different problems were simulated in this study: a 2D asymmetric four element problem subjected to a vertical displacement at the top, a 2D embankment subjected to base shaking, and a 3D embankment subjected to base shaking. These analyses were done with two different soils, silt and clay. In addition to the realistic Young's modulus, relatively smaller Young's moduli were also used to cause the soils to produce smaller stiffness induced stress (first component in the Bishop's effective stress equation); so that the role of suction induced stress (second component in the Bishop's equation) could be investigated.

Example 1: Asymmetric Four-Element Problem Subjected to Quasi-Static Loading

The 2D finite element mesh used for the asymmetric four-element problem is shown in Figure 4.4. The base of the mesh was assumed to be fixed in all direction throughout the analysis and a vertical displacement time history shown in Figure 4.5 was applied at nodes N2, N3 and N6. The predicted responses are discussed below.

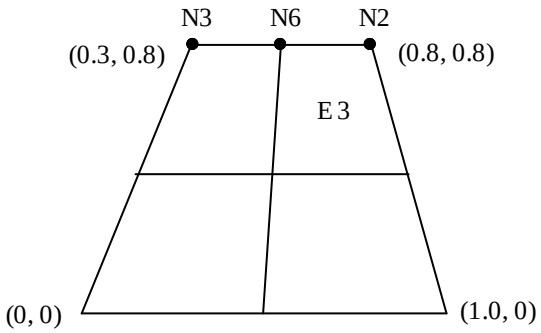

Figure 4.4 Asymmetric four element mesh (all dimensions are in meters)

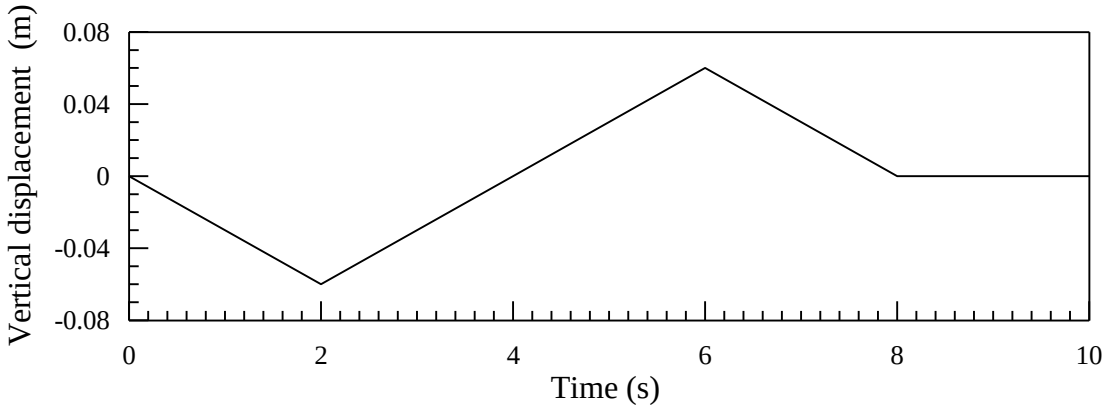

Figure 4.5 Vertical displacement time history (nodes N2, N3 and N6)

Effect of Initial Degree of Saturation and Matric Suction: Stiffer Soil

Analyses were done with three different intial degree of saturations to investigate the effect of initial degree of saturation. The initial degree of saturation values were chosen considering the natural conditions of silt and clay as well as to get incremental matric suctions in a suitable range. Intial degree of saturations in the lower range, 0.2, 0.4 and 0.6, were selected for silt and in the higher range, 0.6, 0.7 and 0.8, were used for clay. The Figures 4.6a through 4.6d show the predicted time histories of incremental degree of saturation, incremental matric suction, incremental horizontal strain and incremental horizontal stress in element E3 (see Figure 4.4), respectively, for silt. The Figures 4.6e through 4.6h show the predicted time histories of incremental degree of saturation, incremental matric suction, incremental horizontal strain and incremental horizontal stress in element E3, respectively, for clay.

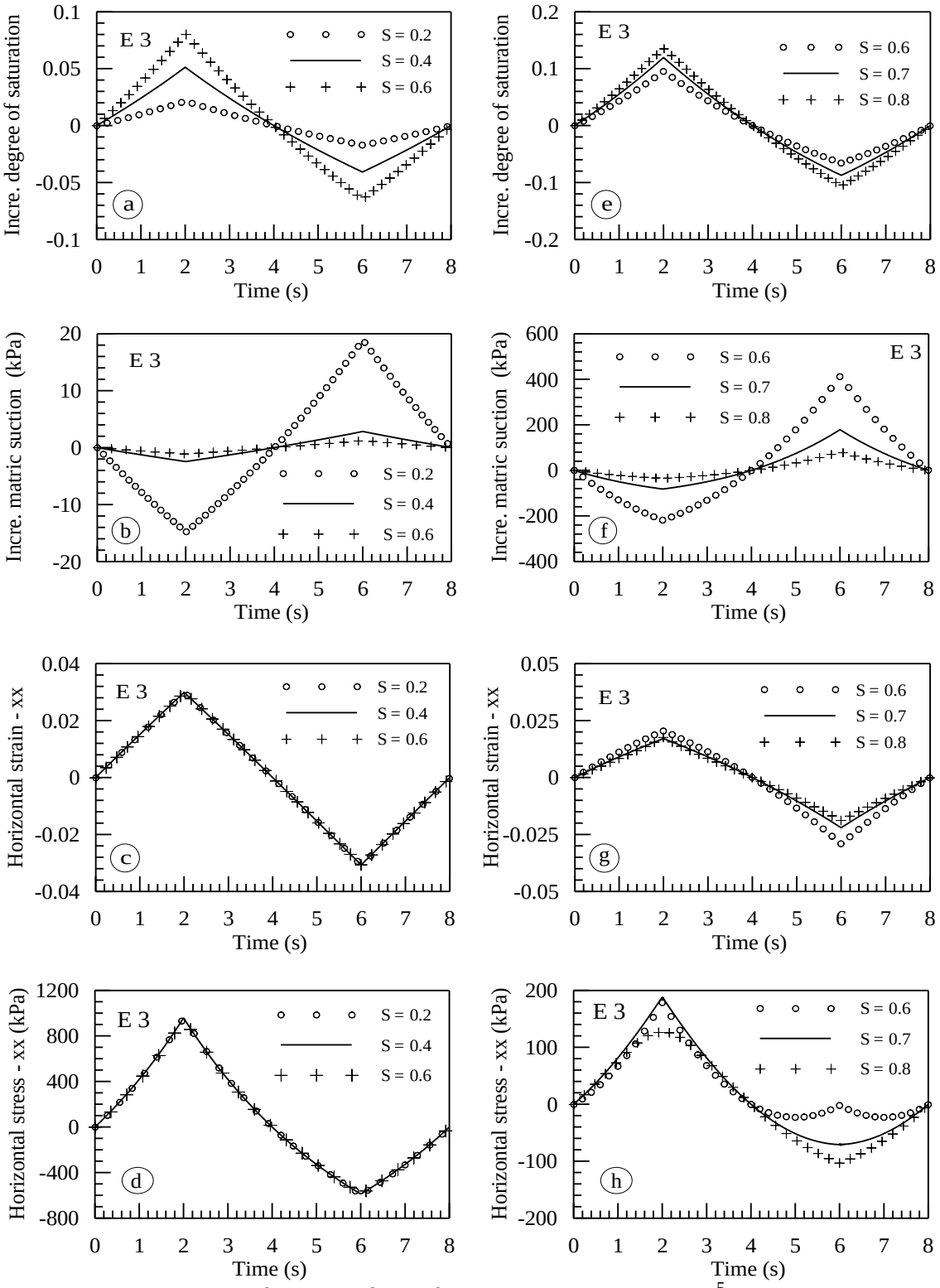

Figure 4.6 Comparison of element fields for Minco silt (E= 1.2 x 10^5 kPa) and Speswhite kaolin (E = 3 x 10^4 kPa)

In the case of silt, even though significant differences are seen in the matric suction for different initial degree of saturation, no noticeable differences are seen in the predicted stress and straintime histories. Such behavior can be explained by comparing the first componenet, $\sigma - p^g$ which is the stiffness related component, and the second component, $\chi\left(p^g - p^l\right)$, which is the suction related component in the Bishop's effective stress equation. The maximum incremental matric suction is around 20 kPa and the maximum incremental stress is 1000 kPa. The suction related component is small compared to the stiffness related component. Therefore, not much difference is seen in the stress and strain histories. In the case of clay, the stiffness related component and the suction related components are large enough to be comparable to each other. Therefore, the effect of matric suction can be seen in the incremental stress and strain time histories. A detailed comparison of the stiffness and the suction related components in the stiffer and softer soils is discussed right after the discussion of softer soil. Predicted time histories of incremental horizontal stress in element E3 shown in Figure 4.6h for clay with initial degree of saturation of 0.6, shows a kink at 6 sec and it is due to poisson effect.

Effect of Poisson Ratio

As shown in Figure 4.6h, when the clay is subjected to vertical compression, the predicted maximum horizontal stress increament for the clay with S = 0.8 (80% degree of saturation), is significantly smaller (differs by around 50 kPa) compared to that in the clay with S = 0.6 or 0.7. At the same time when it is subjected to vertical expansion, the predicted maximum horizontal stress increament is higher when the S = 0.8 and lower

when the S = 0.6. In addition, it shows a small kink for S = 0.8 at t = 2 sec when it is subjected to vertical compression, and a significant kink for S = 0.6 at t = 6 sec when it is subjected to vertical expansion. These kinks are due to the magnitude of poisson ratio and this effect is further studied with relatively higher poisson ratio ($\nu = 0.3$). The predicted results for $\nu = 0.3$ is presented in Figure 4.7. As shown in the figure, when the $\nu = 0.3$, the kink in S = 0.8 curve during the compression at t = 2 sec is totally vanished, and the kink for S = 0.6 during the vertical expansion at t = 6 sec is significantly reduced.

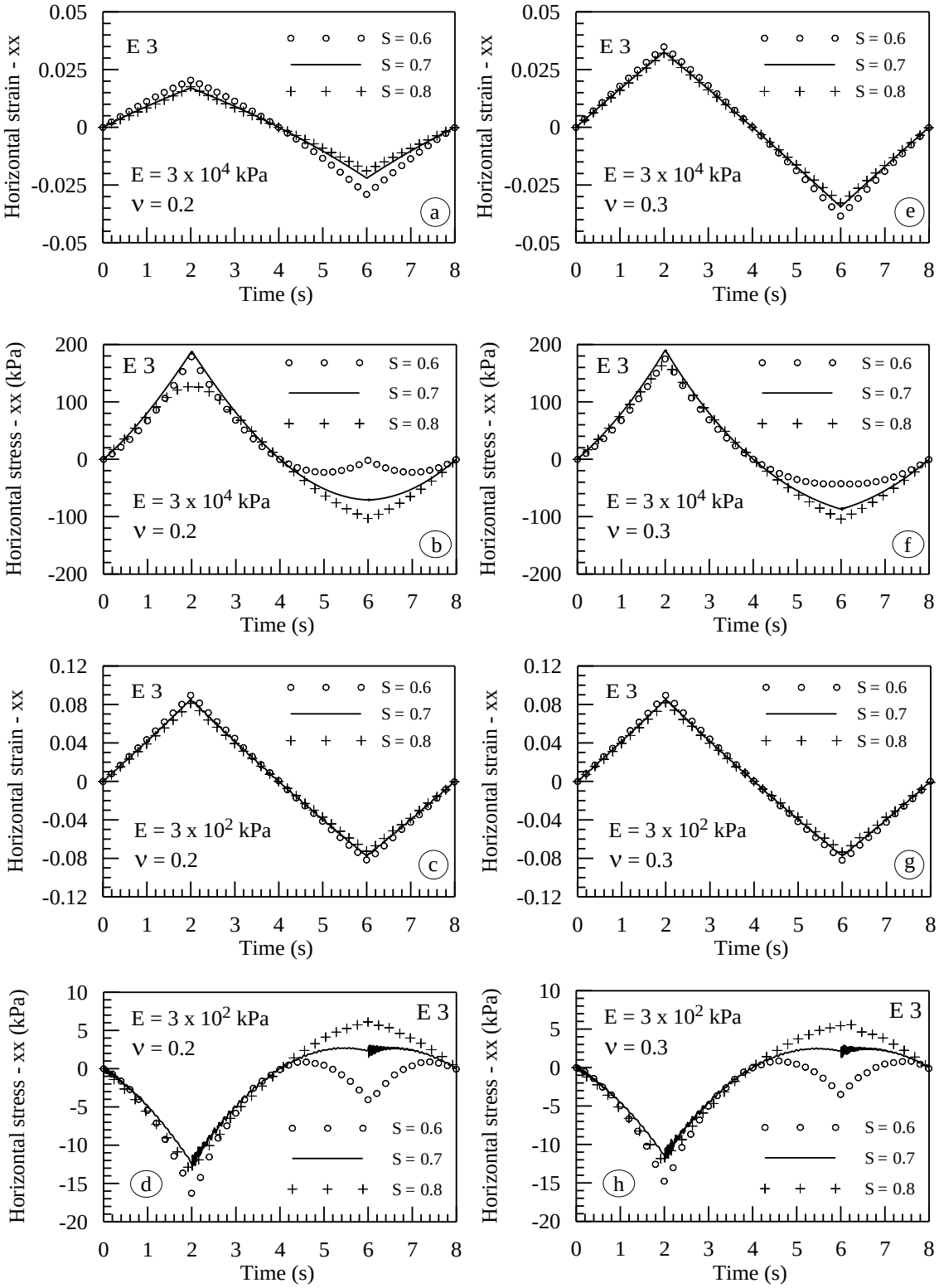

Figure 4.7 Comparison of element fields for Speswhite kaolin with ν = 0.2, 0.3

Effect of Initial Degree of Saturation and Matric Suction: Softer Soil

The same problem was analyzed with smaller Young's moduli for silt and clay to significantly lower the stiffness related stress component caused by the same displacement time history applied before. The predicted responses are shown in Figure 4.8. The results show that the effect of matric suction is significant in the case of both silt and clay soils. When the Young's modulus was reduced, the stiffness induced component was also reduced significantly and the stiffness and suction related components are comparable to each other. The effect of matric suction due to the change in degree of saturation could be seen in the overall behavior. As shown in Figures 4.8d and 4.8h, the predicted stress histories show an opposite variation compared to the predicted histories for stiffer soils (see Figure 4.8d and 4.8h). This opposite variation is due to the magnitude of smaller Young's modulus and this can be easily proved with a simple application of Hooke's low.

Horizontal stresses are calculated using the predicted horizontal and vertical strains. The Hooke's low is used for the stress calculation together with $E = 3.0 \times 10^4$ kPa and $\nu = 0.2$ for the stiffer analysis and $E = 3.0 \times 10^2$ kPa and $\nu = 0.2$ for the softer analysis, and the comparison is shown in Figure 4.9. As shown in Figure 4.9, predicted horizontal and the vertical strains for stiffer and softer analysis show similar variation (see Figures 4.9a, 4.9b, 4.9e, and 4.9f) while the predicted horizontal stress for stiffer and softer analysis shows an opposite variation (see Figures 4.9c, 4.9g). As shown in Figures 4.9c, 4.9d and Figures 4.9g, 4.9h, the calculated stresses and the predicted stress are same and it proves the accuracy of the predicted results.

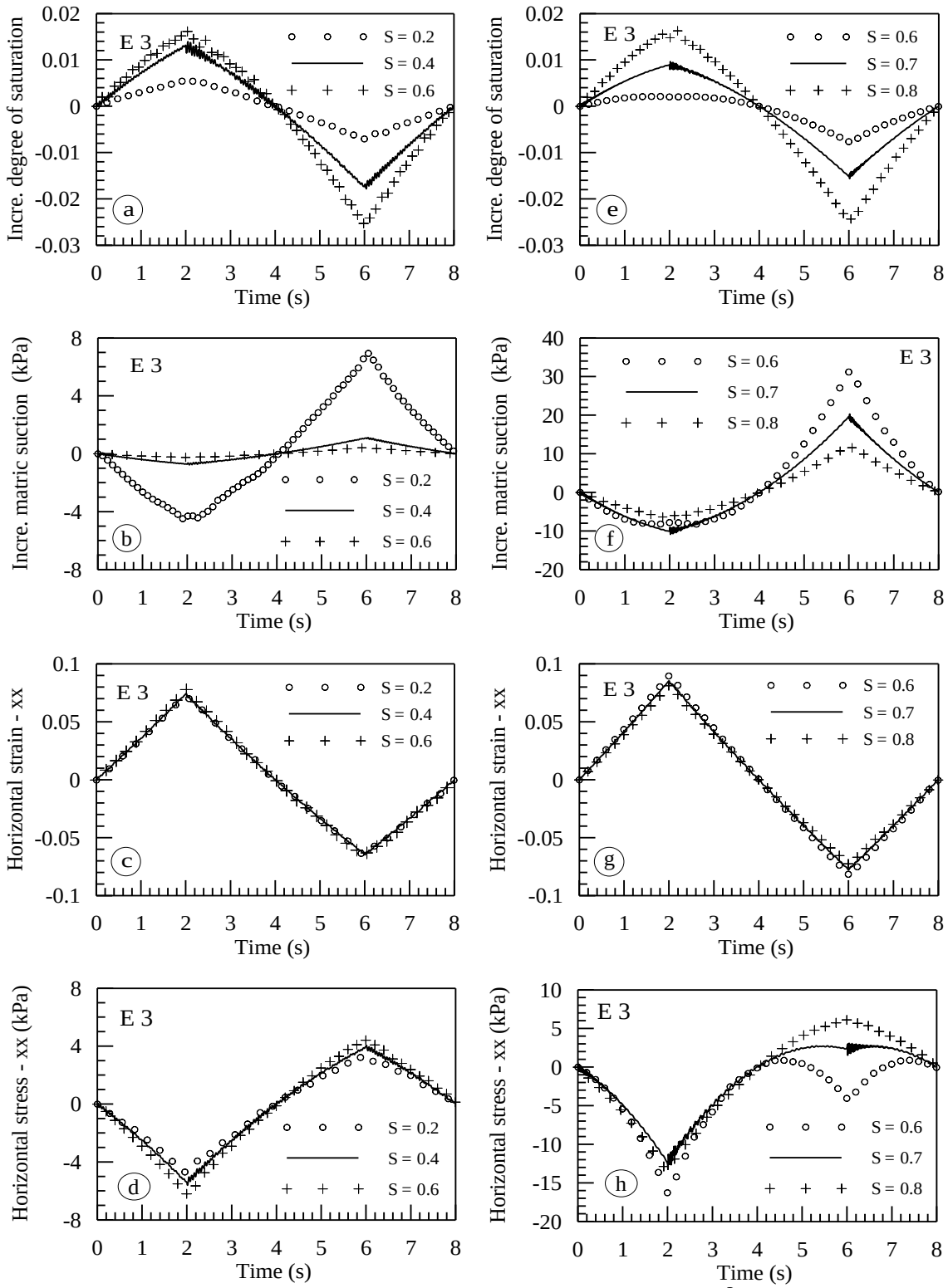

Figure 4.8 Comparison of element fields for Minco silt (E = 1.2 x 10^2 kPa) and Speswhite kaolin (E = 3 x 10^2 kPa)

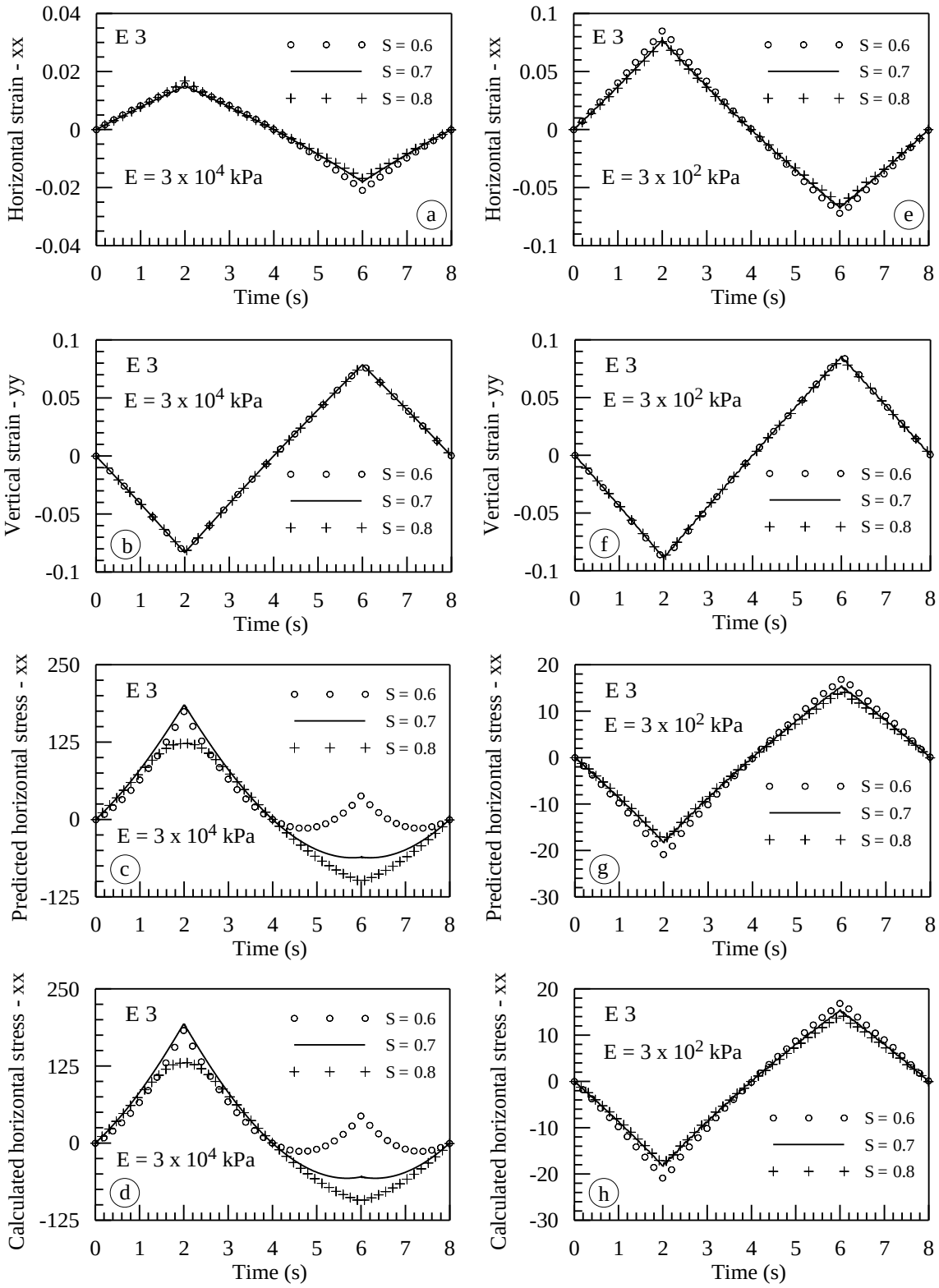

Figure 4.9 Comparison of element fields for stiff and soft Speswhite kaolin

Contribution of the Suction Related Component

From the above discussions it is seen that the effect of suction would be important for soft soils or for soils that show large change in suction such as clay. Analyses with and without taking into account the suction effect were performed and the results are shown in Figure 4.10 for a selected degree of saturation (degree of saturation of 0.6). Figures 4.10a, 4.10b, 4.10c and 4.10d show the element fields for silt and Figures 4.10e, 4.10f, 4.10g and 4.10h show the element fields for clay. There is no significant differences are seen for silt when the effect of suction is taken into account. However, results for clay show significant differences in the element fields. From these results it can be concluded that for an unsaturated silty soil subjected to quasi-static load a code which does not incorporate unsaturated effective stress can give reasonable results but not for unsaturated clay soil which shows larger suction variation.

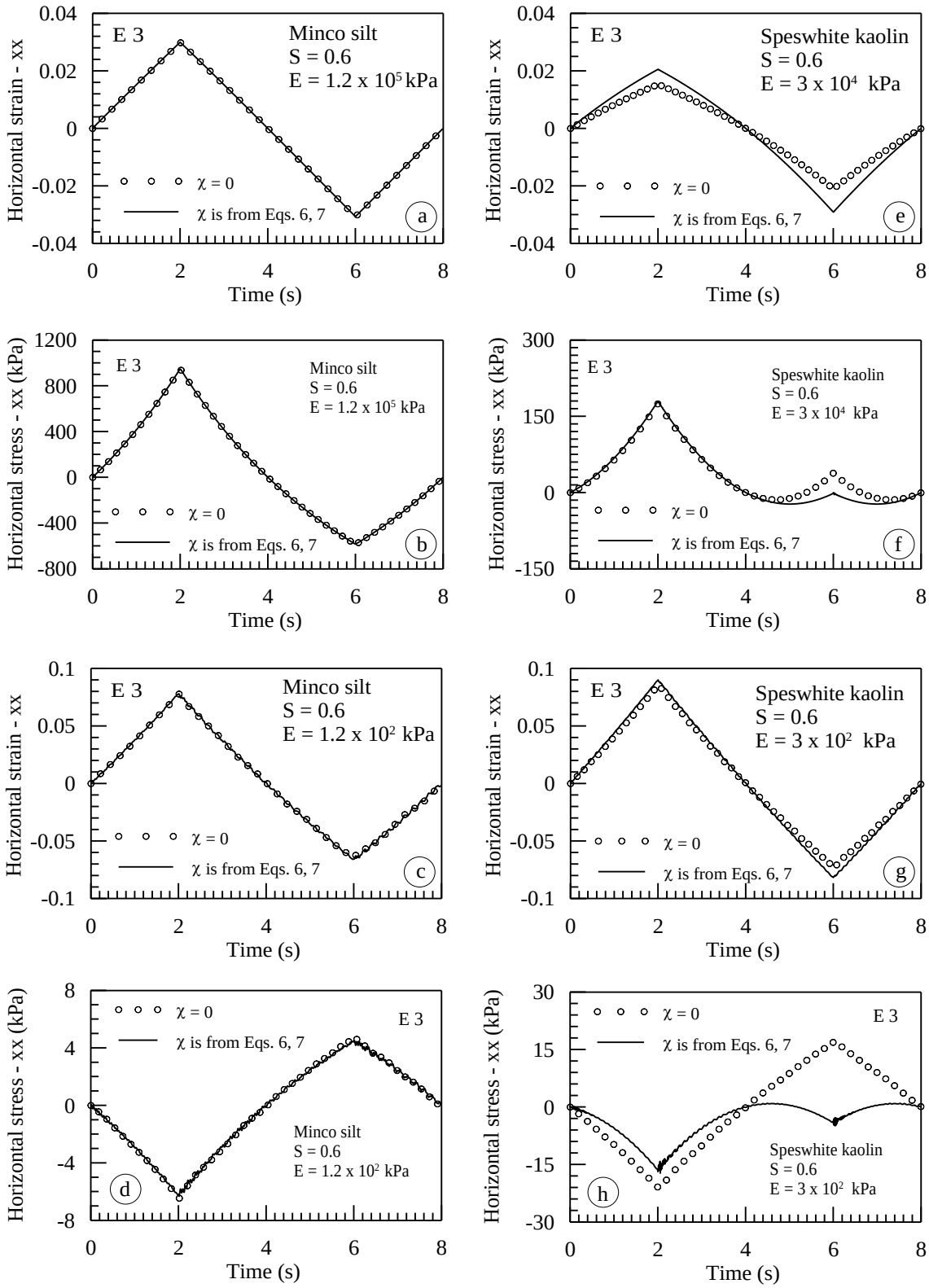

Figure 4.10 Comparison of element fields with and without suction effect

Example 2: 2D Unsaturated Embankment Subjected to Base Shaking

The 2D finite element mesh of unsaturated compacted embankment is shown in Figure 4.11. The mesh consists of 175 quadrilateral elements. For undrained formulation in which only the solid displacements are considered as primary nodal unknowns, there are only 8 degrees of freedom per element. The base of the embankment was assumed to be impermeable and fixed in all direction throughout the analysis. On all other sides of the embankment zero traction is specified for the solid phase. The acceleration time history shown in Figure 4.12 was applied at the base of the embankment. It should be noted here that the dynamics of unsaturated soil is a complex problem compared to the static or quasi-static problem. For dynamic analyses, when the initial degree of saturation changes, the loading on the system also changes in addition to the resistance of the soil. When the initial degree of saturation is different, the mass of the finite element will be changed which will cause different inertial load when subjected to base shaking. At the same time, when the initial degree of saturation changes, the matric suction also changes which causes the soil resistance to change.

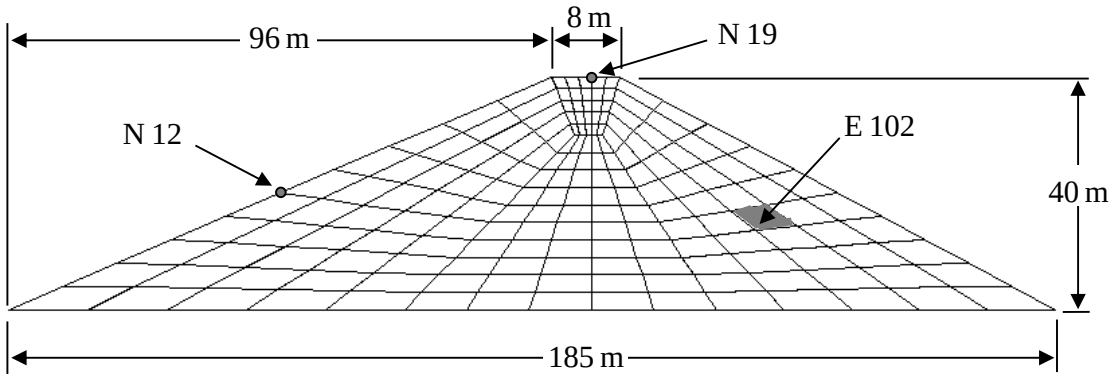

Figure 4.11 2D finite element mesh of the embankment (175 quadrilateral elements)

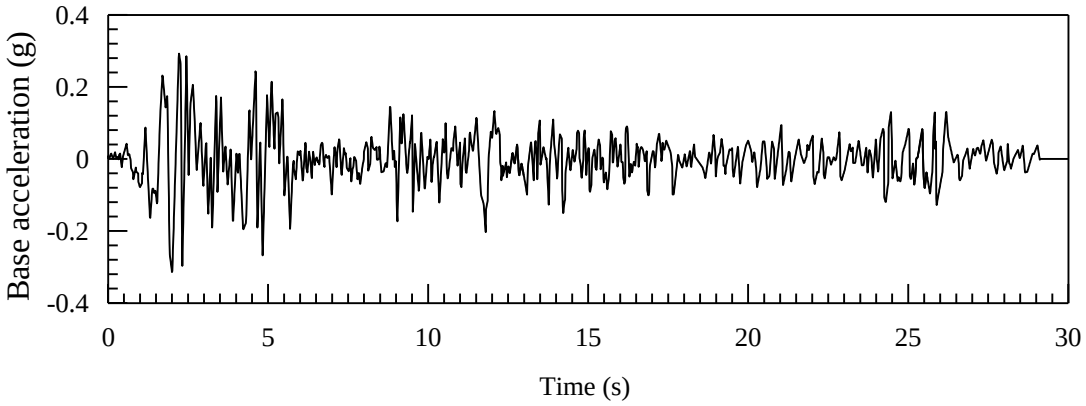

Figure 4.12 Base motion acceleration time history (El Centro, 1940)

Effect of Initial Degree of Saturation and Matric Suction: Silt

The incremental degree of saturation, matric suction, horizontal normal strain and horizontal normal stress in a selected element E102 (see Figure 4.11) are shown in Figures 4.13a, 4.13b, 4.13c and 4.13d, respectively. The analysis with higher initial degree of saturation shows higher incremental degree of saturation and lower incremental matric suction in the selected element. Interpreting the responses embankments subjected to earthquake shaking is complicated compared to the monotonic loading in one direction. The predicted displacement responses may be smaller or larger depending on the cumulative response of the system at the selected time and may not be an indicator of stiff or soft response of the material. Therefore, dynamic analyses of earth structures with different initial degree of saturation, the displacement amplitude may not be a good measure to compare the behavior. Rather frequency can be an ideal choice and here a delay in response or relatively lower frequency can be an evident for the softer response. On the other hand, if the responses are in phase, the amplitude can be used to compare the results.

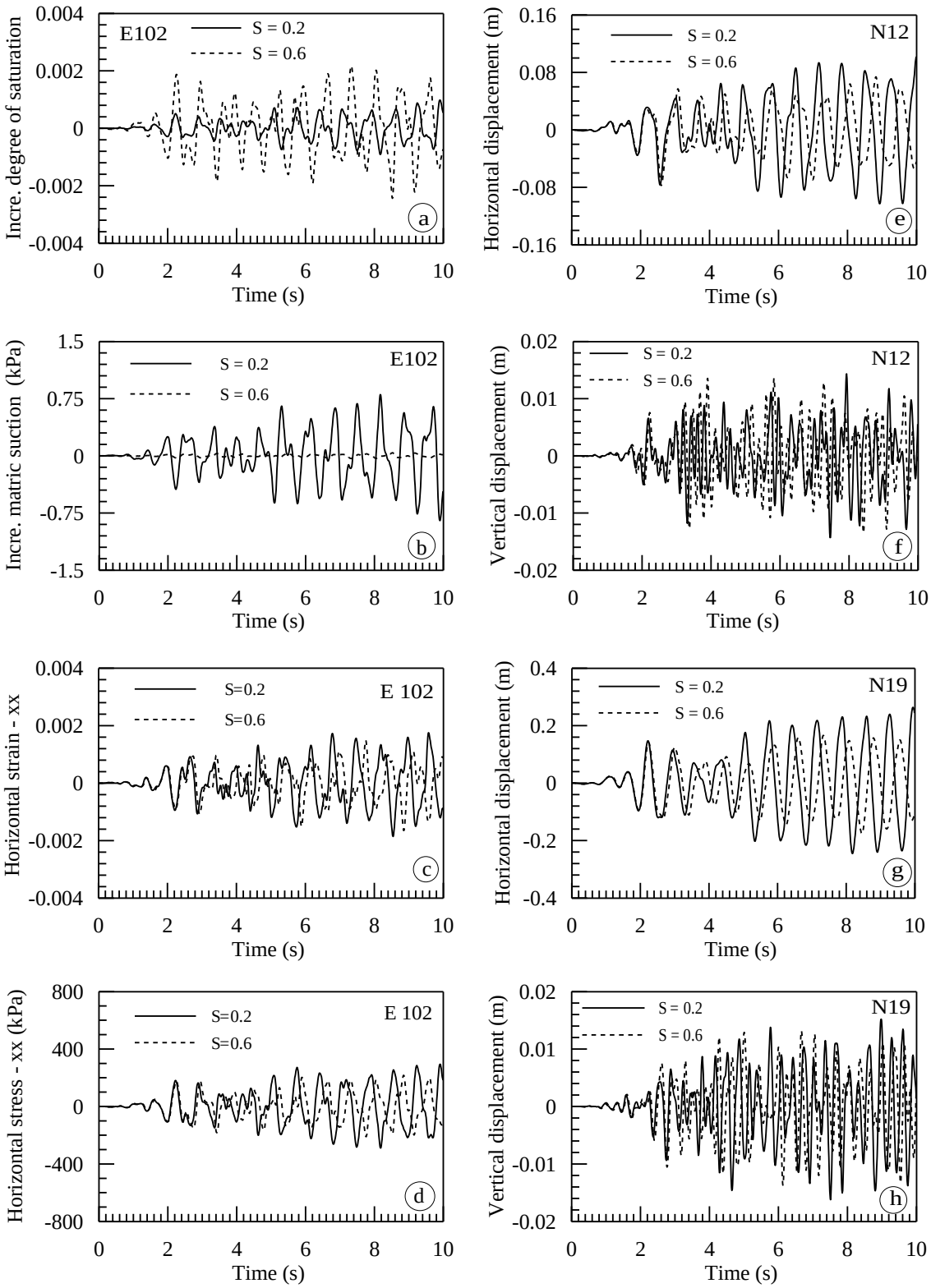

Figure 4.13 Comparison of element and nodal fields for Minco silt

Incremental normal strain and the corresponding incremental normal stress are higher for the soil with higher initial degree of saturation when the responses are in phase. When the responses are out of phase, the delay/lower frequency of the response proves the softer response for the embankment with higher initial degree of saturation. The horizontal and vertical displacement time histories at nodes N12 (on the left side) and N19 (on the top) are shown in Figures 4.13e, 4.13f, 4.13g, and 4.13h. As discussed previously, the horizontal displacement time history at the side of the embankment shows slightly smaller displacement for the embankment with higher initial degree of saturation. At the same time, the delay/lower frequency of the response proves the softer response for higher initial degree of saturation. These element and nodal fields show consistent responses. The vertical displacement time histories show higher frequency responses compared to the horizontal displacement time histories. These observations show that the embankment with higher initial degree of saturation shows softer response.

The same embankment problem was analyzed with a smaller Young's modulus and the results are shown in Figure 4.14. When a smaller Young's modulus is used, the suction related parameter in the Bishop's effective stress equation can be relatively large and its effect can be observed in the element fields. As expected, noticeable differences are seen in incremental stress and strain histories. Since the embankment is very soft, the displacement time histories show very low frequency responses and larger displacements compared to the analysis with higher Young's modulus. No noticeable displacement are seen when the initial degree of saturation changes, however, a shift (delay) in the response is seen for the embankment with higher initial degree of saturation.

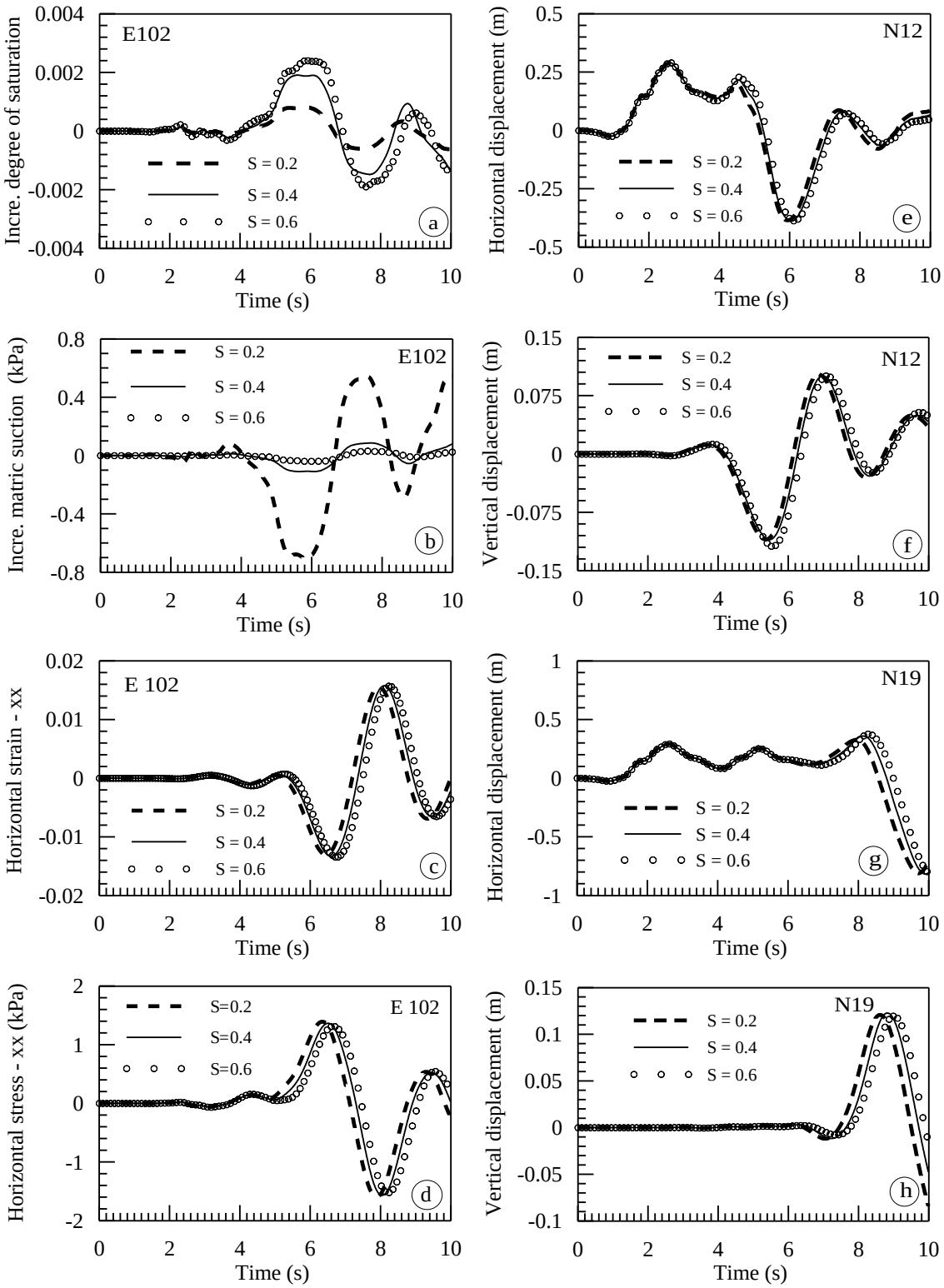

Figure 4.14 Comparison of element and nodal fields for Minco silt with smaller E (E = 1.2 x 10^2 kPa)

Effect of Initial Degree of Saturation and Matric Suction: Clay

A different range of initial degree of saturation was selected to force the suction to be within the tail portion of the soil water characteristic curve to avoid any sudden jump in the suction for a small change in degree of saturation. However, it should be noted that the suction for clay is very large compared to silt for a given degree of saturation (see Figures 4.1 and 4.2). Therefore, second component in the Bishop's equation can be significant for clays. The 2D embankment described before is analyzed with clay soil. The simulation results are shown in Figure 4.15. The Figure 4.15 shows that the predicted responses for different initial degree of saturations show a relatively in phase behavior. Hence, the amplitude is a good measure to compare the stiffness with different degree of saturation. In the case of clay, the embankment with higher initial degree of saturation shows smaller incremental suction. However, the incremental strain and corresponding stress are larger for the embankment with higher initial degree of saturation. Such larger stress can be explained by the larger horizontal displacement seen on the side of the embankment. In contrast to the silt, higher incremental suction does not always produce larger stress in an element. The horizontal displacement time histories at the top of the embankment show that the embankment with higher initial degree of saturation shows larger horizontal displacement, i.e., softer response. This is consistent with the prediction made for silt. Results of the clay embankment with a smaller Young's modulus are shown in Figure 4.16. Similar to soft silt, the soft clay embankment shows low frequency response with larger horizontal and vertical displacements.

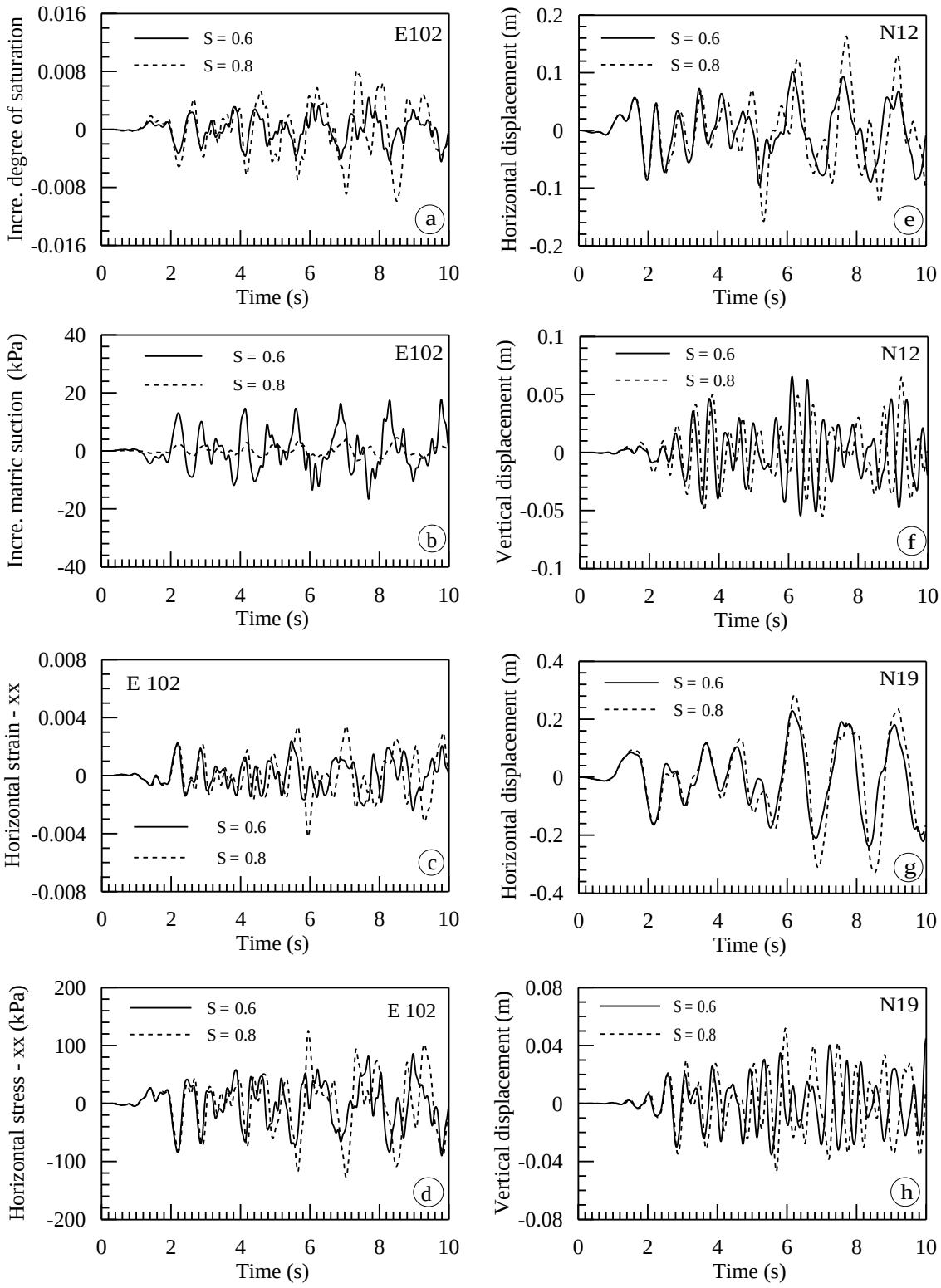

Figure 4.15 Comparison of element and fields for Speswhite kaolin

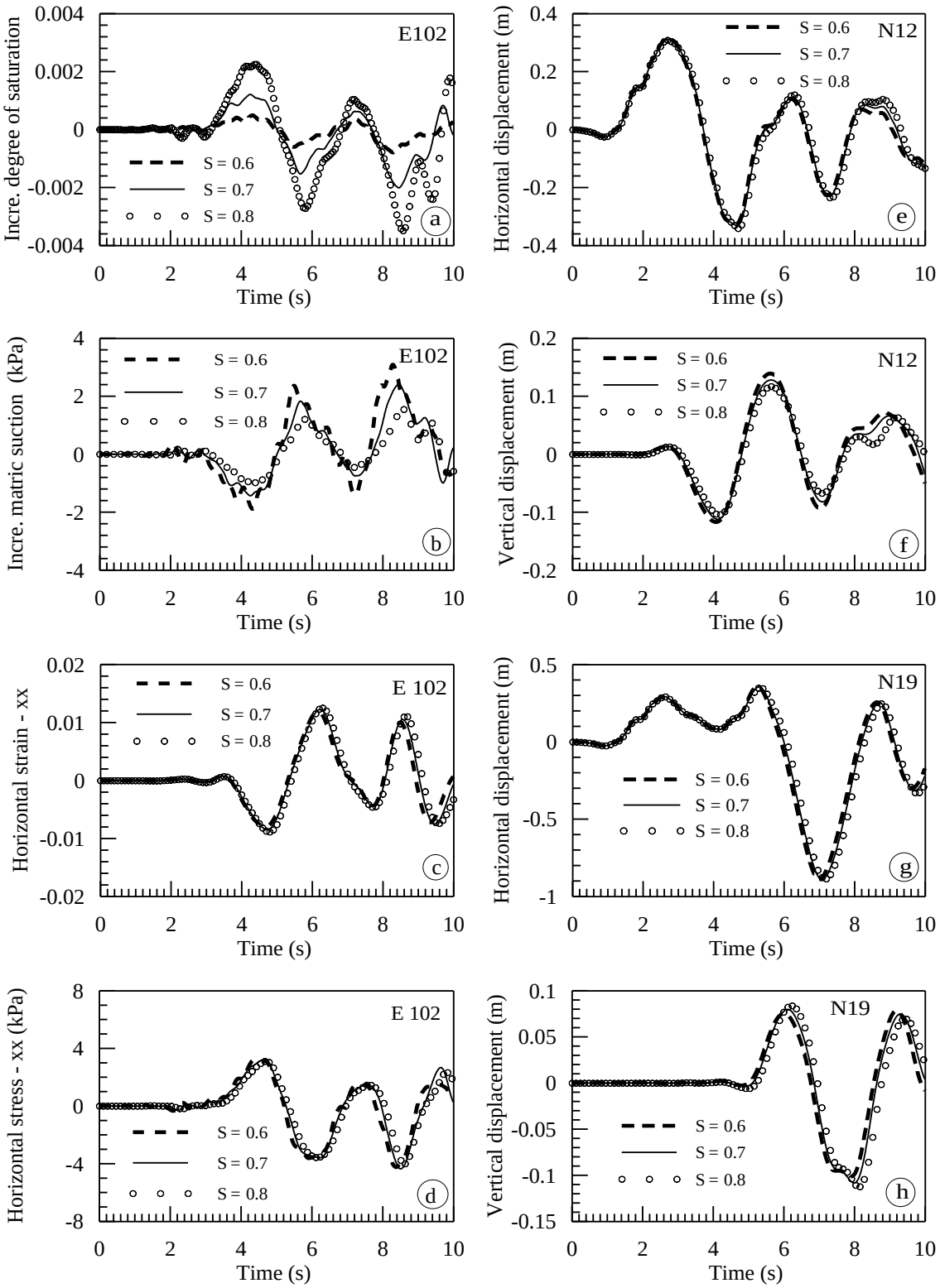

Figure 4.16 Comparison of element and nodal fields for Speswhite kaolin with smaller E ($E = 3.0 \times 10^2$ kPa)

Contribution of Suction Related Component

The simulation results of the embankment with and without taking into account the suction effect are shown in Figure 4.17 for silt (Figures 4.17a through 4.17d) and clays (Figures 4.17e through 4.17h) for a selected degree of saturation. The effect of suction is not seen from the results of silt embankment. However, the effect of suction can be seen for when clay is used. From these results it can be concluded that for an unsaturated silty soil subjected to base motion a code which does not incorporate unsaturated effective stress can give reasonable results but not for unsaturated clay soil which shows larger suction variation.

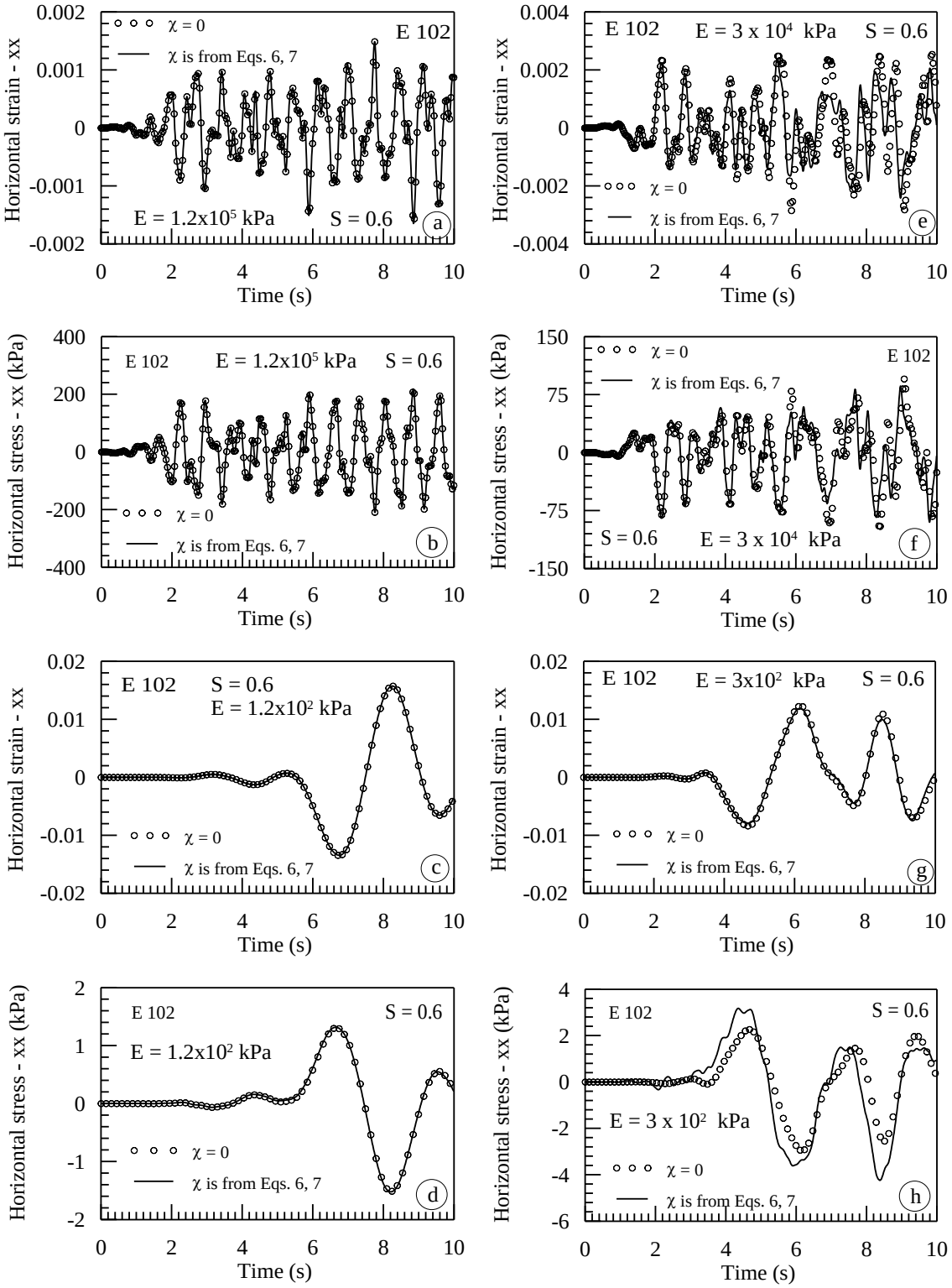

Figure 4.17 Comparison of element fields with and without matric suction effect for Minco silt (left side) and Speswhite kaolin (right side)

Example 3: 3D Unsaturated Embankment Subjected to Base Shaking

When compared the computational efficiencies of complete and simplified formulations, it was found that the simplified formulation is 36 times more computationally eficient (Ravichandran and Muraleetharan, 2009). It would not be possible to perform a 3D analysis using complete formulation, but it is possible to conduct a 3D analysis using simplified formulation. A 3D analysis of the embankment (see Figure 4.18) was carried out and the results elements fields predicted by 3D and 2D analyses are compared in Figure 4.19.

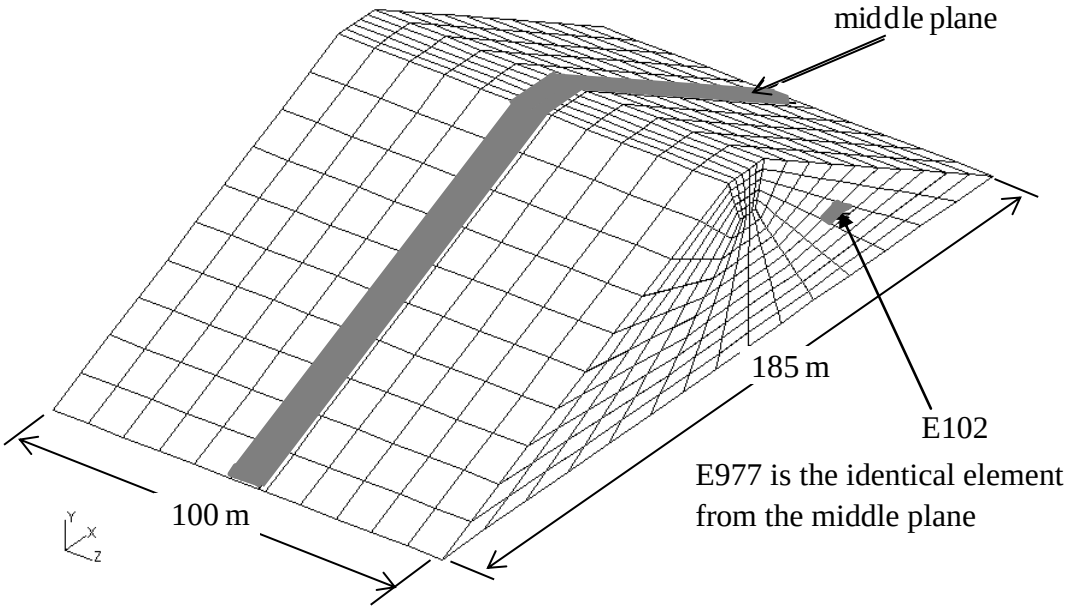

Figure 4.18 The 3D finite element mesh of the embankment (1925 brick elements)

The 3D mesh (see Figure 4.18) was created by extruding the 2D mesh shown in Figure 4.11 for 100 m length in the z-direction having 11 comparable slices. Similar to the 2D problem, the base of the 3D embankment was fixed in all direction. The front and back faces were fixed in the z-direction. Zero traction is specified on the all other faces

and so that the embankment is can freely deform when subjected to base shaking. These boundary conditions are similar to what is seen in reality. The 2D and the 3D analyses show very smilar results for the example shown. The 2D analysis with 175 quadrilateral elements took 10 minutes and the 3D analysis took 3 days, 20 hours and 49 minutes. This is approximately 422 times longer CUP time on a 1.6 GHz clock speed Intel dual core machine.

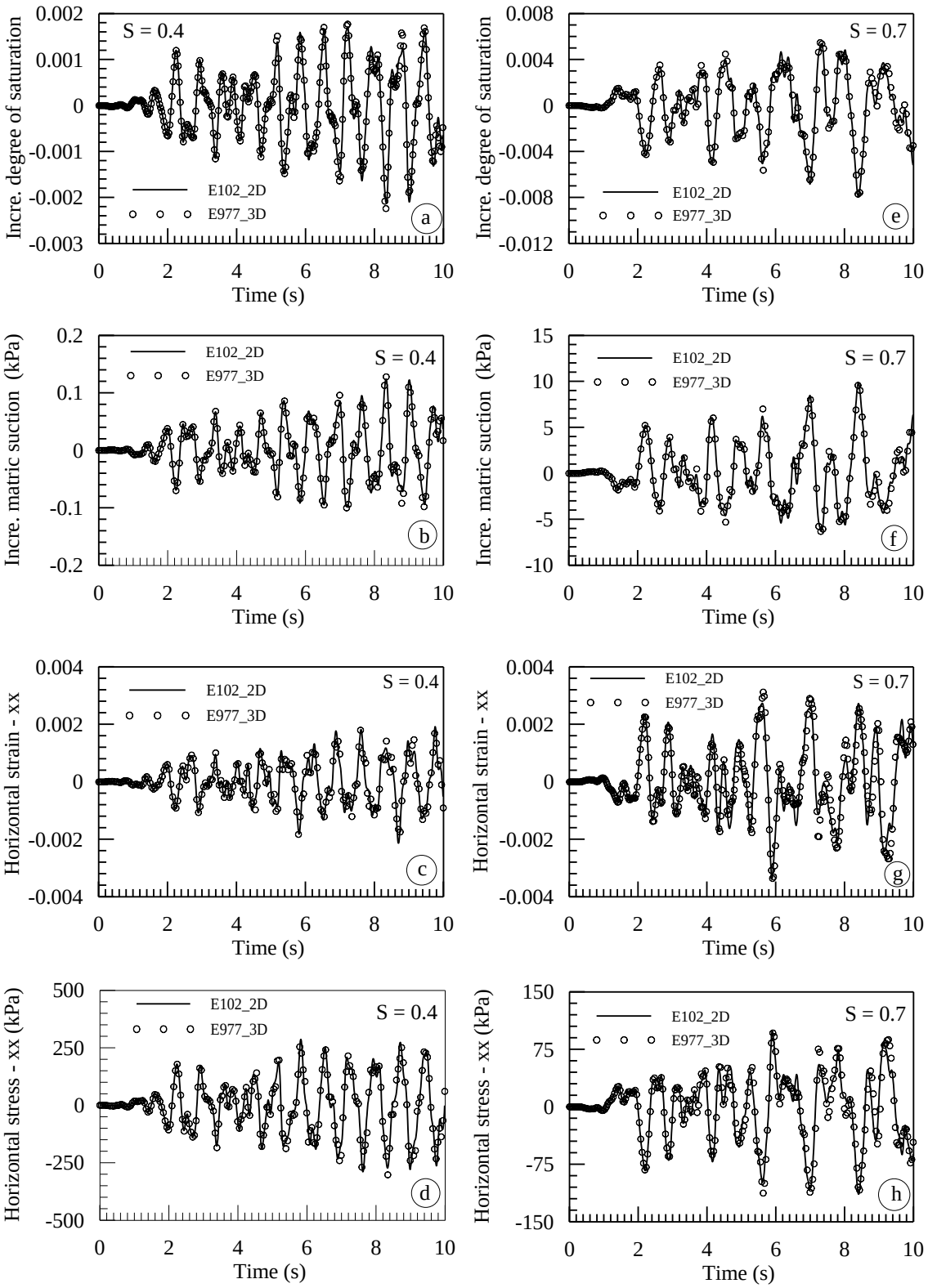

Figure 4.19 Comparison of 2D and 3D analysis results for both silt and clay

Summary of the Study

In this study, an in-depth analysis on the deformation behavior of unsaturated soils is performed using simplified formulation. Incremental stresses, incremental strain, and other variables were computed at various initial degree of saturation and compared for two different soils. The predicted responses of unsaturated clay and silt show that the influence of suction/ suction induced stresses is insignificant in the unsaturated silty soils. However, when the silt is relatively soft, the suction considerably influences the overall response. In the case of unsaturated clayey soils, the suction or the degree of saturation significantly influences the overall responses. And also the influence of suction in unsaturated clayey soils is relatively large compared to the influence in unsaturated silty soils. The calculated results of clayey soils show that the poisson ratio is a significant parameter, whose effects depends not only on the initial degree of saturation but also in the loading type (compression/expansion). From these results it can also be concluded that for an unsaturated silty soil, a numerical tool which does not incorporate the suction would give reasonable results. However, such numerical tool cannot be used for unsaturated clayey soils. Further studies have to be carried out at lower degree of saturation, where the influence of suction is expected to be much higher. However, with currently available SWCC models, calculating the moisture-suction relation in low degree of saturation range is a challenge. Therefore, before conducting further studies at low range of degree of saturation, the applicability and accuracy of the available SWCC models in low range of degree of saturation should be extensively studied. If necessary, the available SWCC models should be modified or new models should be developed.

CHAPTER FIVE

UNDERSTANDING THE INFLUENCE OF DEGREE OF SATURATION ON THE BEHAVIOR OF SOIL-PILE SYSTEMS

Introduction

Pile foundations are an integral part of many civil engineering structures such as highway bridges, wharves, towers, and other tall buildings, with the structural load transferred to the supporting soil through the foundation. The dynamic behavior of superstructure is greatly influenced by the characteristics of the supporting soil. Therefore, a safe and economical design of the foundation requires a greater understanding of the interaction between the structure and the supporting soil. Deep foundations in seismic areas are typically designed in either a loosely coupled or uncoupled manner. In this method, acceleration design response spectrum (ADRS) of free-field (without the presence of pile foundation and superstructure) will be calculated using site-response analysis software such as SHAKE2000, DMOD2000 or DEEPSOIL and the ADRS will be used to calculate the site specific design coefficients. However, SSI studies (described in Chapter 2) show that the presence of structure significantly alters the soil-pile system response. For example, the dynamic response of a building with three basement floors and multiple stories was studied by Wartman et al. (2001) using FLUSH software. The response spectral values of the predicted horizontal acceleration at the base of the structure were 35% higher than those of the free field

conditions. Therefore, coupled unsaturated soil-pile interaction analysis under various loading and environmental conditions is important for safe and economical designs.

The characteristics of soil-pile interaction might differ when the pile is supported by unsaturated soils, which consists of three bulk phases: solid, water and air. The effect of unsaturated soil condition varies with soil type and the amount of water present in the soil. The factors affecting the soil-pile systems have been reported in the Chapter 2. The degree of saturation is also reported as a factor based on the study of Georgiadis et al. (2003), and in which they determined that the load capacity (ultimate pile load) increases as the degree of saturation decreases. The analysis also showed an excessive settlement due to collapse exhibited by the unsaturated soil under the tip of the pile. This settlement is perhaps attributed to wetting-induced collapse behavior of unsaturated soils (Miller et al., 2001). Another important point to note is this settlement could not be recognized with saturated finite element analyses (Georgiadis et al., 2003). However, this literature study shows the importance of unsaturated soil-pile interaction analysis and the importance to understand the influence of degree of saturation/ suction on the overall response of soil-pile systems. Therefore, to investigate the behavior of unsaturated soil-pile systems and the influence of degree of saturation and suction on the overall response of soil-pile systems, a wide range of numerical simulations were carried out and the details are presented below.

Simulation Study

Problem Description

In this study, the overall response of piles located in unsaturated soil is investigated with two different initial degree of saturation, using the reduced formulation of TeraDysac. The effect of degree of saturation on the spectral acceleration and the period is analyzed and discussed. The development and dissipation of suction (difference between pore gas pressure and pore liquid pressure) around the pile foundation is also calculated and compared with that of free-field responses.

The finite element mesh used for the simulation is shown in Figure 5.1. The structure consists of a single column with a large mass on top (superstructure) supported on a pile foundation. The structural element nodes are connected to the solid nodes and move together i.e., no special interface elements are utilized between the soil and the structure to capture the opening and closing of gaps or relative movement in the vertical direction. The structural element consists of three components: superstructure, pier and the foundation. The superstructure is modeled by a single element of concentrated mass at the top of the pier. Very high density is used for the superstructure element to represent the actual mass of the superstructure. The acceleration-time history of applied base motion is shown in Figure 5.2.

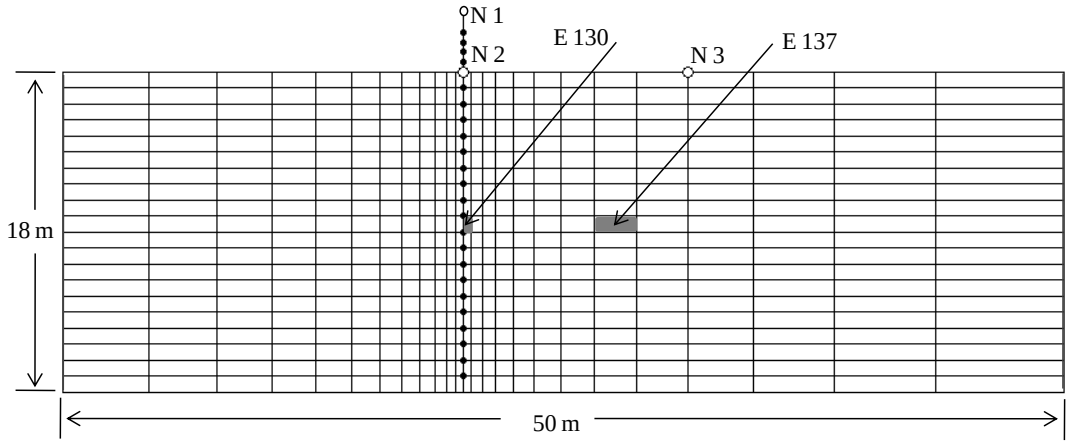

Figure 5.1 The 2D finite element mesh for the example problem

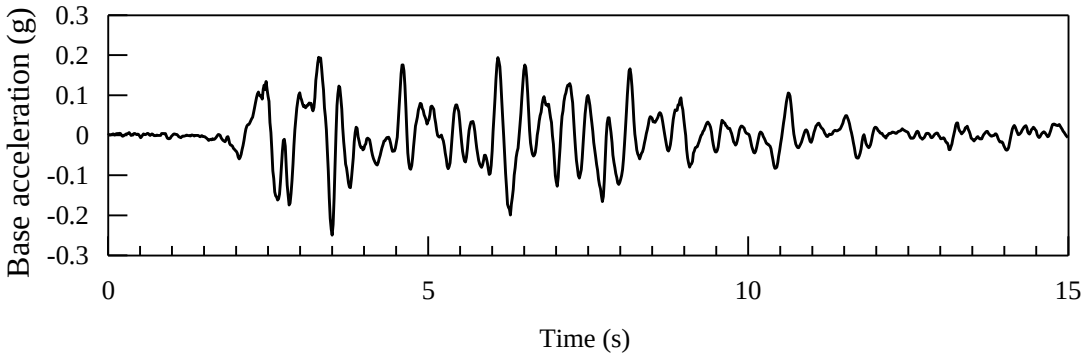

Figure 5.2 Time history of applied base motion acceleration

Material Models and Model Parameters

The stress-strain behavior of the solid skeleton is modeled using an elastoplastic material model based on bounding surface concept. The bounding surface model for saturated soil was developed by Dafalias and Herrman (Dafalias and Herrman, 1986) and the saturated soil model was later modified by Muraleetharan and Nedunuri (Muraleetharan and Nedunuri, 1998) to incorporate the suction related behavior such as loading collapse (LC curve) proposed by Alonso et al (Alanso et al., 1990) and Wheeler and Sivakumar (Wheeler and Sivakumar, 1995). The elastoplastic material model parameters calibrated using laboratory tests (Vinayagam, 2002) and are listed in Table

5.1 and the corresponding suction related model parameters are listed in Table 5.2. The in situ stresses were calculated for the mesh and used as the initial stresses for the dynamic analysis. A lateral earth pressure coefficient of 0.5 was used to calculate the corresponding horizontal stresses. The moisture-suction relationship of the soil is modeled using the soil-water characteristics curve proposed by van Genuchten (1980). The behavior of structural elements is assumed to be linear elastic. Timoshenko beam theory is utilized to represent the beam behavior. The structural properties and the elastic material model parameters are listed in Table 5.3. The predicted responses are discussed in the next section.

Table 5.1 Material properties and model parameters of Minco silt

Parameter	Value
Slope of the isotropic consolidation line on e - $\ell n\ p'$ plot, λ	0.02
Slope of an elastic rebound line on e - $\ell n\ p'$ plot, κ	0.002
Slope of the critical state line in q - p' space , M_c (compression)	1.0
Ratio of extension to compression value of M (M_e / M_c)	1.00
Value of parameter defining the ellipse1 in compression (R_C)	2.60
Value of parameter defining the hyperbola in compression (A_C)	0.1
Parameter defining the ellipse 2 (tension zone) (T)	0.05
Projection center parameter (C)	0.00
Elastic nucleus parameter (S)	1.00
Ratio of triaxial extension to compression value of R (R_e / R_c)	1.0
Ratio of triaxial extension to compression value of A (A_e / A_c)	1.0
Hardening parameter (m)	0.02
Shape hardening parameter in triaxial compression (h_c)	2.00
Ratio of triaxial extension to compression value of h (h_e/h_c)	1.00
Hardening parameter on I-Axis (h_o)	2.00

Table 5.2 Suction related parameters of Minco silt

Parameter	dos = 43%	dos = 70 %
m	80	140
B	0.12	0.12
N	1.66	2.017
A	0.27	0.27
r	1.27	1.57
b	0.0133	0.0133

Table 5.3 Properties of structural elements

Property	Value
Mass on top of the superstructure (Mg)	49.1
Cross sectional area (m^2)	0.132
Length (m)	20.57
Second moment of area (m^4)	6.01x10-3
Mass per unit length (Mg/m)	0.37
Young's modulus (GPa)	69.35x103
Poisson's ratio	0.33
Shear modulus (GPa)	26.07x103

Results and Discussion

Analyses were performed for initial degree of saturations of 43% and 70% to investigate the effect of degree of saturation on the response of coupled soil-pile system subjected to earthquake loading. The horizontal displacement time histories at nodes N1 and N2 are shown in Figures 5.3a and 5.3b, respectively. The soil with initial degree of saturation of 70% shows slightly larger horizontal displacement compared to the soil with 43% initial degree of saturations i.e., the soil with higher initial degree of saturation shows softer response compared to the lower initial degree of saturation. The horizontal spectral accelerations obtained at nodes N1, N2 and N3 using 5% damping are shown in Figure 5.4. Simulations with higher initial degree of saturation show higher spectral accelerations values at all three nodes (See Figures 5.4a, 5.4b, 5.4c). The soil with higher

initial degree of saturation seems to show higher amplification factor compared to that of lower initial degree of saturation. The response spectra at nodes N1, N2 and N3 for initial degree of saturations of 43% and 70% are shown in Figures 5.4d and 5.4e, respectively.

In both cases, highest amplification is predicted at node N1 and the lowest amplification is predicted at node N3 (free field). However, the periods of these acceleration spectra do not show considerable change. The response spectrum of the applied base motion is shown in Figure 5.4f. When comparing the spectral acceleration values, the simulations show that the soil has amplified the base motion by a factor of approximately 7, 5 and 2.5 at nodes N1, N2 and N3, respectively.

The predicted incremental matric suction time histories in element E130 and E137 are shown in Figure 5.5. The element E130 is located very close to the pile and the element E137 is located away from the pile. It appears that both elements show decrease in matric suction during earthquake shaking. Also, the element near the pile shows slightly lower change in matric suction compared to the one far away from the pile. In both elements the soil with lower initial degree of saturation shows higher incremental matric suction.

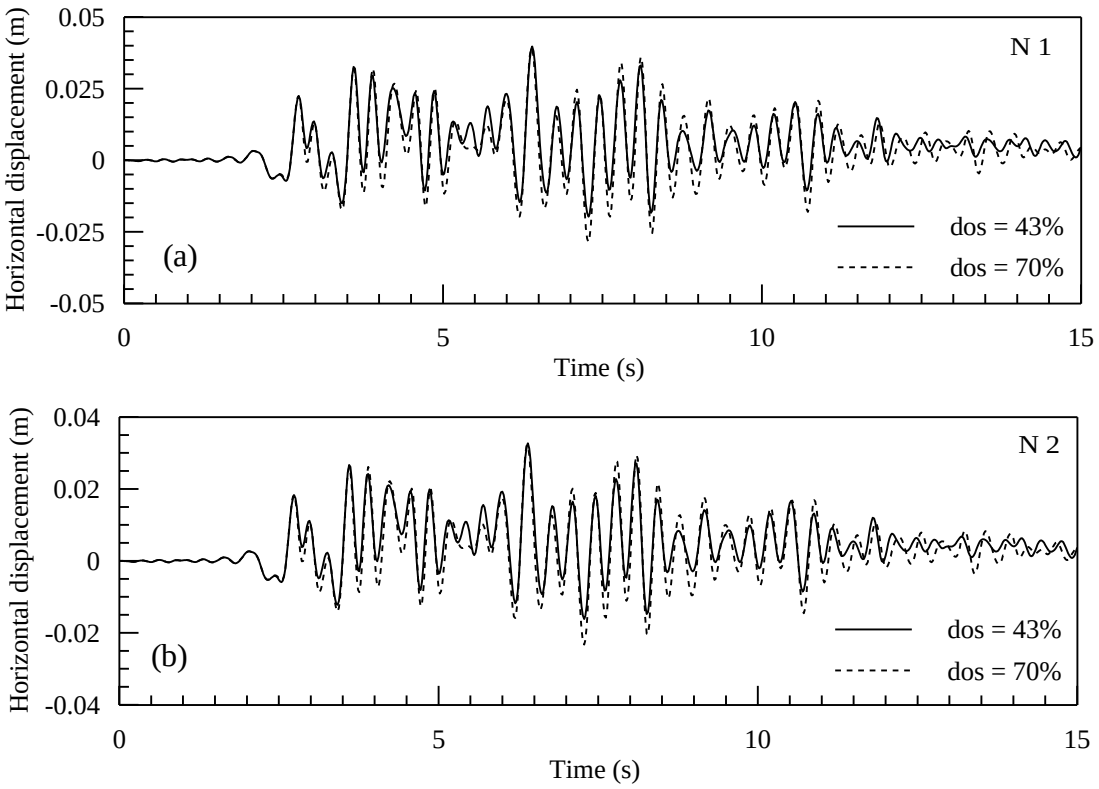

Figure 5.3 Comparison of horizontal displacement histories

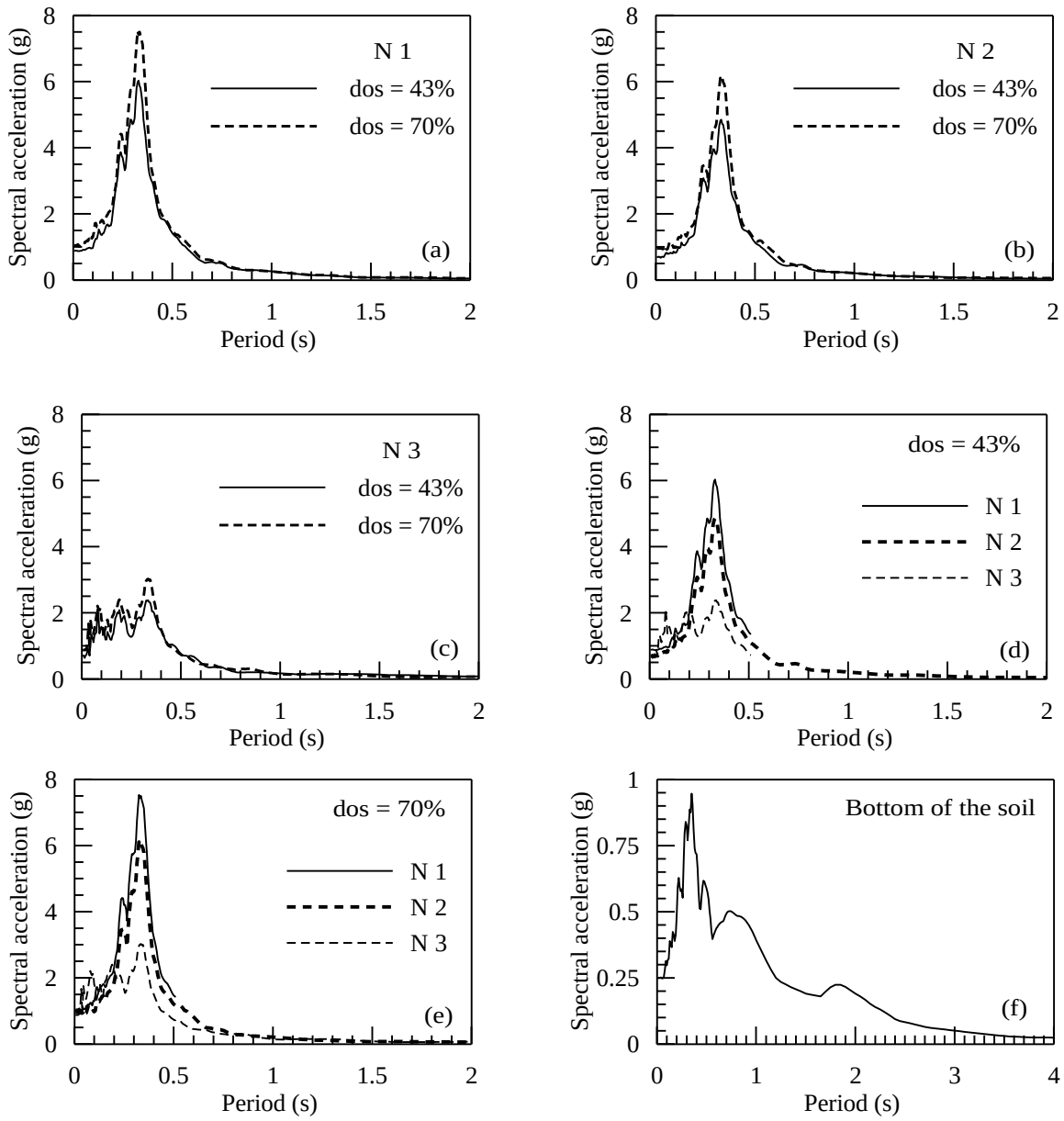

Figure 5.4 Comparison of spectral accelerations

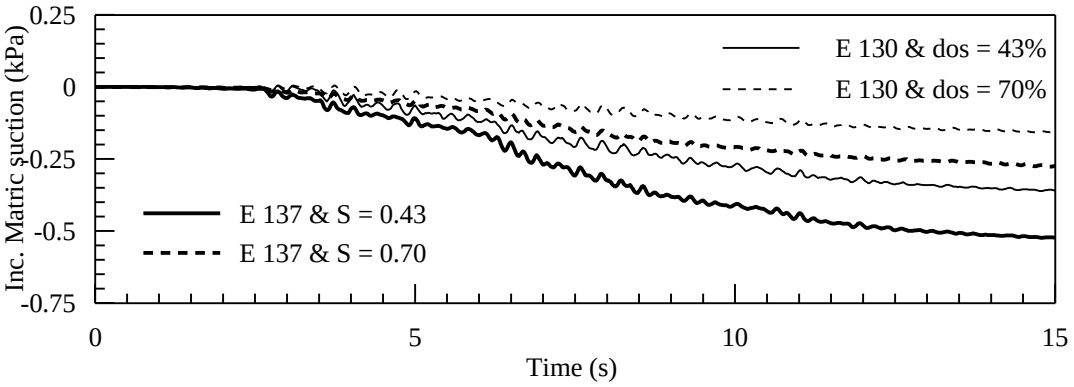

Figure 5.5 Time history of incremental suction in elements E130 and E137

Summary of the Study

Effect of degree of saturation on soil-pile interaction response is investigated using finite element simulations. The results show that the initial degree of saturation influences the free-field responses and the response of coupled soil-pile systems. For a given base motion, soil-pile system with higher initial degree of saturation produces larger amplification compared to the system with lower initial degree of saturation. In addition, the free field response shows lower amplification factor compared to the response of coupled soil-pile system. Therefore, the standard practice of using free-field soil motion to design or analyze the pile/structure with a fixed base assumption should be utilized with caution.

Since the reduced finite element formulation is used in this study, further investigations using partially reduced or complete formulations may reveal better insights into the dissipation of pore pressures and their effects on the soil-pile system responses. However, among the finite element formulation described in Chapter 3, the simplified formulation is computationally very efficient and that can be used for deformation

analyses without eliciting numerical instability. However, the material damping will not be taken into account in a simulation with simplified formulation as the damping matrix does not naturally appear in the governing equation of this formulation. It is another reason for the calculated peak spectral acceleration become high. This no-damping condition is one of the deficiencies in applying the simplified formulation as an effective method to derive greater insights into dynamic response of soil-pile system. However because of the other advantages of this formulation, the no-damping issue must be fixed and the performance of the simplified formulation should be improved.

As suggested in the previous study, further studies of SPI have to be carried out at low range of degree of saturation, where the influence of suction is expected to be much higher. However, before conducting SPI studies at low range of degree of saturation, the applicability and accuracy of available SWCC models in low range of degree of saturation should be studied. If necessary, the available SWCC models should be modified or new models should be developed to perform more accurate numerical simulations with low range of degree of saturation.

CHAPTER SIX

IMPROVING THE PERFORMANCE OF THE SIMPLIFIED FINITE ELEMENT FORMULATION

Introduction

In recent years, various forms of nonlinear governing equations and finite element formulations have been developed for studying the behavior of unsaturated soils and it is summarized in Chapter 3. Among these finite element formulations, the simplified formulation is computationally efficient that can be used without eliciting any numerical instability to analyze the deformation behavior of unsaturated soil-structure systems. However, since the relative acceleration and relative velocities of both water and air phases are neglected in this formulation, the viscous damping matrix does not appear naturally at the governing equation level. This no-viscous damping condition is one of the deficiencies in applying the simplified formulation as a method to derive greater insights into soil-pile system, especially in dynamic simulations without numerical instability.

In this study, the simulation capability of the simplified formulation is enhanced by integrating the full Rayleigh damping formulation. The modification to the finite element equation and the performance evaluation study is presented in this chapter. The capability of the improved formulation is scrutinized by comparing the simulation results with the results of a commercial software that has a similar formulation and capable of performing soil-pile interaction analysis but for saturated/dry soil conditions without true unsaturated soil mechanics theory. Subsequent to performing parametric studies on the Rayleigh

damping parameters, the improved formulation is also used to investigate the effects of the initial degree of saturation and performance of the formulation with elastoplastic constitutive model. The analyses reveal that the Rayleigh damping model improves the performance of the simplified finite element formulation in the predicting the behavior of unsaturated soil-pile systems.

Importance of Incorporating an External Damping Model

Compared to structural engineering systems, the presence of viscous fluids and their permeability coefficients greatly enhances the complexity in soil damping. In the fully coupled governing equations of the dynamics of unsaturated soils, a damping matrix naturally exhibits and it is viscous damping. The components of the viscous damping matrix are related to the permeability coefficients and the porosity of the soil. However, it must be noted that the viscous damping does not vary either with the strain level or frequency. Material damping or hysteretic damping is the second type of damping presents in soils. Area of the hysteresis loop formed by loading, unloading and reloading processes is a measure of energy lost and the hysteresis damping. The hysteretic damping is nil or insignificant when the soil behave in elastic condition, i.e. in elastic analysis or non-linear analysis with small strain problems. However it is significant in non-linear large strain analyses. In such cases, the hysteretic damping can be mitigated through use of an appropriate elastoplastic constitutive model.

In the case of simplified finite element formulation, the damping does not appear naturally in the governing equation level. If an elastic analysis is performed, the system exhibits no damping since the hysteretic damping vanishes due to the construct of the

elastic constitutive model. Therefore, an external damping must be applied to the system to obtain reasonable results. The Rayleigh construct is but one such example of external damping formulation used in soil dynamics (Rayleigh and Lindsay, 1945).

Rayleigh Damping Model

In this model, the damping is considered propositional to both the mass and the stiffness of the system. The damping matrix for the finite element formulation is calculated using Equation 6.1 given below (Phillips and Hashash, 2009):

$$\mathbf{C}^{\mathrm{R}} = \alpha^{R}\mathbf{M} + \beta^{R}\mathbf{K} \tag{6.1}$$

where the $\mathbf{C}^{\mathrm{R}}$ is Rayleigh damping matrix, $\mathbf{M}$ is mass matrix, $\mathbf{K}$ is the stiffness matrix, the α^{R} and β^{R} are mass and stiffness related Rayleigh damping coefficients, respectively.

Rayleigh Damping Model for Unsaturated Soils

The two types of stiffness matrices derived for soils, as mentioned previously, are the fluid stiffness and the solid stiffness. Therefore, the Rayleigh damping formulation can be further expanded as follows:

$$\mathbf{C}^{\mathrm{R}} = \alpha^{R}\mathbf{M} + \beta^{R}\left(\mathbf{K}_{\mathbf{p}} + \mathbf{K}_{\mathbf{s}}\right) \tag{6.2}$$

The Equation 6.2 is further modified as shown in Equation 6.3 by assigning different stiffness coefficients for pore fluid stiffness matrix and solid stiffness matrix so that the contribution of each stiffness matrix can be evaluated for better prediction. It is expressed as follows:

$$\mathbf{C}^{\mathrm{R}} = \alpha^{R}\,\mathbf{M} + \beta_{p}^{R}\,\mathbf{K_p} + \beta_{s}^{R}\;\mathbf{K_s} \tag{6.3}$$

For the full Rayleigh damping formulation, the viscous damping parameters α^{R} and β^{R} are given by:

$$\alpha^{R} = \xi_{tar}\left(\frac{4\pi}{T}\right)\left(\frac{n}{n+1}\right)$$

$$\beta^{R} = \frac{\xi_{tar}T}{\pi\left(n+1\right)}$$

where ξ_{tar} is the target damping, ***n*** is an odd integer (1, 3, 5 or 7) and ***T*** is the fundamental period of the soil deposit given by:

$$T = \frac{4H}{V_{s,avg}}$$

where H is the depth of the soil deposit and $V_{s,avg}$ is average shear wave velocity.

Incorporating the Rayleigh Damping Model with the Simplified Formulation and Performance Analysis

The spatially discrete governing equation of the ***simplified formulation*** is given in matrix form in Equation 6.4:

$$\mathbf{M\ddot{u}} + \mathbf{C}^{\mathrm{R}}\mathbf{\dot{u}} + \mathbf{K_p u} + \mathbf{f_I} = \mathbf{f_E} \tag{6.4}$$

The spatially discrete governing equations for the ***improved-simplified formulation*** that includes Rayleigh damping can be written in matrix form as follows:

$$\mathbf{M\ddot{u}} + \mathbf{C}^{\mathrm{R}}\mathbf{\dot{u}} + \mathbf{K_p u} + \mathbf{f_I} = \mathbf{f_E} \tag{6.5}$$

To improve the performance of the simplified formulation by incorporating the Rayleigh damping model, the simplified finite element formulation (Equation 6.4) of TeraDysac is modified based on the improved-simplified finite element formulation (Equation 6.5). To examine the performance of the *improved-simplified finite element formulation*, wide range of numerical simulations were performed with the simplified finite element formulation and the improved-simplified finite element formulation, and the predicted results are compared. The details of the simulation study and the results are presented below.

Performance Analysis

Problem Description

The 2D finite element mesh used for the TeraDysac simulations is shown in Figure 6.1. The soil mesh consists of 630 quadrilateral elements. The structural element is represented by Timoshenko beam theory. The structure consists of a single column with an element at top with a larger density. The larger density is used to model the self weight of the superstructure. The soil and the structural nodes are merged together at the interfaces.

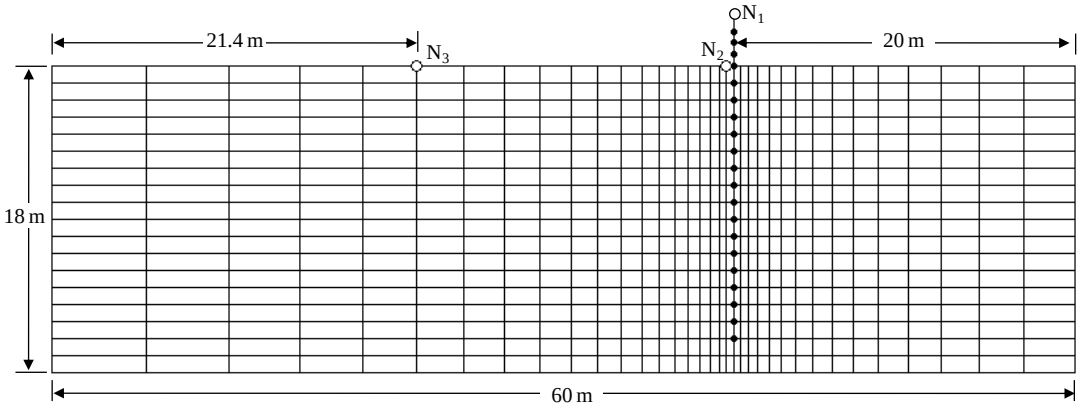

Figure 6.1 Finite element mesh for the TeraDysac simulation

To examine the accuracy or the performance of the improved simplified formulation, the simulations were also carried out using PLAXIS software. The reason to choose PLAXIS is, no other unsaturated finite element software which uses Rayleigh damping model and capable of coupled soil-pile interaction analysis, could be accessed. Although PLAXIS does not solve the equations for unsaturated soils, soil type and the loading are selected in such a way so as to elicit reasonable results that can be compared to unsaturated soil simulations. Figure 6.2 shows the finite element mesh used for the PLAXIS simulations.

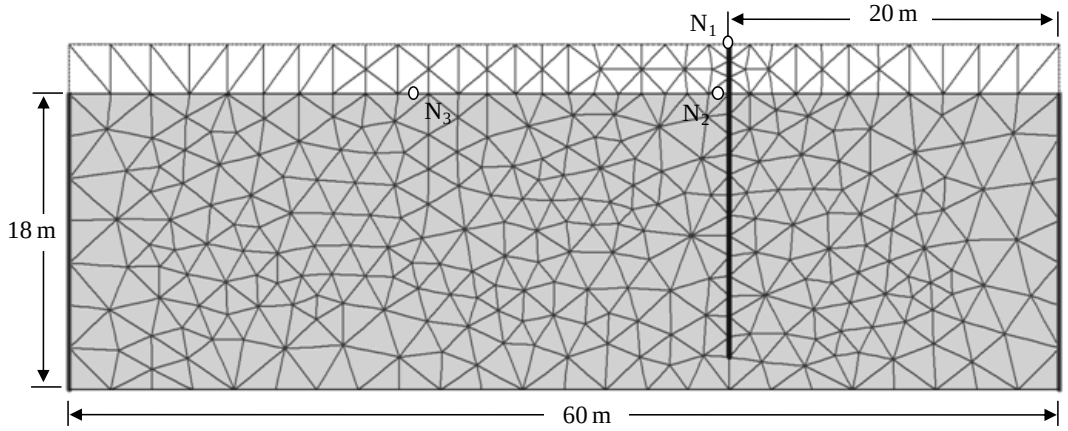

Figure 6.2 Finite element mesh for the PLAXIS simulation

Material Model and Model Parameters

Although both PLAXIS and TeraDysac have elastoplastic constitutive models that can replicate the soil behavior more realistically, linear elastic models are used for comparison purposes to eliminate the influence of hysteretic damping on the predicted results. Linear elastic models represent the soil behavior only when the soil is within a low strain range. Consequently, the loading applied to the system must be kept low in order for the linear elastic model to properly describe the soil behavior of the soil for purposes of comparison.

The engineering properties and the linear elastic model parameters of Minco silt are listed in Table 6.1. The structure is also assumed to be linear elastic and the model parameters used for the structural elements are given in Table 6.2. The Rayleigh damping coefficients for the Minco silt at 70% and 25% degree of saturation are calculated considering the 1^{st} and 2^{nd} modes frequencies of the soil response as the significant frequencies. The shear wave velocity of the Minco silt deposit is calculated using the shear modulus and the density of the deposit. This unsaturated SPI simulation study is conducted with two different initial degrees of saturation: 25% and 70%. The dynamic response of the soil deposit for a given earth quake loading with slightly varied fundamental period is also investigated by varying the stiffness (Young's modulus) of the soil.

Table 6.1 Linear elastic model parameters and soil properties of Minco silt

Properties			Value
Solid grain density		Mg/m^3	2.67
Liquid density		Mg/m^3	1.0
Gas density	$x10^{-3}$	Mg/m^3	2.1
Bulk modulus of liquid	$x10^{6}$	kPa	2.2
Bulk modulus of gas		kPa	101.3
Young's Modulus	$x10^{5}$	kPa	1.2
Poisson's ratio			0.3

Table 6.2 Linear elastic model parameters for structural elements

Properties			Pile	Superstructure
Density		Mg/m^3	2.803	386.5
Cross section area		m^2	0.132	0.132
2^{nd} moment of	$x10^{-3}$	m^4	6.01	6.01
Young's Modulus	$x10^{10}$	kPa	6.935	6.935
Poisson's ratio			0.33	0.33

The moisture-suction relation of Minco silt is modeled using the soil water characteristics curve (SWCC) proposed by Fredlund and Xing (1994). The model parameters were obtained by fitting the experimental data of Minco silt (Ananthanathan, 2003). The calibrated parameters are: $\boldsymbol{a}$ = 3 kPa, $\boldsymbol{n}$ = 1.675, $\boldsymbol{m}$ = 1, $\boldsymbol{Cr}$ = 2500, and θ_r = 0.

Results and Discussion

To evaluate the effectiveness of the improved simplified formulation, a series of simulations were carried out using the improved simplified formulation of TeraDysac and compared with predictions of PLAXIS. In addition, detailed Unsaturated Soil-Pile Interaction (USPI) simulation studies were carried out using the improved simplified formulation. Parametric studies were also performed to investigate the influence of the fundamental period of the soil deposit.

Comparison of Simplified, Improved, and PLAXIS Predictions

Although both software programs have various boundary conditions that realistically represent the boundaries of the simulation model, rigid-box boundary conditions (with the bottom fixed in all directions, and left and right fixed in horizontal directions with free vertical movement) is used in both software simulations to lessen the differences in the simulation procedure. The amplitude of the earthquake-time history shown in Figure 6.3 was downsized by five and applied to the finite element models shown in Figure 6.1 (TeraDysac) and Figure 6.2 (PLAXIS).

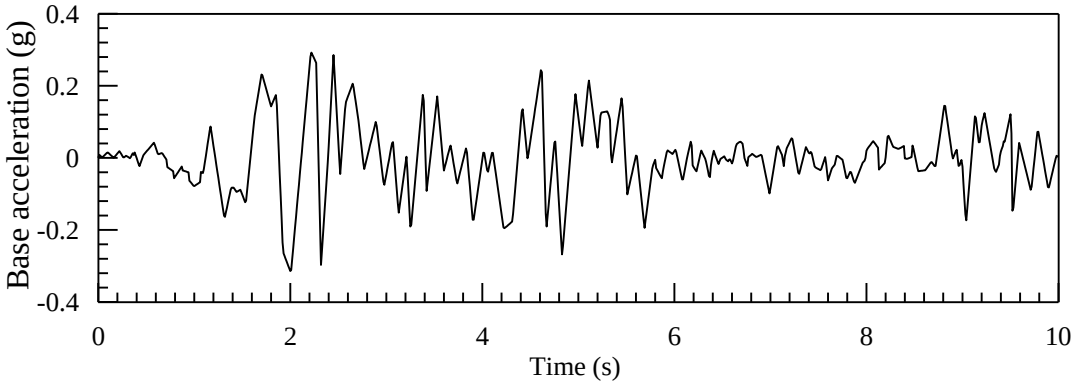

Figure 6.3 El Centro earthquake (1940) acceleration time history

The comparison of the horizontal spectral accelerations predicted by Simplified formulation, Improved Simplified formulation, and PLAXIS at the ground level far from the pile (node N3), adjacent to the pile (node N2) and at the superstructure level (node N1) are shown in Figure 6.4. For the Improved Simplified formulation the target damping of 5% and n of 3 were used. Figures 6.4a, 6.4b and 6.4c show the predictions for an initial degree of saturation of 70% and Figures 6.4d, 6.4e and 6.4f for an initial degree of saturation of 25%. For both initial degrees of saturations, the simplified formulation predicts unrealistic peak horizontal spectral acceleration of approximately 7g at the superstructure level (node N1) and approximately 6g at the ground level (node N2) for the minor earthquake loading. A comparison of predominant frequencies of the applied motion and the soil layer confirmed that the amplification observed from Simplified formulation prediction was not due to the resonant effect (the fundamental period of the soil layer is about 0.45 sec and the applied motion is higher). The Improved Simplified formulation predicts reasonable spectral acceleration values (maximum of approximately 2g) with results comparable to that predicted by PLAXIS. As the damping parameters, T, n and ξ, will influence the responses predicted by the Improved Simplified Formulation, these parameters must be calibrated more accurately for realistic predictions.

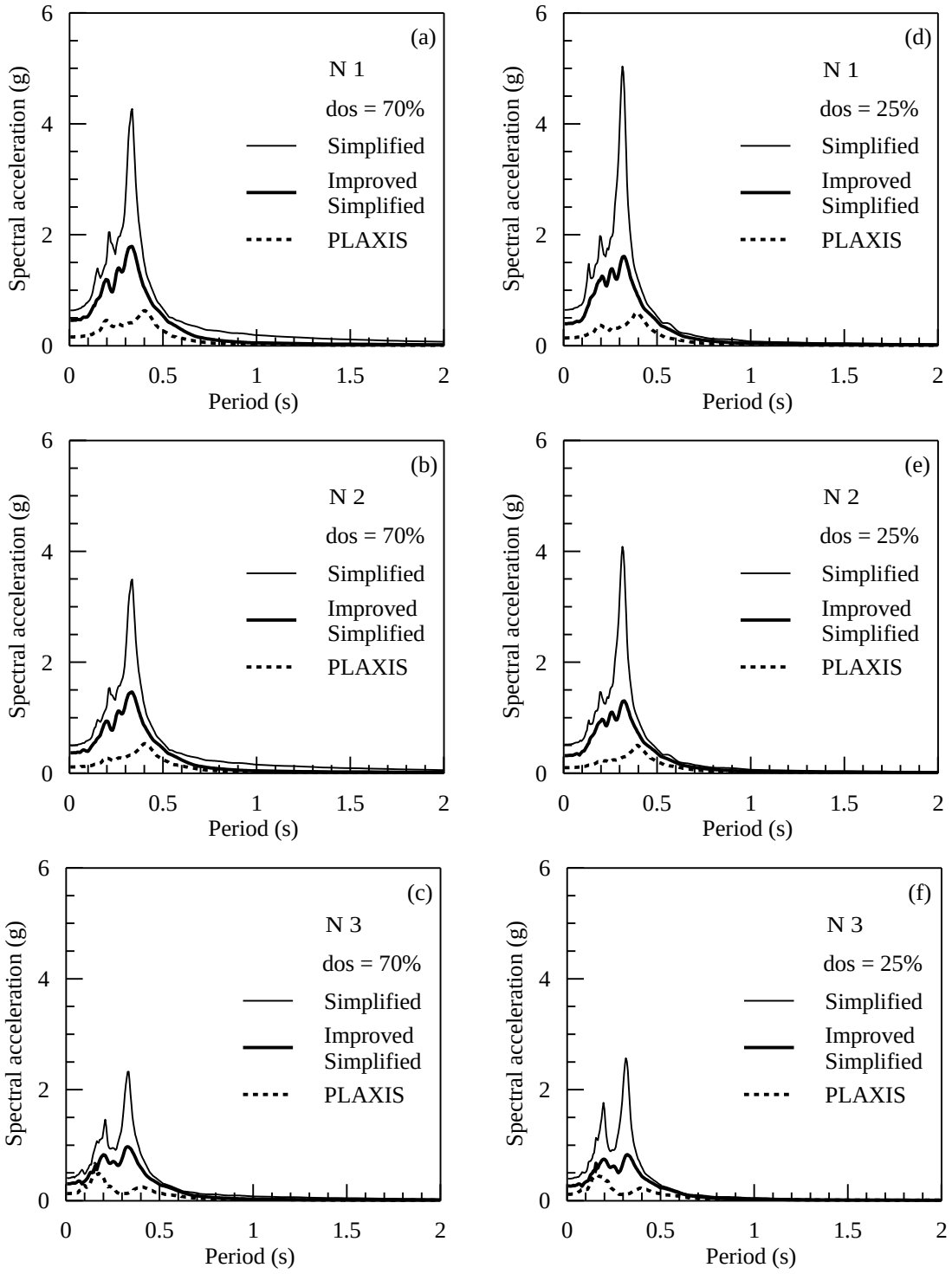

Figure 6.4 Comparison of Simplified, Improved Simplified, and Plaxis predictions

Parametric Study on the Rayleigh Damping Parameters

The finite element mesh shown in Figure 6.1 is used in the parametric studies with more realistic boundary conditions. The 2D level ground boundary condition that replicates the flexible shear beam container used in geotechnical centrifuge modeling is also used for all the parametric studies. In the 2D level ground boundary condition, the displacement fields at the bottom are fixed in all directions, horizontal displacement on the left and right vertical boundaries are equal, the vertical displacement on the left and right vertical boundaries is unconstrained and the top is traction free. The earthquake time history shown in Figure 6.3 was used for all parametric studies shown in this section.

Effect of ξ

The predicted responses for $\xi = 5\%$, 10% and 15% are shown in Figure 6.5 for initial degree of saturations of 70% and 25%, respectively. The increase in the damping coefficient reduces the peak spectral acceleration without affecting the predominant period. Although 0.5% to 5% is the range suggested for nonlinear site response analysis using 1-D models (Park and Hashash, 2001), the proposed finite element model requires more damping to obtain reasonable spectral accelerations.

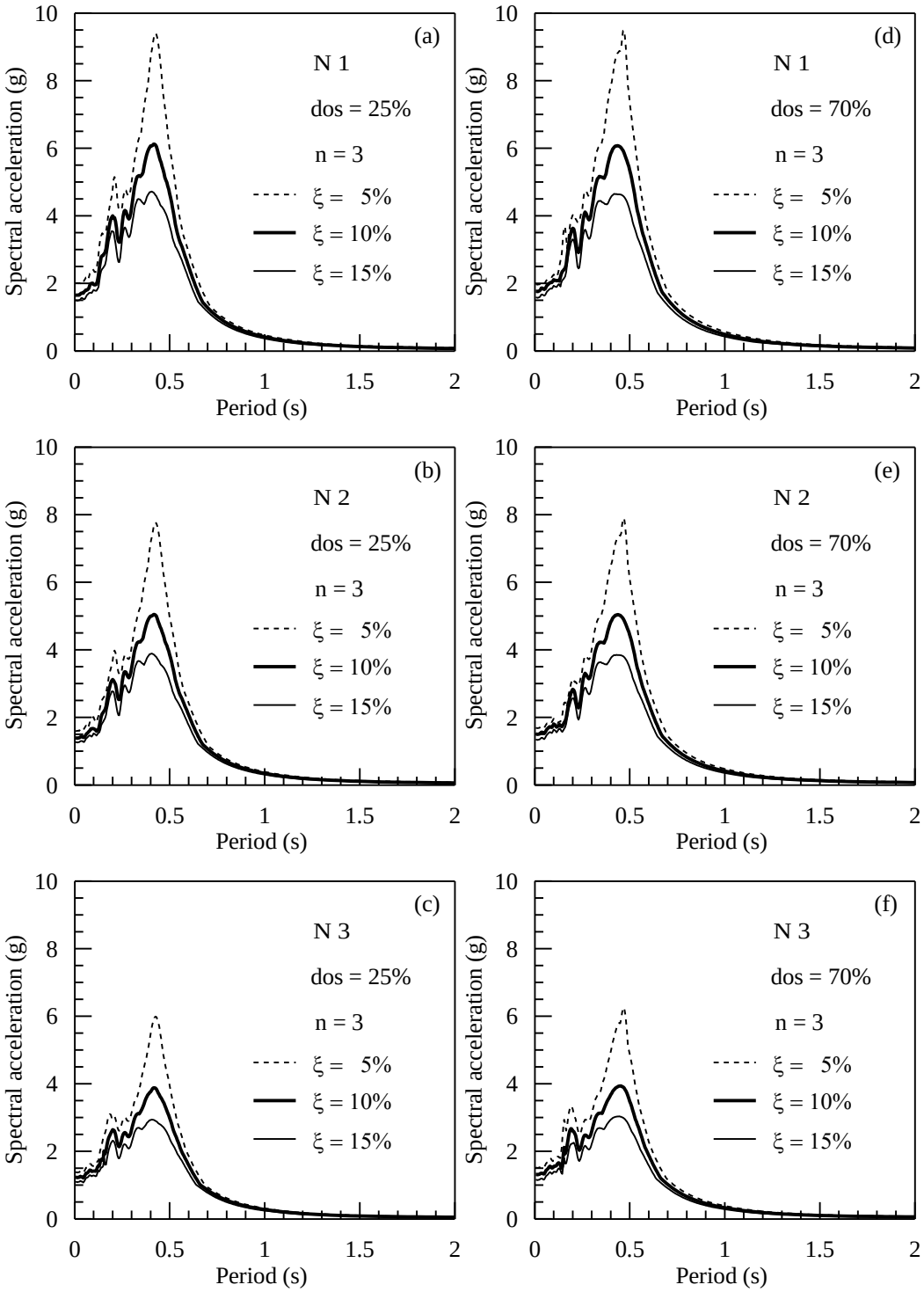

Figure 6.5 Effect of Rayleigh damping parameter ξ on the spectral accelerations

Effect of n

There is a continuous discussion regarding what frequencies (mode shapes) should be used in the calibration of full Rayleigh damping parameters for nonlinear analyses. Although some researchers recommend using n = 5 (Park and Hashash, 2001), calibrations at either higher or lower mode shapes are also necessary (Park and Hashash, 2004). To investigate the influence of the value of *n*, the spectral accelerations at node N1 for *n* = 0, 3 and 5 are compared in Figure 6.6 for initial degrees of saturations of 70% and 20%. In general, these results show the effect of ***n*** to be insignificant. Similar observations were made at nodes N2 and N3 but are not detailed in this dissertation since there are no significant differences.

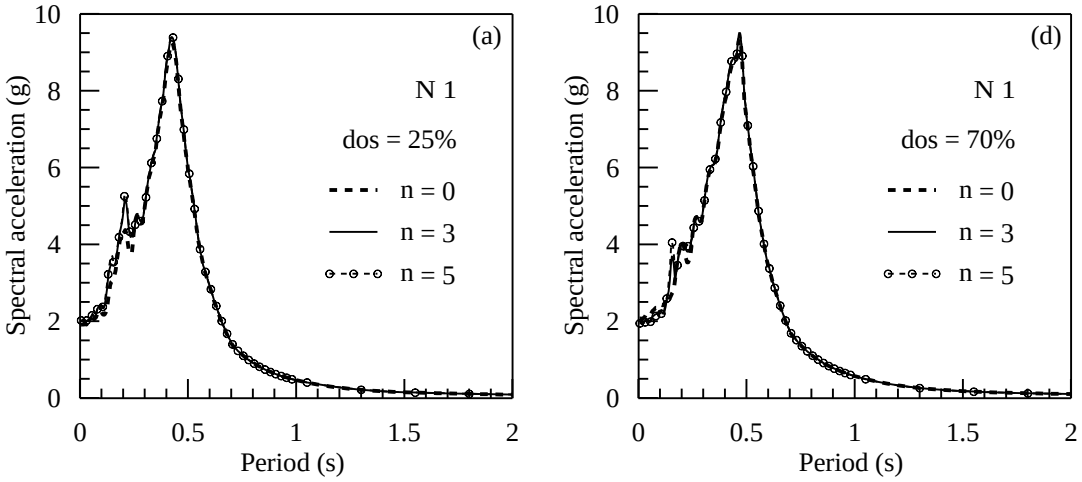

Figure 6.6 Effect of Rayleigh damping parameter **n** on the spectral accelerations

Effect of T

The fundamental period mainly depends upon the density and the shear modulus (Young's modulus and Poisson's ratio) of the soil. Therefore the influence of the fundamental period of the soil deposit is evaluated through multiple simulations with

different Young's moduli and with different base motions based upon the time histories of the El Centro (Figure 6.3) and Kobe earthquakes (Figure 6.7).

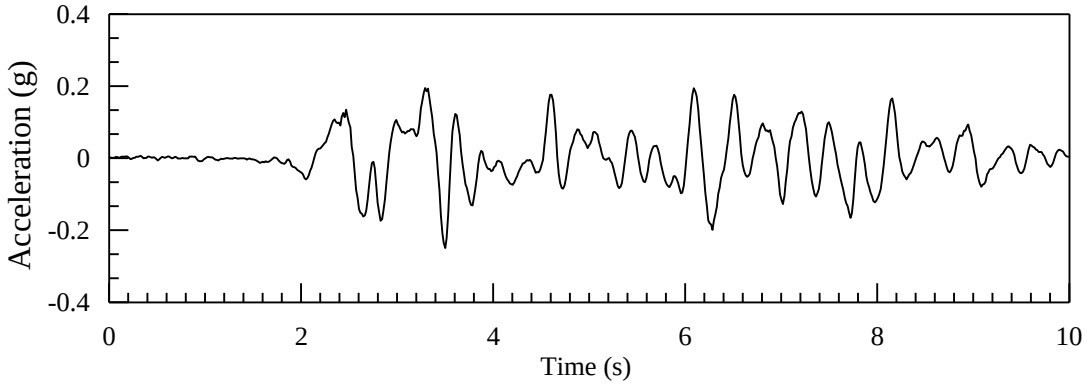

Figure 6.7 Acceleration time history of Kobe earthquake (1995)

As shown in Figures 6.8a, 6.8b, and 6.8c, the predicted spectral acceleration values for the El Centro earthquake load are higher when the actual value ($E = 1.2 \times 10^5$ kPa) and a value of $E = 6.5 \times 10^5$ kPa were used for the Young's Modulus of the Minco silt. However, the predicted spectral acceleration values are lower when the $E = 4.25 \times 10^5$ kPa. The fundamental periods of the Minco silt at the above Young's moduli are 0.44 sec and 0.19 sec, respectively. At 0.44 sec and 0.19 sec periods, the spectral acceleration of the applied El Centro history are higher; 0.19g, 0.2g respectively (see Figure 6.8a). Therefore, as discussed previously the response spectral acceleration will be higher when the fundamental period of the soil deposit and the period corresponding to the peak or higher spectral acceleration of the applied motion are identical. Based upon this observation, the simulation with the Kobe earthquake time history was expected to produce a higher spectral acceleration when the Young's modulus is about $E = 1.95 \times 10^5$ kPa (fundamental period = 0.35sec), and the predicted spectral acceleration values shown in Figures 6.8d, 6.8e, and 6.8f evidently prove the above observation.

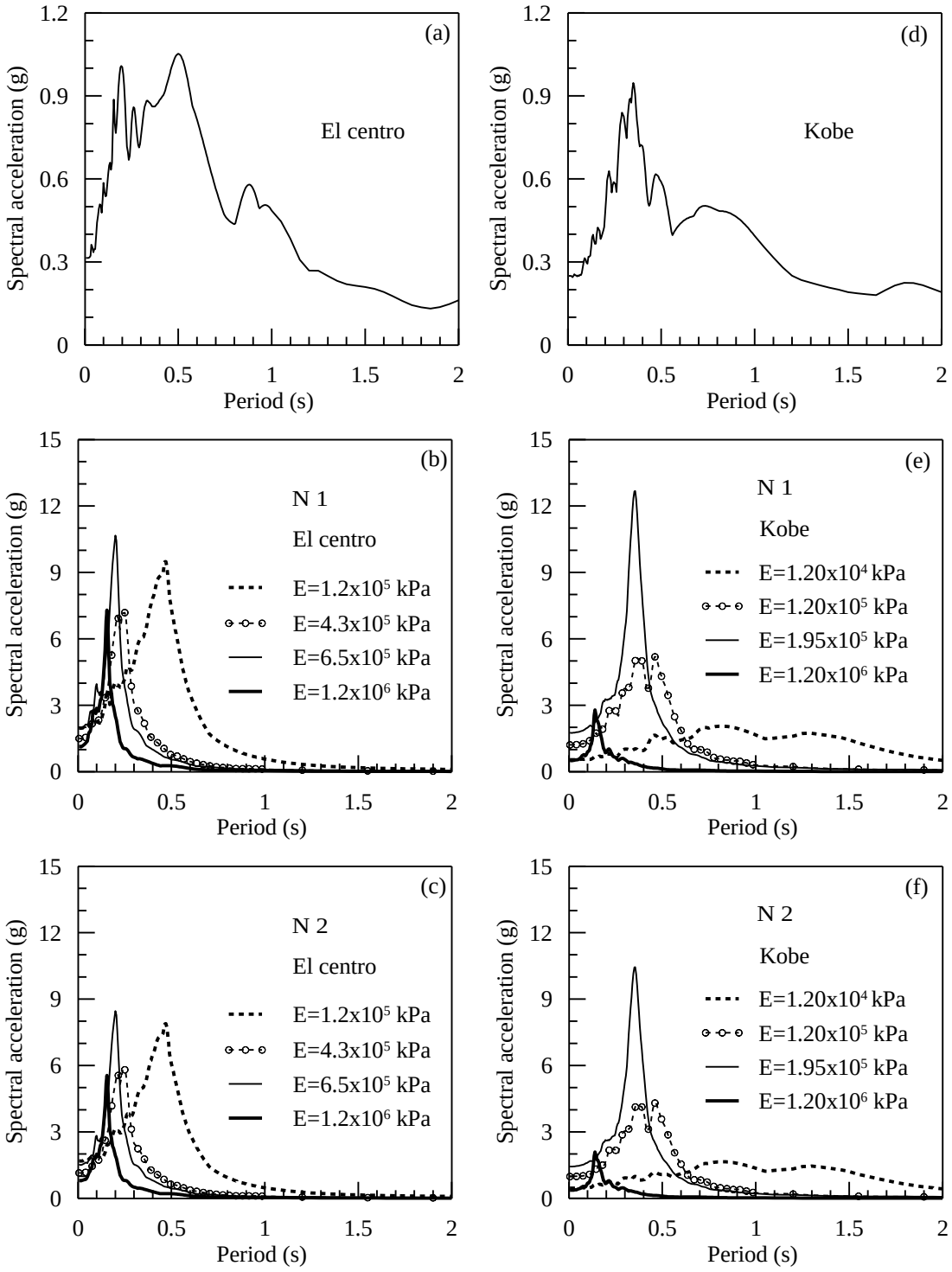

Figure 6.8 Effect of soil stiffness and fundamental period of soil deposit on the spectral accelerations

In dynamic analysis, for a specified loading/shaking, the shaking induced acceleration or displacement is expected to be higher when the Young's modulus is lower, as in softer soils. However, the period of the dynamic response increases for these softer soils. Therefore the period of the applied loading and the fundamental period of the soil deposit may differ, in which case, the soft soil may exhibit lower amplitude response. Thusly, prior to a possible maximum acceleration reached in as single direction, the shaking may induce acceleration in the opposite direction, thusly yielding a smaller acceleration. Therefore, to study and compare the stiffer and softer responses of soils, both the amplitude and the period (or frequency) of responses should be considered. Similarly, unsaturated soils with lower degrees of saturation (stiffer soil) may show a higher amplitude than soils with higher degrees of saturation when the period of the applied loading and the fundamental period of the soil deposit are identical.

Comparison of Elastic and Elastoplastic Predictions

Realistic predictions using finite element model require the use of realistic constitutive models for each component. Although the linear elastic model is characterized by easy to implement methodologies and results analysis, it is only applicable within a small strain range As the analyses of the soil-pile system under dynamic loading requires the use of elastoplastic model to obtain reasonable predictions, the original bounding surface model proposed by Dafalias and Herrmann (1986) was modified for unsaturated soils incorporating the suction effects proposed by Alonso et al. (1990). These constitutive model parameters are listed in Tables 6.3 and 6.4, and the predicted results are shown in Figure 6.9. The finite element mesh shown in Figure 6.1

and the acceleration time history shown in Figures 6.3 were used. At all three locations (N1, N2 and N3), the elastoplastic model predicts considerably lower spectral accelerations compared to elastic predictions. The predominant period was also observed to shift slightly to the left.

Table 6.3 Bounding surface based elastoplastic model parameters for the Minco silt

Parameter	Value
Slope of the isotropic consolidation line on e - $\ell n\ p'$ plot, λ	0.02
Slope of an elastic rebound line on e - $\ell n\ p'$ plot, κ	0.002
Slope of the critical state line in q - p' space , M_c (compression)	1.00
Ratio of extension to compression value of M (M_e / M_c)	1.00
Value of parameter defining the ellipse1 in compression (R_C)	2.60
Value of parameter defining the hyperbola in compression (A_C)	0.10
Parameter defining the ellipse 2 (tension zone) (T)	0.05
Projection center parameter (C)	0.00
Elastic nucleus parameter (S)	1.00
Ratio of triaxial extension to compression value of R (R_e / R_c)	1.00
Ratio of triaxial extension to compression value of A (A_e / A_c)	1.00
Hardening parameter (m)	0.02
Shape hardening parameter in triaxial compression (h_c)	2.00
Ratio of triaxial extension to compression value of h (h_e/h_c)	1.00
Hardening parameter on I-Axis (h_o)	2.00

Table 6.4 Suction related elastoplastic model parameters for Minco silt

Parameter	dos = 25%	dos = 70%
m	60	140
B	0.12	0.12
N	1.526	2.017
A	0.27	0.27
r	1.57	1.57
b	0.0133	0.0133

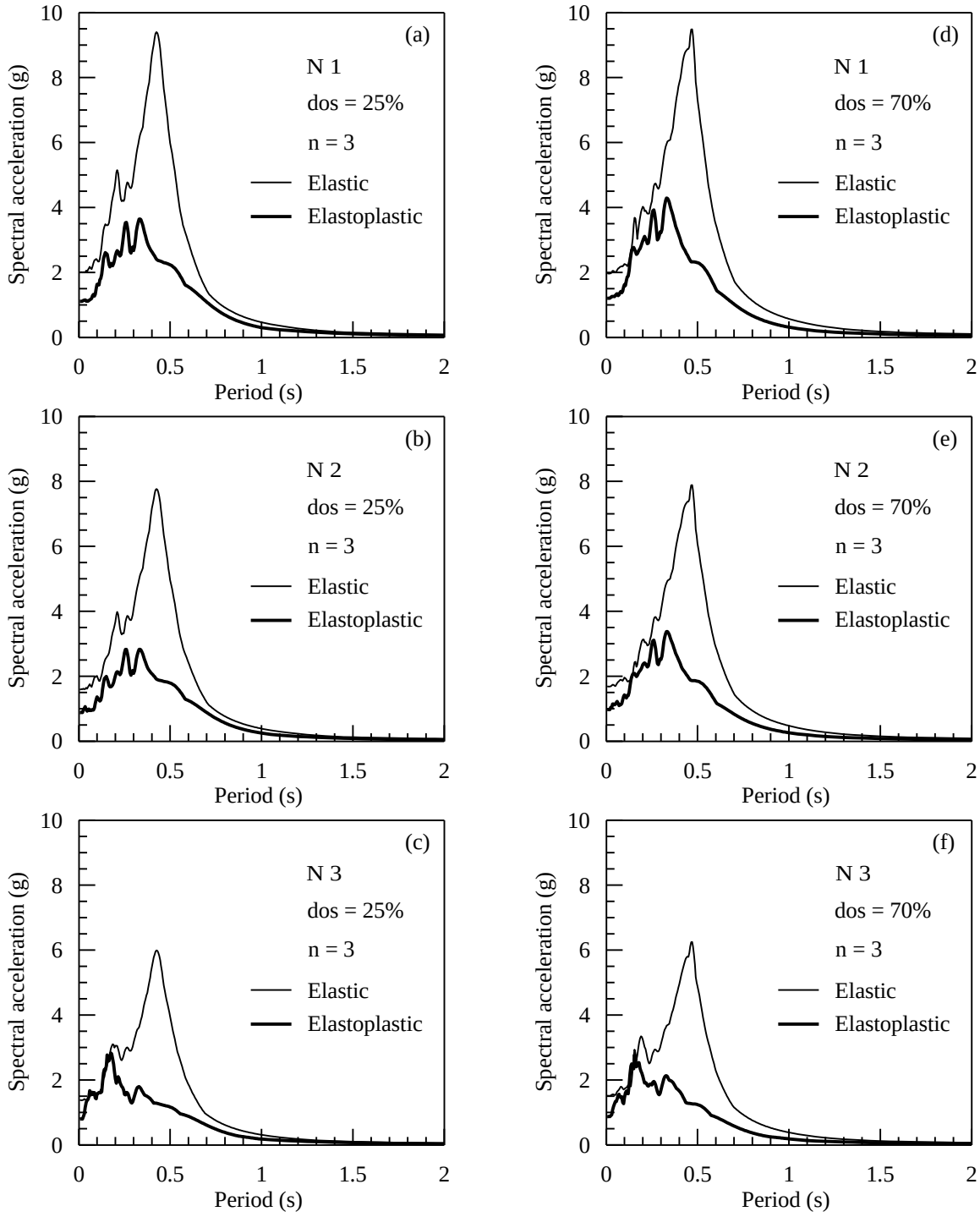

Figure 6.9 Comparison of spectral accelerations predicted with elastic and elastoplastic constitutive models

Summary of the Study

The numerical analyses and comparisons determine that the incorporation of Rayleigh damping model improves the performance of the simplified formulation. The unsaturated soil-pile interaction analyses show that the presence of pile significantly alters the acceleration at the ground level. The horizontal spectral acceleration, which is calculated near to the pile are relatively high compared to free-field motion. Therefore, the standard practice of using free-field ground motion to design the pile with a fixed base assumption should be utilized with caution or must incorporate the soil-pile interaction. In addition, the parametric studies show that the target damping coefficient has significant influence on the predicted responses. A commonly used 5% damping still shows higher acceleration and the parametric study shows that it can be controlled by increasing the target damping values. The fundamental period or the soil stiffness also influences the predicted response. A second supportive parametric study shows that the use of more realistic elastoplastic constitutive model significantly improves the reliability of predicted responses.

As suggested in the previous studies, further studies of SPI have to be carried out at low range of degree of saturation, where the influence of suction is expected to be much higher. However, before conducting SPI studies at low range of degree of saturation, the applicability and accuracy of available SWCC models in low range of degree of saturation should be studied. If necessary, the available SWCC models should be modified or new models should be developed. Therefore, extensive studies about the SWCC models of unsaturated soils are carried out and presented in the next chapter.

CHAPTER SEVEN

SWCCs OF UNSATURATED SOILS AND THE DEVELOPMENT OF NEW MODELS

Introduction

In addition to the governing equations, the finite element modeling of unsaturated soil responses requires mathematical models for various relationships. Two of the most important relationships are the stress-strain relationship and moisture-suction relationship. Most of the widely used stress-strain relationships are phenomenological models that are developed based upon observed responses and fundamental plasticity theories. Concurrently, most of the mathematical equations for moisture-suction relation available in the literature were also developed based on observed responses. The accurate predictions of unsaturated soil responses depend upon how well these mathematical equations represent the actual variation.

In this chapter, new soil-water characteristic curve models, which can be used over the full range of degree of saturation (dry to fully saturated conditions) is presented. The new model has the flexibility to use either with a residual water content (lower bound value for the water potential) or with a maximum suction value (the upper bound value for the suction). The capability of the new model is verified by matching the experimental data of twelve soils which includes sandy, silty, and clayey soils. As elucidated by the finite element modeling community, any constitutive law should not only represent the measured data well but should also be numerically stable when used in

numerical tools. The performance of the proposed moisture-suction model in the finite element simulation of unsaturated soils with low degree of saturation is investigated by simulating the behavior of a compacted embankment subjected to earthquake loading.

Factors Influencing the SWCC/ Moisture-Suction Variation

The amount of water present in the soil can be expressed in various forms such as degree of saturation, volumetric water content, or gravimetric water content. Also, the SWCC for a given soil can differ depending upon the wetting or drying process used to vary the moisture content in the soil sample. The portion of the SWCC obtained by the wetting a dry sample is called the primary wetting curve. Similarly, the curve obtained by drying a wet sample is called the primary drying curve. The primary drying curve always exhibits higher suction compared to the wetting curve (Figure 7.1) at a given degree of saturation (Ng and Pang 1999; Parlange 1976; Mualem 1977, 1984; Jaynes 1985; Hogarth et al. 1988; Nimmo 1992; Pham et al. 2003; Yang et al. 2004). Although the wetting and drying curves differ, the mathematical models for moisture-suction relation are represented by a single equation (Brooks-Corey 1964; van Genuchten 1980; Fredlund and Xing 1994).

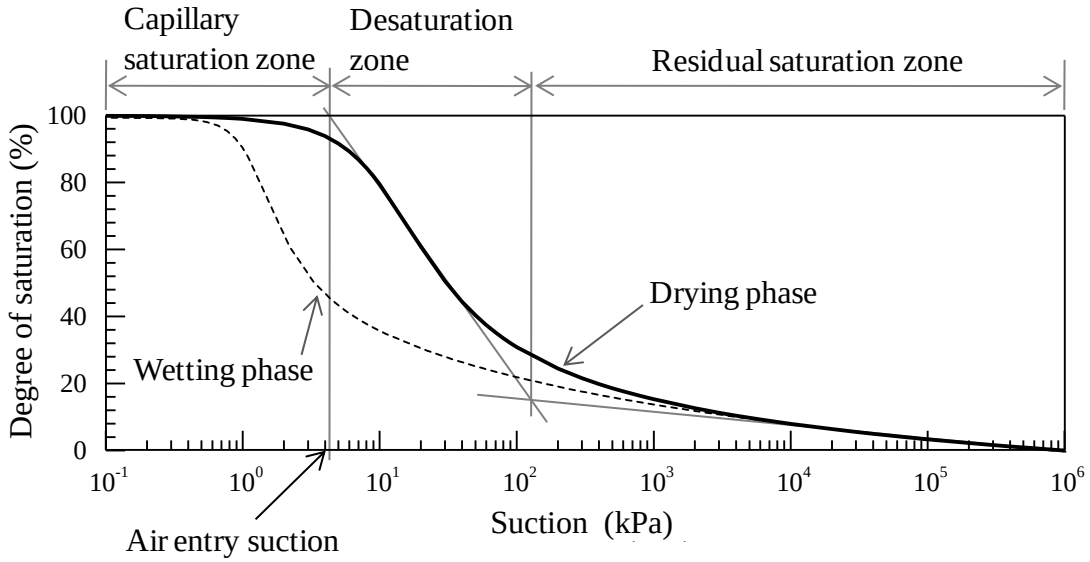

Figure 7.1 Typical SWCC with different regions of saturation

Various mathematical models have been developed to fit the measured moisture-suction relationship of natural soils (Gardner, 1956; Brooks and Corey, 1964; Brutsaert, 1966; van Genuchten; 1980; McKee and Bumb, 1987; Kosugi, 1994; Fredlund and Xing, 1994), all of which confirm an inverse proportional relationship between the degree of saturation and suction. The shape of the soil water characteristic curves significantly depends on pore size distribution and air-entry suction of the soil. Many researchers have identified the factors which influence the pore size distribution and the air-entry suction of the soil. Kawai et al. (2000) showed that the void ratio (***e***) affects the air-entry suction (***a)*** and proposed an inverse relation between ***a*** and ***e*** as shown in Equation 7.1.

$$a = 160\ e^{-2.51} \tag{7.1}$$

Another study by Vanapalli et al. (1999) showed that the initial degree of saturation has significant influence on the shape of SWCCs at lower suction range. For example, a higher initial degree of saturation makes the curves steeper, whereas the effect of initial

degree of saturation is insignificant at higher suction values. Through a series of experiments on undisturbed samples of completely decomposed volcanic soil with net normal stress levels of 0, 40 and 80 kPa, Ng and Pang (2000) showed the effect of net normal stress to be insignificant. Fredlund and Rahardjo (1993) and Vanapalli et al. (1999) found that the air-entry suction parameter ***a*** increases with increasing equivalent pressure. The influence at high suction was investigated by Vanapalli et al. (1999), which showed that the SWCC exhibits similar behavior at high suctions (20000–300000 kPa) even if all other parameters differ.

Popular SWCC Models of Unsaturated Soils

Although there are numerous SWCC models available in the literature, the B-C (Brooks and Corey, 1964), v-G (van Genuchten, 1980) and F-X (Fredlund and Xing, 1994) models are being widely used. Therefore before developing the new model, these three models were extensively investigated and the results are presented below.

The Brooks and Corey (B-C) Model

The B-C model (Equation 7.2) is one of the basic SWCC models developed with two parameters. This model does not provide a continuous mathematical function for the entire range of degree of saturation, and it is the major weakness of this model.

$$\frac{\theta - \theta_r}{\theta_s - \theta_r} = \begin{cases} 1 & if \quad \psi < a \\ (\psi / a)^{-n} & if \quad \psi > a \end{cases} \tag{7.2}$$

where ***a*** and ***n*** are the fitting parameters, ψ is suction, θ is volumetric water content, θ_r is residual water content and θ_s is saturated water content.

In a calibration procedure with B-C model, the fitting parameter ***a*** can be adjusted to fit the initiation point of the desaturation zone (air-entry state) with experimental air-entry prediction. The curve can be moved along the axis of suction by changing the ***a*** value, and there will be no significant change in the slope of the desaturation zone due to the variation in ***a*** (see Figure 7.2a). The parameter ***n*** controls the slope of the curve in the desaturation zone, which is related to the pore-size distribution of the soil. The slope of the curve proportionally varies with the ***n*** (see Figure 7.2b) and therefore the ***n*** can be adjusted to fit the experimental results in the desaturation zone. In the B-C model, there is no fitting parameter to control the curve in residual zone and it is another shortcomings.

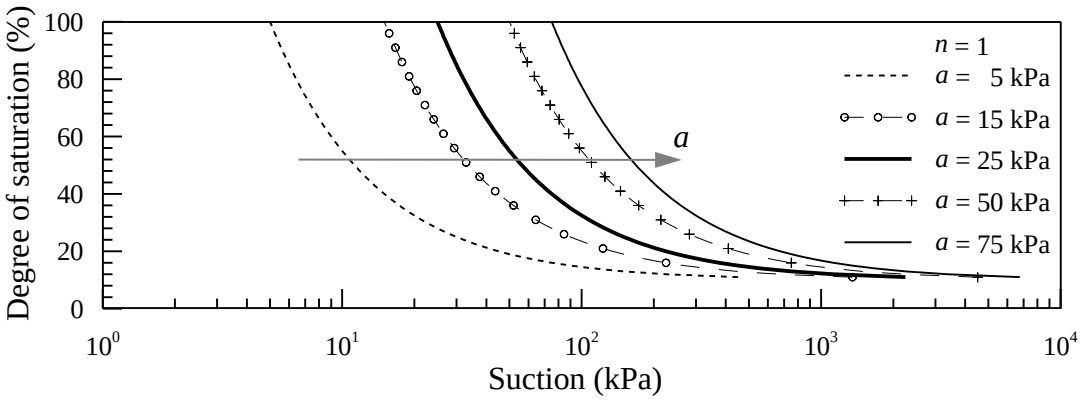

(a)

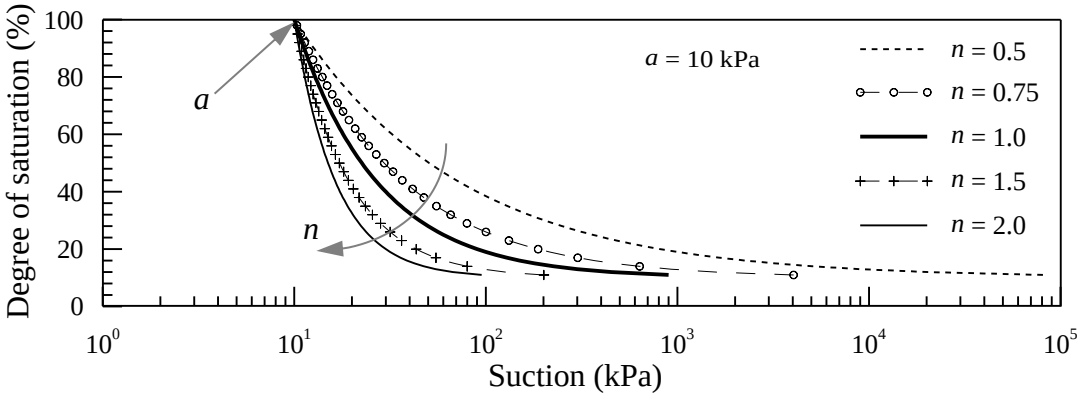

(b)

Figure 7.2 Role of fitting parameters in the B-C model

The van Genuchten (v-G) Model

The v-G model (Equation 7.3) provides a single equation for the entire range of degree of saturation. This model is flexible compared to the B-C model, since it has an additional fitting parameter ***m***.

$$\frac{\theta - \theta_r}{\theta_s - \theta_r} = \frac{1}{\left(1 + (a\psi)^n\right)^m} \tag{7.3}$$

where the fitting parameter ***m*** is related to the symmetry of the model and the other parameters are same as in the B-C model.

The role of the fitting parameters ***a*** (see Figure 7.3a) and ***n*** (see Figure 7.3b) in the v-G model is very similar to the B-C model. However in the B-C model, the ***a*** is the initiation point of the desaturation zone and in the v-G model, it is related to a point within the desaturation zone. When the ***n*** increases, the degree of saturation at a given suction will increase if the suction is less than 1/***a*** value, but the degree of saturation will decrease if the suction is greater than the 1/***a*** value (see Figure 7.3b). The fitting parameter ***m*** can be used to adjust the residual zone of the curve and it is one of the advantages of v-G model over the B-C model. However the ***m*** is not very effective, as it significantly affects the capillary saturation zone which is related to the sir-entry suction, and the desaturation zone which is related to the pore-size distribution of the soil. (see Figure 7.3c).

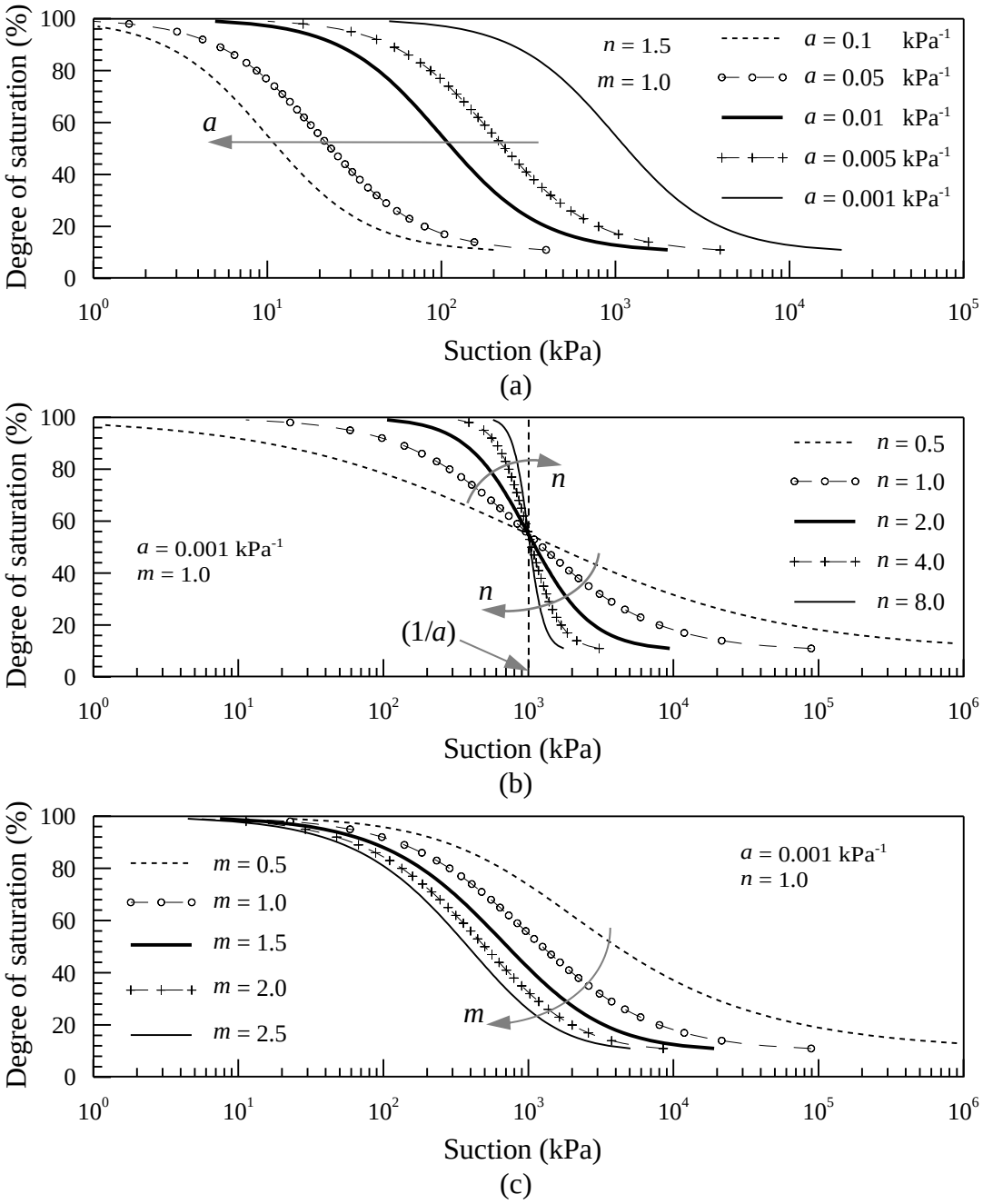

Figure 7.3 Role of fitting parameters in the van Genuchten model

The Fredlund and Xing (F-X) Model

The F-X model (Equation 7.4) is proposed with a limiting value for the maximum suction (1,000,000 kPa at zero water content) while the B-C and the v-G models predict a

maximum suction of infinity which is not realistic. Capability of predicting the SWCC for entire range of degree of saturation is considered as the major advantage in this model. This model is rather similar to the v-G model other than the correction factor $C(\psi)$ and "ln-term" in the equation. The "ln-term" is important and very effective in bringing the curve to a higher maximum suction value (1000000 kPa) without reaching the zero water content in low suction range. Fredlund and Xing (1994) also suggested another form of the F-X model (Equation 7.5) which is applicable if a residual water content is to be considered.

$$\frac{\theta}{\theta_s} = \frac{C(\psi)}{\left(\ln\left(\exp + (\psi/a)^n\right)\right)^m} \tag{7.4}$$

$$\frac{\theta - \theta_r}{\theta_s - \theta_r} = \frac{C(\psi)}{\left(\ln\left(\exp + (\psi/a)^n\right)\right)^m} \tag{7.5}$$

$$C(\psi) = 1 - \frac{\ln\left(1 + \frac{\psi}{Cr}\right)}{\ln\left(1 + \frac{1000000}{Cr}\right)}$$

where the *Cr* is a parameter related to residual water content and all other parameters are same as in the v-G model. The role of the fitting parameters ***a*** (see Figure 7.4a), ***n*** (see Figure 7.4b), and ***m*** (see Figure 7.4c) in the F-X is very similar to the v-G model.

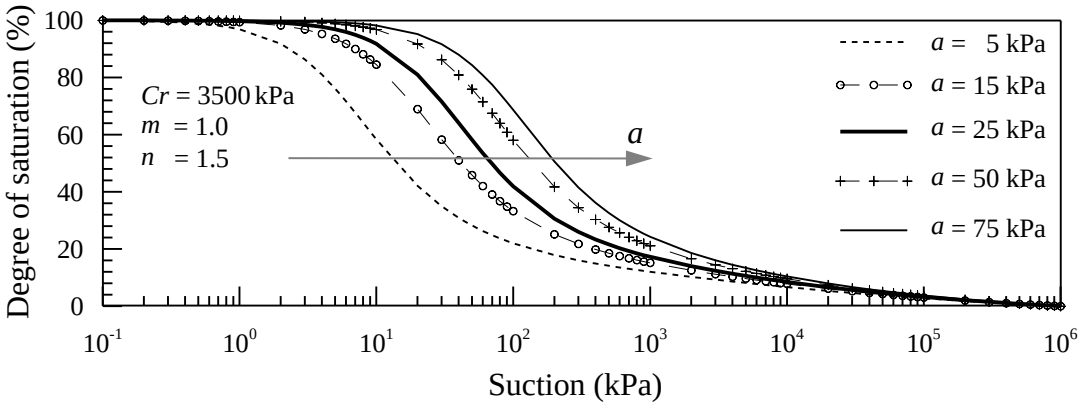

(a)

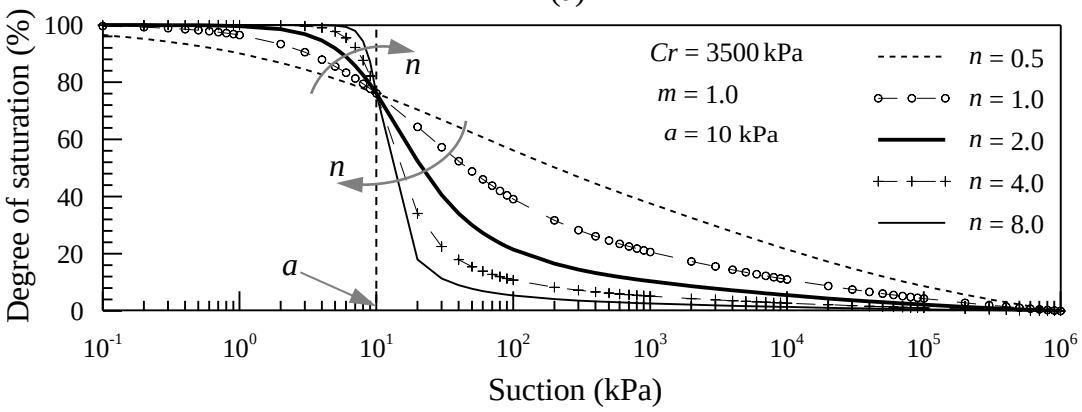

(b)

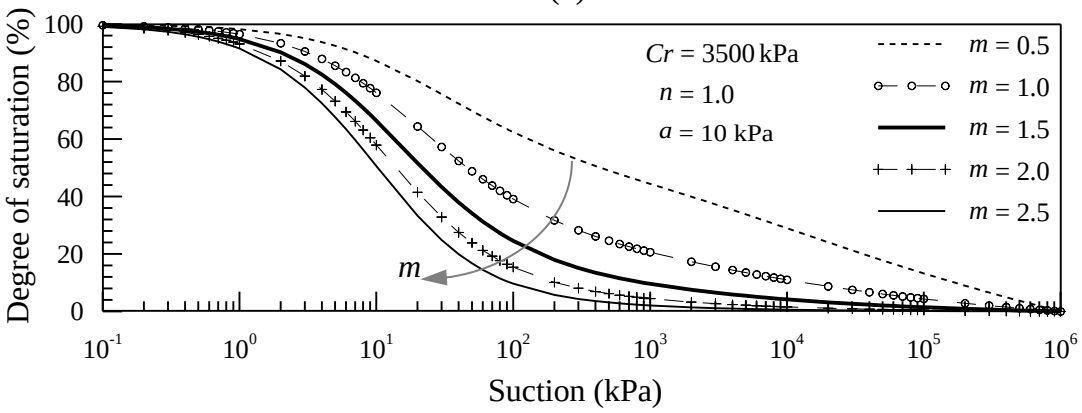

(c)

Figure 7.4 Role of fitting parameters in the F-X model

A correction factor $C(\psi)$ is introduced in this model, to achieve a maximum suction of 1,000,000 kPa at dry condition. However, as Leong and Rahardjo (1997) identified,

when the *Cr* is relatively low, the correction factor $C(\psi)$ affects the capillary saturation and desaturation zones (see Figure 7.1) significantly. Also it is difficult to choose the best set of fitting parameters, since the value of *Cr* can be chosen from a very wide range (1-1,000,000).

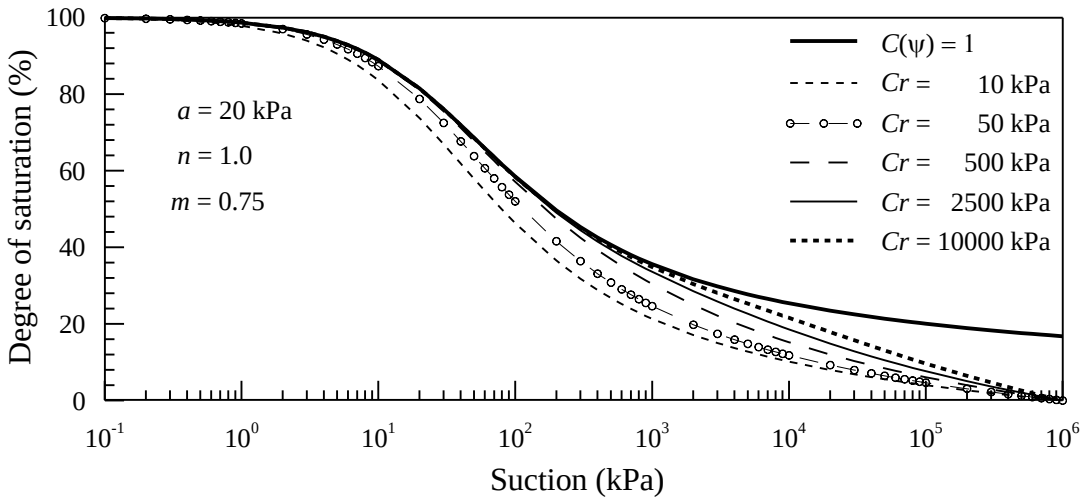

Figure 7.5 Role of ***Cr*** in the F-X model

Leong and Rahardjo (1997) suggested two other forms of the correction factor $C(\psi)$ (see Equations 7.6 and 7.7).

$$C_1(\psi) = \left(\frac{\ln\left(2 - \frac{\psi}{\mathrm{A}}\right)}{\ln 2} \right)^B \tag{7.6}$$

$$C_2(\psi) = \left(1 - \frac{\psi}{10^6}\right)^B \tag{7.7}$$

where A is maximum suction and B is a constant.

These factors are successful in avoiding the effect of $C(\psi)$ in the initial portion of the curve, but not very effective in the residual saturation zone. In the residual saturation

zone, these factors usually produce a wave shape curve (see Figures 7.6 and 7.7) when the suction is very high (close to maximum suction), and because of that, it is difficult to fit with experimental curves.

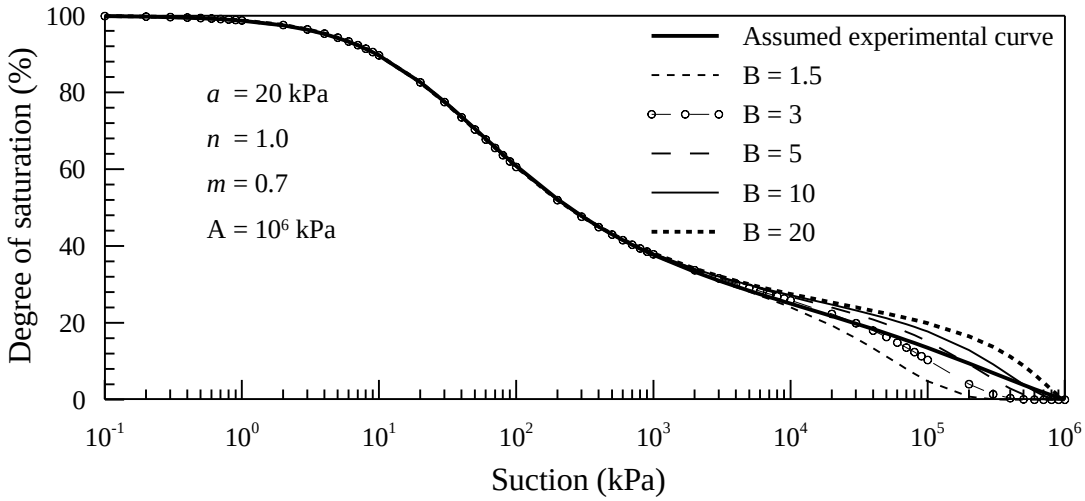

Figure 7.6 Role of the **B** when the F-X model is used with factor $C_1(\psi)$

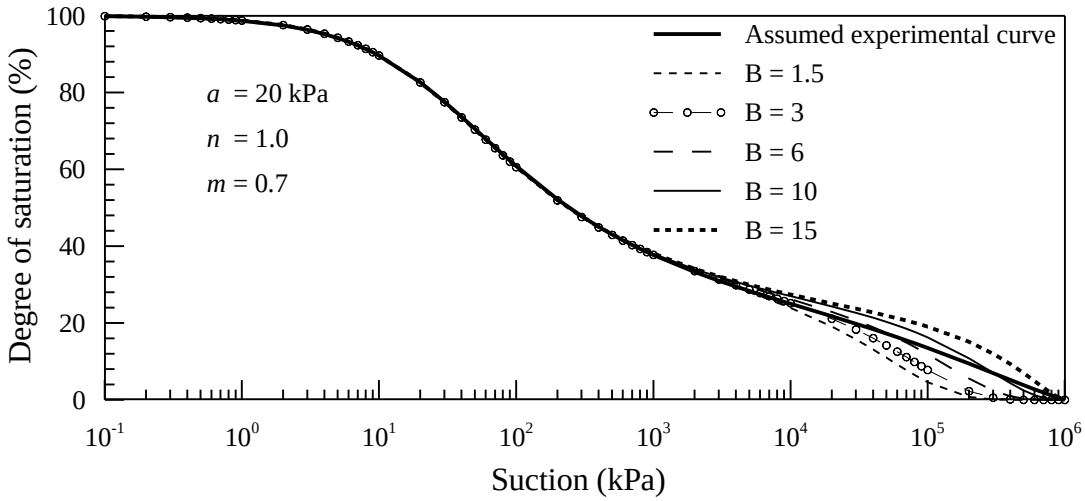

Figure 7.7 Role of the **B** when the F-X model is used with factor $C_2(\psi)$

Limitations and Issues of the Popular SWCC Models

Among the three popular SWCC models, for the B-C and v-G models, a reasonable residual water content value (lower bound value for the water potential) has to be specified. However these two models calculate an infinity/unrealistic suction when the water content of the soil is less than or equal to the specified residual water content, i.e. at zero or less normalized water content. In the F-X model, the maximum suction value (upper bound value for the suction) is assumed to be 1,000,000 kPa for any soils, which has no theoretical basis. Fredlund and Xing (1994) have also suggested another form of the model to use with a residual water content value, and this model also calculates infinity/unrealistic suction when the normalized water content is zero or less.

In simulations of unsaturated soils using numerical tools a user should be able to set the residual water content value to zero or to any other reasonable values. However a maximum suction value should be specified to avoid the calculation of infinity/unrealistic suction when the normalized water content is close to zero. The maximum suction value cannot be assumed to be 1,000,000 kPa for any soils (F-X model); rather it should be decided based on the experimental data. However, if there is a need, it should be able to perform numerical simulations without calculating a maximum suction value.

Capability of calculating maximum suction value of 1,000,000 kPa is considered as the major improvement of the F-X model over the other models. However, as Leong and Rahardjo (1997) pointed out, the correction factor $C(\psi)$ significantly affects the desaturation zone of the curve when the Cr is relatively low. Since the desaturation zone is related to the $\boldsymbol{a}$ and $\boldsymbol{n}$ values, the influence of the correction factor in the desaturation

zone should be avoided. In addition, the *Cr* value in the F-X model can vary from 1 to 1,000,000 kPa and it creates difficulties in achieving the best set of model parameters.

Incorporating the maximum suction as part of the model will increase its flexibility in fitting the measured data well especially in low saturation ranges. In addition, researchers may wish to use both lower bound and upper bound concepts in a single numerical simulation with multiple unsaturated soil layers (i.e. in real boring logs for geotechnical engineering projects). For example, there might be a need to specify residual water content for clayey soils while preserving a maximum suction for sandy soils in a single simulation. Therefore, a model that can be used either with residual water content or maximum suction is desirable. Therefore, there is a real need for a new SWCC model which should be able to use with a residual water content and/or a maximum suction value at zero normalized water content condition.

Development of a New SWCC Model (S-R-1 Model)

The S-R-1 model is developed primarily to use with both residual water content concept and maximum suction concept. The new model is developed by modifying the F-X model and by simplifying some of the calculations. The new model is given by the following equations (Equation 7.8).

$$\frac{\theta - \theta_r}{\theta_s - \theta_r} = \frac{N(\psi)}{\left(1+\ln\left(1+\left(\psi / a\right)^n\right)\right)^m} \tag{7.8}$$

The function $N(\psi)$ is given by $\left(1-\sqrt{\frac{\psi}{\psi_{max}}}\right)^{Nr}$. The parameters ***a, n*** and ***m*** are the fitting parameters, and ***Nr*** is a number related to residual water content.

The correction function $N(\psi)$ is used to bring the normalized water content to zero when the suction is equal to ψ_{max}. If θ_r is set to be zero, the suction will be equal to ψ_{max} at dry condition. If a residual water content is to be considered without limiting the maximum suction value, the *Nr* has to be set to zero, so that the Equation 7.8 will be simplified ($N(\psi) = 1$) to a form shown in Equation 7.9. On the other hand, if the residual water content of the soil has to be considered with a limiting maximum suction value, a calibrated N_r value can be used together with residual water content. In this case, the maximum suction will be equal to ψ_{max} when the $\theta = \theta_r$. The factor $N(\psi)$ is effective only in the residual saturation zone, thus the prediction or the value of other model parameters will not be affected due to the $N(\psi)$.

$$\frac{\theta - \theta_r}{\theta_s - \theta_r} = \frac{1}{\left(1+\ln\left(1+\left(\psi / a\right)^n\right)\right)^m} \tag{7.9}$$

The derivative of the moisture-suction relation is used in the development of governing equations for the unsaturated soil and to determine the specific moisture capacity function for problems involving flow in unsaturated media. The derivative of the proposed model is given below.

$$\frac{dS}{d\psi} = \frac{-\ N\left(\psi\right)}{\left(1+\ln\left(1+(\psi / a)^n\right)\right)^m}\left(\frac{Nr}{2\left(\sqrt{\psi\ \psi_{max}} - \psi\right)} + \frac{mn\ (\psi / a)^n}{\psi\left(1+(\psi / a)^n\right)\left(1+\ln\left(1+(\psi / a)^n\right)\right)}\right)$$

$$\frac{d\theta}{d\psi} = \left(\theta s - \theta r\right)\frac{dS}{d\psi}$$

Role of the Fitting Parameters in the S-R-1 Model

The role of fitting parameters ***a***, ***m*** and ***n*** in the proposed model are presented in Figures 7.8a, 7.8b and 7.8c, respectively. These parameters influence the shape of the curve similar to the F-X model. However, as presented in Figure 7.8d, the 1,000,000 kPa suction at dry condition is successfully achieved without affecting the slope of the curve within the desaturation zone by adjusting the correction factor $N(\psi)$.

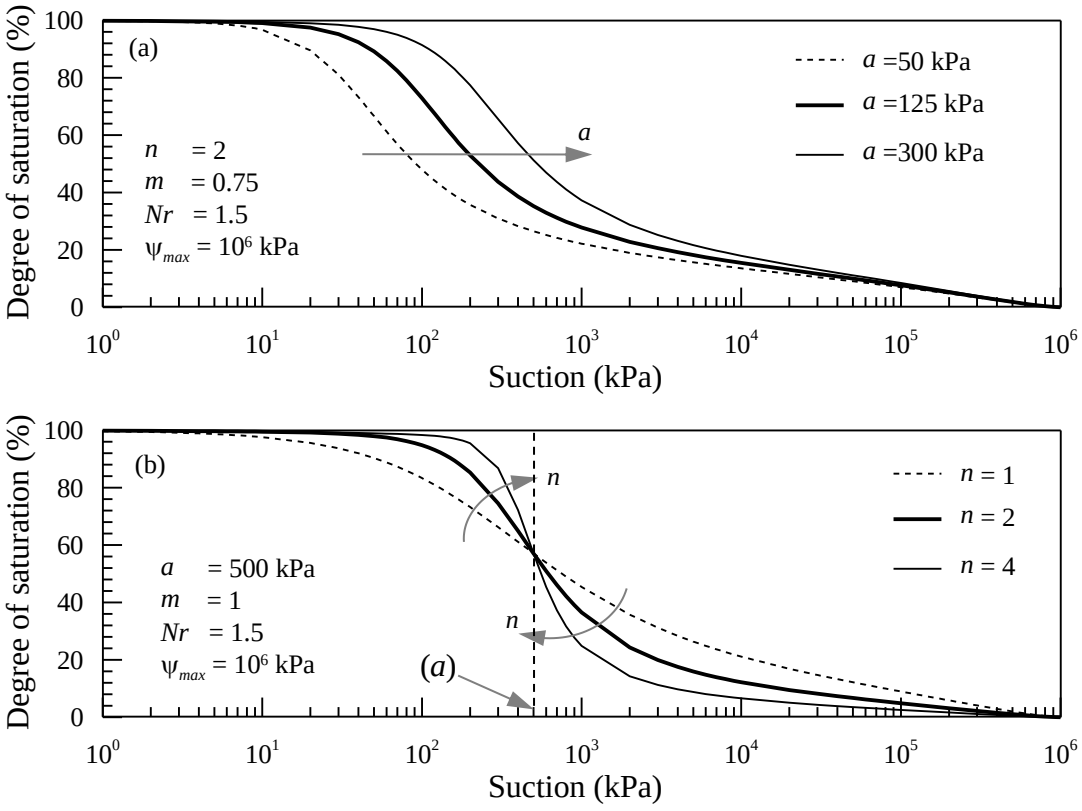

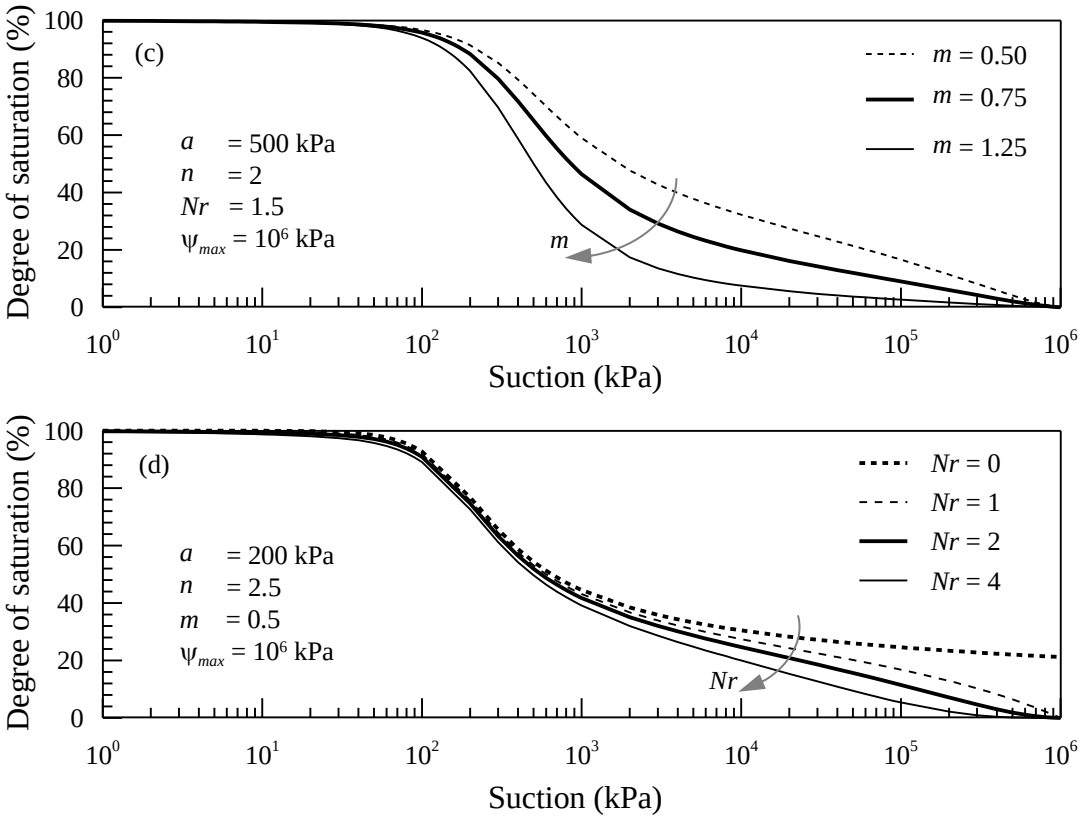

Figure 7.8 Role of the fitting parameters in the S-R-1 model

Predictive Capability of the S-R-1 Model

The capability of the new model to predict the moisture-suction relation is examined by fitting the experimental data of eight different soils including high plastic soils. The index properties and the calibrated model parameters of these soils are listed in Table 7.1 and the calibrated S-R-1 SWCCs are shown in Figure 7.9.

Table 7.1 Properties of the selected soils and calibrated SWCC model parameters

Soil Type	Properties	Calibrated Model Parameters							Reference
		Model	a (*kPa*)*	n	m	N_r	C_r (*kPa*)	ψ_{max} (*kPa*)	
Columbia sandy loam	n = 0.458	B-C	5.25	1.08	-	-	-	-	Brooks & Corey 1964
		v-G	0.18	11.0	0.110	-	-	-	
		F-X	6	8.50	0.490	-	5000	-	
		S-R	6.9	8.50	0.480	1.0	-	10^5	
Silt loam	n = 0.396	B-C	11	0.27	-	-	-	-	Reisenauer 1963
		v-G	0.037	1.65	0.310	-	-	-	
		F-X	22	2.50	0.440	-	50	-	
		S-R	50	1.90	0.780	1.0	-	10^5	
Madrid clay sand CL	G_s = 2.71 n = 0.275 LL = 28% PI = 8%	B-C	32	0.31	-	-	-	-	Escario & Juca 1989
		v-G	0.028	2.55	0.125	-	-	-	
		F-X	65	1.80	0.670	-	10000	-	
		S-R	110	1.90	0.630	2.0	-	10^6	
Indian head till (CL)	G_s = 2.73 LL = 36% PI = 19%	B-C	275	0.26	-	-	-	-	Vanapalli et al. 1999, Oloo & Fredlund 1995
		v-G	0.001	0.95	0.325	-	-	-	
		F-X	360	1.10	0.550	-	10000	-	
		S-R	1500	1.00	0.650	1.5	-	10^6	
Arlington soil (CL)	G_s = 2.46 n = 0.403 LL = 44% PI = 22%	B-C	68	0.15	-	-	-	-	Puppala et al. 2006
		v-G	0.01	1.75	0.100	-	-	-	
		F-X	120	1.50	0.320	-	10000	-	
		S-R	230	1.75	0.275	1.8	-	10^6	
DFW soil (CL)	G_s = 2.65 n = 0.447 LL = 50% PI = 32%	B-C	19	0.085	-	-	-	-	Puppala et al. 2006
		v-G	0.05	1.70	0.050	-	-	-	
		F-X	50	0.90	0.320	-	35000	-	
		S-R	130	0.90	0.270	1.5	-	10^6	
Maryland clay (CH)	G_s = 2.68 n = 0.448 LL = 64% PI = 40%	B-C	1350	0.325	-	-	-	-	Li et al. 2007
		v-G	0.000	1.65	0.245	-	-	-	
		F-X	2500	2.25	0.330	-	5000	-	
		S-R	4000	2.50	0.440	1.2	-	10^6	
Madrid gray clay (MH)	G_s = 2.64 n = 0.507 LL = 71% PI = 35%	B-C	260	0.25	-	-	-	-	Escario & Juca 1989
		v-G	0.001	0.75	0.425	-	-	-	
		F-X	1900	0.50	1.400	-	4000	-	
		S-R	6000	0.62	1.200	1.8	-	10^6	

* The unit of parameter ***a*** in the v-G model is kPa^{-1}, in the other models it is kPa.

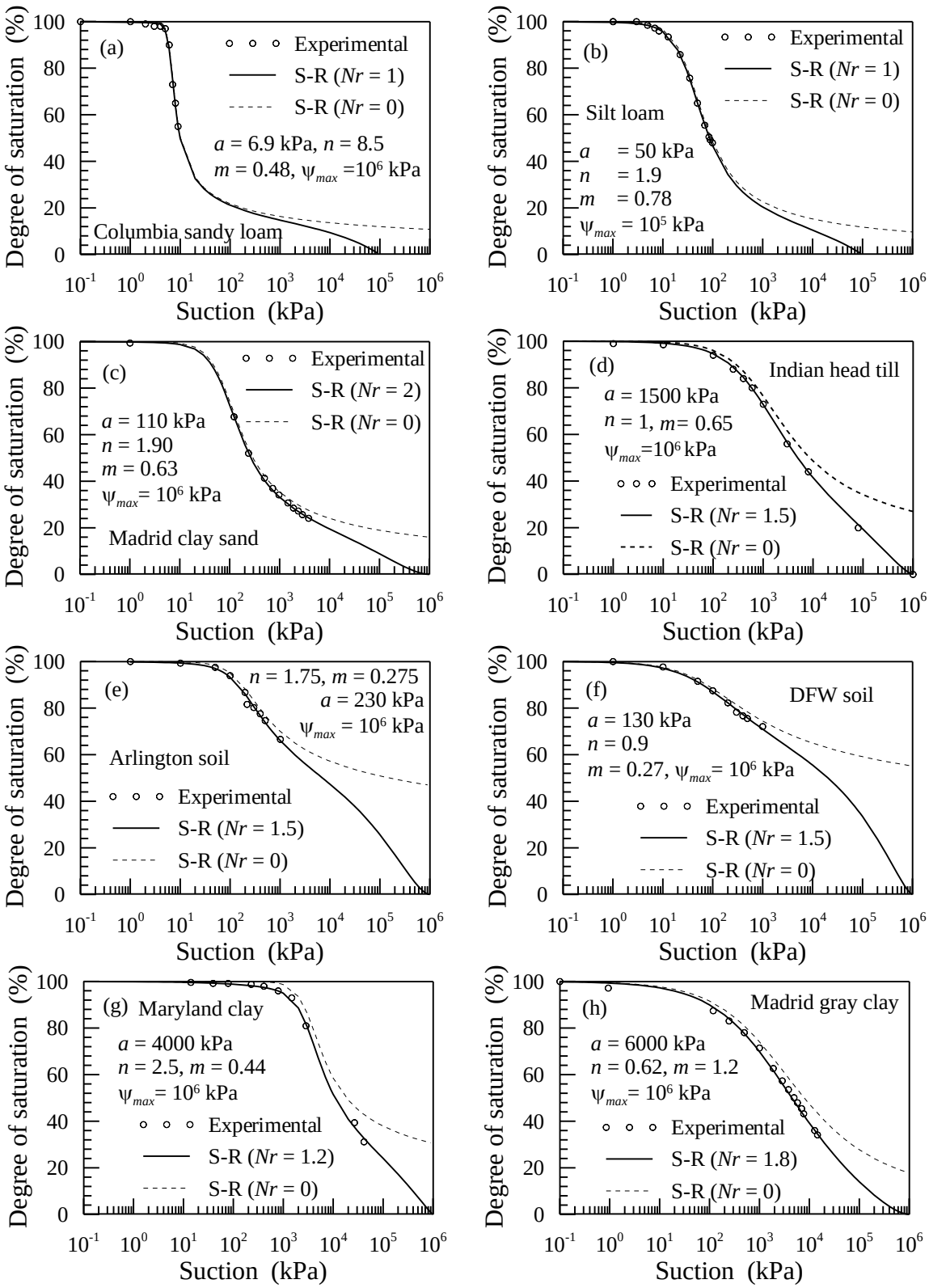

Figure 7.9 SWCC data of various soils fitted with the S-R-1 model

The results show that the new model fits the experimental data well. It should be noted that experimental data are not available for the whole range of degree of saturation of the soils used in this study. However, the inclusion of the maximum suction as a model parameters increases the flexibility of the model to fit data in the low suction range. Also, the maximum suction represents the last point in the SWCC. Therefore, the proposed model can be used to predict moisture-suction relation with confidence for the range of degree of saturation in which actual measurement is not available. The proposed model can also be used with appropriate maximum suction for *zero normalized water content* that will represent dry condition when the irreducible water content is zero. It can also be used without specifying maximum suction value by setting *Nr* to zero. Unlike the correction factor *Cr* in F-X model, the correction factor *Nr* in the new model has a small range (1 to 5) for any soil. The correction factor ranges from 1 to 2.5 for clayey soils, and 1.5 to 3.5 for silt and sandy soils. If the *Nr* is less than or equal to 5, the slope of the curve in the desaturation zone will not be affected by the value of $N(\psi)$.

The B-C, v-G and F-X models were also calibrated by fitting these experimental data and compared with the new model, the comparison is presented in Figure 7.10. As shown in the figure, obvious differences were seen in the low degree of saturation region when B-C and v-G models were used. In addition to the above mentioned soils, the experimental SWCC data of Minco silt (Ananthanathan, 2002) and Speswhite Kaolin (Sivakumar, 1993) were also calibrated using all four models. The calibrations of these two soils are shown in Figures 7.11 and 7.12, respectively (along with the finite element simulation details).

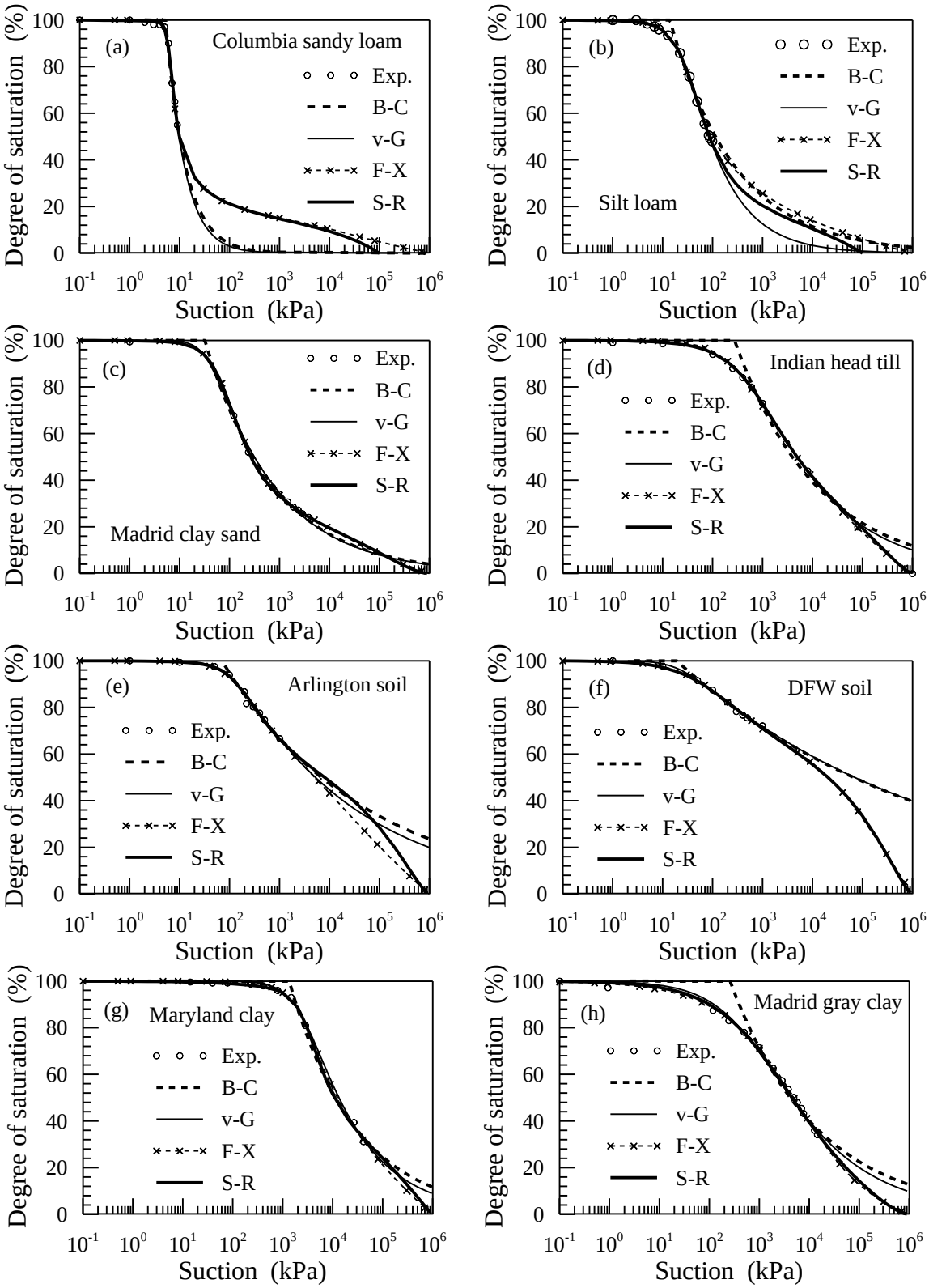

Figure 7.10 SWCC data of various soils fitted with all four SWCC models

Based on the capability analysis, it can be summarized that the new model preserves all the advantages of the available models and eliminates the shortcomings found in the other models. The performance of the new model in finite element simulations is also studied for a wide range of degree of saturation and the results are presented in the next section.

Performance of the S-R-1 Model in Finite Element Simulations

One of the primary applications of mathematical representation of soil-moisture relation in geotechnical engineering is in the finite element modelling of unsaturated soils. In general, mathematical equations become complex when they represent the true behaviour while the complex equations simultaneously limit the applicability via numerical instabilities. Therefore, the performance of the SWCC should be studied in addition to the capability analysis to fit the experimental data.

Material models and model parameters

Minco silt and Speswhite kaolin are used in this study. The range of matric suction is relatively low for the Minco silt compared to the Speswhite kaolin. Soil is a non-linear elastoplastic material and shows nonlinear behavior stating from small strain. Therefore, linear elastic approximation does not represent the actual stress-strain relationship especially in large strain range. However, for verifications purposes, such as the problems presented here, linear elastic model is simple and numerically stable and analyzing the results of linear elastic predictions is easy compared to elastoplastic models. Although an elastoplastic material model based on bounding surface concept (Muraleetharan and Nedunuri 1998) for unsaturated soil is available in the simulation tool, the linear elastic

model is used to avoid any complication arise due to a nonlinear material model. The linear elastic model parameters for the Minco silt and the Speswhite kaolin are listed in Table 7.2.

Table 7.2 Linear elastic model parameters for Minco silt and Speswhite kaolin

Properties			Value	
			Minco silt	Speswhite kaolin
Solid grain density		Mg/m^3	2.67	2.62
Liquid density		Mg/m^3	1.0	1.0
Gas density	$x10^{-3}$	Mg/m^3	2.1	2.1
Bulk modulus of liquid	$x10^6$	*kPa*	2.2	2.2
Bulk modulus of gas		*kPa*	101.325	101.325
Young's Modulus	$x10^5$	*kPa*	1.2	0.3
Poisson's ratio			0.3	0.2

The SWCC model parameters for Speswhite kaolin were calibrated using laboratory experimental results (Sivakumar (1993). The model parameters for the B-C model are: $\boldsymbol{a}$ = 15 kPa, $\boldsymbol{n}$ = 0.165, irreducible degree of saturation = 0%, for the v-G model are: $\boldsymbol{a}$ = 0.067 kPa^{-1}, $\boldsymbol{n}$ = 2.85, $\boldsymbol{m}$ = 0.058, irreducible degree of saturation = 0%, for the F-X model are: $\boldsymbol{a}$ = 28 kPa, $\boldsymbol{n}$ = 1.65, $\boldsymbol{m}$ = 0.365, *Cr* = 5,000 kPa and for the new model are: $\boldsymbol{a}$ = 60 kPa, $\boldsymbol{n}$ = 1.5, $\boldsymbol{m}$ = 0.385, *Nr* = 2 and the calibrated curves are shown in Figure 7.11.

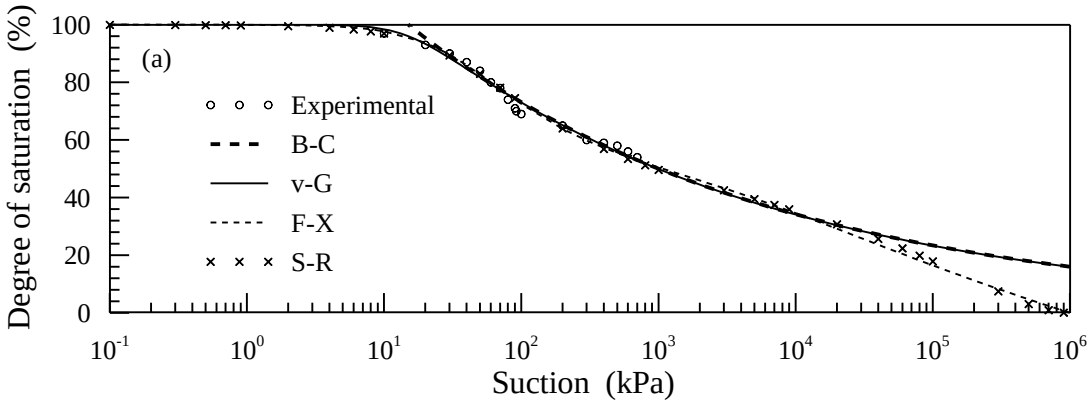

Figure 7.11 SWCC data of Speswhite kaolin fitted with all four SWCC models

The model parameters for Minco silt were calibrated using laboratory experimental results for soil-water characteristics of the Minco silt presented by Ananthanathan (2002). The model parameters for the **B-C** model are: $\boldsymbol{a}$ = 1.75 kPa, $\boldsymbol{n}$ = 0.475, irreducible degree of saturation = 0%, for the v-G model are: $\boldsymbol{a}$ = 0.55 kPa^{-1}, $\boldsymbol{n}$ = 3.5, $\boldsymbol{m}$ = 0.137, irreducible degree of saturation = 0% for the F-X model are: $\boldsymbol{a}$ = 3.25 kPa, $\boldsymbol{n}$ = 1.65, $\boldsymbol{m}$ = 1.05, Cr = 2,500 kPa, and the new model are: $\boldsymbol{a}$ = 5.85 kPa, $\boldsymbol{n}$ = 1.725, $\boldsymbol{m}$ = 1.015, Nr = 2.65 and the calibrated curves are shown in Figure 7.12.

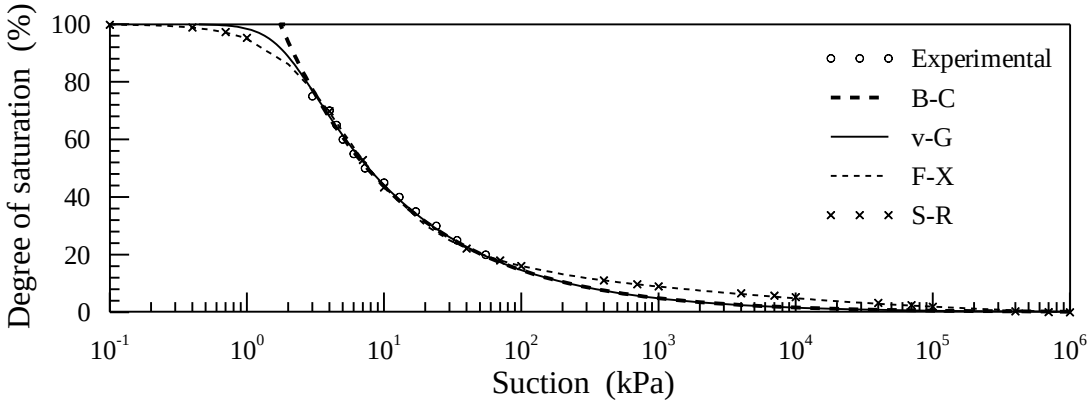

Figure 7.12 SWCC data of Speswhite kaolin fitted with all four SWCC models

Simulation Problem 1: A Four-Element Problem Subjected to Quasi-Static Loading

An arbitrary 2D asymmetric four-element mesh shown in Figure 7.13a is used for the simulation of consolidation problem. The base of the mesh was assumed to be fixed in all direction and the vertical edges assumed to be free to move only in the y-direction throughout the analysis. A vertical displacement time history shown in Figure 7.13b was applied at the top of the mesh (at nodes N1, N2 and N3).

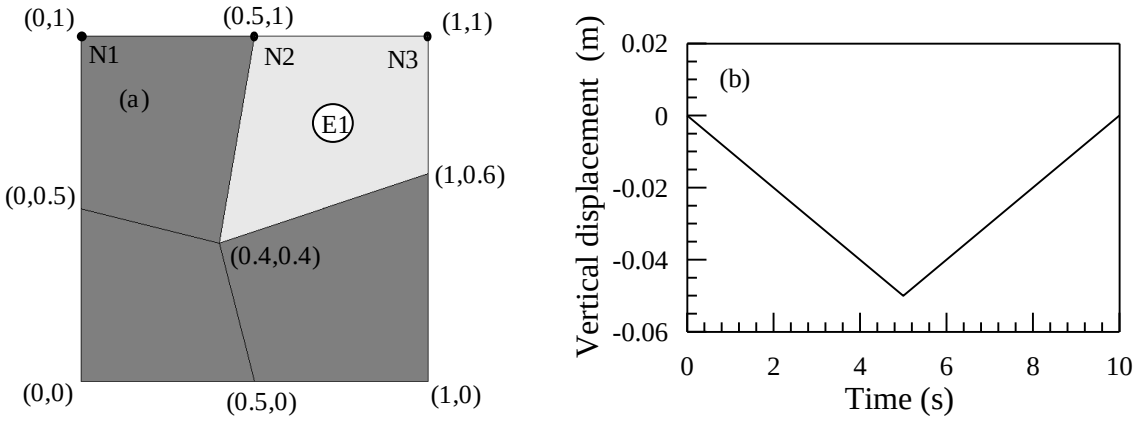

Figure 7.13 FE mesh and the loading history for the problem #1, (a) Asymmetric four element mesh (all dimensions are in meters), (b) Loading

The calculated responses for an initial degree of saturation of 70% are shown in Figure 7.14. The time histories of incremental matric suction and degree of saturation predicted by the finite element program in element E1 are shown in Figures 7.14a and 8.14(b) for Minco silt and Figures 7.14c and 7.14d for Speswhite kaolin. The results show that all four SWCC models predict similar responses for the initial degree of saturation of 70%. For Minco silt, as seen in Figure 7.14a, the B-C model predicts slightly lower incremental suction compared to other models. On the other hand, the B-C model predicts slightly higher suction for Speswhite kaolin. It should be noted that, for

both soils, the difference in suction variation is small. This may be because all SWCCs matched the experimental data well in the range of degree of saturation experienced by the selected element.

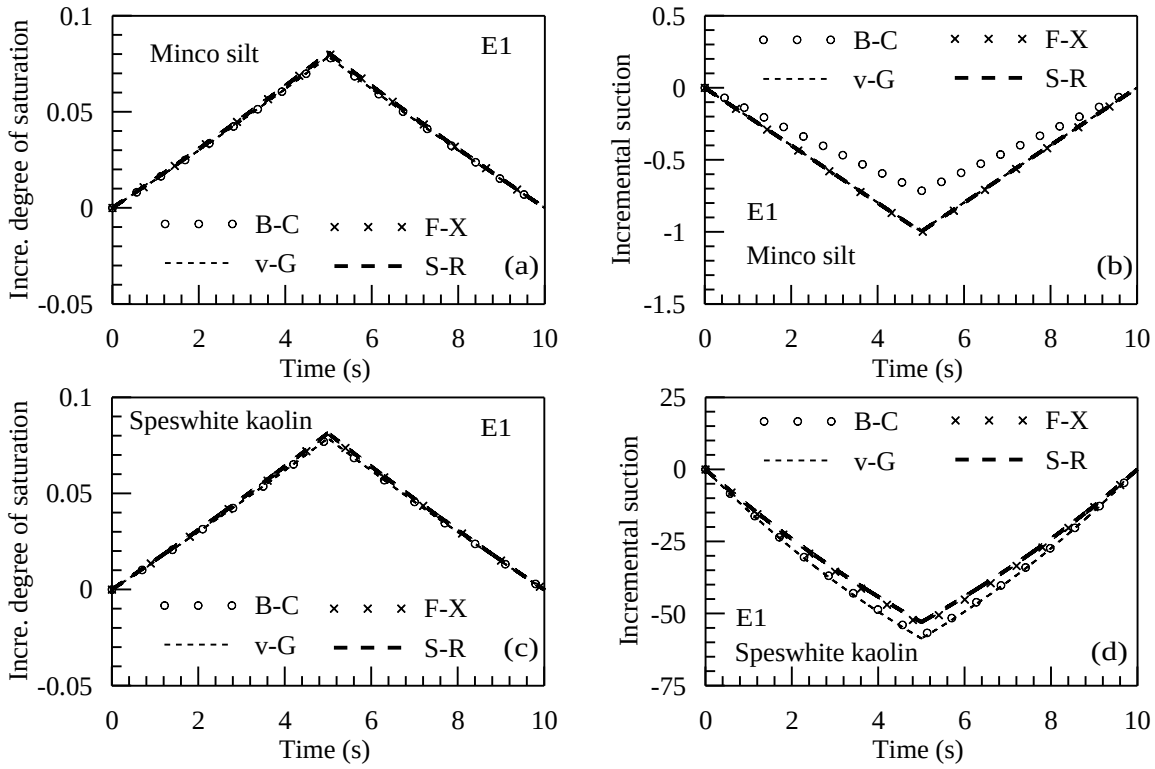

Figure 7.14 Consolidation simulations with 70% initial degree of saturation

Simulation Problem 2: 2D Unsaturated Embankment Subjected to Base Shaking

The 2D finite element mesh of unsaturated compacted embankment is shown in Figure 7.15. The mesh consists of 292 quadrilateral elements. The base of the embankment was assumed to be impermeable and fixed in all directions throughout the analysis. Zero traction was specified for the solid phase on the other sides of the embankment. The acceleration time history shown in Figure 7.16 was applied at the base of the embankment. In this example, simulations were performed with Speswhite kaolin. The performance of all four models in dynamic simulations was investigated with various

initial degree of saturation. However, since these models show significant differences in lower degree of saturation, only the results calculated with 10% initial degree of saturation is presented in this chapter.

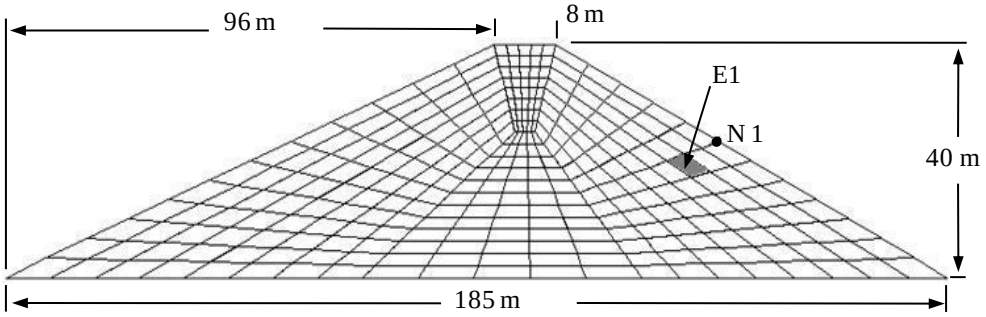

Figure 7.15 The 2D finite element mesh of unsaturated compacted embankment

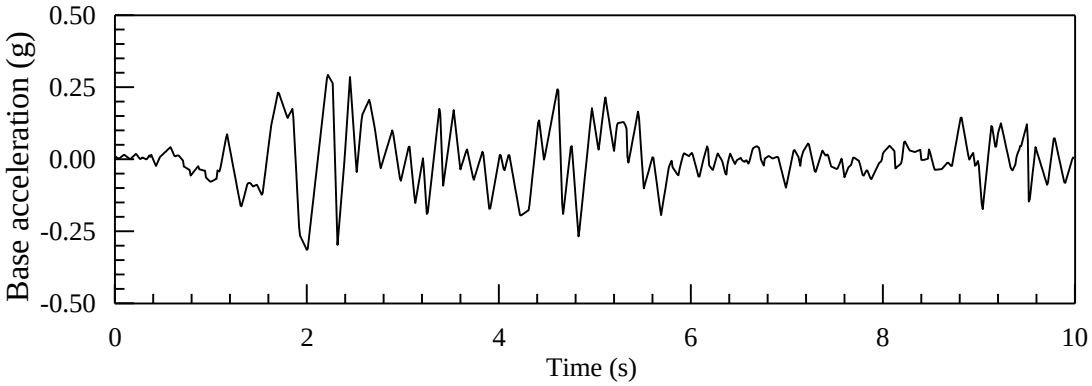

Figure 7.16 The acceleration-time history of applied base motion

The calculated degree of saturation and suction variation in the element E1 (see Figure 7.15) are shown in Figures 7.17a and 7.17b, respectively. The time histories of horizontal and vertical displacements at the node N1 are shown in Figures 7.17c and 7.17d, respectively. As shown in the Figure 7.17a, 7.17b the B-C and v-G models show negligible change in the degree of saturation and a high variation in the suction compared to the suction variation calculated by the S-R-1 and the F-X models. Also the predicted vertical displacement time histories are not identical for all four models.

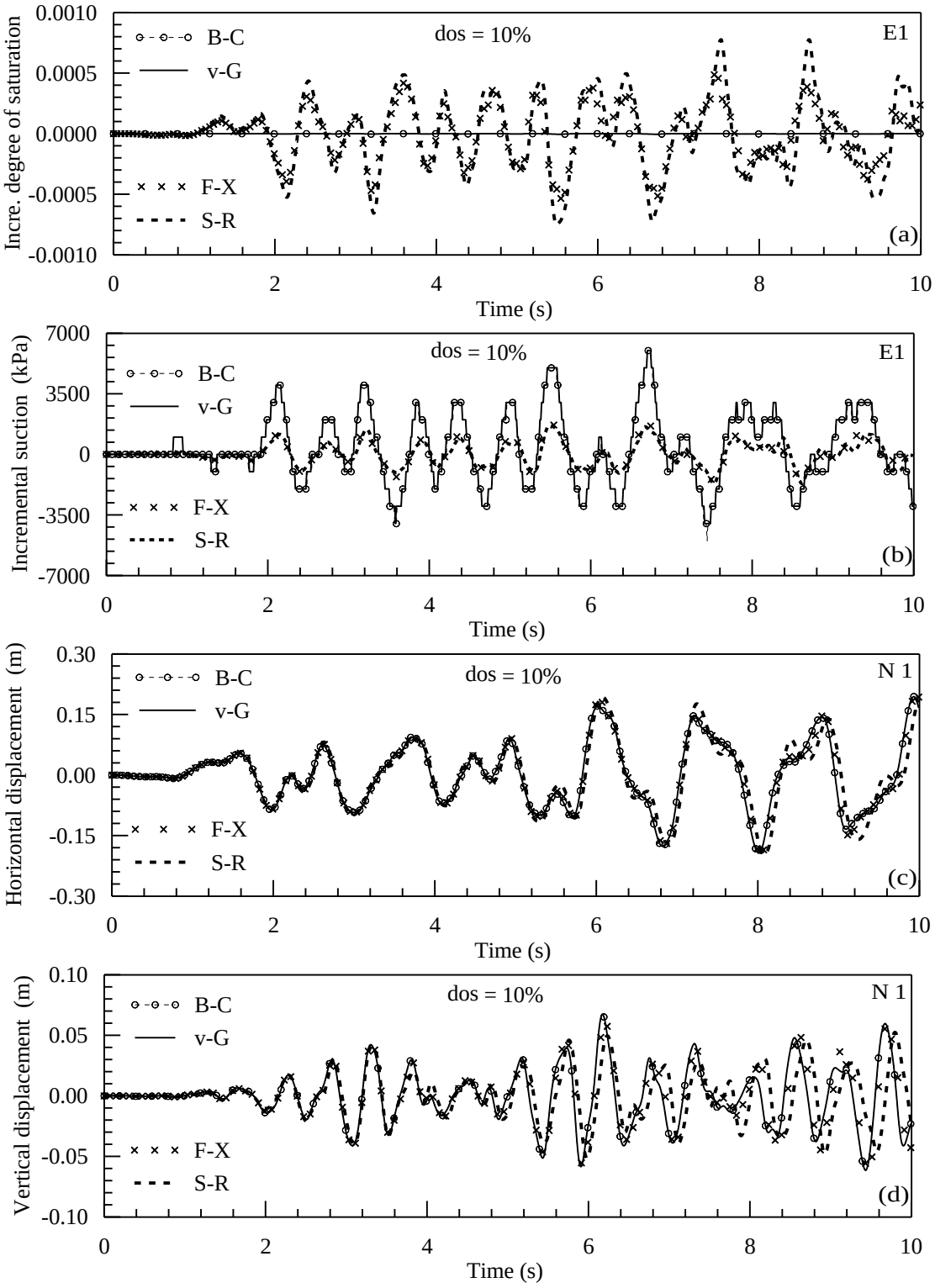

Figure 7.17 Embankment simulations with 10% initial degree of saturation

The effect of initial degree of saturation on the dynamic response of the compacted embankment is examined by finite element simulation that uses the proposed model to relate the moisture-suction relation. The predicted time histories of matric suction, degree of saturation in the element E1 shown in Figure 7.18. As shown in Figure 7.18a, higher variation in the degree of saturation is predicted for the soil with 70% of initial degree of saturation. However, the calculated suction variation for 70% initial degree of saturation is negligible compared to the variation calculated for 10% of initial degree of saturation. This is mainly due to the effect SWCC i.e., at low degree of saturation, a small change in degree of saturation shows very large change in suction (see Figure 7.12). The horizontal and vertical displacement time histories at node N1 are shown Figures 7.18c, 7.18d. Simulations with higher initial degree of saturation shows softer response as expected.

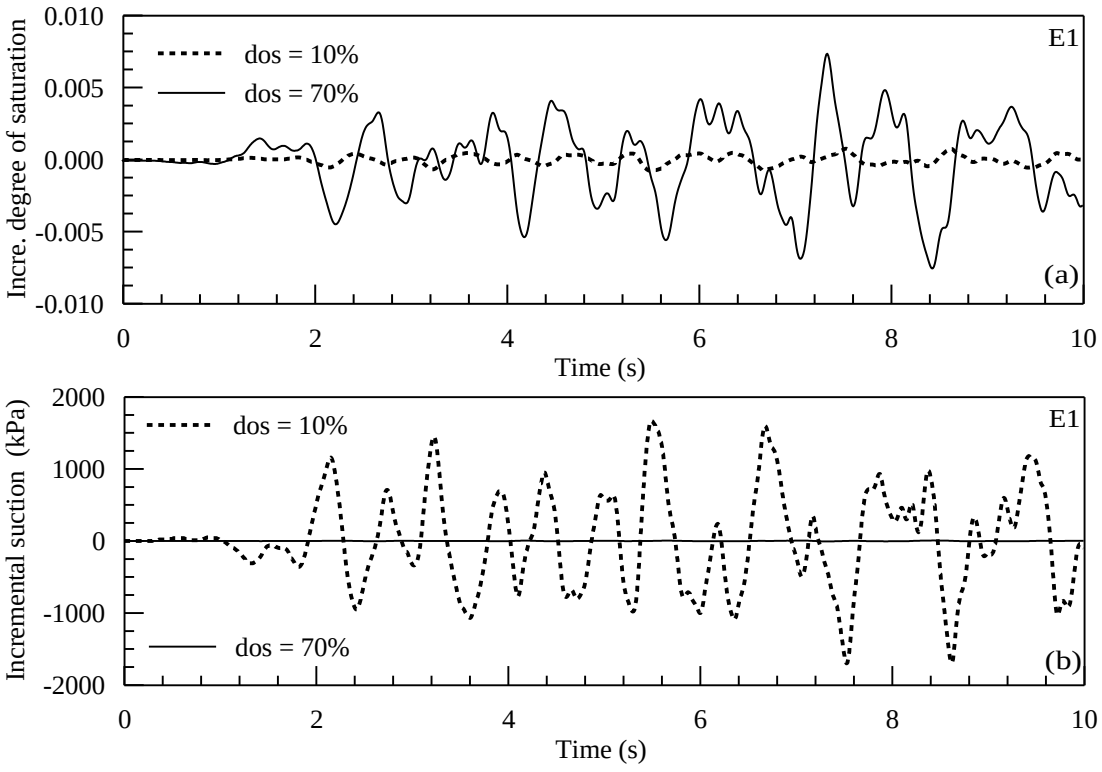

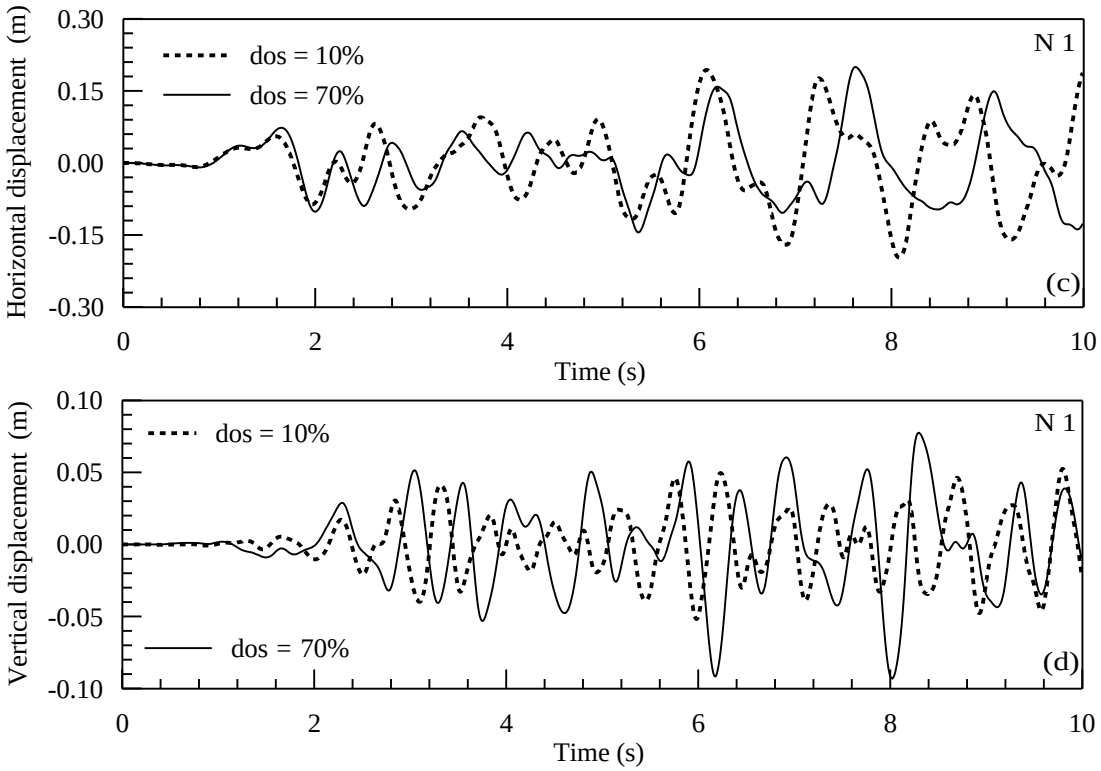

Figure 7.18 Simulations with 10%, 70% degrees of saturation using the S-R-1 model

Dependency of Fitting Parameters in the S-R-1 and the other SWCC Models

In the S-R-1 and other popular SWCC models, the fitting parameters have a physical meaning. In all these models, the parameter ***n*** is related to the pore-size distribution, and thus the value of ***n*** varies with soil type. For sandy soils the ***n*** will be relatively higher (just about 6 or more) and for clayey soils it will be approximately less than 3. The parameter ***a*** is related to the air-entry suction in all four models, thus the curve can be moved along the suction axis by changing the ***a***. However, unfortunately the fitting parameters are not independent in all these models. For example, same curves with different ***n*** values can be achieved by increasing the ***a*** and ***m*** simultaneously. When the value of ***m*** changes, the slope of the curve will change slightly and the curve will also

move along the suction axis. Therefore the ***a*** and ***n*** values have to be re-adjusted to fit the experimental data. The initiation point of the desaturation zone (see Figure 7.1) is the actual air-entry suction. However in v-G, F-X, and S-R-1 models, the predicted ***a*** value will be within the desaturation zone, i.e. parameter ***a*** will not be equal to the actual air-entry suction. It is another disadvantage of v-G, F-X, and S-R-1 models. In the F-X model, the parameter C_r will affect the initial portion of the curve when the C_r value is relatively small. So, it will further increase the dependency of the fitting parameters or it will increase the number of parameter combinations. Therefore, a new SWCC model with independent fitting parameters is should be developed.

A New SWCC Model with Independent Fitting Parameters (S-R-2 Model)

A new SWCC model with independent fitting parameters is developed and expressed in Equation 7.10. In this model, the actual air-entry suction is also included as a model parameter.

$$\frac{\theta-\theta_r}{\theta_s-\theta_r} = \frac{N(\psi)}{\left(1+\ m\ln\left(1\ +\ \frac{1}{m}\left(\psi/a\psi_{aev}\right)^n\right)\ \right)^{0.5}} \tag{7.10}$$

$$N(\psi)\ =\ 1\ -\ \left(\frac{N_r}{N_r\ -\ 1\ +\ \psi_{max}/\psi}\right)^{0.5}$$

where ***a***, ***n***, ***m***, and N_r are the fitting parameters; ψ_{aev} is the actual air-entry suction, ***a*** is a non-dimensional parameter that represents the ratio between the air-entry suction and the suction at inflection point in the curve. The parameter ***n*** is related to the pore-size

distribution of the soil, and ***m*** is related to asymmetry of the model. ψ is the suction, ψ_{max} is the maximum suction or suction at zero normalized water content, and N_r is a number related to residual water content. The function $N(\psi)$ does not affect the initial portion (portion in the low suction range) of the curve. The effect of $N(\psi)$ over a range of N_r value (0 to 10) is discussed in the subsequent sections.

Role of the Fitting Parameters of the S-R-2 Model

Understanding the role of each parameter in the analytical model is important to fit the experimental data well and to obtain the best set of parameters. A detailed discussion based on the parametric studies performed upon the role of each parameter is presented below.

Parameter ***a***

The parameter ***a*** is the ratio between the actual air-entry suction of the soil and the suction at the inflection point of the SWCC. The effect of parameter ***a*** on the shape of the S-R-2 SWCC model is shown in Figure 7.19. In the case of B-C, v-G and F-X models, the curve can be shifted along the suction axis by increasing ***a***. However, in the proposed model, ***a*** must be first adjusted until the initiation point of the desaturation zone matches the air-entry suction (ψ_{aev}) of the soil. For sandy soils, since the slope of the curve is steeper, the value of ***a*** will be relatively small (ranges between zero and two). For clayey soils the slope is mild and the value of ***a*** is higher than five. For silty soils, the value of ***a*** falls between the values of clayey and sandy soil (approximately between 1 and 5).

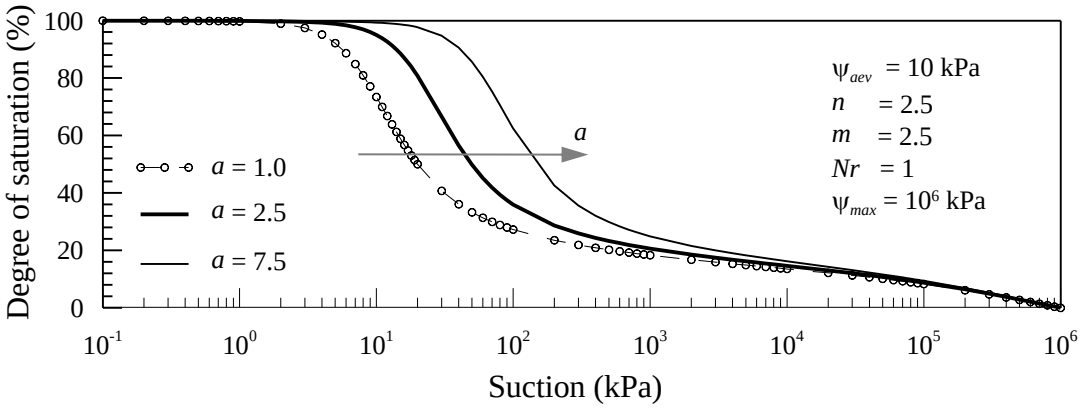

Figure 7.19 Role of the fitting parameter ***a*** in the S-R-2 model

Parameter ***n***

The influence of the parameter ***n*** in the shape of the S-R-2 SWCC is shown in Figure 7.20. As seen here, ***n*** changes the slope of the curve about the inflection point. When ***n*** increases the degree of saturation at a given suction will increase if the suction is greater than $a\psi_{aev}$, and the degree of saturation will decrease if the suction is less $a\psi_{aev}$.

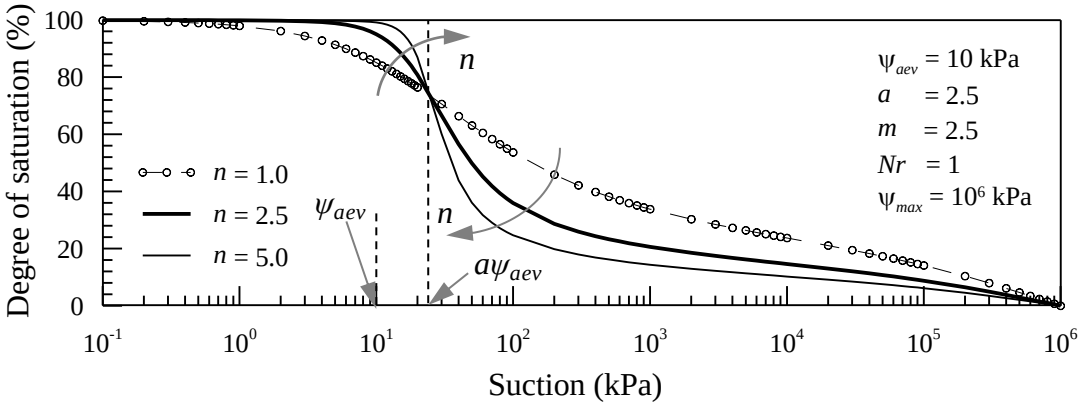

Figure 7.20 Role of the fitting parameter ***n*** in the S-R-2 model

Parameter ***m***

Influence of ***m*** in the shape of the S-R-2 model is shown in Figure 7.21. As seen here, ***m*** in the S-R-2 model does not affect the curve when the suction is within **0** and $a\psi_{aev}$. This indicates that the parameter ***m*** does not alter the shape of the curve that may

require re-adjustment of the parameters ***a*** and ***n***. On the other hand, the parameter ***m*** in the v-G, F-X, and S-R-1 models alters the slope of the curve. This requires readjustment of ***a*** and ***n*** to fit the experimental curve. This not only requires a tedious calibration procedure, but results in multiple possible combinations of model parameters and difference in finite element simulation results for the same soil.

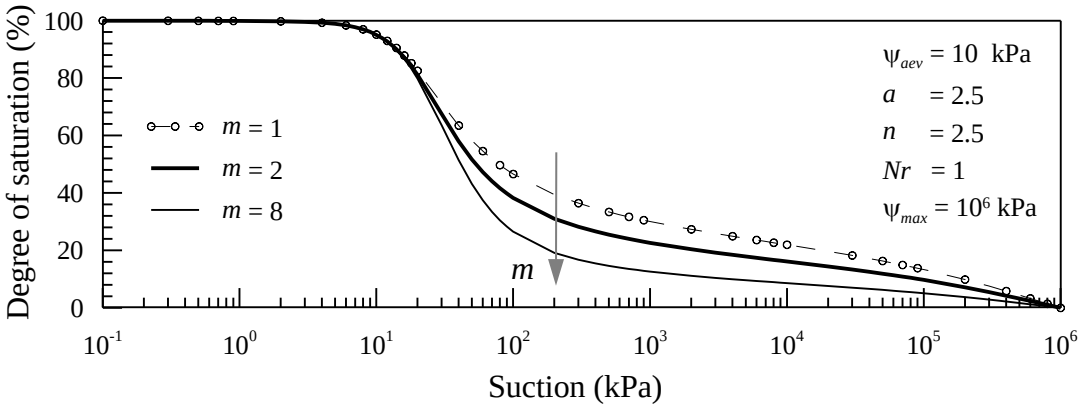

Figure 7.21 Role of the fitting parameter ***m*** in the S-R-2 model

Parameters N_r

The influence of the parameter N_r, a parameter in the correction factor in the new model, in reaching the specified maximum suction is shown in Figure 7.22. As mentioned previously, one of the advantages of the S-R-2 model is the use of maximum suction as a model parameter in which maximum suction must be obtained from experimental results and used in the modeling. In the example shown in Figure 7.22, a maximum suction of 10^6 kPa is used. As seen there, because the parameter N_r does not affect the initial portion (capillary saturation, desaturation zones) of the curve, the effect of N_r on the other model parameters is insignificant.

As shown in Equation 7.10, the correction factor $N(\psi)$ must be 1.0 to use the residual water content concept. Setting $\boldsymbol{N_r}$ equals to zero (given that ψ is not equal to ψ_{max}) can yield this correction factor. Based upon our experience, $\boldsymbol{N_r}$ varies within 1.0 and 5.0 for any soil.

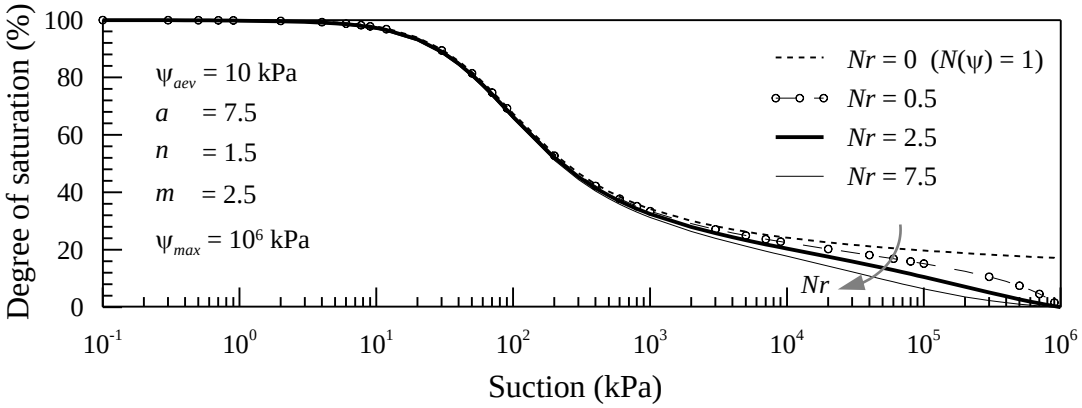

Figure 7.22 Role of the fitting parameter $\boldsymbol{N_r}$ in the S-R-2 model

Predictive Capability of the S-R-2 Model

The capability of the S-R-2 model in predicting the moisture-suction relation for six different soils that include sands, silt and clays is investigated presented in Figures 7.23a through 8.23f. The predicted SWCC without the correction factor $N(\psi)$ is also presented. Figures 7.23a and 7.23b show the calibration of S-R-2 model for Superstition sand (data - Richards 1952) and Lakeland sand (data - Elzeftawy and Cartwright 1981), respectively. Figure 7.23c shows the calibration of SWCC model parameters for Touchet silt loam (data - Brooks & Corey 1964).

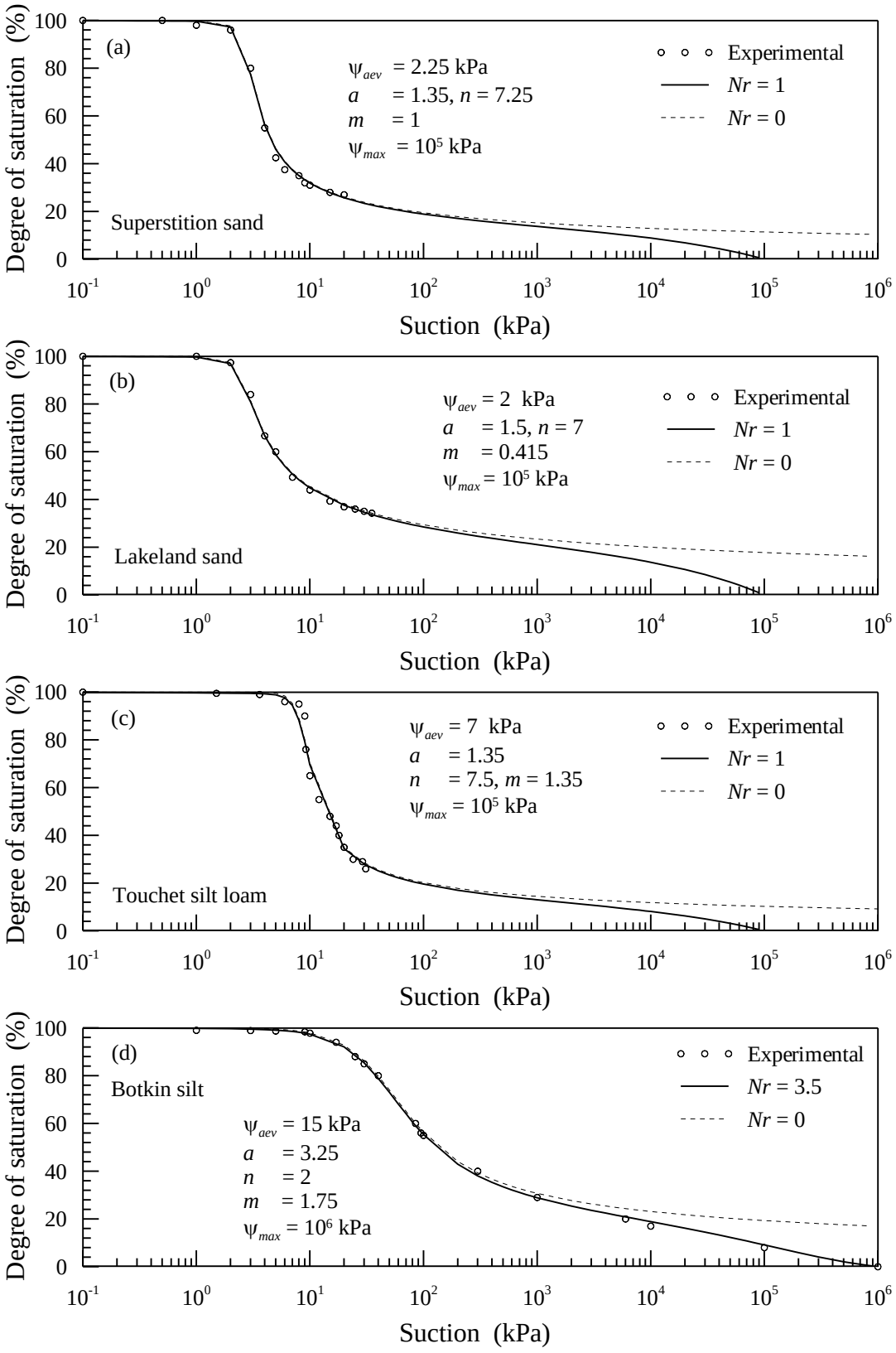
(a)
ψ_{aev} = 2.25 kPa
a = 1.35, n = 7.25
m = 1
ψ_{max} = 10^5 kPa
Experimental
Nr = 1
Nr = 0
Superstition sand
Degree of saturation (%)
Suction (kPa)
(b)
ψ_{aev} = 2 kPa
a = 1.5, n = 7
m = 0.415
ψ_{max} = 10^5 kPa
Lakeland sand
(c)
ψ_{aev} = 7 kPa
a = 1.35
n = 7.5, m = 1.35
ψ_{max} = 10^5 kPa
Touchet silt loam
(d)
Botkin silt
ψ_{aev} = 15 kPa
a = 3.25
n = 2
m = 1.75
ψ_{max} = 10^6 kPa
Nr = 3.5

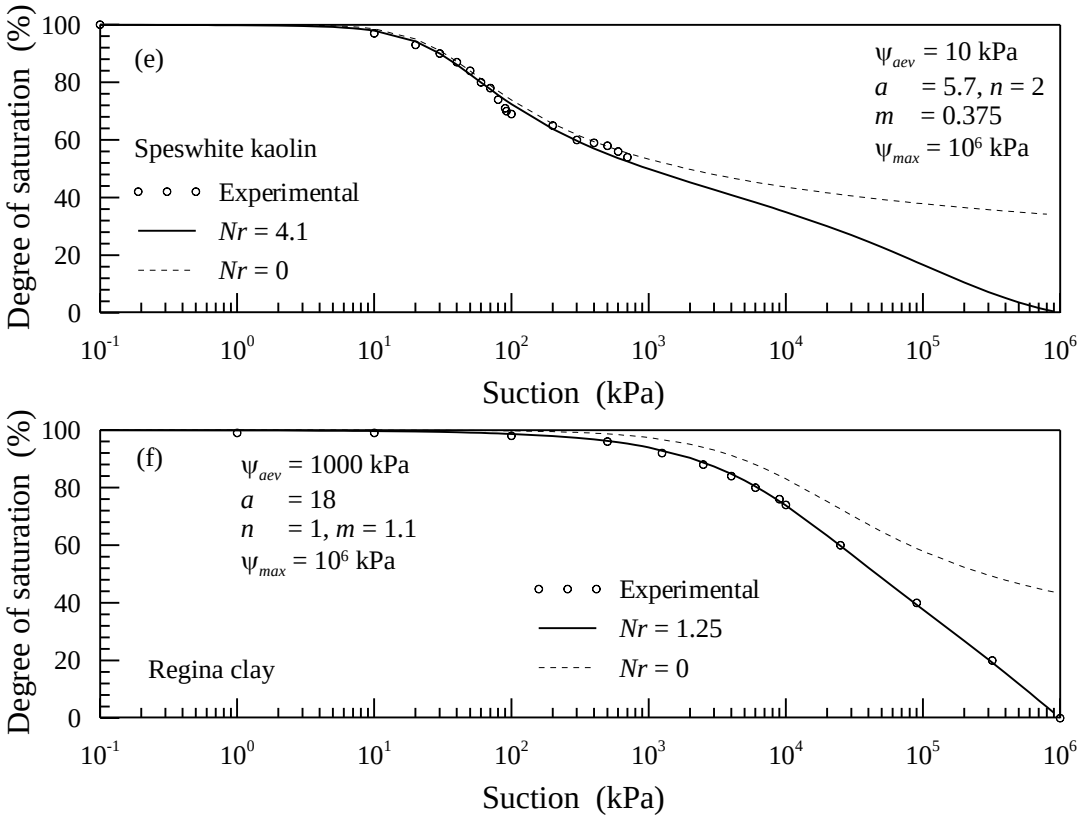

Figure 7.23 SWCC data of various soils fitted with the S-R-2 model

Figure 7.23d shows the calibration of SWCC model parameters for Botkin silt (data - Vanapalli et al. 1999). Figures 7.23e and 7.23f show the calibration of SWCC model parameters for Speswhite kaolin (data - Sivakumar 1993) and Regina clay (data - Vanapalli et al. 1999), respectively. The air-entry suction (ψ_{aev}) and maximum suction (ψ_{max}) for each soil are selected based on the variation of available experimental data.

These results show that the S-R-2 model is effective and flexible enough to fit the experimental data. The number N_r in the new model can be chosen between 1 and 5 for any soil and the correction factor $N(\psi)$ does not affect the initial portion of the curve. The S-R-2 model can be effectively used with either the residual water content concept or with a maximum suction value. In addition to eliminating the dependency of fitting

parameters, the S-R-2 model includes all the advantages of the B-C, v-G, F-X, S-R-1 models. The performance of the S-R-2 model in finite element simulations is investigated by simulating the same problem used for S-R-1 model.

Performance of the S-R-2 Model in Finite Element Simulations

To show the influence of various SWCC models, the dynamic behavior of a compacted earthen embankment made of Speswhite Kaolin subjected to earthquake shaking was simulated using TeraDysac. Since this problem is already described under the S-R-1 model, additional details are not presented here.

Simulations were performed using B-C, v-G, F-X and the S-R-2 models. The SWCC model parameters were calibrated against the experimental data published by Sivakumar (1993). For the S-R-2 model, the parameters are calibrated as follows: $\boldsymbol{\psi_{aev}}$ = 10 kPa, $\boldsymbol{a}$ = 5.7, $\boldsymbol{n}$ = 2, $\boldsymbol{m}$ = 0.375, Nr = 4.1, and $\psi_{max} = 10^6$ kPa. The air-entry suction ($\boldsymbol{\psi_{aev}}$) and the maximum suction (ψ_{max}) values were selected based on experimental data.

As mentioned previously, all the models predict identical responses when the degree of saturation falls in the mid range (30-70%) and show significant differences or become inapplicable in low and/or high degree of saturation range. Therefore, initial degree of saturations of 10% and 90% were selected for the finite element simulations. The degree of saturation corresponding to the residual water content (irreducible degree of saturation) is set to be zero in the B-C and v-G models to simulate identical soil condition in all four models.

The predicted incremental suction time histories in element E1 (see Figure 7.15) are presented in Figure 7.24. As shown in the figures, while the initial degree of saturation

increases the initial suction and the suction variation due to external loading decrease. The comparison study shows that the results predicted using the v-G, F-X models are close for an initial degree of saturation of 90%, the B-C model predicts slightly lower suction variation as shown in Figure 7.24b. As seen in Figure 7.24a, significant differences are observed when the initial degree of saturation is 10 %. At 10% initial degree of saturation, the S-R-2 and the F-X models predict close responses, but the other two models predicts relatively very high suction variation. The accuracy of the predicted response could not be verified due to the lack of experimental results. However, this finite element simulation study shows that the S-R-2 model is numerically stable and can be effectively used to capture the moisture-suction variation with wide range of initial degree of saturation, especially at low degrees of saturation.

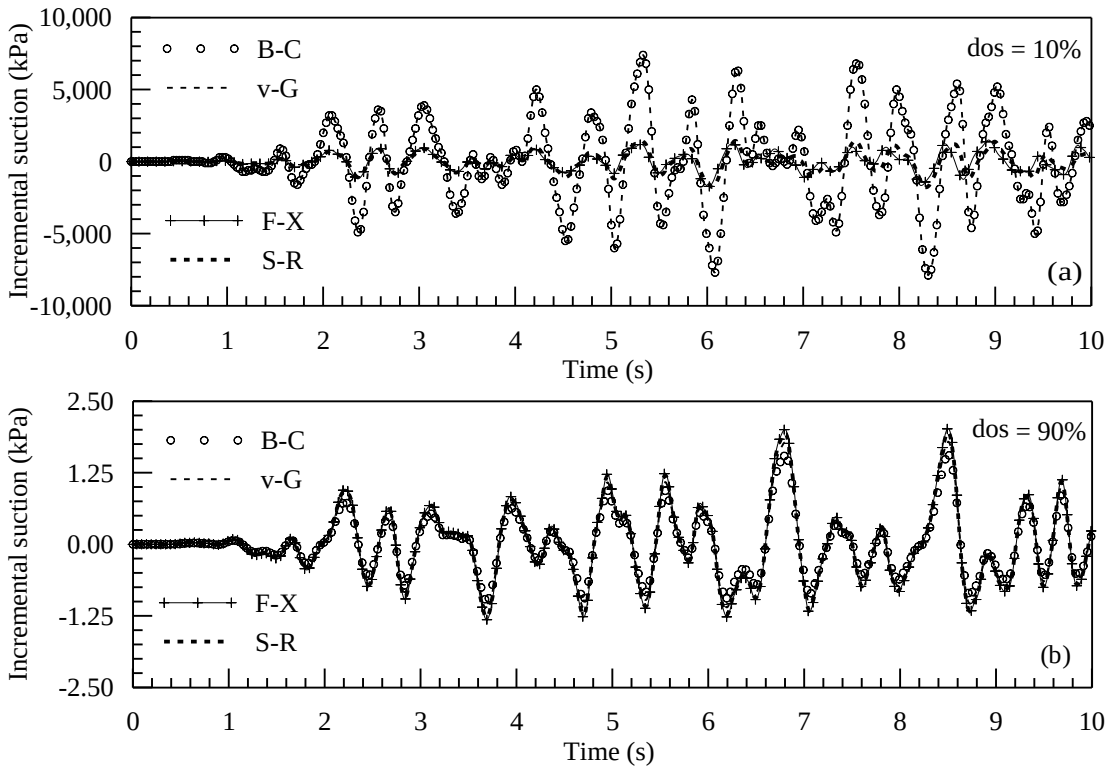

Figure 7.24 Simulations using the S-R-2 and other popular models

Another Form of the S-R-2 Model with Reduced Number of Fitting Parameters

To reduce the numbers of fitting parameters of the S-R-2 model, another form of S-R-2 SWCC model is developed and expressed as S-R-3 model in Equation 7.11. In this model, the parameter *Nr* is replaced with (***m*** +1). Therefore, the only difference between the S-R-2 and S-R-3 is the correction factor *N(ψ)*. In this model also, the actual air-entry suction is included as a model parameter.

$$\frac{\theta-\theta_r}{\theta_s-\theta_r} = \frac{N(\psi)}{\left(1+\ m\ln\left(1\ +\ \frac{1}{m}\left(\psi/a\psi_{aev}\right)^n\right)\right)^{0.5}} \tag{7.11}$$

$$N(\psi)\ =\ 1\ -\ \left(\frac{1+m}{m\ +\ \psi_{max}/\psi}\right)^{0.5}$$

where ***a, n,*** and ***m*** are the fitting parameters; Similar to the S-R-2 model, ψ_{aev} is the actual air-entry suction, ***a*** is a non-dimensional parameter that represents the ratio between the air-entry suction and the suction at inflection point in the curve. The parameter ***n*** is related to the pore-size distribution of the soil. However the parameter ***m*** is related residual water content in this model. ψ is the suction, ψ_{max} is the maximum suction or suction at zero normalized water content.

Role of the Fitting Parameters in the S-R-3 Model

The role of the fitting parameters ***a***, ***n*** in the S-R-3 model is exactly same as the role of those parameters in the S-R-2 model. Even though the parameter *Nr* is replaced with (***m*** +1) in the S-R-3 model, as shown in Figure 7.25, the parameter ***m*** influences the shape of the SWCC curve exactly same as in the S-R-2 model.

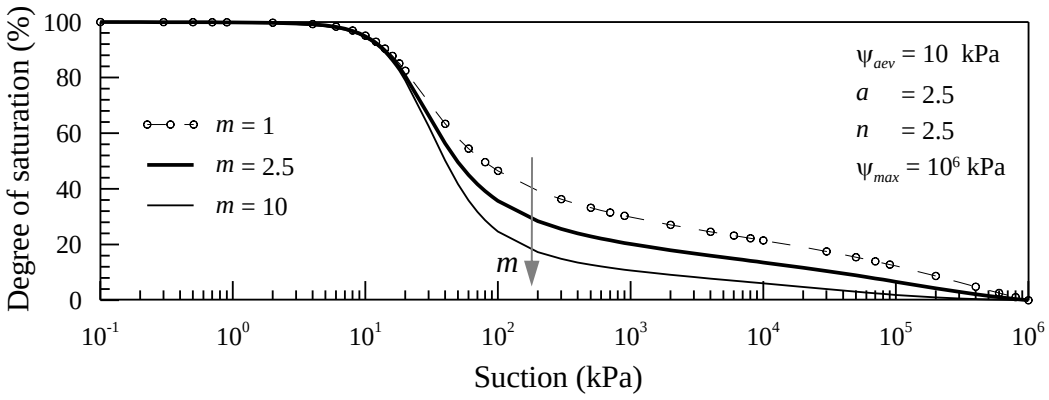

Figure 7.25 Role of the fitting parameter ***m*** in the S-R-3 model

Predictive Capability of the S-R-3 Model

Capability of the S-R-3 model in predicting the moisture-suction relation of different types of soils; Superstition sand, Lakeland sand, Touchet silt loam, Botkin silt, Speswhite kaolin, and Regina clay, is investigated and presented in Figures 7.26a through 8.26f.

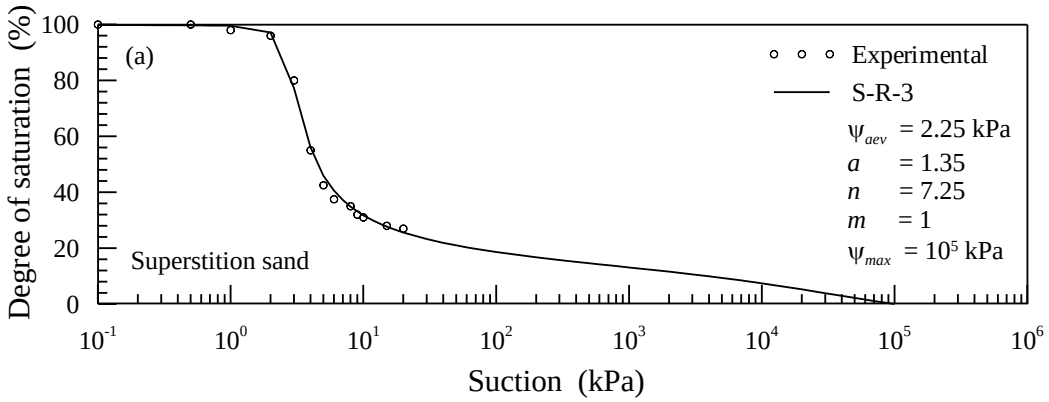

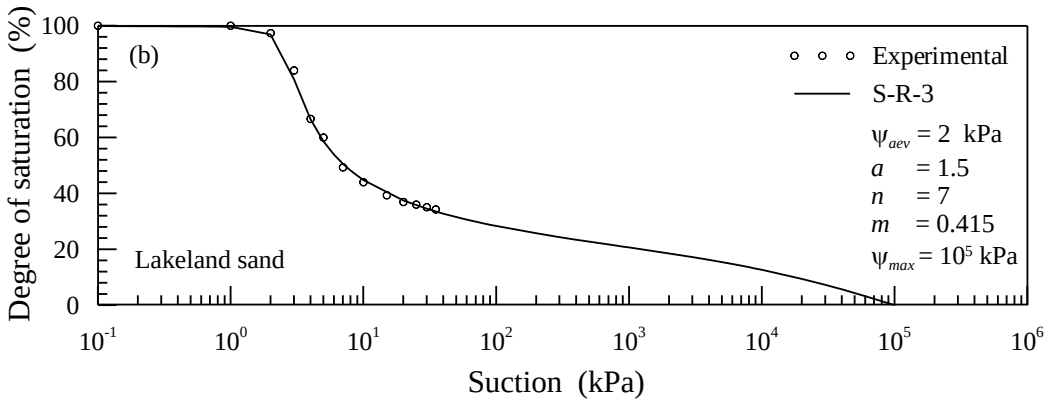

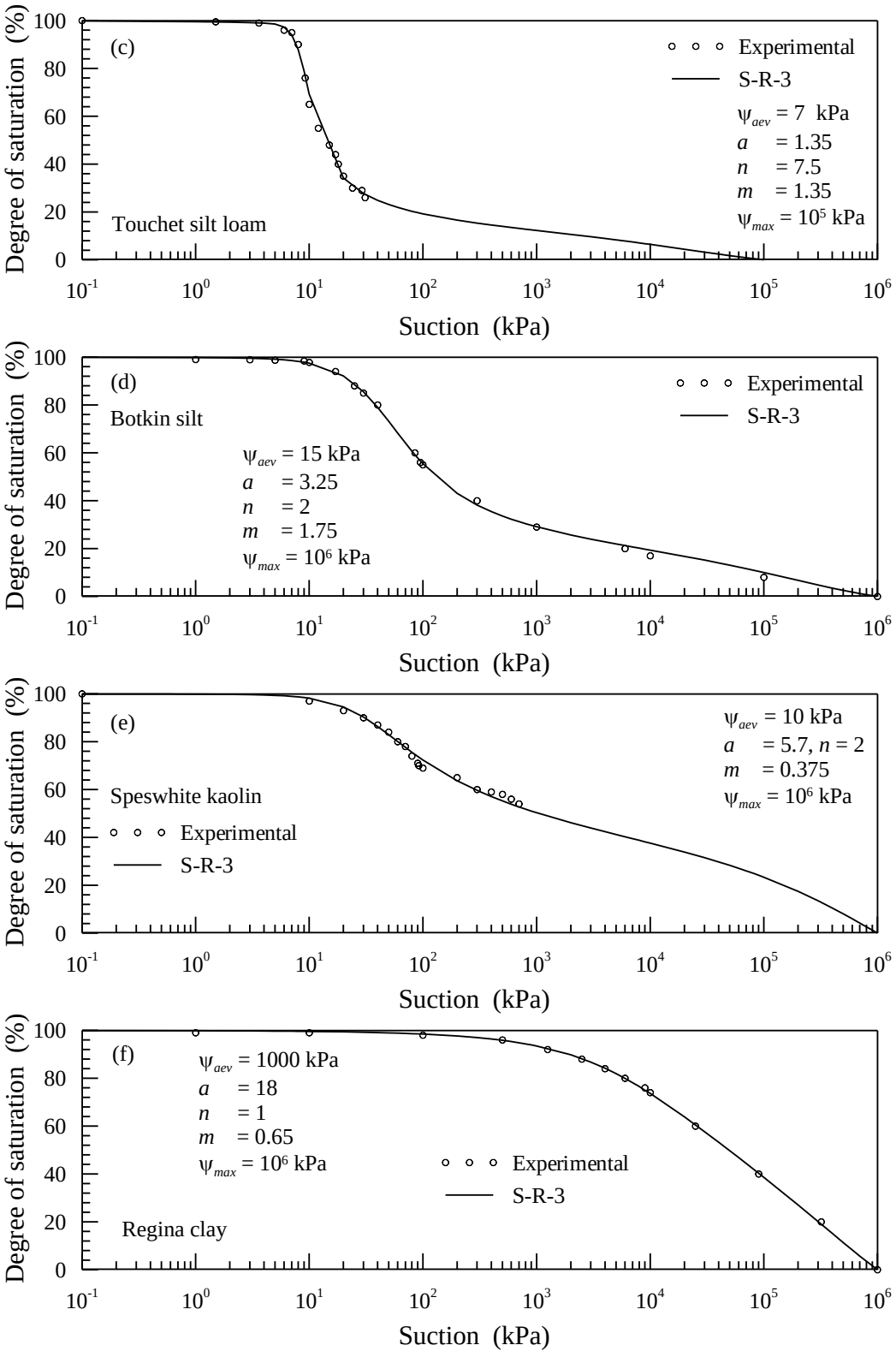

Figure 7.26 SWCC data of various soils fitted with the S-R-3 model

Improving the Performance of Popular SWCC Models and Comparisons

Although there are numerous SWCC models available in the literature, this study is intended to improve the popular B-C, v-G, and F-X models. The B-C and v-G models are modified primarily to make sure that these models no longer calculate infinity/unrealistic suction when the normalized water content is zero or less. And also to make sure that these models have the feature to specify both residual water content and maximum suction values.

Improved Brooks and Corey (I-B-C) Model

The improved Brooks and Corey (I-B-C) model is given in Equation 7.12. To preserve the advantage of the B-C model, no additional fitting parameter is introduced. Even though the maximum suction ψ_{max} is incorporated in the equation, it cannot be considered to be a fitting parameter, as the shape of the SWCC cannot be changed by adjusting the ψ_{max}. The I-B-C model also does not provide a continuous mathematical function for the entire range of dos.

$$\frac{\theta - \theta_r}{\theta_s - \theta_r} = \begin{cases} 1 & if \quad \psi < a \\ \dfrac{C(\psi)}{(\psi / a)^n} & if \quad \psi > a \end{cases} \tag{7.12}$$

$$C(\psi) = 1 - \sqrt{\psi / \psi_{max}}$$

where ψ_{max} is maximum suction and other parameters are same as in the B-C model.

Comparison of the B-C and the I-B-C Models

Capability of the improved B-C (I-B-C) model in predicting the moisture-suction relation is investigated and compared with the B-C model for four different soils. The

comparison of B-C and I-B-C Models for Columbia sandy loam (data - Brooks & Corey 1964) is shown in Figure 7.27. The Figures 7.28 and 7.29 show the comparison for Madrid clay sand and Arlington soil, respectively. The Figure 7.30 shows the comparison for Indian head till (data - Vanapalli et al. 1999).

It should be noted that the experimental SWCC data are not available for the full range of dos (0-100%). Based on the experimental data, the maximum suction of 1,000,000 kPa is chosen for all four soils. The residual water content is assumed to be zero for all four soils. As shown in these figures, the I-B-C model is capable of calculating the moisture-suction relation for full range of dos, whereas the B-C model is not effective. The B-C, I-B-C models are not effective for sandy soils and it is evidently shown in Figure 7.27 as these models failed to keep the SWCC without reaching zero normalized water content in low suction range.

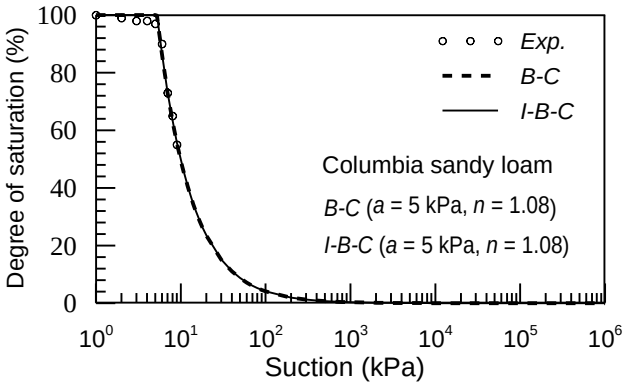

Figure 7.27 B-C and I-B-C SWCCs for Columbia sandy loam

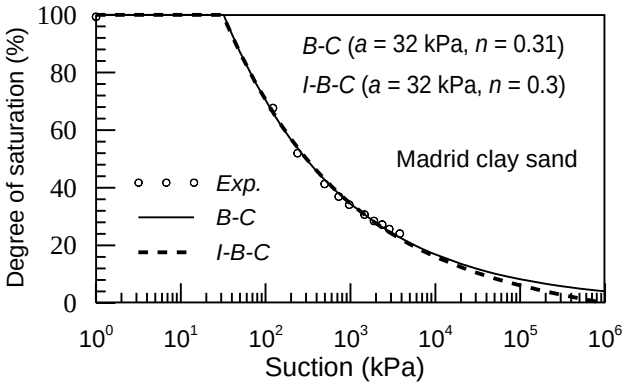

Figure 7.28 B-C and I-B-C SWCCs for Madrid clay sand

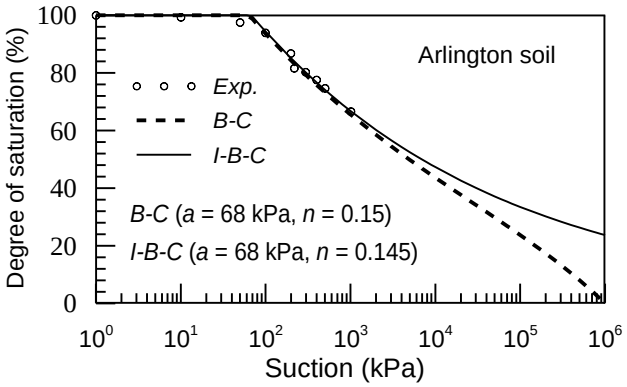

Figure 7.29 B-C and I-B-C SWCCs for Arlington soil

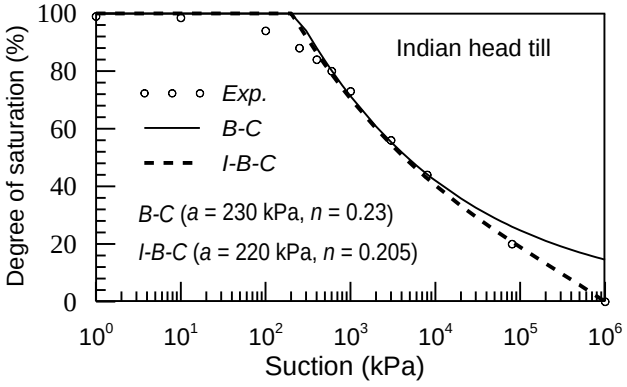

Figure 7.30 B-C and I-B-C SWCCs for Indian head till

Improved van Genuchten (I-v-G) Model

The improved van Genuchten (I-v-G) model is given in Equation 7.13. Since the parameter **a** is related to the air-entry suction, the model is revised so that the parameter **a** has the unit of suction. The I-v-G model is developed with the feature to specify both residual water content and maximum suction value with no additional fitting parameter.

$$\frac{\theta - \theta_r}{\theta_s - \theta_r} = \frac{C(\psi)}{\left(1 + \left(\psi / a\right)^n\right)^m} \tag{7.13}$$

$$C(\psi) = 1 - \left(\frac{m+1}{m + \left(\psi_{max} / \psi\right)}\right)^{0.5}$$

where ψ_{max} is maximum suction and other parameters are same as in the v-G model.

Comparison of the v-G and the I-v-G Models

Capability of the improved v-G (I- v-G) model in predicting the moisture-suction relation is presented for Columbia sandy loam, Madrid clay sand, Arlington soil, and Indian head till in Figures 7.31 through 7.34, respectively. Similar to the I-B-C model, maximum suction of 1,000,000 kPa and residual water content of zero are used for all four soils. As shown in Figures 7.31 through 7.34, the I-v-G model is capable of calculating the moisture-suction relation for full range of dos, whereas the v-G model is not effective. As shown in Figures 7.31, the v-G, I-v-G models are also not suitable for sandy soils as these models also failed to keep the SWCC without reaching zero normalized water content in low suction range.

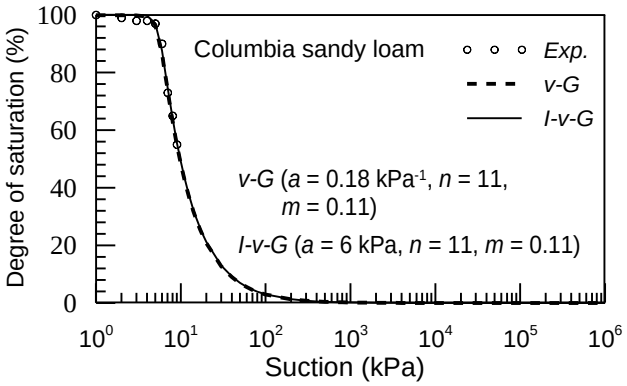

Figure 7.31 v-G and I-v-G SWCCs for Columbia sandy loam

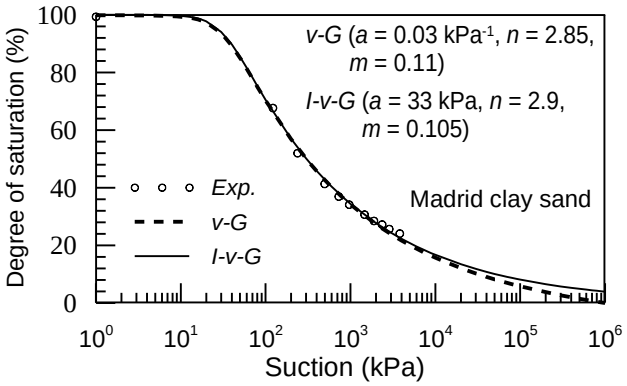

Figure 7.32 v-G and I-v-G SWCCs for Madrid clay sand

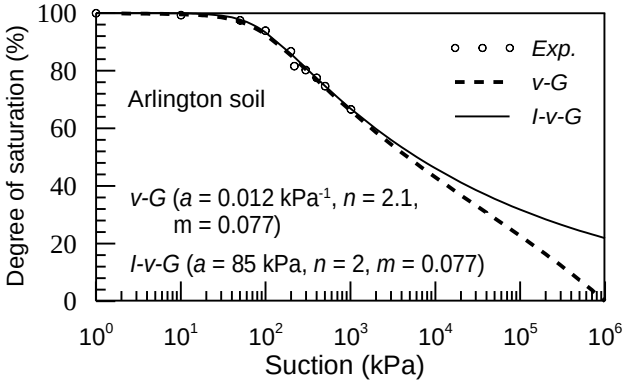

Figure 7.33 v-G and I-v-G SWCCs for Arlington soil

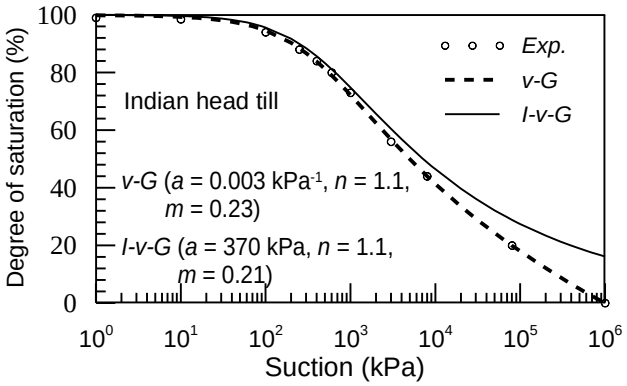

Figure 7.34 v-G and I-v-G SWCCs for Indian head till

Improved Fredlund and Xing (I-F-X) Model

The improved Fredlund and Xing (I-F-X) model is given in Equation 7.14. The I-F-X model is developed with the feature to specify both residual water content and maximum suction value without the parameter C_r, i.e. with only three fitting parameters. Therefore, the effect of C_r in the initial portion of the F-X model (Leong and Rahardjo, 1997) is avoided in the I-F-X model.

$$\frac{\theta - \theta_r}{\theta_s - \theta_r} = \frac{C(\psi)}{\left(\ln\left(e + \left(\psi/a\right)^n\right)\right)^m} \tag{7.14}$$

$$C(\psi) = 1 - \left(\frac{m+1}{m+\left(\psi_{max}/\psi\right)}\right)^{0.5}$$

where all the parameters are same as in the I-v-G model.

Comparison of the F-X and the I-F-X Models

The predictive capability of the I-F-X model in predicting the moisture-suction relation is presented in Figures 7.35 through 7.38. Similar to the I-B-C, I-v-G models, 1,000,000 kPa maximum suction and zero residual water content are used in the

calibration. It can be noted that the I-F-X model is also effective in full range of dos. However the I-F-X model can be considered better as it has only three fitting parameters, whereas the F-X model has four.

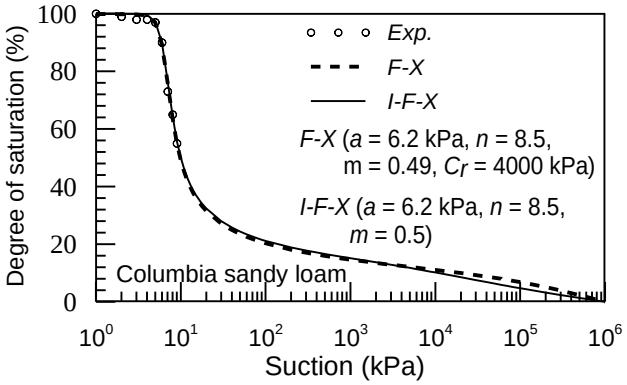

Figure 7.35 F-X and I-F-X SWCCs for Columbia sandy loam

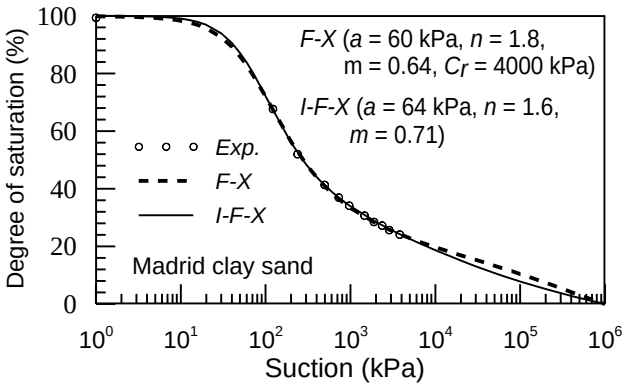

Figure 7.36 F-X and I-F-X SWCCs for Madrid clay sand

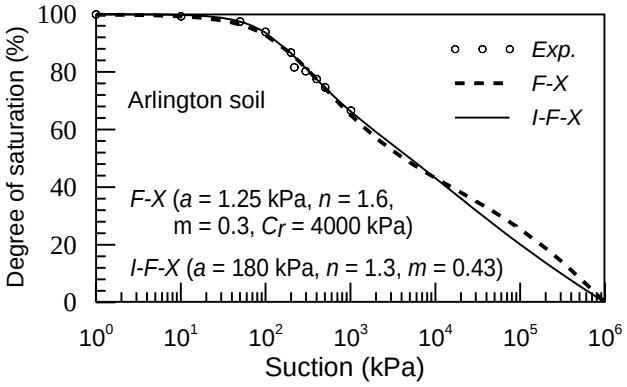

Figure 7.37 F-X and I-F-X SWCCs for Arlington soil

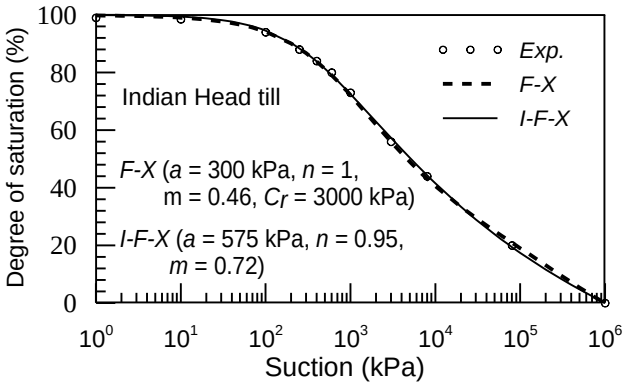

Figure 7.38 F-X and I-F-X SWCCs for Indian head till

Summary of the Study

New mathematical models for the moisture-suction relation of unsaturated soil are developed and their capability to fit experimental data and performance in finite element simulation is examined. The newly developed models are flexible enough to fit with the experimental data in low range of degree of saturation. The new models can be used either with a residual water content (lower bound value for the water potential) or with a maximum suction value (upper bound value) for dry case. If the maximum suction and air entry suctions are available for a soil, this data can be directly used in the proposed model. The performance of the new models is verified by fitting the experimental data of various types of soils. The calibration results show that the new models can be successfully used to model various types of soils over the entire range of degree of saturation without any numerical difficulties. The limitations and the identified issues of the popular SWCC models are now solved with the new models and these models can be effectively used in finite element simulations with low range of degree of saturation.

The finite element simulations conducted using the new SWCC models show that the new models are numerically stable and effective in finite element simulations with low range of degree of saturation. There is no finite element computer code currently available to model the soil behavior from fully dry condition to fully saturated condition. Three inadequacies: difficulties in dealing with multiple nodal variables in the finite element formulation of porous media at these extreme conditions, difficulties in developing stress-strain behavior with appropriate stress state variables at these extreme conditions, and difficulties in accurately calculating the suction at these extreme conditions have prevented the development of such a computer code. In this study, an attempt is made to solve the third difficulty.

The popular B-C, v-G, and F-X SWCC models are also revised to improve their predictive capabilities. The modified SWCC models have the features to specify residual water content and maximum suction values. The performance of the improved models is compared with the prediction of original models and experimental data for four different soils. The comparison study shows that the improved model can be successfully used to model the SWCC of various types of soils over the entire range of degree of saturation.

Suggestions

In finite element simulations, the permeability of unsaturated soil is being calculated using SWCC models. Therefore to ensure or enhance the applicability of the newly developed S-R SWCC models, it is important to develop a permeability model which can be used with the S-R SWCC models.

CHAPTER EIGHT

PERMEABILITY MODELS OF UNSATURATED SOILS AND THE DEVELOPMENT OF A NEW MODEL

Introduction

Engineering problems involving unsaturated soils span numerous sub-disciplines and practices within the general field of civil engineering. These sub-disciplines include hydrology, soil mechanics and soil physics. Modeling of surface and ground water is one of many such examples that require an interdisciplinary approach necessary to accurately elucidate soil behavior. Modeling such problems requires a better understanding of the infiltration of water into the soil, surface runoff, evaporation, and transpiration processes. Other examples that involve unsaturated soil and related to soil mechanics are; contaminant transport through soil, earth slope failure after extended periods of rainfall, seepage through earthen structures, and shrinking and swelling of problematic fine grained soils. Soil expansion, which has been the subject of much unsaturated soil research, poses severe threat to civil engineering infrastructures such as roads, housing, and other transportation facilities. All of these problems share a single commonality: movement (flow) of fluid. The ability of a fluid to move through a given soil is measured by its permeability. Therefore, accurate evaluation of the permeability is important for accurate modeling of the flow, stress and deformation behavior of unsaturated soil.

In the case of saturated soil with void spaces completely filled with a single fluid (water), the coefficient of permeability is correlated to the void ratio and/or the

parameters of the particle size distribution curve such as effective size, D_{10} and uniformity coefficient C_u (Hazen, 1930; Chapuis, 2004) of the soil. On the other hand, the permeability of unsaturated soil with voids filled with multiple fluids is affected not only by the void ratio but also by the degree of saturation of the interested fluid (Lloret and Alonso, 1980). Compared to a pure flow problem, a coupled flow-deformation problem of unsaturated soil is most involved. This complexity is because the volumetric deformation of the solid skeleton, due to external load, can change both the void ratio and degree of saturation of the soil. For example, a reduction in void volume will increase the volumetric water content, thusly increasing the permeability coefficient. It is observed that the permeability coefficient of unsaturated soil varies by an order of magnitude of 10 when the degree of saturation of the soil varies from very low to very high (Fredlund et al., 1994). It should be noted that in most of the finite element simulations of saturated or unsaturated soils, the change in permeability due to the deformation of the solid skeleton is never considered.

The permeability of unsaturated soil is related to volumetric water content, thus the soil-water characteristic curve (SWCC) can be used to predict the permeability coefficient. The SWCC is a relationship between volumetric water content and matric suction that also incorporates the basic soil properties associated with flow, such as the void ratio. Therefore, the permeability coefficient of unsaturated soils can be related to the either the matric suction or volumetric water content variable. When using finite element simulations of unsaturated soil the matric suction is either calculated directly from primary nodal solutions; or through SWCC when the degree of saturation or the

volumetric water content is calculated using secondary solutions. Therefore, it is easy to calculate the permeability coefficient using the matric suction or the volumetric water content in a finite element simulation. Another advantage of using the matric suction-water content variable is that the matric suction is one of the two widely used stress-state variables in unsaturated soil theories.

To simulate a realistic flow behavior by means of numerical tool, it is necessary to have an effective mathematical formula to estimate the permeability-volumetric water content relationship. Such mathematical expressions should also be elemental enough for implementation in a bigger parent finite element or finite difference model and stable enough to avoid numerical instabilities during the simulations, especially in coupled nonlinear problems subjected to complex loading and boundary conditions. In this study, a new relative permeability function for unsaturated soils is developed using the SWCC of the soil. The proposed relative permeability function uses the model parameters of the S-R SWCC models. The predictive capability is verified using experimental data of eight different soils. A comparison with the predictions of the Fredlund method (Fredlund et al., 1994) is also presented. The predictions and the comparisons show that the proposed model accurately predicts the measured permeability data over a wide range of saturation.

Popular Permeability Models/Functions of Unsaturated Soils

Variety of mathematical permeability functions has been developed to predict the permeability of water in unsaturated soil. These models either uses certain model parameters or predicts the permeability function directly from soil-water characteristic curves or other constitutive functions of unsaturated soils. Based on the modeling

techniques, all the currently available permeability models can be classified into three: (a) empirical models, (b) macroscopic models and (c) statistical models.

Empirical Models

The permeability of unsaturated soils is affected by degree of saturation, void ratio, and pore size distribution (Lobbezoo and Vanapalli, 2002) and it is expressed as a scalar product of saturated permeability tensor (k_s) and relative permeability (k_r). This empirical technique is purely a data-driven method. Here, the unsaturated permeability is expressed as a function of saturated permeability and certain fitting parameters of an equation. The fitting parameters depend upon the shape of the experimental curve (Richards, 1931; Wind, 1955; Gardner, 1958; Brooks and Corey, 1964; Rijtema, 1965; Davidson et al., 1969; Campbell, 1973) and are adjusted to match the experimental curve with the empirical equation. Numerous experimental data sets that cover a large spectrum of degree of saturation/suction are required to develop an advanced permeability function. It should be noted that most of the existing unsaturated permeability functions fit well with the experimental data in the mid-range of degree of saturation or suction and exhibit a significant deviation, particularly at low degree of saturation range. Therefore, it is important to conduct experiments with a sufficient number of degrees of saturations to ensure that the measurements cover the full range of saturation or suction conditions (fully saturated to near dry) before developing empirical equations by experimental data fitting. Obtaining of the requisite amount of experimental data especially at a low degree of saturation is a difficult task. As such, most existing permeability models cannot capture the permeability at low degree of saturation.

Macroscopic Models

The macroscopic models are being developed by averaging the microscopic flow behavior over a representative element volume. The representative element size is selected so that the volume or the characteristic length is large enough to include a sufficient number of pores and particles to reduce the microscopic inhomogeneity at the same time small enough to reduce the macroscopic inhomogeneity due to cracks etc. Although the macroscopic models are developed based on fundamental physical laws, the inability of scaling the microscopic properties to the macroscopic level and incorporating the pore size distribution index (Brooks and Corey, 1964), makes it difficult to develop advanced models that replicate actual soil systems.

Statistical Models

The statistical models are developed based upon the assumption that the soil pores consists of a network of interconnected pores. When a fluid occupies a portion of the pore, a fluid-filled tube forms and the flow of that particular fluid occurs only through the flow tubes. In addition to the size and the distribution of these tubes, the degree of saturation also affects the flow of a given liquid. For example, at higher degrees of saturation, the flow tubes will be bigger in cross sections that will result in a larger flow. The statistical method is used to quantify the size and the distribution of these flow tubes. It should be noted, the distribution of the pores and pore sizes affect the suction at given degree of saturation. Therefore, the suction-degree of saturation relationship, known as the Soil Water Characteristic Curve (SWCC) can be indirectly used to develop the hydraulic conductivity function for unsaturated soils (Burdine 1953, Mualem 1976*a*, van

Genuchten 1980, Fredlund et al., 1994, Leong and Rahardjo 1997) i.e., a calibrated SWCC model can be used to predict the permeability of unsaturated soil at various degree of saturation.

The model proposed by Leong and Rahardjo (1997) incorporates the suction and a soil type dependent fitting parameter *p* to calculate the permeability of unsaturated soil. This method was further studied by Fredlund et al. (2001) using almost 300 sets of permeability data to understand the typical values of *p* for common soil types. Based on this study, it is concluded that, the Leong and Rahardjo method is effective for course-grained soils but it is not suitable for fine-grained soils (Fredlund et al. 2001, Lobbezoo and Vanapalli, 2002).

Fredlund et al (F-All) Permeability Model

One of the many permeability functions, the model proposed by Fredlund et al. (1994), which is shown in Equation 8.1, is commonly used in finite element simulations of unsaturated soils. The model uses the SWCC proposed by Fredlund and Xing (1994). Since the residual water content is assumed to be zero in the Fredlund and Xing model, the normalized water content and the degree of saturation are equal. Therefore, this permeability function can be utilized with either volumetric or gravimetric water content or with the degree of saturation.

$$K_r(\psi) = \frac{\int_{\ln(\psi)}^{b} \frac{\theta(e^y) - \theta(\psi)}{e^y}\, \theta'(e^y)\, dy}{\int_{\ln(\psi_{aev})}^{b} \frac{\theta(e^y) - \theta_s}{e^y}\, \theta'(e^y)\, dy} \tag{8.1}$$

The functions θ and C are given by

$$\theta = C(\psi) \frac{\theta_s}{\left(\ln\left(e + (\psi/a)^n\right)\right)^m} \text{ and } C(\psi) = 1 - \frac{\ln\left(1+\psi/C_r\right)}{\ln\left(1+10^6/C_r\right)}$$

where ψ is the soil suction, $K_r(\psi)$ is the relative permeability at suction ψ, ψ_{aev} is the air-entry value of the soil under consideration, y is a dummy variable of integration representing a suction, b = ln(l,000,000), θ is the volumetric water content and θ' is the derivative of θ. C_r is a parameter related to residual water content, and ***a***, *n* and *m* are the fitting parameters of the F-X SWCC model. The parameter ***a*** is related to the air-entry suction, the parameter *n* represents the pore size distribution of the soil, and parameter *m* is related to the asymmetry of the SWCC.

The F-All model involves a complicated integration procedure (refer Fredlund et al., 1994) for calculating the permeability using the corresponding SWCC. It also exhibits a significant deviation at low degree of saturation (high suction) values.

Development of a New Permeability Model for Unsaturated Soils

The pore-size distribution is an important property in unsaturated soils, because it directly influences the soil suction and permeability. In most of the popular soil-water characteristic curves (SWCCs), a fitting parameter ***n*** which is related to the pore-size distribution is used to relate to the soil suction and the degree of saturation. The permeability of water in unsaturated soils is governed not only by the pore-size distribution but also by the volumetric water content (θ/θ_s) or the degree of saturation. The permeability of water will increase with the volumetric water content (θ/θ_s) because the effective space (available space) for the water flow increases with the volumetric

water content. There are many available permeability models which relate the permeability of the unsaturated soils to the SWCC model parameters (van Genuchten 1980, Fredlund et al. 1994).

Most of the available permeability models relate permeability only to the volumetric water content and pore-size distribution; in those models the permeability is related only to the available effective space for water flow. In reality, the permeability is influenced not only by the effective space (proportional) but also by the soil suction (inverse proportional), because the suction provides additional friction to the flow. Because the effect of suction is significant in high suction ranges, most of the available permeability models failed to predict the accurate permeability values in this range. Therefore, the permeability functions should be related to the volumetric water content, pore-size distribution, and the soil suction (Equation 8.2) for more accurate predictions.

$$K_r = f\left(\theta/\theta_s,\ n,\ \psi\right) \tag{8.2}$$

Most of the permeability function available in the literature failed to predict the permeability at high suction range accurately. In this proposed model, further consideration is given for the accuracy in high suction ranges. The newly proposed relative permeability function is given below (Equation 8.3).

$$K_r(\psi) = F(\psi)\left[1-\left[1-\left(\theta/\theta_s\right)^{\left(1.25\ -\ \frac{1}{2n}\right)}\right]^{n/3.5}\right]^{n} \tag{8.3}$$

The function $F(\psi)$ is given by

$$F(\psi) = \left(\frac{1}{1+\left(\psi/a\psi_{aev}\right)^{1.5}}\right)^{0.25} \left(\frac{\theta}{\theta_s}\right)^{\left(1+\left(\frac{10\theta_s}{n}\right)^{1.75}\right)}$$

where $K_r(\psi)$ is the relative permeability at suction ψ. ***a***, ***n,*** and ***m*** are the fitting parameters of the S-R-1, S-R-2, and S-R-3 SWCC models. An important point to note is, when the fitting parameters of the S-R-1 SWCC model are used along with the proposed permeability model, the value of $a\psi_{aev}$ in the permeability model should be set to the value of ***a*** in the S-R-1 SWCC model.

Predictive Capability of the Proposed Permeability Model

The predictive capability of the new model was investigated using experimental results of eight different type of soils found in the literature. In this study, the fitting parameters of S-R-2 and S-R-3 SWCC models are used along with the proposed relative permeability model. Soil were chosen based upon the availability of both moisture-suction and moisture-permeability relationships. The dataset includes sand, silts and clays, the available properties of which and the reference are listed in Table 8.1. The fitting parameters of the S-R-2 and S-R-3 SWCC models were first calibrated by matching the experimental data. It should be noted that the experimental permeability values are not matched by adjusting the model parameters; the calibrated SWCC model parameters are instead directly used to predict the relative permeability.

Table 8.1 Properties of the selected soils

Soil	*Porosity*	*PI (%)*	*Reference*
Lakeland sand	0.375	0	Elzeftawy & Cartwright 1981
Superstition sand	0.500	0	Richards 1952
Columbia sandy loam	0.458	unknown	Brooks & Corey 1964
Touchet silt loam	0.430	3	Brooks & Corey 1964
Silt loam	0.396	unknown	Reisenauer 1963
Guelph loam	0.520	10	Elrick & Bowmann 1964
Yolo light clay	0.375	10	Moore 1939
Speswhite kaolin	0.560	unknown	Peroni et al. 2003

It should be noted that the experimental moisture-suction data for these soils are unavailable for the either the full range (0-100%) of degree of saturation or possible suction ranges. For the Superstition sand and Lakeland sand, the available experimental data show an approximate saturation range between 30 to 100% degrees (see Figures 8.1 through 9.8); for the Columbia sandy loam between 50 to 100%; for Touchet silt loam between 20 to 100%; for silt loam between 50 to 100%; for Guelph loam between 45 to 100%; for Yolo light clay between 45 to 100%; and for the Speswhite kaolin between 55 to 100%. For each soil, the SWCC model parameters were adjusted to match the experimental data. In this study, the SWCC model parameters are adjusted not only to match the measured data but also to reach an assumed maximum suction for each soil. A maximum possible suction of 10^5 kPa and 10^6 kPa are assumed for sandy and clayey soil, respectively. The permeability coefficients of the above mentioned eight soils were predicted using the proposed permeability model that uses the same fitting parameters that were calibrated by matching with experimental data.

The calibrated models parameters of the S-R-2 and S-R-3 SWCC models and predicted permeability function for these eight soils are shown in Figures 8.1 through 8.8. Figure 8.1 illustrates the prediction of relative permeability of Superstition sand, which is compared with experimental data (from Richards, 1952) and prediction from the Fredlund et al. model (1994) model. Figure 8.1a presents the calibrated S-R-2 SWCC along with the model parameters and corresponding (S-R-2) permeability predictions are shown in Figure 8.1b. Figure 8.1c presents the calibrated S-R-3 SWCC along with the model parameters and corresponding (S-R-3) permeability predictions are shown in Figure 8.1d. As shown in these figures, the proposed permeability model shows better prediction while the Fredlund et al. method shows small deviation at higher suction range (at a low degree of saturation).

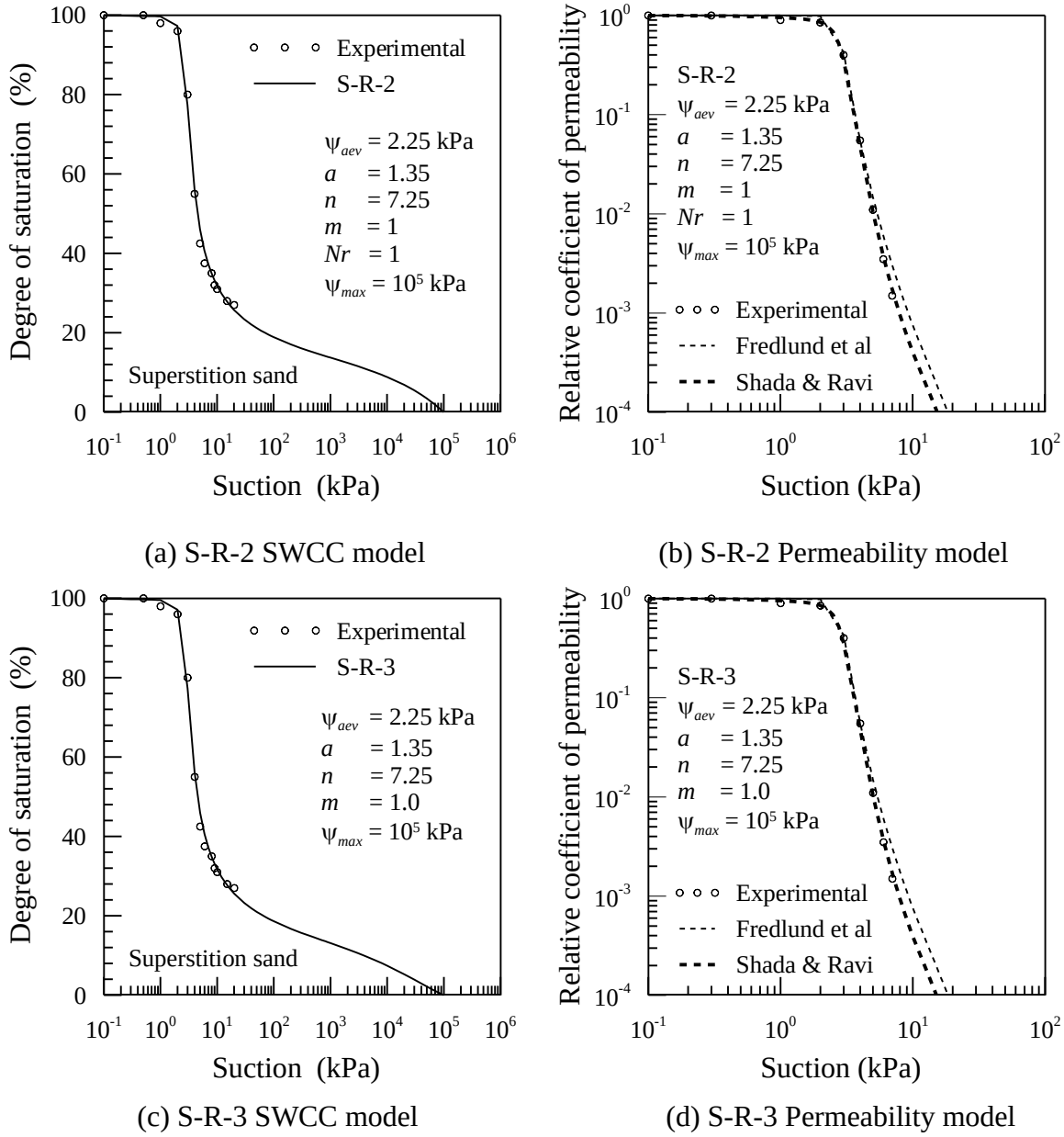

(a) S-R-2 SWCC model

(b) S-R-2 Permeability model

(c) S-R-3 SWCC model

(d) S-R-3 Permeability model

Figure 8.1 Calibrated SWCCs and calculated permeability functions for Superstition sand (experimental data - Richards 1952)

Similar to the Figure 8.1, the Figure 8.2 illustrates the SWCC calibrations and the relative permeability predictions for Lakeland sand. As shown in these figures, the proposed permeability model shows better prediction while the Fredlund et al. prediction significantly differs in the higher suction range. When the suction is approximately 100

kPa, the difference between the predictions by Fredlund et al. and the proposed model is approximately one order of magnitude. When the suction is approximately 1000 kPa, the difference increases approximately to two orders of magnitude.

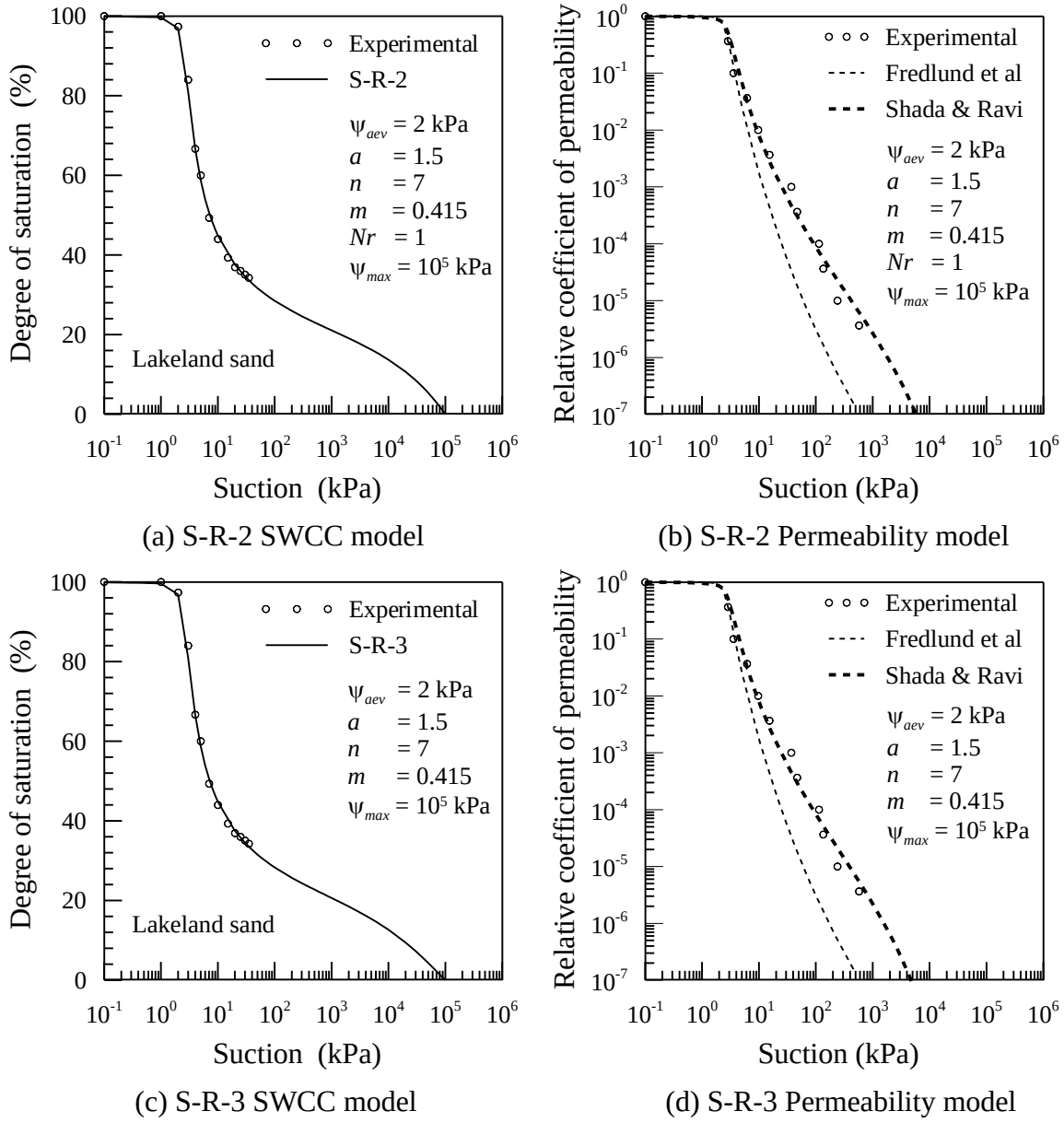

(a) S-R-2 SWCC model

(b) S-R-2 Permeability model

(c) S-R-3 SWCC model

(d) S-R-3 Permeability model

Figure 8.2 Calibrated SWCCs and calculated permeability functions for Lakeland sand (experimental data - Elzeftawy and Cartwright 1981)

The Figure 8.3 illustrates the SWCC calibrations and the permeability predictions for Columbia sandy loam. As shown in these figures, the new model and the Fredlund et al. model predict the experimental data well in the lower suction range. The accuracy in the higher suction range could not be verified because the lack of experimental data.

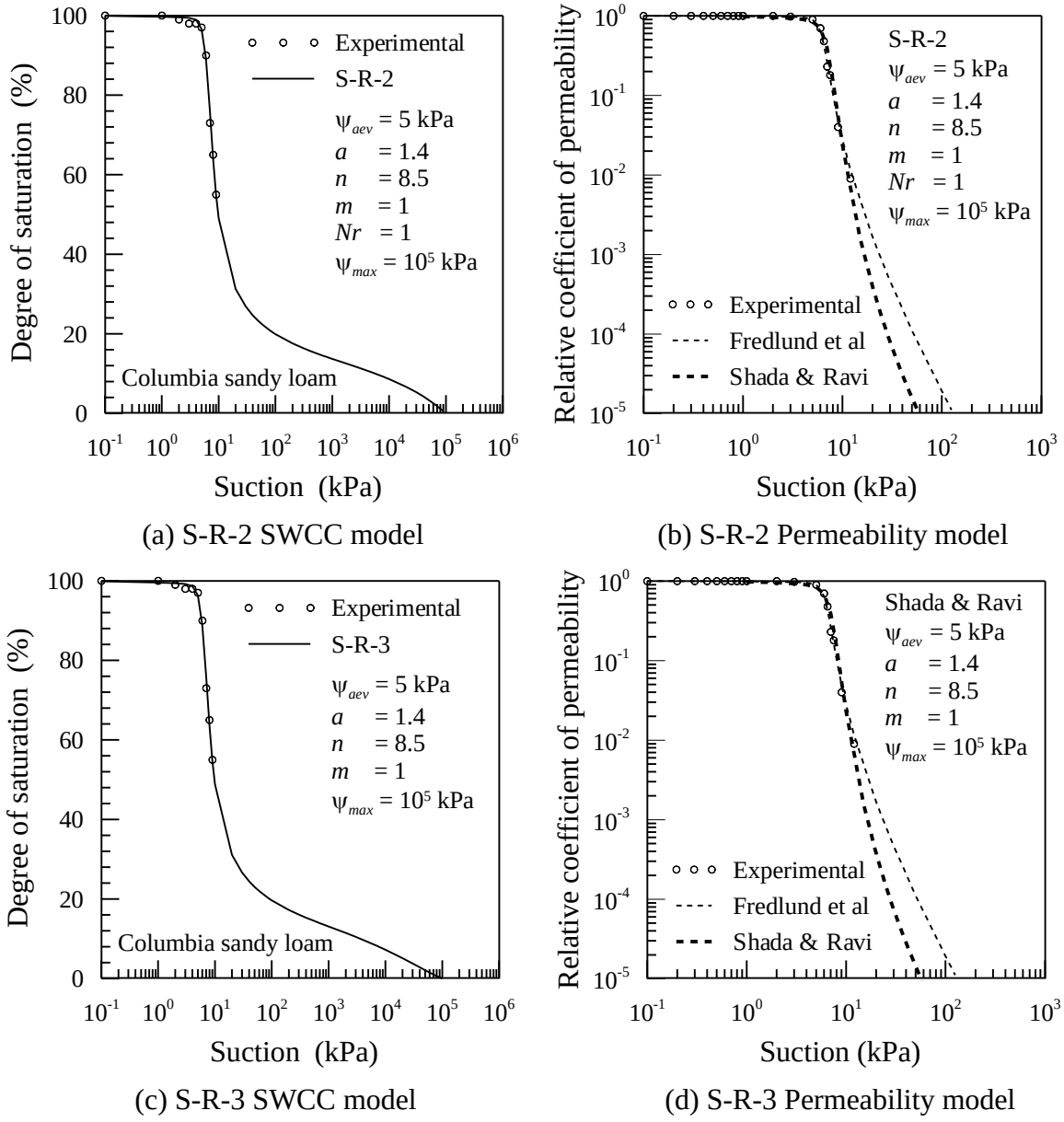

Figure 8.3 Calibrated SWCCs and calculated permeability functions for Columbia sandy loam (experimental data - Brooks & Corey 1964)

The Figure 8.4 illustrates the calibrated SWCCs and the predicted permeability functions for Touchet silt loam (GE3). As shown in these figures, similar to the Columbia sandy loam, a similar discrepancy is observed for the Touchet silt loam.

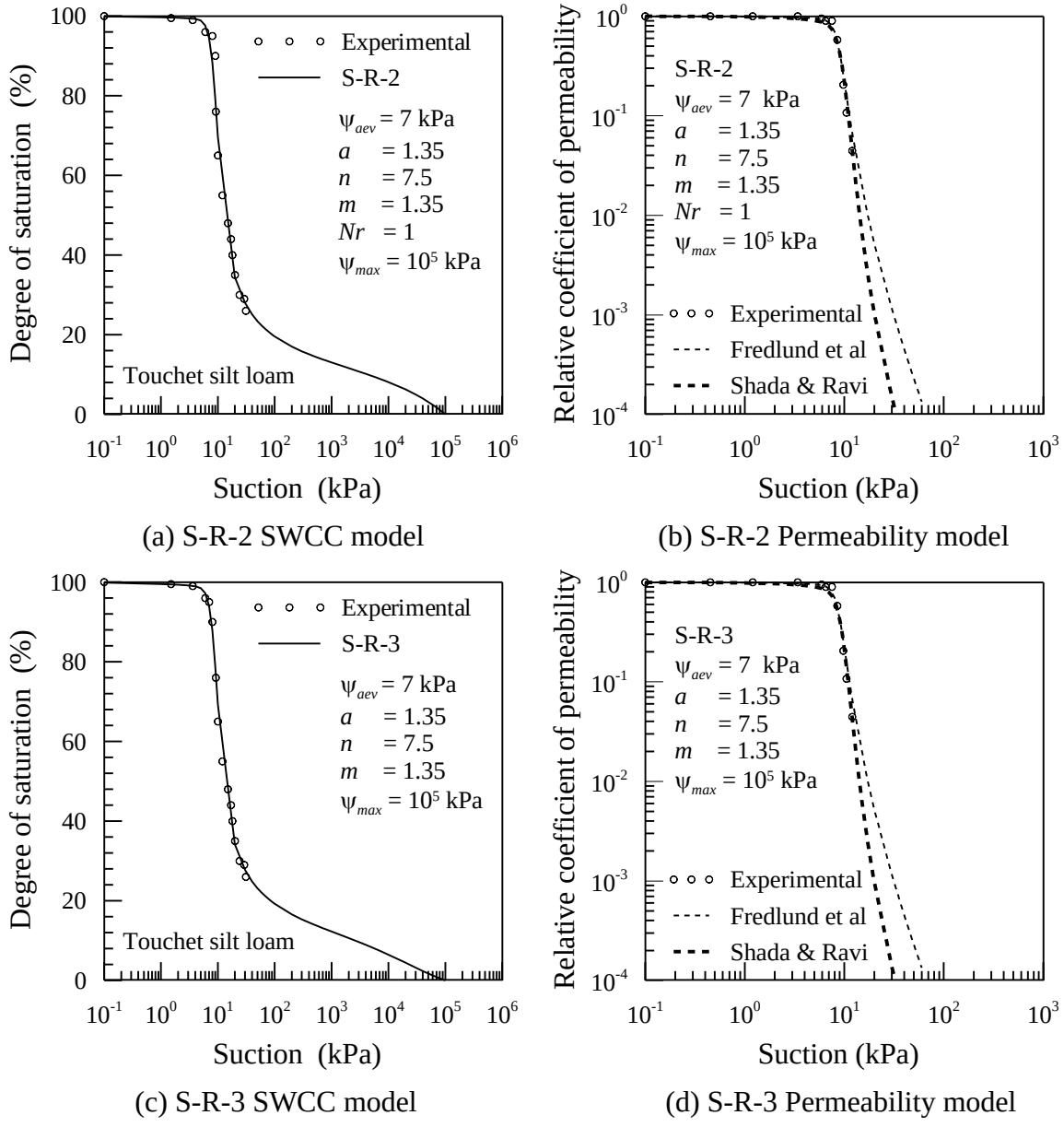

(a) S-R-2 SWCC model

(b) S-R-2 Permeability model

(c) S-R-3 SWCC model

(d) S-R-3 Permeability model

Figure 8.4 Calibrated SWCCs and calculated permeability functions for Touchet silt loam (GE3) (experimental data - Brooks & Corey 1964)

The Figure 8.5 illustrates the calibrated SWCCs and the predicted permeability functions for Silt loam. As shown in these figures, the particular interest is the observation that the proposed model matches the experimental data well while the Fredlund et al. model is shifted to the right.

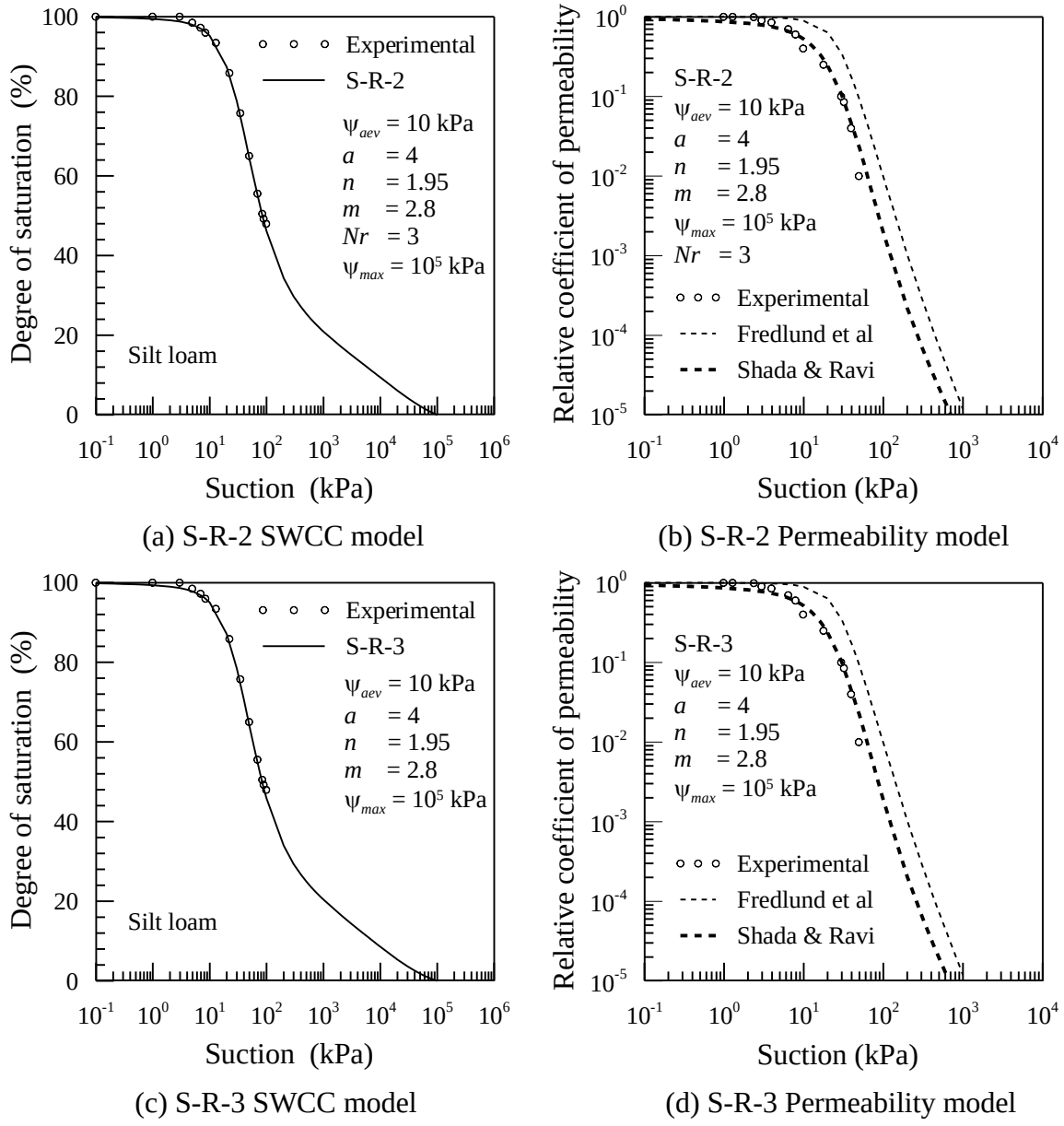

(a) S-R-2 SWCC model

(b) S-R-2 Permeability model

(c) S-R-3 SWCC model

(d) S-R-3 Permeability model

Figure 8.5 Calibrated SWCCs and calculated permeability functions for Silt loam (experimental data - Reisenauer 1963)

Figures 8.6, 8.7, and 8.8 show the predictions and comparisons of the relative permeability of Guelph loam (data from Elrick & Bowmann 1964), Yolo light clay (data from Moore 1939), and Speswhite kaolin (data from Peroni et al. 2003), respectively. Although the predictions are comparable for Guelph loam, both permeability models show slight deviations from the measured data. In the case of Yolo light clay, the difference between the experimental data and the Fredlund et al. prediction increases as the suction increases (Figure 8.7) while the proposed model matches the experimental data well. Experimental data for the Speswhite kaolin is available only for a narrow range of suction (Figure 8.8). Therefore additional discussion on the permeability predictions is not elucidated for the Speswhite kaolin.

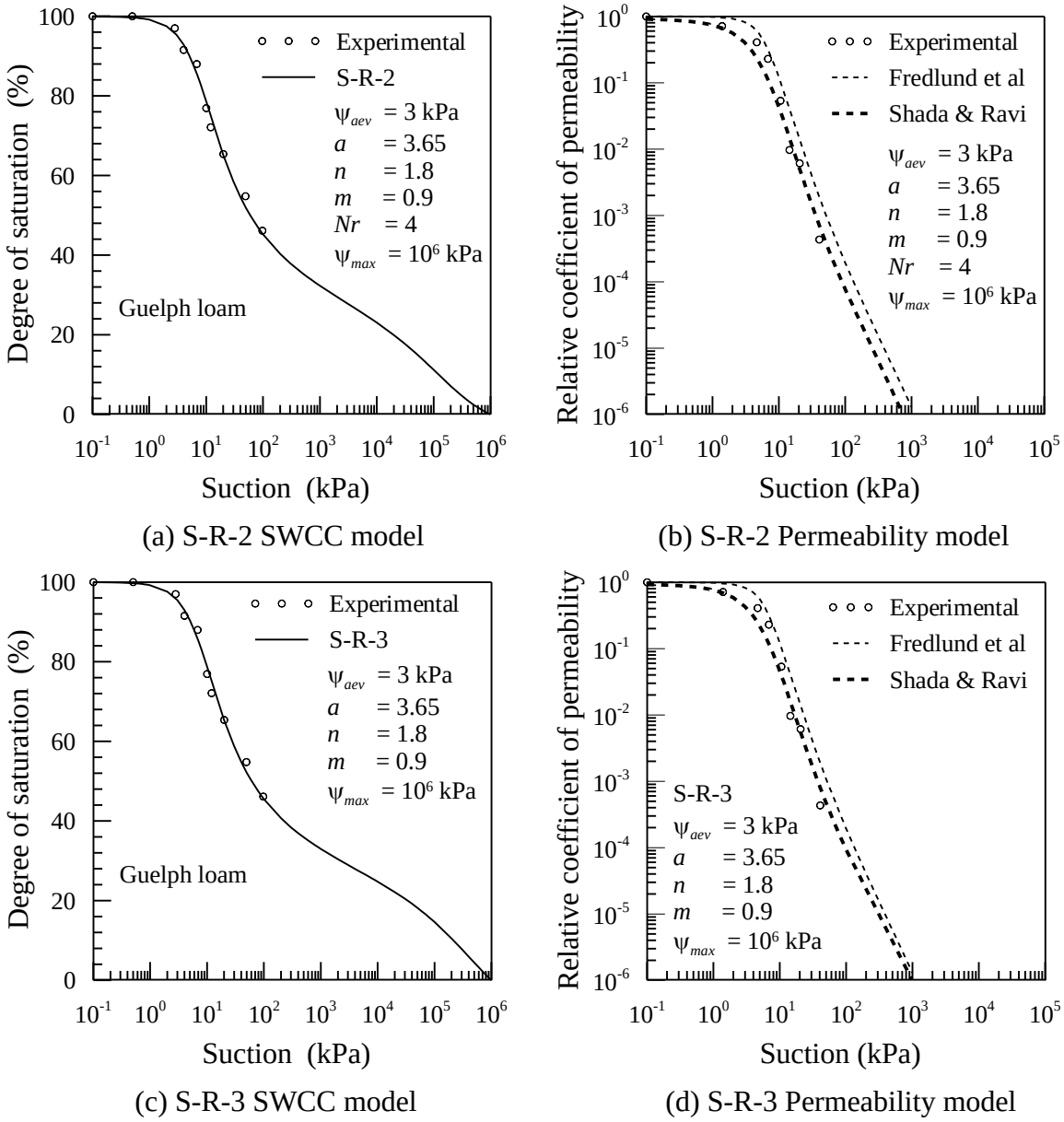

(a) S-R-2 SWCC model

(b) S-R-2 Permeability model

(c) S-R-3 SWCC model

(d) S-R-3 Permeability model

Figure 8.6 Calibrated SWCCs and calculated permeability functions for Guelph loam (experimental data - Elrick & Bowmann 1964)

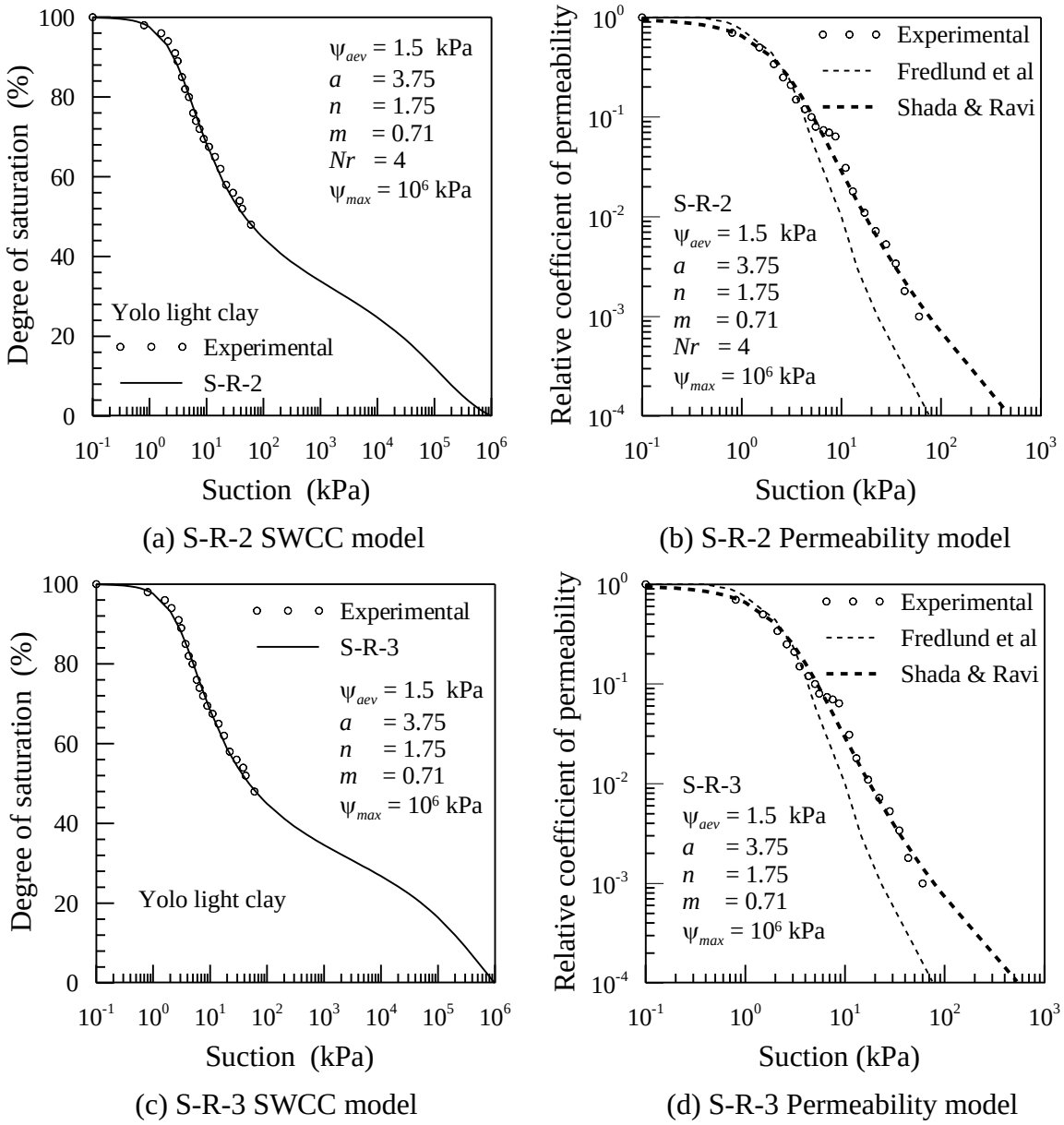

(a) S-R-2 SWCC model

(b) S-R-2 Permeability model

(c) S-R-3 SWCC model

(d) S-R-3 Permeability model

Figure 8.7 Calibrated SWCCs and calculated permeability functions for Yolo light clay (experimental data - Moore 1939)

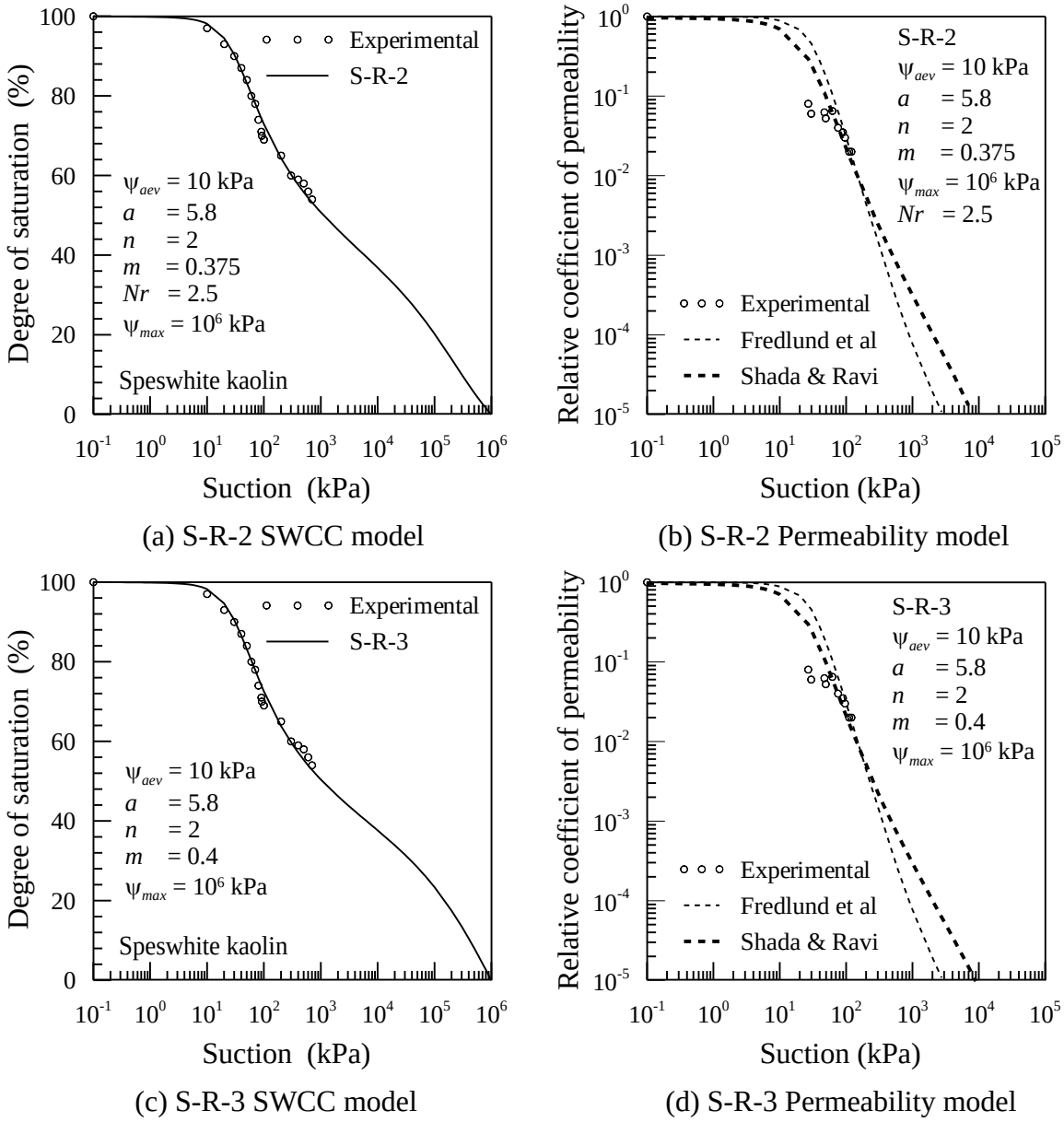

Figure 8.8 Calibrated SWCCs and calculated permeability functions for Speswhite kaolin (experimental data - Peroni et al. 2003)

From these observations, it can be summarized that the proposed permeability model predicts the experimental data well while the Fredlund et al. model (one of the currently available popular models) shows significant differences in the higher suction range.

Summary of the Study

A new relative permeability function for water in unsaturated soil was developed using the model parameters of S-R SWCC models. The capability and the accuracy of the new permeability function were verified by comparing the predictions of the new permeability function with both experimental values and predictions of F-All permeability model for eight different soils. The comparisons show that the new model predicts the experimental data well over a wide range of suction (0 - 1,000,000 kPa) and the accuracy of the new model in higher suction range is better than the F-All model.

The proposed relative permeability model must be used with the corresponding parameters of S-R SWCC models. The model parameters of the proposed relative permeability model and the S-R SWCC models are identical. It should be noted that measuring SWCC for a soil over wide range of degree of saturation is easier than measuring the permeability coefficient. Therefore, the model parameters can be obtained by calibrating against the measured SWCC for the soil instead of the permeability coefficients. Based on the results of other simulation studies it can also summarized that the new model can be effectively used to calculate the permeability of water in unsaturated soils in finite element simulations.

CHAPTER NINE

FINITE ELEMENT MODEL FOR COUPLED DEFORMATION-FLOW ANALYSIS OF UNSATURATED SOILS

Introduction

A finite element model of coupled deformation-flow analysis of unsaturated soils should consist of the following basic elements: (i) *a capable finite element formulation*, (ii) *an effective soil-water characteristic curve model*, and (iii) *an effective relative permeability model*. Importantly all these elements should be implemented together in a software, which can be used for coupled deformation-flow simulations. In the previous chapters, the details of all these basic elements and TeraDysac software are presented in detail. In this chapter, the information about the implementation of the key elements and the results of example simulations are presented.

The partially reduced formulation (u-p-p formulation) is capable of coupled deformation-flow analysis of unsaturated soils, as this formulation neglects only the relative acceleration of the pore fluids but takes the relative velocity of the pore fluids into account. Therefore the u-p-p formulation is implemented in TeraDysac along with the S-R-2 SWCC model and the S-R relative permeability model. A screen print view of the user-interface of TeraDysac that shows the availability of the implemented u-p-p formulation in the drop-down list of "Physics Type" is shown in Figure 9.1.

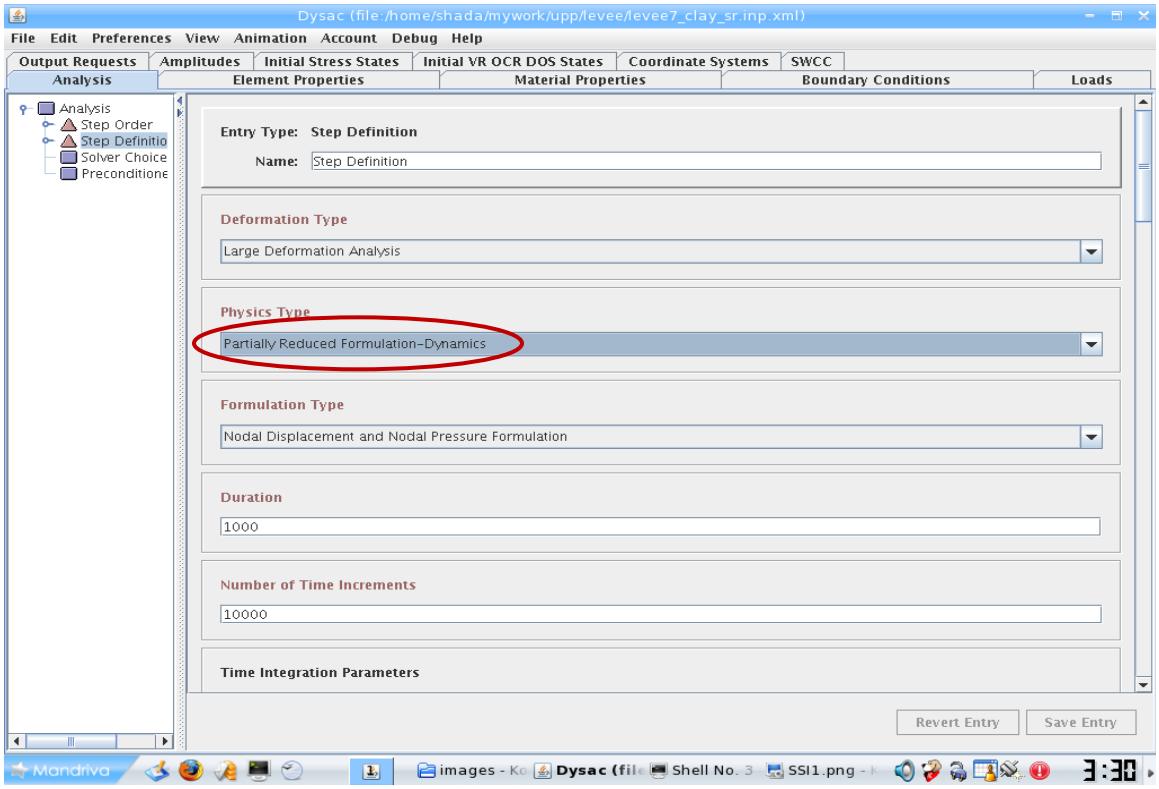

Figure 9.1 The availability of the u-p-p formulation in the user-interface of TeraDysac

The new S-R-2 SWCC models and the S-R relative permeability model are also implemented in TeraDysac. Improved computational efficiency, flexibility, and increased applicability are the key advantages of these models. Figure 9.2 shows the availability of the S-R-2 (Shada-Ravi) SWCC model in the user-interface of TeraDysac.

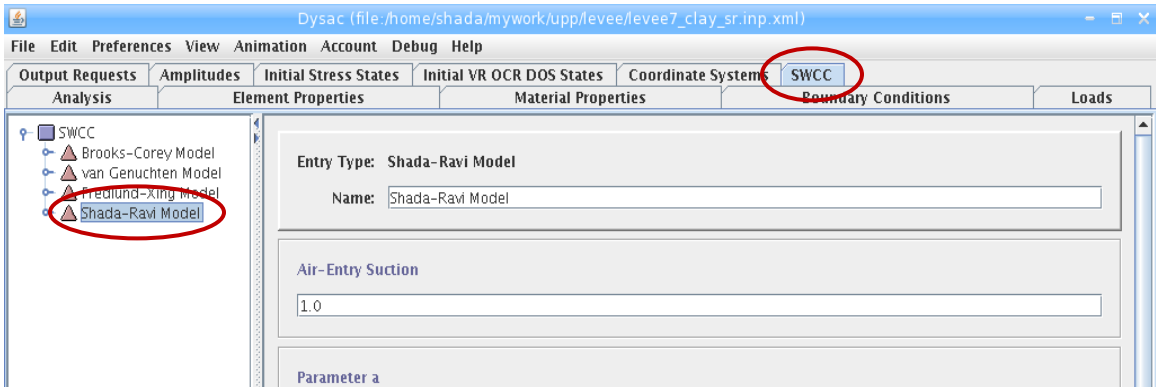

Figure 9.2 Availability of the S-R-2 SWCC model in the user-interface of TeraDysac

In addition to these elements, nodal pore liquid pressure and nodal pore gas pressure boundary conditions are also implemented in TeraDysac. Using these boundary conditions, flow/seepage through unsaturated soils can be generated by creating hydraulic gradient in the numerical simulations. In addition, to model some of the actual physical condition, these boundary conditions are very effective. For example, if a node or a side of the problem is open to atmosphere, the pore gas pressure should be set to zero at that node or side, and it can be done effectively using the nodal pore gas pressure boundary condition. Figure 9.3 shows the availability of the implemented nodal pore pressure boundary conditions in the user-interface of TeraDysac.

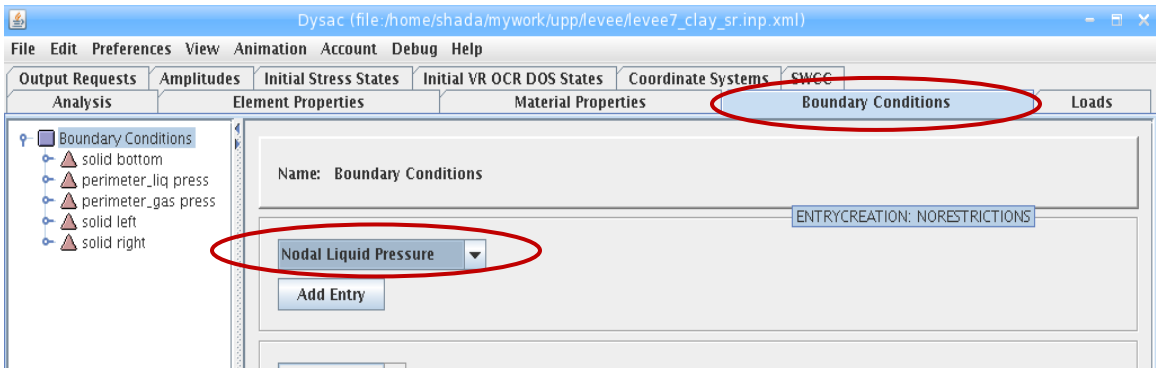

Figure 9.3 Availability of the nodal liquid pressure boundary condition in TeraDysac

It is necessary to state here that the implementation of the coupled deformation-flow analysis finite element model along with the key elements, is remarkably enhanced the applicability of TeraDysac software. The ability of the implemented finite element model in simulating (i) flow through unsaturated soils and (ii) coupled deformation flow response of unsaturated soil-pile system is studied and presented below.

Example Analysis 1: Flow through Unsaturated Embankment

Problem Description

The performance of the formulation in predicting flow behavior of unsaturated soil is examined by simulating flow through embankment problem. The 2D finite element mesh of unsaturated compacted embankment is shown in Figure 9.4. The mesh consists of 310 four-node quadrilateral elements. The left (AB) and right (IJ) vertical edges of the embankment were assumed to be fixed in x-direction and free to move in y-direction. The base of the embankment (AJ) was assumed to be impermeable (no flow) and fixed (no displacement) in all direction throughout the analysis. On all other sides of the embankment zero traction was specified for the solid phase. For the gas phase, atmospheric pressure was applied on the perimeter (BC, CD, DE, EF, FG, GH and HI) of the embankment at the beginning. The liquid pressure time history shown in Figure 9.5 was applied on the left side of the embankment (only on BC, CD). 60% initial degree of saturation is used for the whole embankment. The initial pore liquid pressure in the applied pressure history is the pore liquid pressure corresponding to 60% degree of saturation.

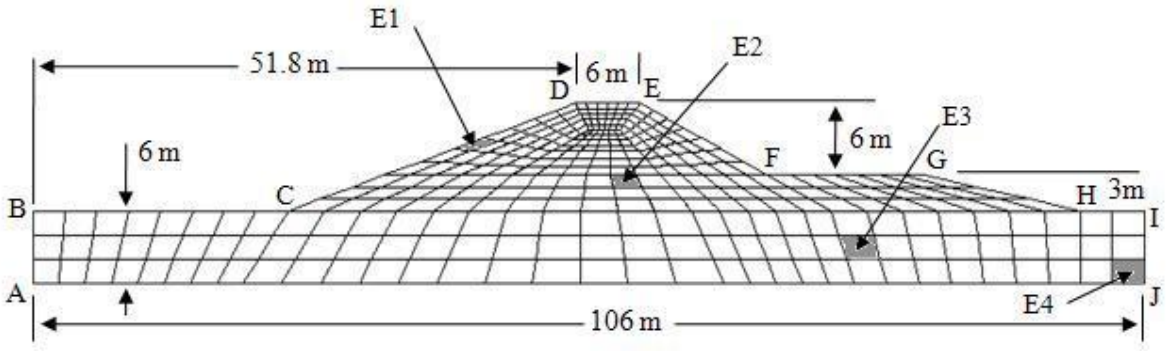

Figure 9.4 The 2D finite element mesh of the compacted embankment

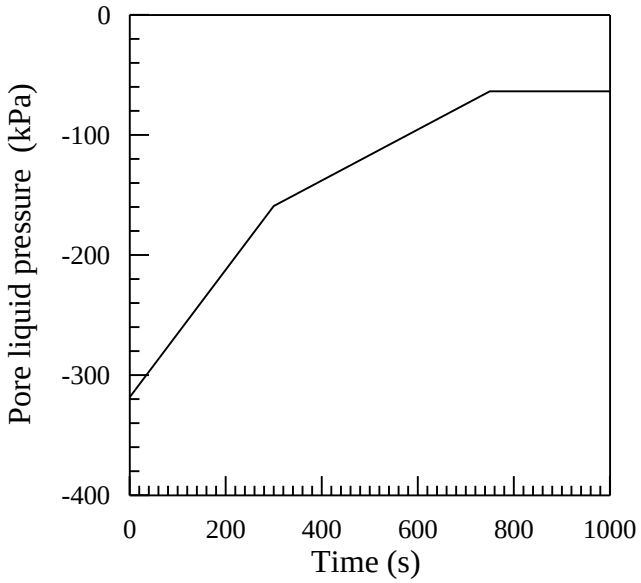

Figure 9.5 History of applied pore liquid pressure (applied along BCD, Figure 9.4)

Material Models and Model Parameters

A clayey soil, Speswhite kaolin, is used in the finite element simulation of flow through unsaturated earthen embankment. Although, the material can undergo elastoplastic deformation, a linear elastic material model is used in the simulation to avoid any complication arise due to the nonlinear material deformation. The linear elastic model parameters for the Speswhite kaolin are listed in Table 9.1.

Table 9.1 Linear elastic model parameters for Speswhite kaolin

Properties			Value
Solid grain density		Mg/m^3	2.62
Liquid density		Mg/m^3	1.0
Gas density	$x10^{-3}$	Mg/m^3	2.1
Bulk modulus of liquid	$x10^{6}$	kPa	2.2
Bulk modulus of gas		kPa	101.325
Viscosity of liquid	$x10^{-6}$	kPa·s	1.0
Viscosity of gas	$x10^{-8}$	kPa·s	1.0
Young's Modulus	$x10^{5}$	kPa	0.3
Poisson's ratio			0.2

The moisture-suction variation of the Speswhite kaolin is modeled using the S-R-2 SWCC model. The model parameters of the S-R-2 SWCC model are calibrated using experimental results for the Speswhite kaolin presented by Sivakumar (1993). The model parameters were adjusted until the model curve matches with the experimental curve. The calibrated curve of the S-R-2 model together with the fitting parameters (ψ_{aev} = 10 kPa, $\boldsymbol{a}$ = 5.7, $\boldsymbol{n}$ = 2, $\boldsymbol{m}$ = 0.375, Nr = 4.1, ψ_{max} = 10^6 kPa), is shown in Figure 9.6. These calibrated parameters are used for the calculation of relative permeability of both liquid and gas phases during finite element simulation.

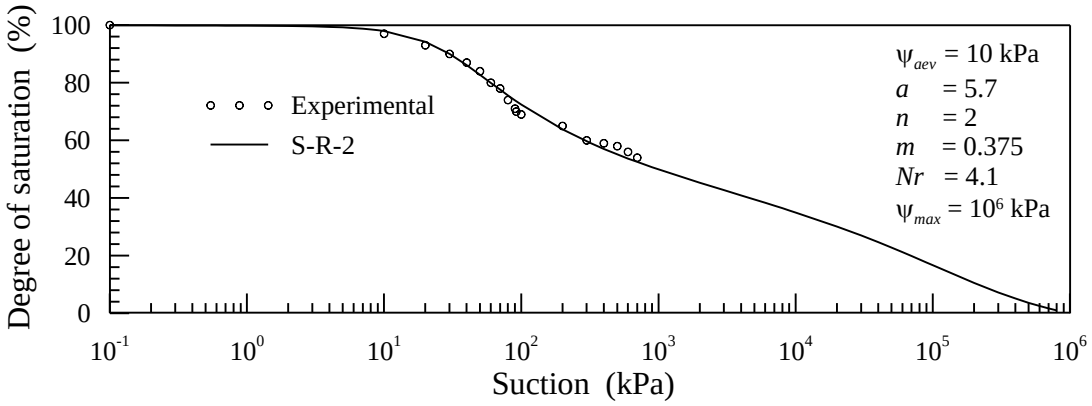

Figure 9.6 Calibrated S-R-2 model and the fitting parameters for Speswhite kaolin

Results and Discussion

Comparisons of predicted time histories of incremental pore liquid pressure and degree of saturation in selected elements (E1, E2, E3, and E4, see Figure 9.4) are shown in Figures 9.7 and 9.8, respectively. Contour plots of degree of saturation and pore liquid pressure at different simulation time are shown in Figures 9.9 and 9.10, respectively. The degree of saturation and pore liquid pressure in the left side of the embankment (Element E1) show a quick response to the applied liquid pressure boundary condition, while the

element located away from the applied liquid pressure boundary condition (E4) shows delayed response. To gain about 5% degree of saturation increment, it took about 250 sec for the Element E1, about 400 sec for the Element E2, about 750 sec for the Element E3, and about 910 sec for the Element E4. As shown in Figure 9.9, the degree of saturation in the left side of the embankment increases from 60% to 82% in first 1000 sec, while the degree of saturation in the right side almost remains at 60%. In addition, the degree of saturation increases uniformly from the left side of the embankment to the right side. The contour plots shown in Figures 9.9 and 9.10 evidently shows the calculated flow of water through the unsaturated embankment. Therefore the coupled deformation-flow analysis finite element model is capable of simulating flow through the unsaturated soils and related geotechnical problems.

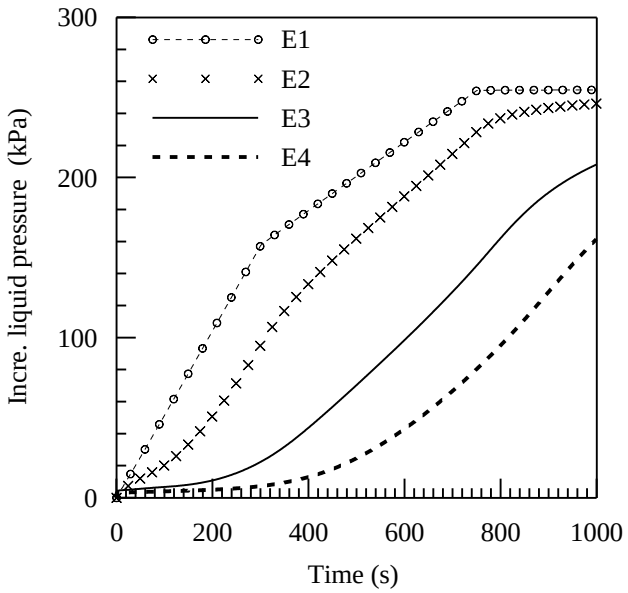

Figure 9.7 Time history of predicted incremental pore liquid pressure

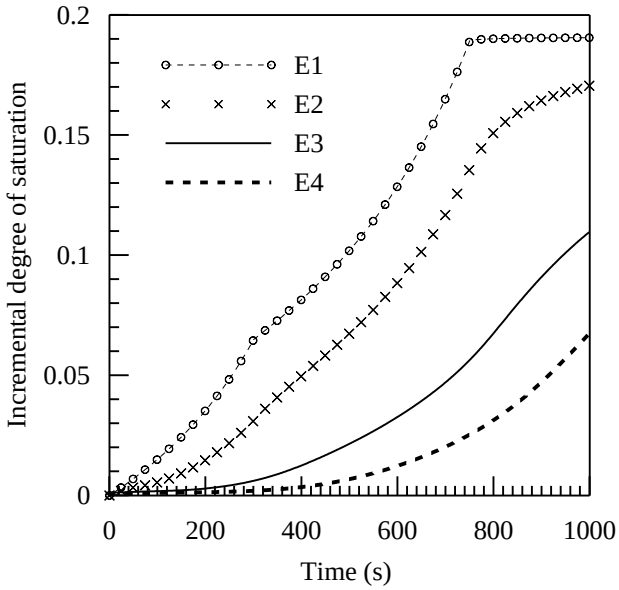

Figure 9.8 Time history of predicted incremental degree of saturation

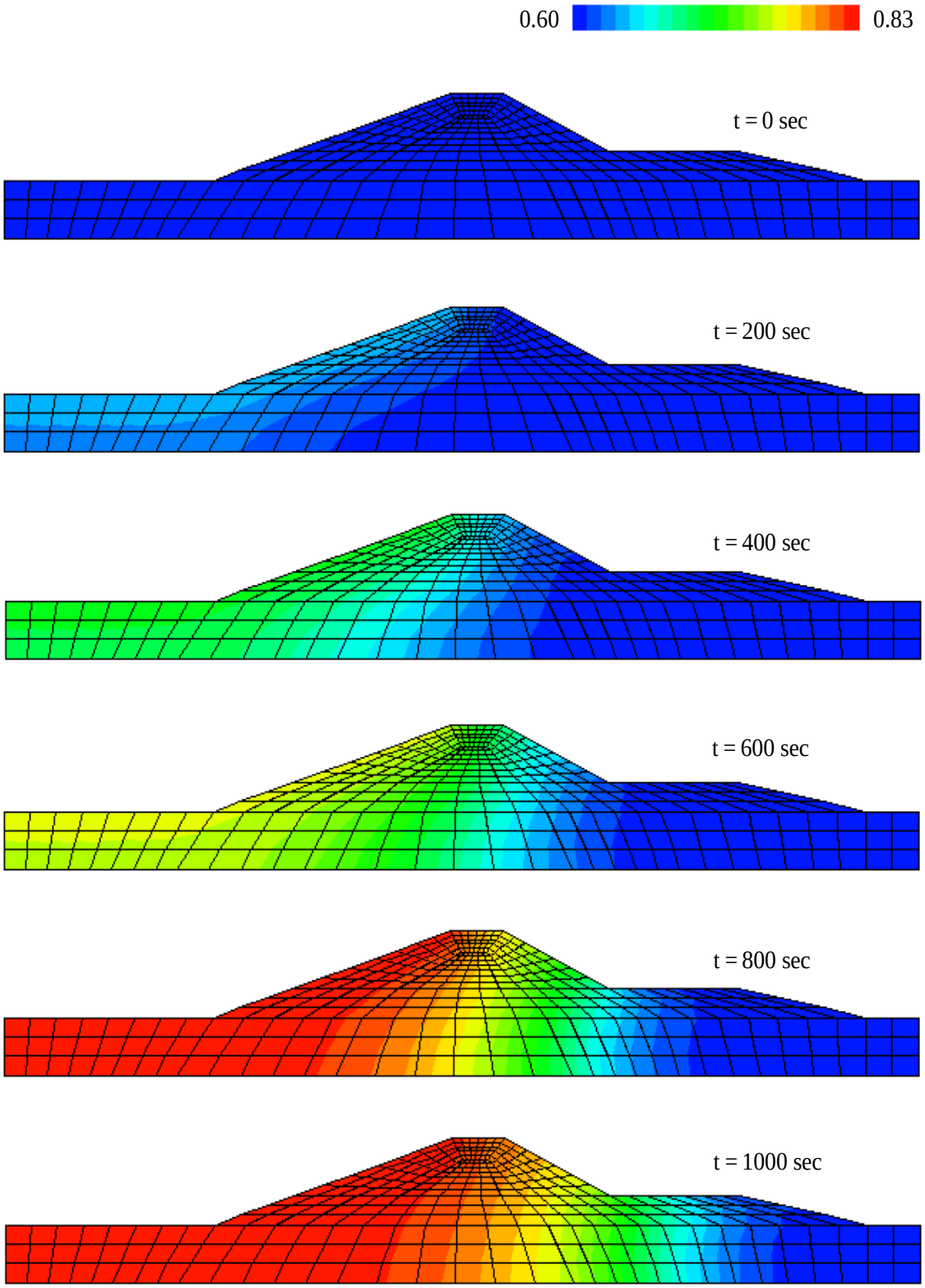

Figure 9.9 Contour plots of predicted degree of saturation at different simulation times

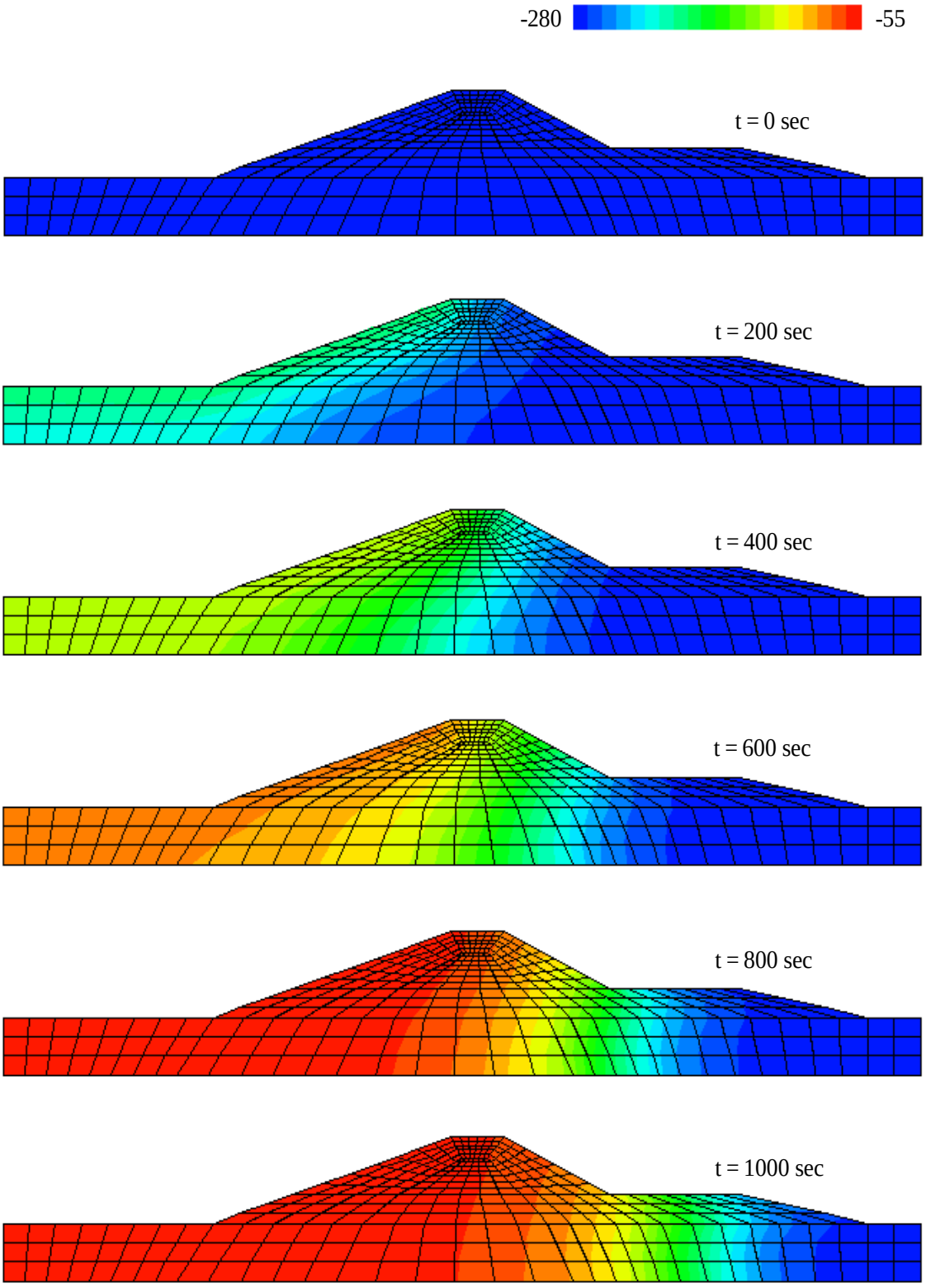

Figure 9.10 Contour plots of predicted pore liquid pressure at different simulation times

Example Analysis 2: Coupled Deformation-Flow Analysis of Unsaturated SPI

Problem Description

The 2D finite element mesh used for the SPI simulation is shown in Figure 9.11. The soil mesh consists of 630 quadrilateral elements. The structure consists of a single column with an element at the top with larger density. The top element with the larger density is used to model the superstructure and its self weight. The Timoshenko beam theory is used to represent structural elements. The soil and the structural nodes are merged together at the interfaces. The acceleration-time history of applied base motion is shown in Figure 9.12.

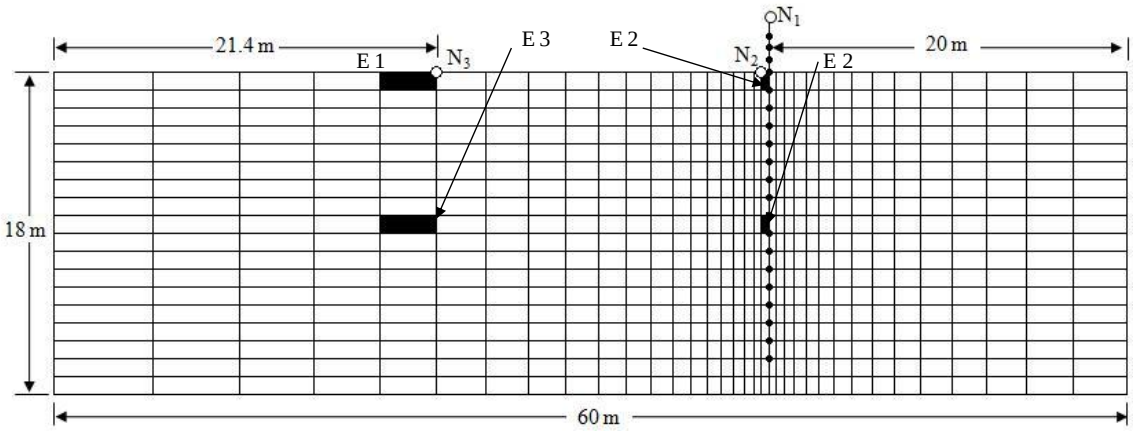

Figure 9.11 The finite element mesh used for the SPI simulation

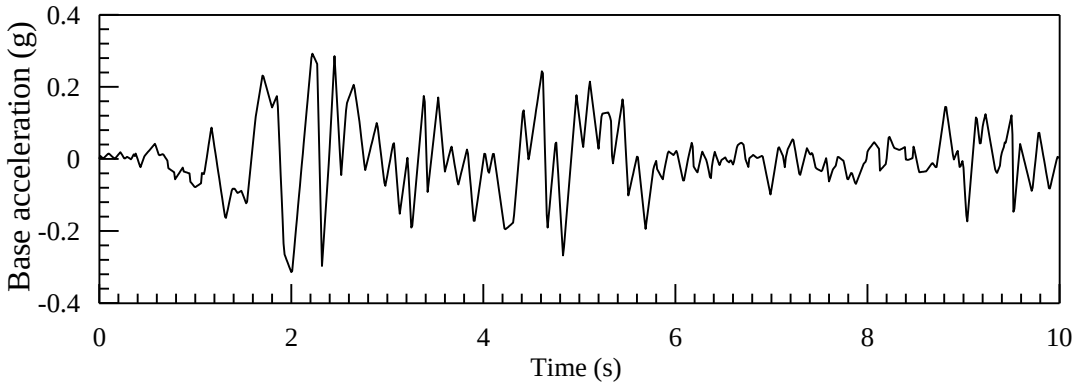

Figure 9.12 The acceleration-time history of applied base motion

Material Model and Model Parameters

Realistic predictions using finite element model require the use of realistic constitutive models for each component. Analyses of the soil-pile system under dynamic loading require an elastoplastic model to obtain reasonable predictions. Therefore the bounding surface based elastoplastic model proposed by Muraleetharan and Nedunuri (Muraleetharan and Nedunuri, 1998) for unsaturated soils is used in this study. The soil is modeled with the properties of Minco silt. The bounding surface model parameters used to model the stress-strain relationship of the Minco silt are listed in Tables 9.2 and 9.3. The structure is also assumed to be linear elastic and the model parameters used for the structural are given in Table 9.4.

Table 9.2 Bounding surface based elastoplastic model parameters for the Minco silt

Parameter	Value
Slope of the isotropic consolidation line on $e - \ell n\ p'$ plot, λ	0.02
Slope of an elastic rebound line on $e - \ell n\ p'$ plot, κ	0.002
Slope of the critical state line in $q - p'$ space , M_c (compression)	1.00
Ratio of extension to compression value of M (M_e / M_c)	1.00
Value of parameter defining the ellipse1 in compression (R_C)	2.60
Value of parameter defining the hyperbola in compression (A_C)	0.10
Parameter defining the ellipse 2 (tension zone) (T)	0.05
Projection center parameter (C)	0.00
Elastic nucleus parameter (S)	1.00
Ratio of triaxial extension to compression value of R (R_e / R_c)	1.00
Ratio of triaxial extension to compression value of A (A_e / A_c)	1.00
Hardening parameter (m)	0.02
Shape hardening parameter in triaxial compression (h_c)	2.00
Ratio of triaxial extension to compression value of h (h_e/h_c)	1.00
Hardening parameter on I-Axis (h_o)	2.00

Table 9.3 Suction related elastoplastic model parameters of Minco silt

Parameter	dos = 70%
m	140
B	0.12
N	2.017
A	0.27
r	1.57
b	0.0133

Table 9.4 Linear elastic model parameters of structural elements

Properties			Pile	Superstructure
Density		Mg/m^3	2.803	386.5
Cross section area		m^2	0.132	0.132
2^{nd} moment of area	$x10^{-3}$	m^4	6.01	6.01
Young's Modulus	$x10^{10}$	kPa	6.935	6.935
Poisson's ratio			0.33	0.33

The moisture-suction variation is modeled using the S-R-2 SWCC model. The model parameters of the S-R-2 SWCC model are calibrated using experimental results for the Minco silt presented by Ananthanathan (2003). The model parameters were adjusted until the model curve matches with the experimental curve and the following parameters were calibrated ψ_{aev} = 1 kPa, $\boldsymbol{a}$ = 3.75, $\boldsymbol{n}$ = 1.6, $\boldsymbol{m}$ = 12, Nr = 2, and $\psi_{max} = 10^6$ kPa.

Results and Discussion

Spectral Accelerations

To investigate the capability of the finite element model to predict the coupled deformation-flow response of unsaturated soil-pile system, simulations were performed

with initial degree of saturations of 70%. The horizontal spectral accelerations obtained at nodes N1, N2 and N3 (see Figure 9.11) using 5% damping are shown in Figure 9.13. The response predicted at the node N1 represents the response of superstructure. The N2 and N3 predicts the surface responses, however the response of N2 will be influenced by SPI, whereas the N3 represents the free-field. This problem is also analyzed using the improved simplified formulation i.e. analyzed assuming an undrained condition and the predicted results are presented in the same Figure. As shown in the Figure 9.13, the spectral accelerations values predicted using the coupled deformation-flow simulation and the undrained simulation are identical, especially the peak spectral accelerations are exactly same. However, at low range of period, i.e. in high range of frequency, the coupled deformation-flow simulation predicts slightly higher spectral accelerations values.

In both cases, highest amplification is predicted at node N1 and the lowest amplification is predicted at node N3 (free-field). However, the periods of these acceleration spectra do not show considerable change. The response spectrum of the applied base motion is shown in Figure 9.13d. When comparing the spectral acceleration values, the simulations show that the soil has amplified the base motion by a factor of approximately 7, 5 and 2.5 at nodes N1, N2 and N3, respectively.

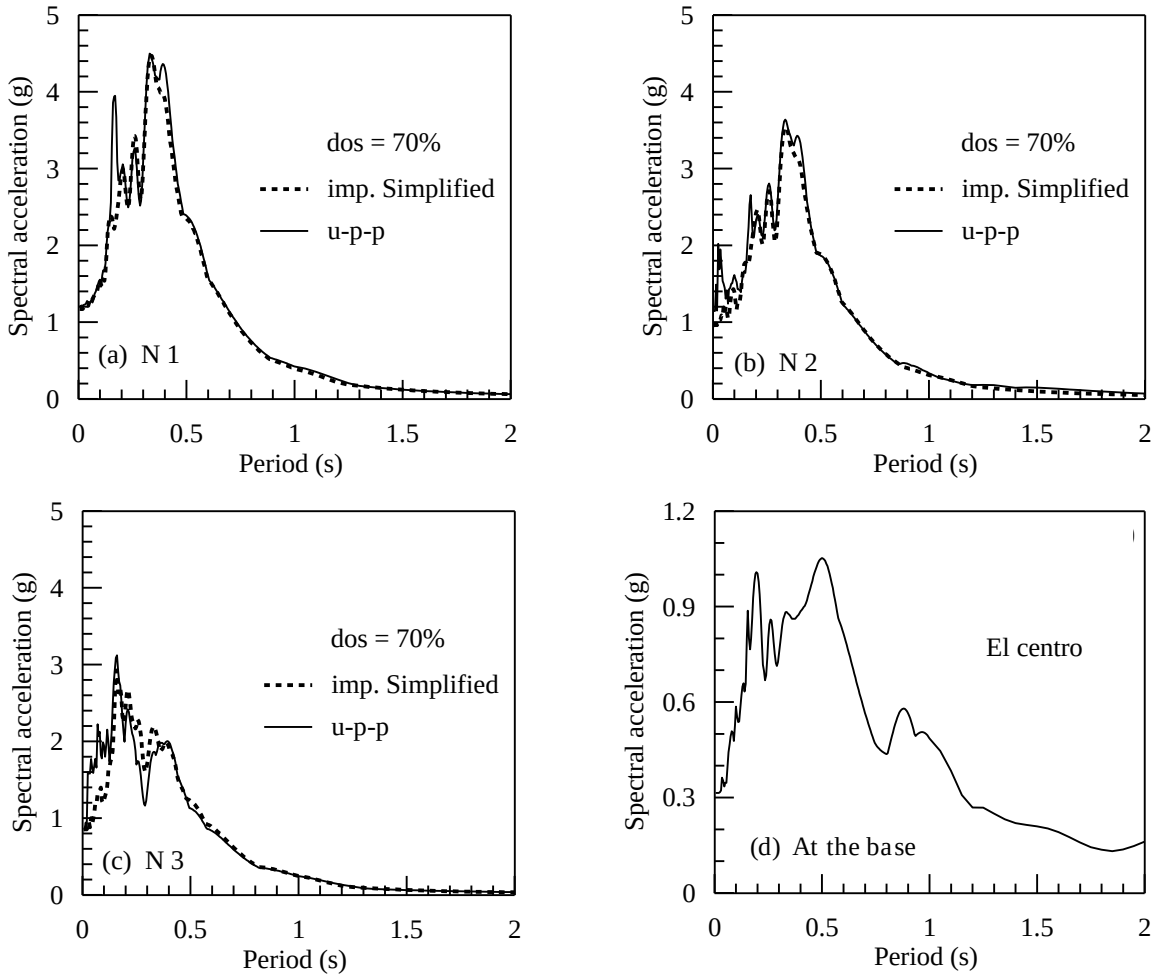

Figure 9.13 Comparison of predicted spectral accelerations and the base acceleration

Horizontal Displacement-Time Histories

The predicted horizontal displacement-time histories at nodes N1 and N2 are shown in Figure 9.14. The coupled deformation-flow simulation predicts slightly higher plastic deformation compared to the undrained or deformation simulation. However, similar to the spectral acceleration, highest displacement is predicted at the node N1 and the lowest displacement is predicted at node N3 (free-field) in both cases.

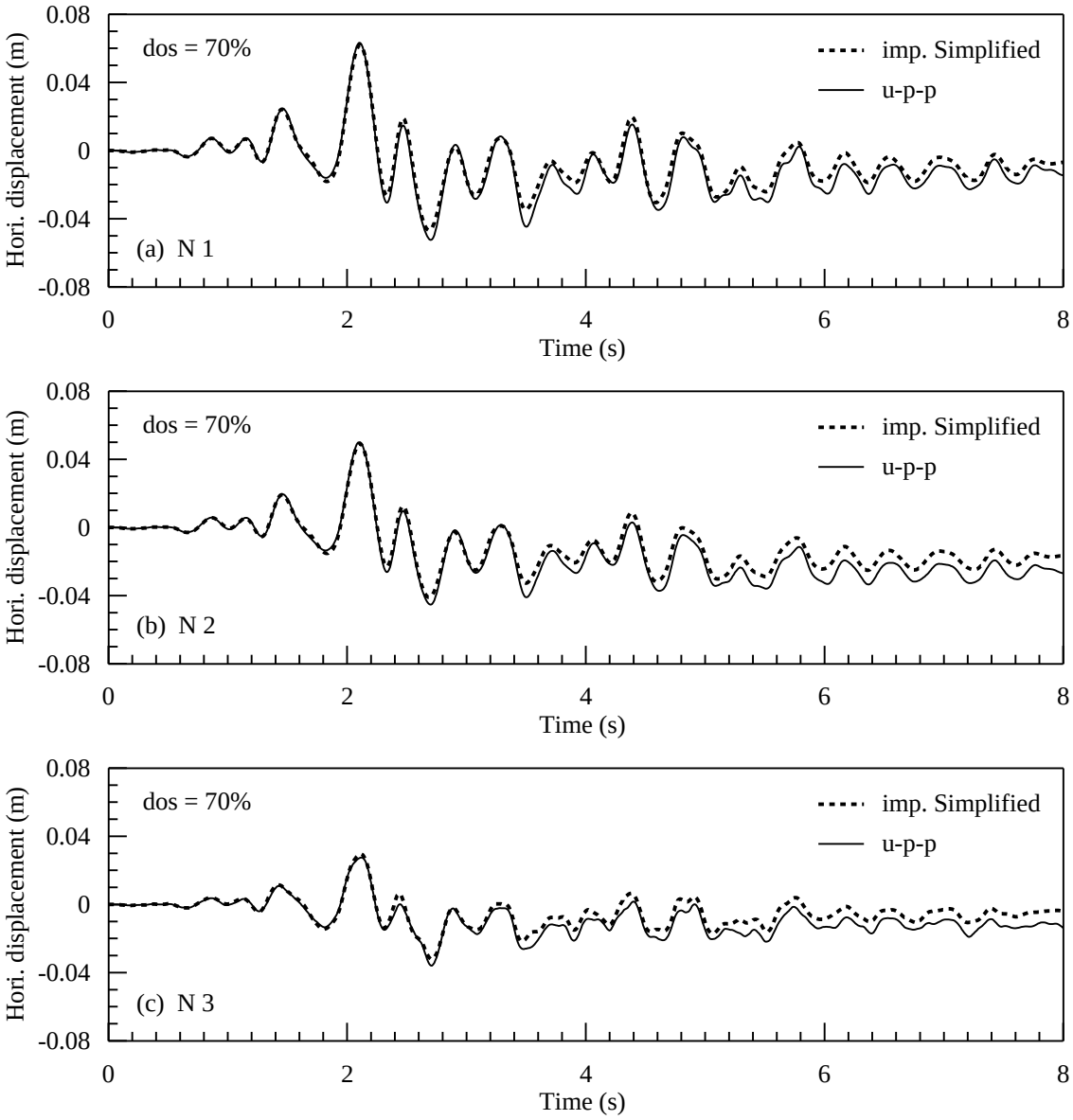

Figure 9.14 Comparison of the predicted horizontal displacement-time histories

Incremental Suction-Time Histories

The incremental suction-time histories are predicted in four elements; E1, E2, E3 and E4 (see Figure 9.11) and presented in Figure 9.15. The E1 and E2 are surface elements, however, the E1 is located away from the pile in the free-field and the element E2 is located very close to the pile. Similar to the E1 and E2, the elements E3 and E4 are

located away from the pile and close to the pile, respectively. However the E3 and the E4 are located at the halfway depth of the pile, whereas the E1 and E2 are surface elements.

Based on the coupled deformation-flow analysis, it can be summarized that all four elements show decrease in suction during earthquake shaking. Also, the surface element near the pile (E2) shows slightly higher change in suction compared to the one far away from the pile (E1). The undrained/ deformation analysis is also predicts decrease in suction in Elements E1, E3, and E4 (Figures 9.15a, 9.15c, and 9.15d), whereas it calculates increase in suction in the element E2 (Figure 9.15b). This increment should be calculated because of the expansion of element (E2) volume. However, the prediction of the coupled deformation-flow analysis can be considered to be more reliable, because it calculates the suction variation based on both deformation and flow characteristics. It can also be further supported that the degree of saturation is expected to increase during an earthquake loading; therefore the suction can be projected to decrease. These figures also show the influence of the presence of the pile foundation on the development and dissipation of suction.

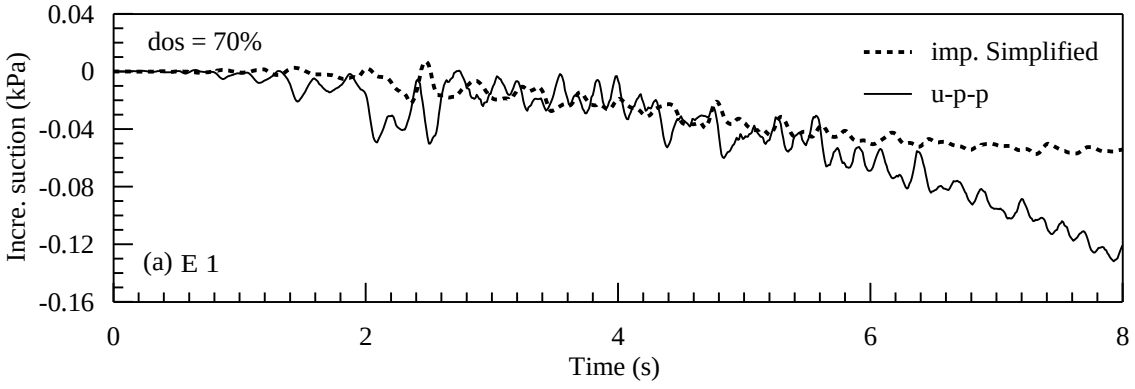

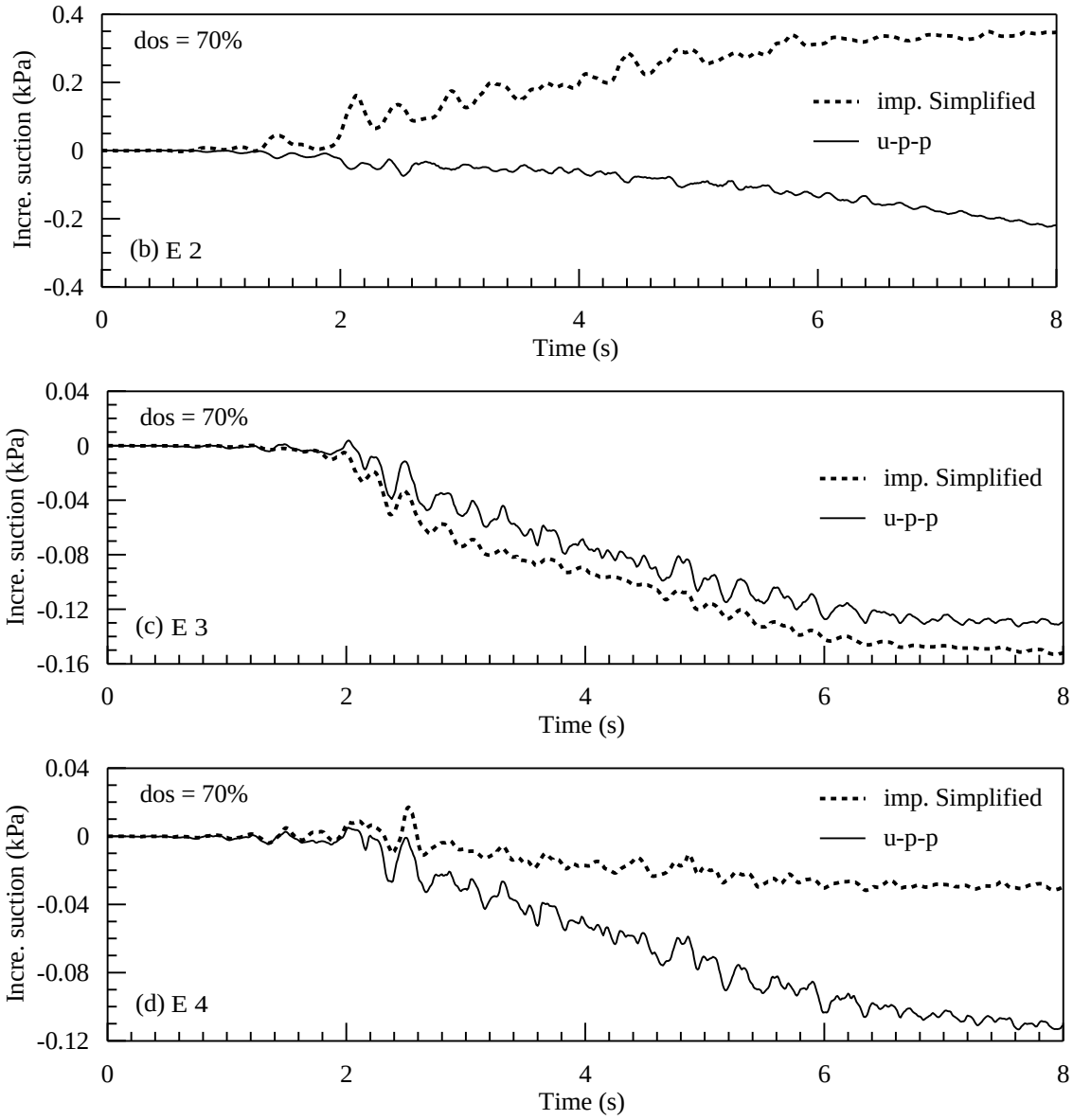

Figure 9.15 Comparison of predicted incremental suction-time histories

Summary of the Study

A finite element model for coupled deformation-flow analysis of unsaturated soil-structure systems is implemented in TeraDysac and used for simulations of *flow through unsaturated embankment*, *coupled deformation-flow analysis of unsaturated soil-pile*

system. Therefore, it can be summarized that the coupled deformation-flow analysis finite element model of TeraDysac software is capable of simulating problems related to flow through unsaturated soils and coupled deformation-flow behavior of unsaturated soil-structure systems. In addition, the SPI simulation studies show increased accuracy in the predictions of coupled deformation-flow analysis compared to the predictions of the undrained/ deformation analysis.

The implemented coupled deformation-flow analysis finite element model consists of the following key elements: (i) *partially reduced finite element formulation*, (ii) *effective soil-water characteristic curve models*, (iii) *effective relative permeability models*, and (iv) *nodal pore pressure boundary conditions*. Using the nodal pore pressure boundary condition, flow of water can be effectively generated by creating a hydraulic gradient. In addition, if a node or side is open to atmosphere, the pore gas pressure should be set to zero at the node or side and it can be done using the nodal pore gas pressure boundary condition. It is necessary to state here that the implementation of the coupled deformation-flow analysis finite element model is remarkably enhanced the performance and applicability of TeraDysac software.

CHAPTER TEN

VALIDATION OF THE COUPLED DEFORMATION-FLOW ANALYSIS FINITE ELEMENT MODEL

Classical Procedure of Centrifuge Modeling of SPI Problems

The classical modeling procedure of soil-pile interaction modeling can be divided into three major stages. The first stage is model construction. The procedure of model construction varies depending on the problem type. It is a common practice to use pluviation technique to place soil at dry condition in the model container. The pluviation height directly depends on the target density of the soil. Based on the prototype pile type i.e. drilled shaft or driven shaft, the method of piling will vary. To model driven shaft prototype pile, the model pile will be driven into the soil after completing the pluviation. For drilled shaft prototype pile, once the necessary depth is achieved by the pluviation, the model pile will be placed and then the pluviation process can be continued. If necessary, piles can also be casted after the completion of pluviation. In addition, instruments/sensors will be placed wherever necessary.

Once the model is constructed, the model will be brought to the centrifuge machine and connected to the flight/shake table with perfect alignment. Another important step in the second phase is to saturate the model. Usually the saturation process will be started from the bottom of the model to saturate the model uniformly. The saturation process will be stopped once the water level reaches the soil surface. If it is a dry test, the saturation process will be skipped.

The last part is spinning and testing. Once the saturation process is over, the centrifuge machine and surrounding area will be carefully checked and arranged for the centrifugal/spinning process. Upon making sure the safety, the spinning process will be started and it will be continued until the soil experiences the target centrifugal force and adequate consolidation. Once a steady state is achieved with adequate consolidation, external loads (static or dynamic) will be applied to the system using remotely-operated control unit.

Ineffectiveness of the Classical Method for Modeling with Unsaturated Soil

An apparent method to perform centrifuge modeling with unsaturated soils is to prepare the physical model with required degree of saturation using the typical procedure and test it. However, there is a high possibility for excessive evaporation and moisture loss in the near surface soil layer. Therefore, the initial degree of saturation cannot be maintained at a required range throughout the modeling process. Therefore the typical procedure cannot be used for unsaturated condition. Furthermore, the amount of evaporation and its effects increase as the spinning duration increases. Increased air circulation and variation in surrounding temperature might cause/increase the evaporation. Centrifuge modeling with clayey soils usually takes more time to achieve adequate consolidation and it might even create cracks/fractures in near surface soil layer. In addition, it is relatively difficult to prepare a model with wet soils, i.e. at a partially saturated condition. It will be trouble-free if the model can be prepared with dry soil and then a uniform degree of saturation profile can be achieved while spinning. Therefore a

scheme should be developed to achieve uniform degree of saturation profile while spinning.

A New Centrifuge Modeling Scheme for Unsaturated SPI Modeling

To achieve uniform degree of saturation profile in centrifuge modeling, a new scheme is developed and successfully used for a series of centrifuge tests performed at UC Boulder. The new method is proposed to achieve the uniform degree of saturation profile by creating a steady flow through the soil layer. It should be noted that in this method, the inflow (spray water) and the outflow (drainage) should be uniform. For the uniformity of the inflow, the inflow water should be uniformly supplied to the whole surface area of the model. Also the surface soil and other test setups in the model surface should not be disturbed by the method of water supply. Therefore it is planned to spray the water to the whole area of the model using uniformly positioned nozzles. It is also very important to use same type of nozzles and supply same amount of water for each nozzle. Therefore the inflow tubes should be arranged in such a way to supply same amount of water to each nozzle. Another important point to note is the pressure of the water stored in the tank #1. As it is planned to spray the water it is very important to store the water with an adequate pressure.

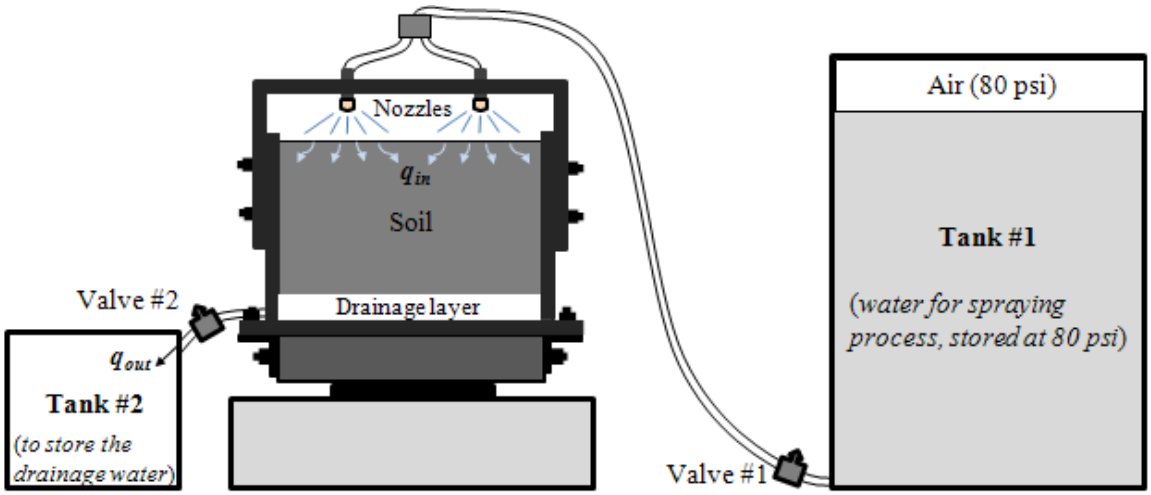

Figure 10.1 A figure explaining the proposed scheme

To get the uniformity in the drainage/outflow, it is designed to place a drainage layer at the bottom of the model i.e. below the soil layer. Drainage tubes should be placed in all four sides of the drainage layer and it is better to place the drainage tubes as low as possible. All the drainage tubes should be joined and connected to the valve #2 (see Figure 10.1) and then with the tank #2 (see Figure 10.1).

The valves #1 and #2 should be remotely operatable i.e. should be able to open/close from the control room while spinning. If those valves are remotely operatable, a steady flow through the model (uniform degree of saturation profile) can be achieved by adjusting the inflow and outflow rates i.e. by adjusting the valves #1 and #2.

Suggestions to Improve the Effectiveness of the Scheme

It is essential to have an uninterested soil layer between the drainage layer and the interested soil layer. Because the degree of saturation of bottom soil layers will remain at near saturation condition due to capillary rise, unless an excellent drainage system is build to avoid the capillary rise. A near saturation condition in the bottom layers will

create difficulties in achieving a uniform degree of saturation profile with a target degree of saturation. By having an uninterested soil/gravel layer in between the drainage layer and the interested soil layer, the worries about the capillary rise can be solved. It can also be reduced by improving the drainage and locating the drainage outlets at the bottom of the model or in the sides but as low as possible.

It is important to make sure that the surface is flat and the water will not flow through any weak interfaces. If the soil surface is not flat enough, there is a possibility of surface flow, which will affect the uniformity of infiltration, thus the uniformity of the degree of saturation profile. Furthermore, there is a possibility for weak interfaces to be formed due to the presence of instruments' wires unless special consideration is given. The issues due to the presence of wires can be minimized by directing all the wires to a corner of the box and placing sufficient amount of soil. It will be more effective, if more soil can be placed at that corner to increase the slope slightly.

Developing a method to reuse the drainage water for spraying purpose would be another valuable recommendation. The amount of water available for spraying purpose is limited as it should be stored in a tank (Tank #1 in Figure 10.1). However if the drainage water (water in Tank #2 in Figure 10.1) can be filtered and restored to the Tank #1, this method will be very effective.

Physical Modeling of Soil-Pile Interaction Using the Classical and the New Scheme

Problem Description

The objectives of this study were to understand the effect of degree of saturation on soil-pile interaction behavior and use the experimental data to validate the accuracy of the finite element model. Dynamic behavior of steel pipe pile in sandy soil (Ottawa sand) was modeled in this study. An SCDOT standard steel pipe pile with 24 inch outside diameter and 0.5 inch wall thickness was selected as the prototype pile. The physical model was designed with two piles (with adequate spacing): Pile #1 and Pile #2. Pile #1 is for static-cyclic load test and the Pile #2 is for dynamic load test. A concentrated mass of 323g was attached to the Pile #2 to represent the superstructure. The Figure 10.2 shows the plan view and three section views of the physical model.

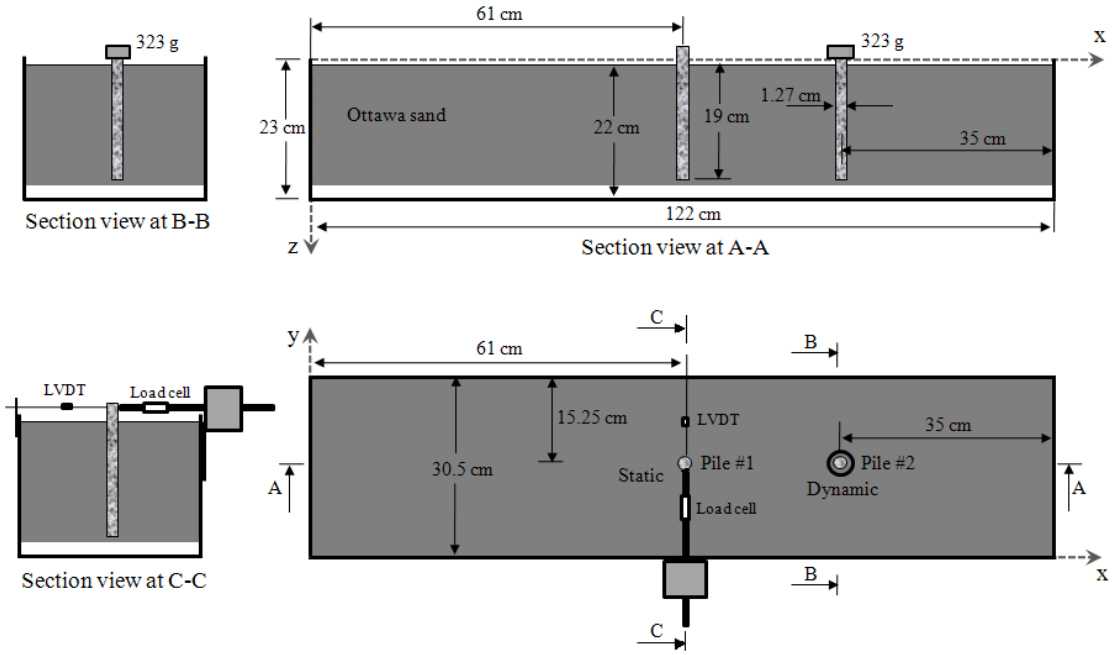

Figure 10.2 Plan and section views of the physical model (dimensions are in cm)

Saturated and Dry Soil-Pile Interaction Modeling Using the Classical Method

Model Construction

The first step in the model construction was to construct a drainage system at the bottom of the container. The drainage system is not necessary for a dry test; however it is important for a saturated test. A drainage tube system was constructed at the bottom (outside) of the container as shown in Figure 10.3. To facilitate a uniformly distributed drainage in the saturation process, the base of the container was lined with a thin layer of Gravel. To control sand flow and to improve the drainage, a filter paper layer was also placed right above the gravel layer. Pictures of the container with drainage tube system and the Gravel drainage layer are shown in Figure 10.3 and Figure 10.4, respectively.

Figure 10.3 The container with drainage tube system

Figure 10.4 The container with the drainage layer

Once the drainage layer placed properly, the dry pluviation was started. To obtain a uniform profile with approximately about 45% relative density, a pluviation height of 1cm was used and this height was calibrated previously. To place the instruments, the soil was leveled at needed depths, and the instruments were placed based on the instrumentation layout shown in Figure 10.5. The coordinates of the instrumentation locations are given in Table 10.1 through Table 10.4. The instruments; accelerometers (A_1-A_{10}), water content transducers (WC_1-WC_8), and Pore pressure transducers (PP_1 and PP_2) were placed in the soil at different locations while placing the soil. At the end of the pluviation or model construction, the LVDTs were placed at the surface of the model.

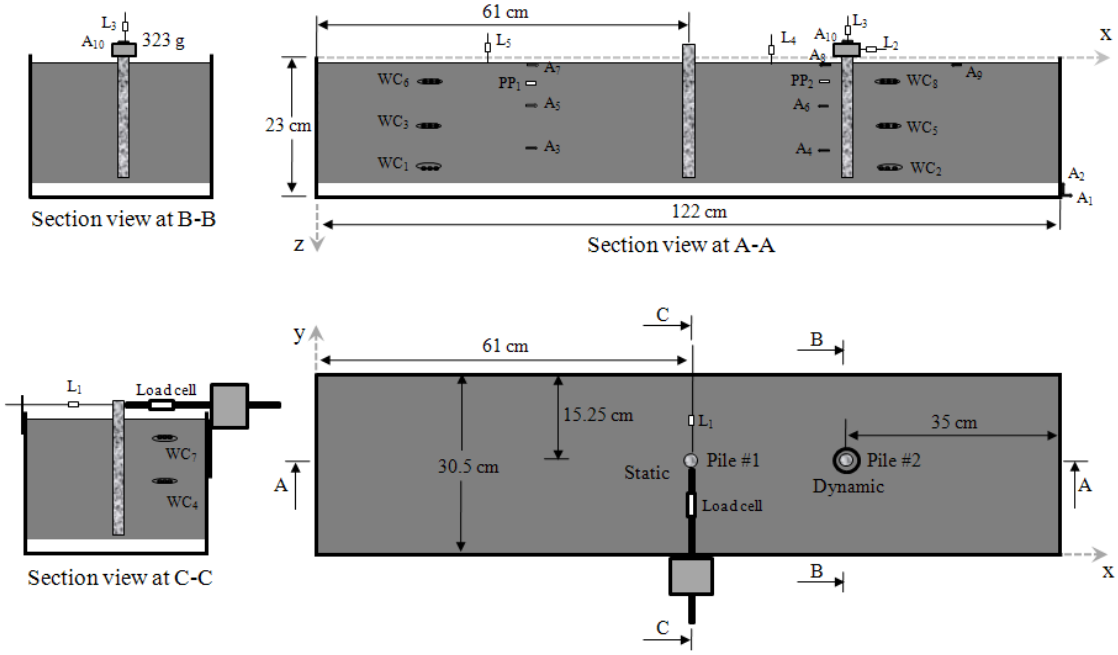

Figure 10.5 Instrumentation layout of the physical model (dimensions are in cm)

Table 10.1 Coordinates of WCs' location

Instrument Type	Instru. Name	x (cm)	y (cm)	z (cm)
WC	WC_1	21	15.25	19
WC	WC_2	95.5	15.25	19
WC	WC_3	21	15.25	11.5
WC	WC_4	61	15.25	11.5
WC	WC_5	95.5	15.25	11.5
WC	WC_6	21	15.25	4.5
WC	WC_7	61	15.25	4.5
WC	WC_8	95.5	15.25	4.5

Table 10.2 Coordinates of PPTs' location

Instrument Type	Instru. Name	x (cm)	y (cm)	z (cm)
PPT	PP_1	36	15.25	4.5
PPT	PP_2	83	15.25	4.5

Table 10.3 Coordinates of accelerometers' location

Instrument Type	Direction	Instru. Name	x (cm)	y (cm)	z (cm)	
Acc	V	A_1				at the base of the container
Acc	H	A_2				
Acc	H	A_3	36	15.25	15	
Acc	H	A_4	83	15.25	15	
Acc	H	A_5	36	15.25	8	
Acc	H	A_6	83	15.25	8	
Acc	H	A_7	36	15.25	1	
Acc	H	A_8	83	15.25	1	
Acc	H	A_9	103.5	15.25	1	
Acc	H	A_{10}				at the mass of pile #2

Table 10.4 Coordinates of LVDTs' location

Instrument Type	Direction	Instru. Name	x (cm)	y (cm)	z (cm)
LVDT	H	L_1			At the top of pile #1
LVDT	H	L_2			At the top of pile #2
LVDT	V	L_3			At the top of pile #2
LVDT	V	L_4	74	15.25	1
LVDT	V	L_5	28.5	15.25	1

When the depth of the soil layer was 9cm, the model piles were driven into the soil to a depth of 8.5cm and supported as shown in Figure 10.6. The Figure 10.6 also shows the process of pluviation (Figure 10.6a), leveling (Figure 10.6b), and placement of an accelerometer (Figure 10.6c). The pluviation and the instrumentation procedures were continued and completed as summarized in Table 10.5.

(a) *(b)* *(c)*

Figure 10.6 Some of the important steps of model construction; (a) pluviation, (b) leveling process, and (c) supporting the piles and instrumentation

Table 10.5 Summary of model preparation procedure

Layer #	Soil type	Thickness of the layer, cm	Depth (Z), cm
1	Gravel	2.5	20.5
		(Filter paper was placed)	
2	Ottawa Sand	1.5	19
		(2 WCs (WC_1, WC_2) were placed)	
3	Ottawa Sand	4	15
		(2 Accelerometers (A_3, A_4) were placed)	
4	Ottawa Sand	3.5	11.5
		(3 WCs (WC_3, WC_4, WC_5) and the piles were placed)	
5	Ottawa Sand	3.5	8
		(2 Accelerometers (A_5, A_6) were placed)	
6	Ottawa Sand	3.5	4.5
		(3 WCs (WC_6, WC_7, WC_8) and 2 PPTs (PP_1, PP_2) were placed)	
7	Ottawa Sand	3.5	1
		(5 LVDTs (L_1-L_5) and 4 Accelerometers (A_7, A_8, A_9, A_{10}) were placed)	

In order to apply a static-cyclic loading, a hydraulic actuator system was attached with the model container as shown in Figure 10.7. A load cell and an LVDT were also attached to the loading system to measure the horizontal load and the displacement. This loading system can be remotely operated from the centrifuge control room.

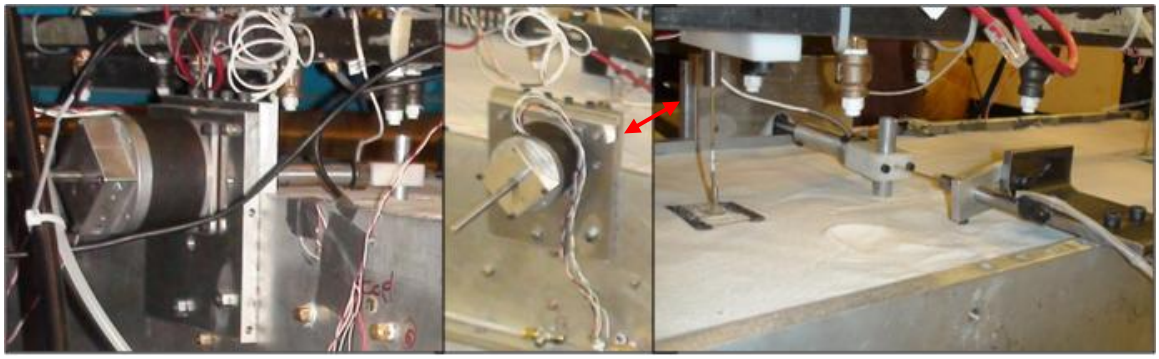

Figure 10.7 The hydraulic actuator and static loading unit

Steps before Spinning

After the completion of model construction i.e. model with lateral loading unit, the model was carefully brought to the centrifuge machine and connected to the shake table using nuts and bolts. Then the wires of the instruments and the lateral loading system were connected with the monitoring unit.

For a saturated test, the model should be saturated before starting the spinning process. Therefore, to saturate the model, the saturation tube (see Figure 10.8) was connected with valve #2 (see Figure 10.8), while keeping the tank#2 disconnected from the valve #2.

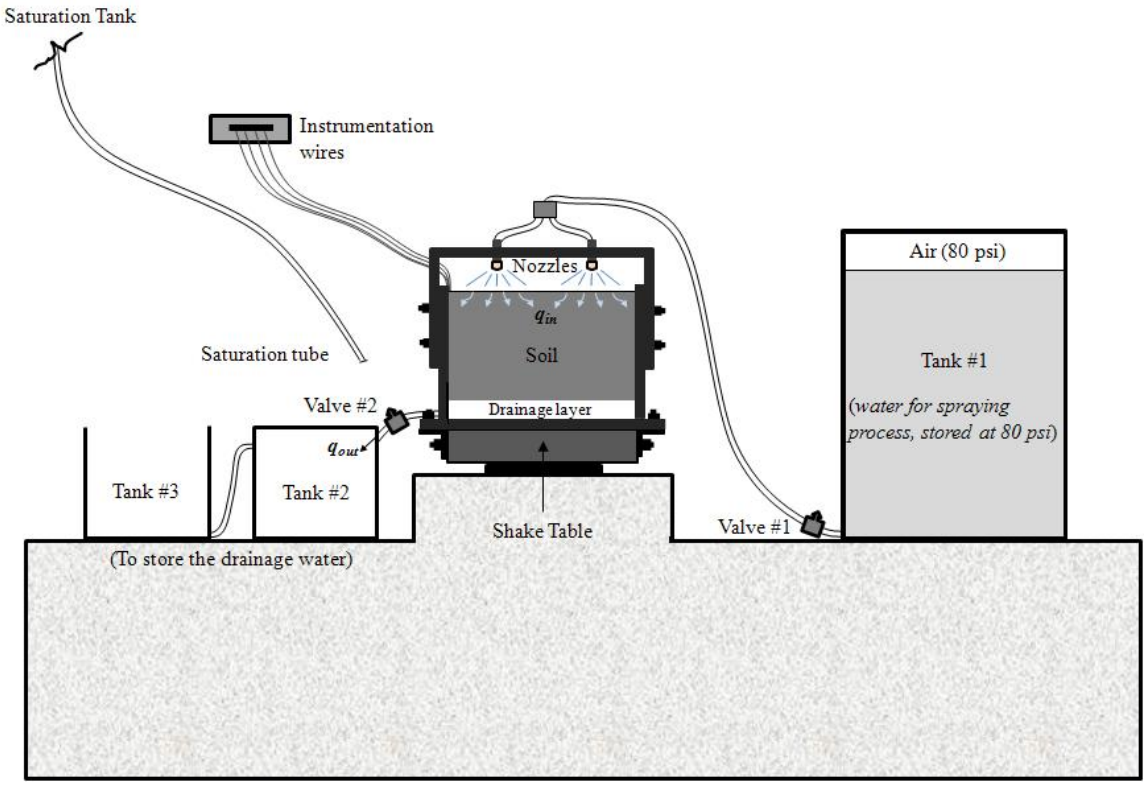

Figure 10.8 A layout showing the drainage system and the model in centrifuge flight

The saturation tank was kept open to the atmosphere; however it had approximately about 10ft elevation head, which pressured the water to flow through the model. The saturation process was stopped and the saturation tube was disconnected after getting the water level slightly above the soil surface.

Spinning and Loading

Once all the steps discussed above are completed, the centrifuge machine and surrounding were arranged for spinning, and then the spinning process was started. Once the target acceleration is achieved, the static and the dynamic tests were performed, i.e. the loading process was started. The applied acceleration history i.e. the history measured at the bottom of the centrifuge model (at shake table level) is presented in Figure 10.9.

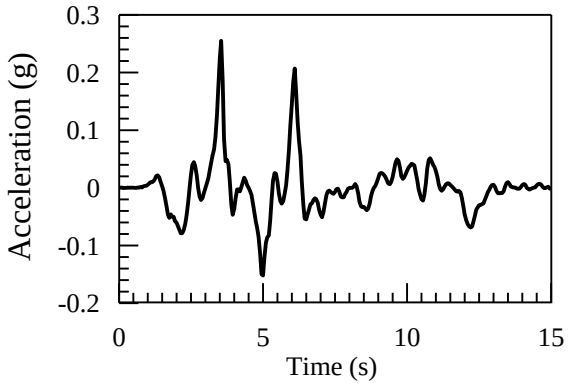

Figure 10.9 Acceleration-time history of the applied motion

Results and Discussion

Measured Acceleration and Corresponding Spectral Acceleration

Using the classical modeling procedure, the tests were performed at dry and saturated conditions. This problem is also analyzed with an initial degree of saturation of 50% using the coupled deformation-flow analysis finite element model (TeraDysac) and the predicted results are compared with centrifuge data (presented in the next section). The horizontal acceleration time histories measured at Accelerometer A3 and A4 are presented in Figure 10.10a and 10.11a, respectively. The spectral acceleration for these two acceleration histories were calculated using 5% damping and presented in Figures 10.10b and 10.11b, respectively. It should be noted that the Accelerometer A3 and A4 are placed at the pile tip level, however the A3 is placed far away from the pile to measure the acceleration history without SPI influence, and the A4 is placed close to the pile to measure the acceleration history with the SPI influence. To study the SPI influence more visibly, the results which are measured or calculated with SPI influence (Accelerometer A4) and without SPI influence (Accelerometer A3) are presented in same figures; Figures 10.12 and 10.13. As shown in Figures 10.10 and 10.11, the amplitude of the acceleration

history which is measured at dry condition is higher than the amplitude of the acceleration history which is measured at saturated condition. As shown in Figures 10.12 and 11.13, the amplitude of the SPI influenced acceleration which is measured at the pile tip level is lower than the amplitude of the acceleration which is measured without the SPI influence.

The horizontal acceleration time histories measured at Accelerometer A7 and A8, and corresponding spectral acceleration are presented in Figures 10.14 through 10.17. The Accelerometer A7 is identical to the Accelerometer A3, i.e. the A3 and A7 are placed away from the pile in a same vertical plan, however the A7 is placed at the surface level. The Accelerometer A8 is identical to the Accelerometer A4; however it is also placed at the surface level. As shown in Figures 10.16 and 10.17, the amplitude of the SPI influenced acceleration which is measured at the surface level is higher than the amplitude of the acceleration which is measured without the SPI influence for both dry and saturated condition. As shown in Figure 10.14, when the soil is at dry condition, the amplitude of the free-field (Accelerometer A7) acceleration is measured to be higher than that of saturated condition. However when the soil is saturated, the amplitude of the acceleration measured with the SPI influence (Accelerometer A8) is higher than that of dry condition. Therefore, beyond the comparison of these two variations, it can be concluded that the response of SPI is significantly governed by the water potential or degree of saturation of the surrounding soil.

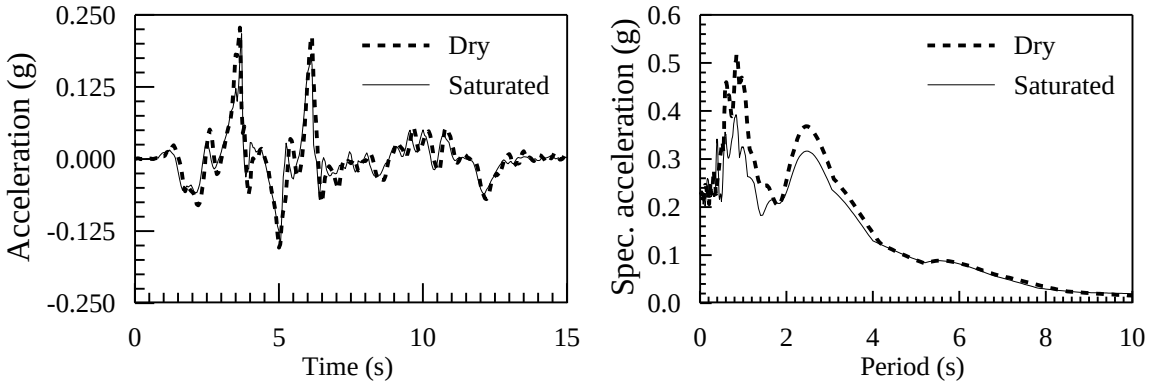

Figure 10.10 Results measured without SPI influence at pile tip level

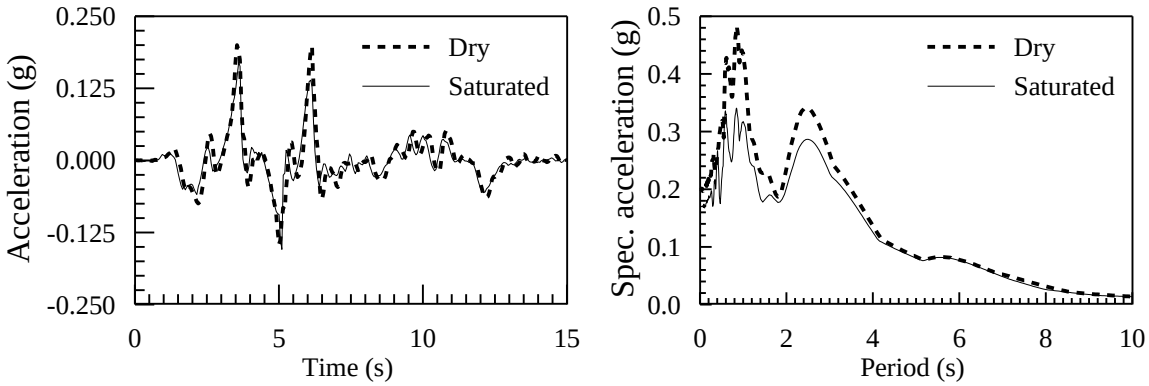

Figure 10.11 Results measured with SPI influence at pile tip level

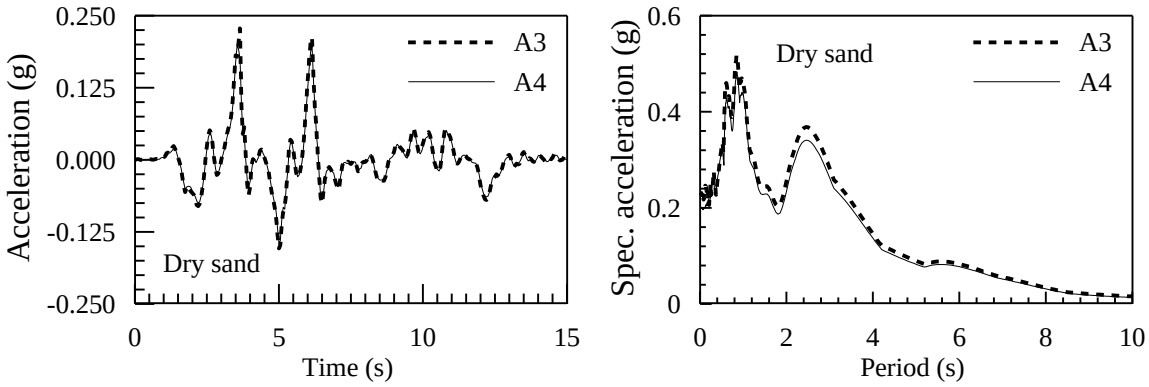

Figure 10.12 Comparison of results measured with and without SPI influence, at pile tip level, at dry condition

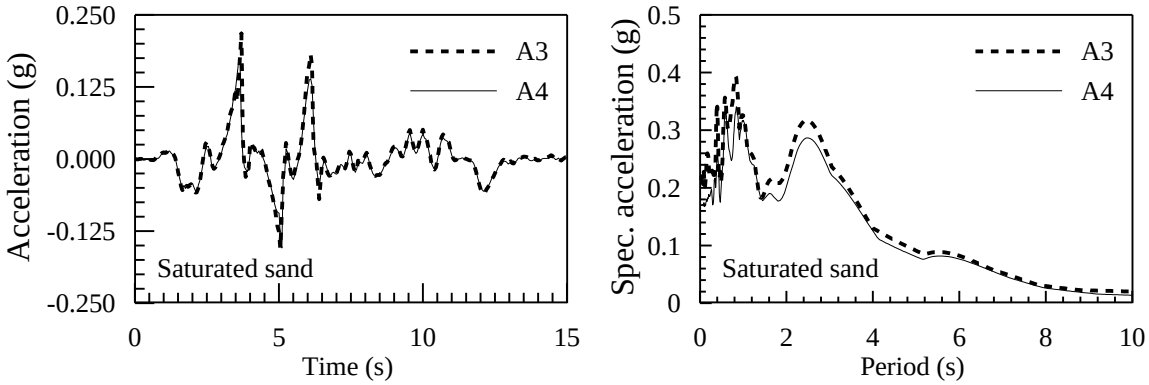

Figure 10.13 Comparison of results measured with and without SPI influence, at pile tip level, at saturated condition

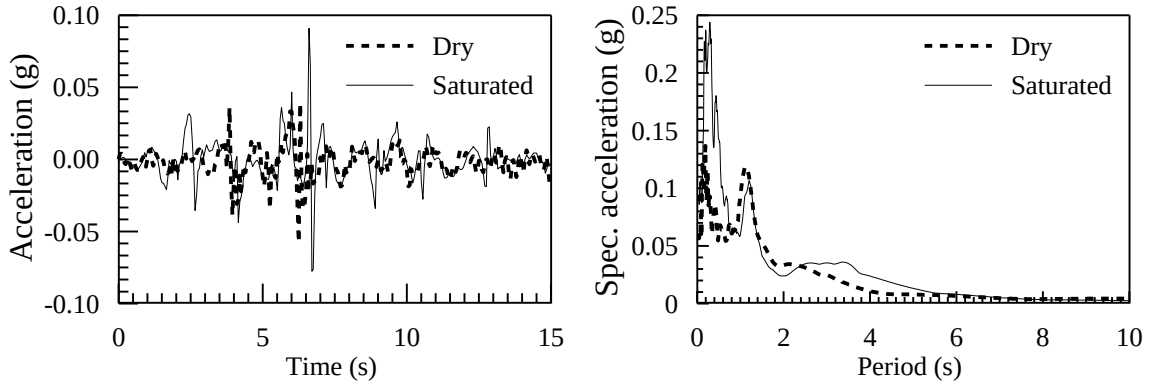

Figure 10.14 Results measured without SPI influence at surface level

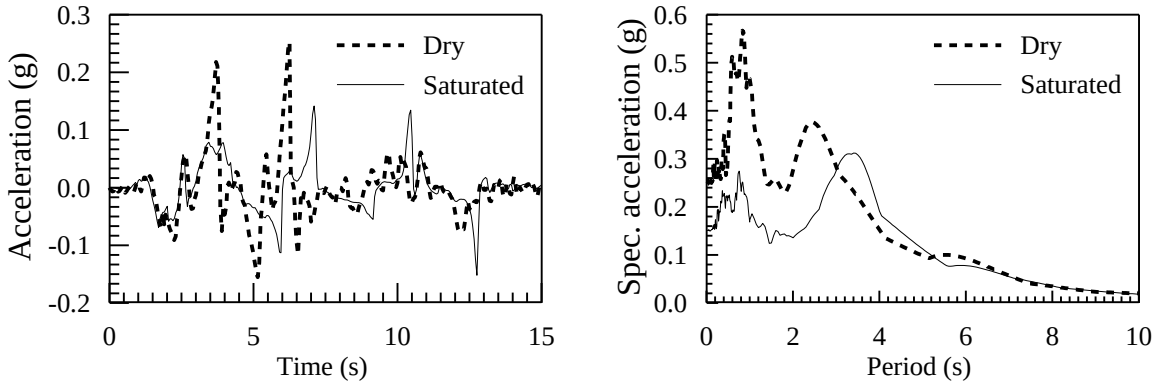

Figure 10.15 Results measured with SPI influence at surface level

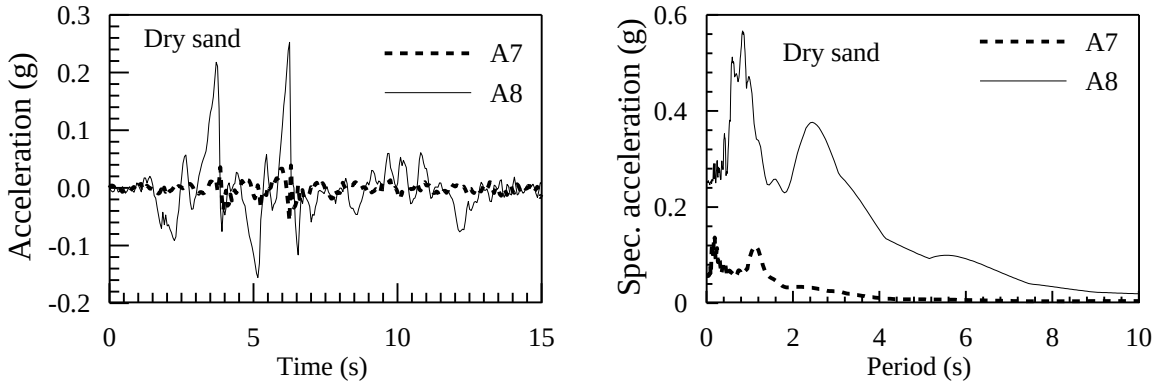

Figure 10.16 Comparison of results measured with and without SPI influence, at surface level, at dry condition

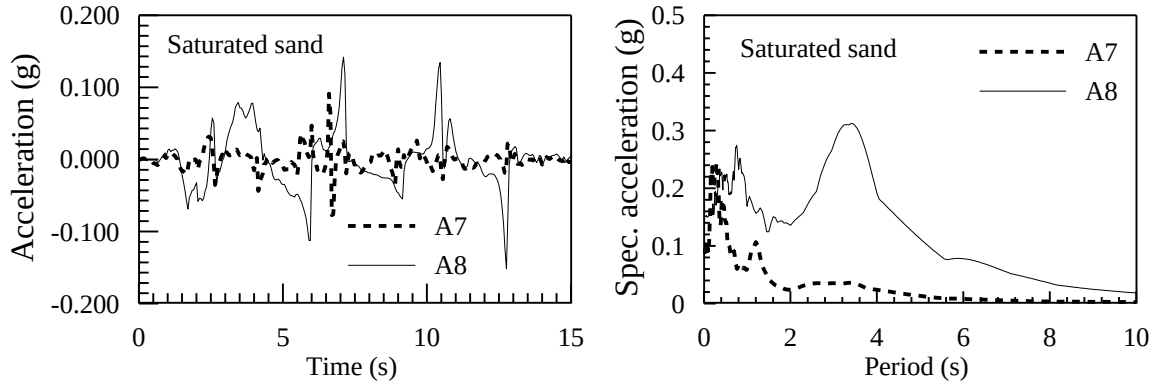

Figure 10.17 Comparison of results measured with and without SPI influence, at surface level, at saturated condition

Settlement and Horizontal Displacement

The horizontal displacement time history at the superstructure level i.e. at the top of the pile is measured using LVDT2 and shown in Figure 10.18a. Vertical settlement is also measured at three different locations and presented in Figures 10.18b through 11.18d. The Figure 10.18b shows the vertical settlement of the pile foundation (measured at superstructure level), Figure 10.18c shows the free-field settlement measured using LVDT4 (see Figure 10.5), and Figure 10.18d shows the free-field settlement measured using LVDT5 (see Figure 10.5). As shown in these Figures, the displacement/settlement measured at saturated condition is higher than the displacement/settlement measured at

dry condition. As shown in Figure 10.18b, when the soil is at dry condition, the settlement of the pile is measured to be zero or almost zero. However, when the soil is at saturated condition, the maximum settlement of the pile foundation is measured to be approximately 420 mm. The maximum free-field settlement measured using the LVDT4 is approximately about 220mm when the soil is saturated, whereas it is about 30 mm when the soil is at dry condition. Using the LVDT5, the maximum free-field settlement of about 200 mm is measured when the soil is saturated, whereas it is also about 30 mm when the soil is at dry condition. Even though the LVDT4 and LVDT5 are placed away from the pile, the LVDT4 is located closer to the pile compared to the LVDT5. Based on all these measurements, it can be concluded that the settlement of the soil increases when the water potential or the degree of saturation increases, and it also increases when the distance from the pile foundation decreases.

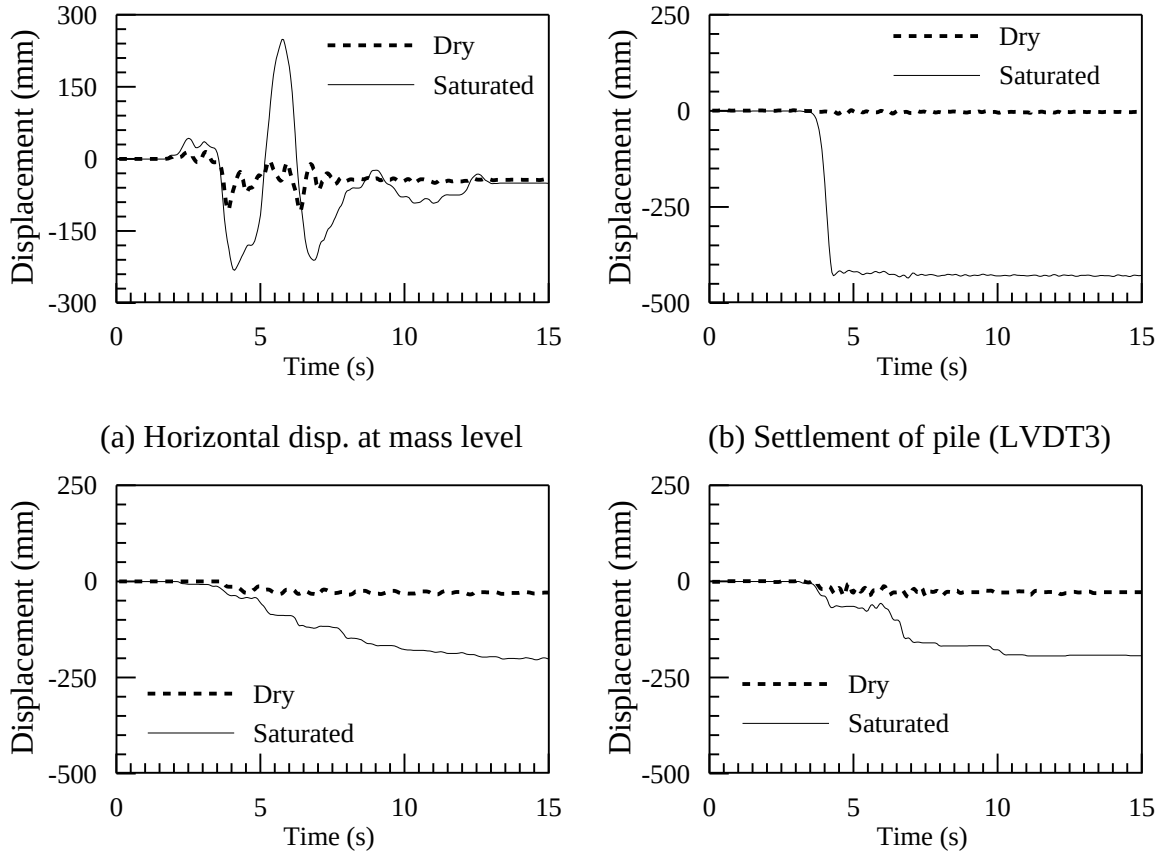

(a) Horizontal disp. at mass level

(b) Settlement of pile (LVDT3)

(c) Free-field settlement (LVDT4)

(d) Free-field settlement (LVDT5)

Figure 10.18 Comparison of settlement and horizontal displacement measured at dry and saturated conditions

Unsaturated Soil-Pile Interaction Modeling Using the Newly Proposed Scheme

Model Construction

The model is constructed as presented in the last section i.e., the procedure used for the saturated modeling is used. Based on the proposed scheme for unsaturated modeling, to achieve uniform degree of saturation profile, it is important to spray the water in the whole surface area of the model. Therefore, a nozzle system with twelve nozzles was constructed and connected with the model so that it can be used to spray the water in the whole surface area. The tubing of the nozzle system was arranged in a way to get same

water flow in all the nozzles. A picture of the nozzle system with equally distributed tubing is shown in Figure 10.19.

Figure 10.19 The nozzle system with equally distributed tubing

Steps before Spinning

After the completion of model construction i.e. model with lateral loading unit and the nozzle system, the model was carefully brought to the centrifuge machine and connected with the shake table. Then the instruments' wires and the lateral loading system wires were connected with monitoring unit. Before starting the spinning process, the model should be saturated. Therefore the saturation tube (see Figure 10.20) was connected with valve #2 (see Figure 10.20), while keeping the tank #2 disconnected from valve #2.

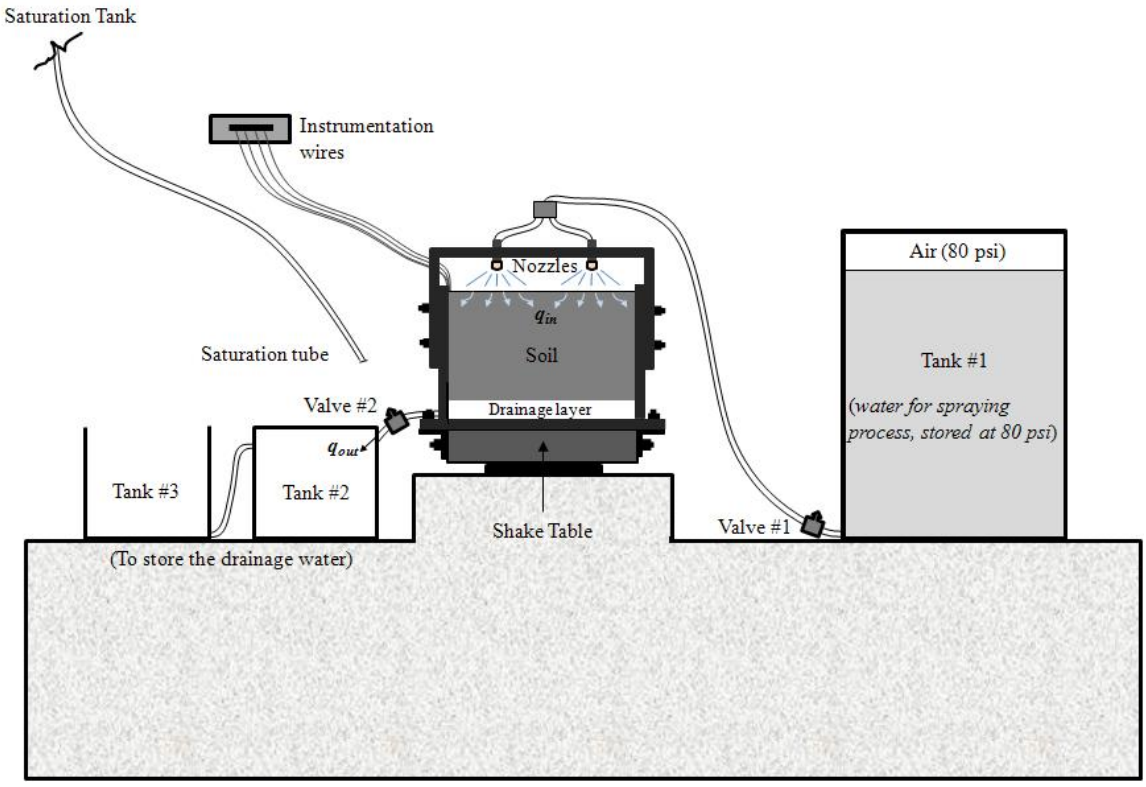

Figure 10.20 A layout showing the drainage system and the model at the centrifuge flight

The saturation tank was kept open to the atmosphere; however it had approximately about 10ft elevation head, which pressured the water to flow through the model. The saturation process was stopped and the saturation tube was disconnected after getting the water level slightly above the soil surface.

Before starting the spinning process, the model was covered with plastic to make sure that the water is not sprayed out outside the model and also to reduce the effect of air circulation. The Figure 10.21 shows the model with the plastic cover.

Figure 10.21 The model with plastic cover

The tank #2 (see Figure 10.20) should be connected with the model to collect the drainage water. There will be no flow through a valve if the valve is closed in the control system even if it is physically open. Therefore using the control unit the valve #2 was closed while keeping it open physically and it will help to activate the drainage later (while spinning) using the control system. The valve #1 was also closed using the remote control system while keeping it open physically.

Spinning and Loading

Once all the steps discussed above are completed, the centrifuge machine and surrounding were arranged for spinning, and then the spinning process was started. Once the target acceleration is achieved, the drainage process was activated by opening the valve #2 using the control system. The moisture sensor readings were monitored while draining the water out. The readings of five moisture sensors which were located in a vertical section are monitored, and a display of the monitoring program is shown in Figure 10.22. The moisture sensors were previously calibrated for the relationship between the sensor reading and the degree of saturation. After getting the target reading

in the bottom moisture content sensor, the spraying process was also started by opening the valve #1. While monitoring the moisture sensor readings, the drainage and the spraying process were adjusted as needed. After achieving a steady flow i.e. approximately same reading in all the sensors (uniform degree of saturation profile), the static and the dynamic tests were performed, i.e. the loading process was started. The applied acceleration history i.e. the history measured at the bottom of the centrifuge model (at shake table level) is presented in Figure 10.23. To simulate the elastic response of SPI, an acceleration load with a_{max} of 0.07g is used in this modeling. The tests were performed with approximately 10% and 15% degree of saturation.

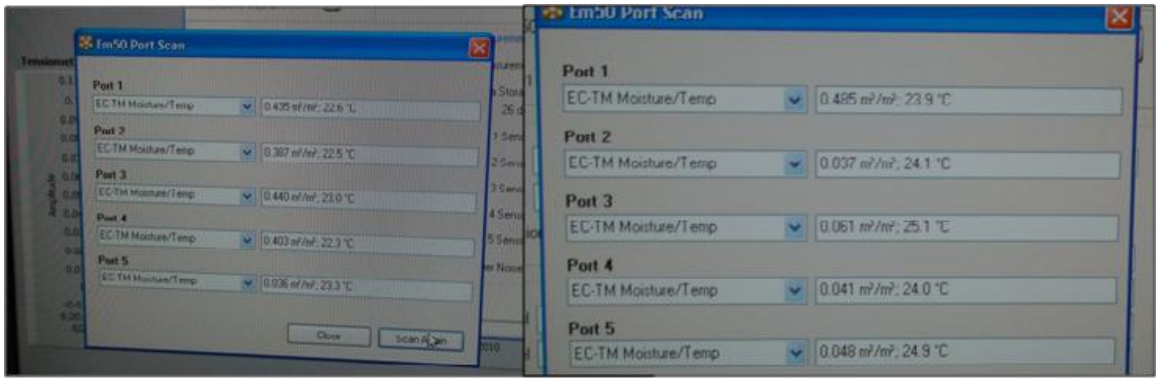

Figure 10.22 A display of moisture sensor readings

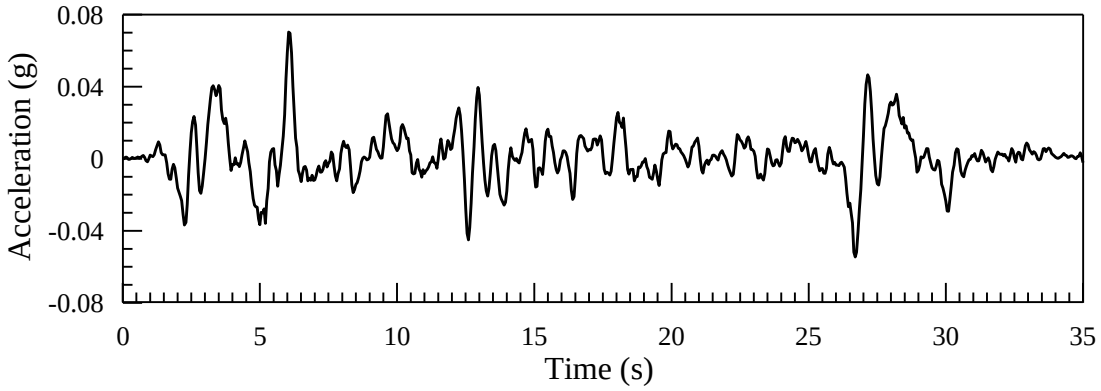

Figure 10.23 The time history of applied acceleration

Results and Discussion

Measured Acceleration and Corresponding Spectral Acceleration (Calculated)

Using the newly proposed scheme, two unsaturated centrifuge modeling were performed with approximately 10% and 15% degree of saturation. It should be noted that the Accelerometer A3, A4, A7, and A8 are placed at the same locations as explained in the saturated modeling section. I.e. Accelerometer A3 and A4 are placed at pile tip level, however the A3 is placed away from the pile and the A4 is placed close to the pile. The Accelerometer A7 is identical to the Accelerometer A3; however it is placed at the surface level. The Accelerometer A8 is identical to the Accelerometer A4; however it is also placed at the surface level.

The time history of horizontal acceleration measured using the Accelerometer A3 and corresponding spectral accelerations are presented in Figures 10.24a and 10.24b, respectively. The spectral accelerations were calculated using 5% damping. The time history of horizontal acceleration measured using the Accelerometer A4 and corresponding spectral accelerations are presented in Figures 10.25a and 10.25b, respectively. To study the SPI influence more visibly, the results which are measured with the SPI influence (Accelerometer A4) and without SPI influence (Accelerometer A3) are presented in same figures; Figures 10.26 and 10.27. As shown in these Figures, the amplitude of the acceleration history which is measured at 15% degree of saturation is higher than the amplitude of the acceleration history which is measured at 10% degree of saturation. As shown in Figures 10.26 and 10.27, the amplitude of the SPI influenced

acceleration which is measured at the pile tip level is lower than the amplitude of the acceleration which is measured without the influence of SPI.

The time histories of horizontal acceleration measured using the Accelerometers A7 and A8, and corresponding spectral acceleration are presented in Figures 10.28 through 11.31. As shown in these Figures, the amplitude of the acceleration history which is measured at 15% degree of saturation is higher than the amplitude of the acceleration history which is measured at 10% degree of saturation. Also the amplitude of the acceleration which is measured (at the surface level) without the SPI influence is slightly higher than the amplitude of the acceleration which is measured with the SPI influence at both 10% and 15% degree of saturations. Therefore it can be concluded that the degree of saturation significantly influences the response of SPI. It can also be concluded that the presence of pile foundation significantly influences the overall response of soil-pile systems.

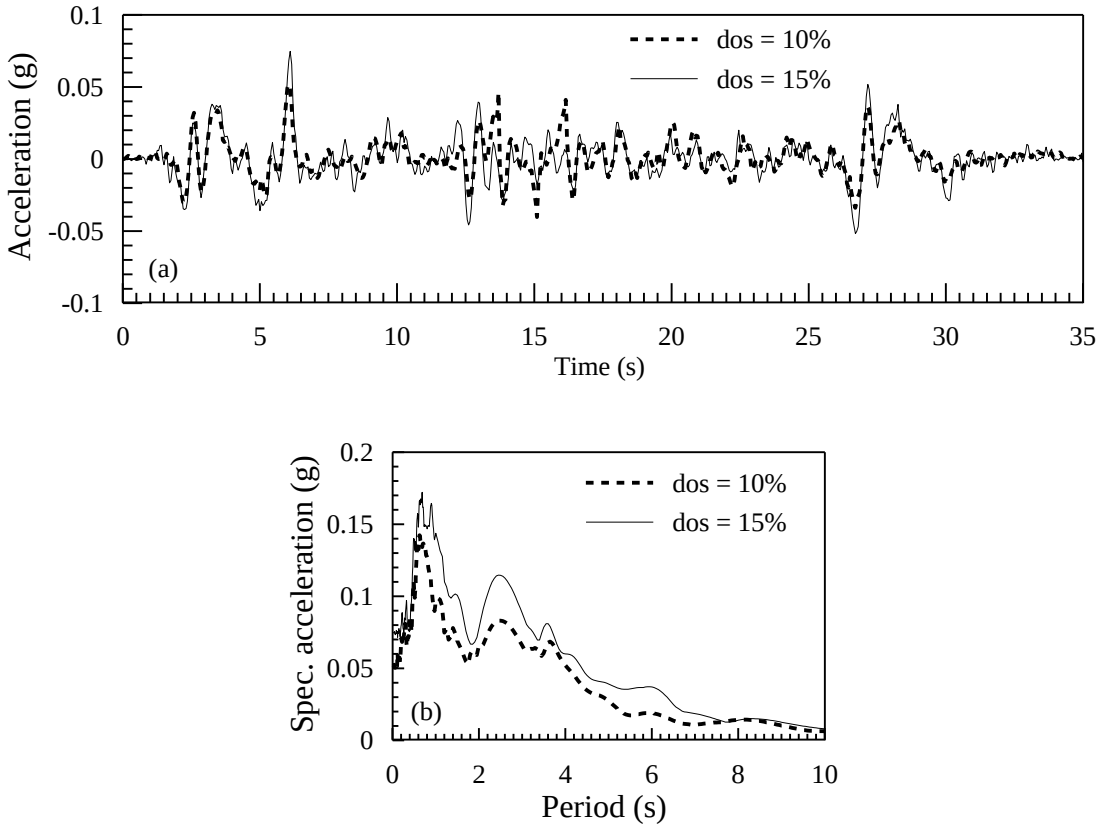

Figure 10.24 Results measured without SPI influence at pile tip level

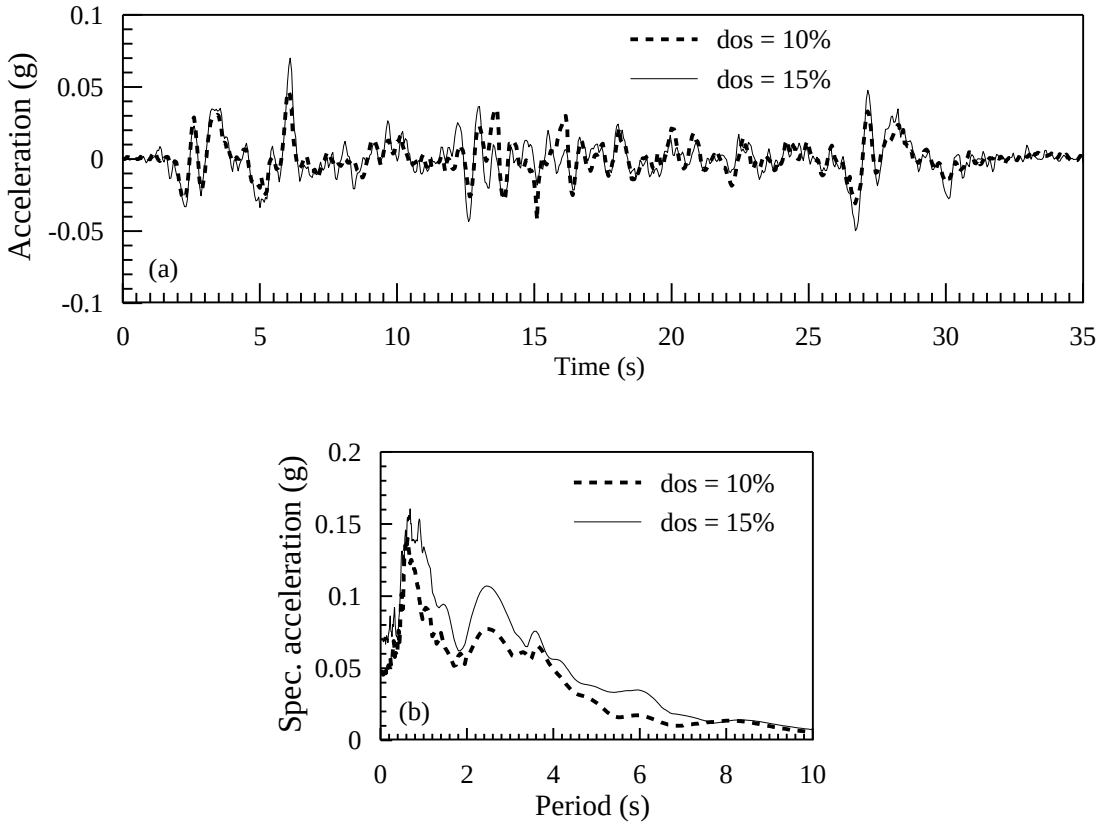

Figure 10.25 Results measured with SPI influence at pile tip level

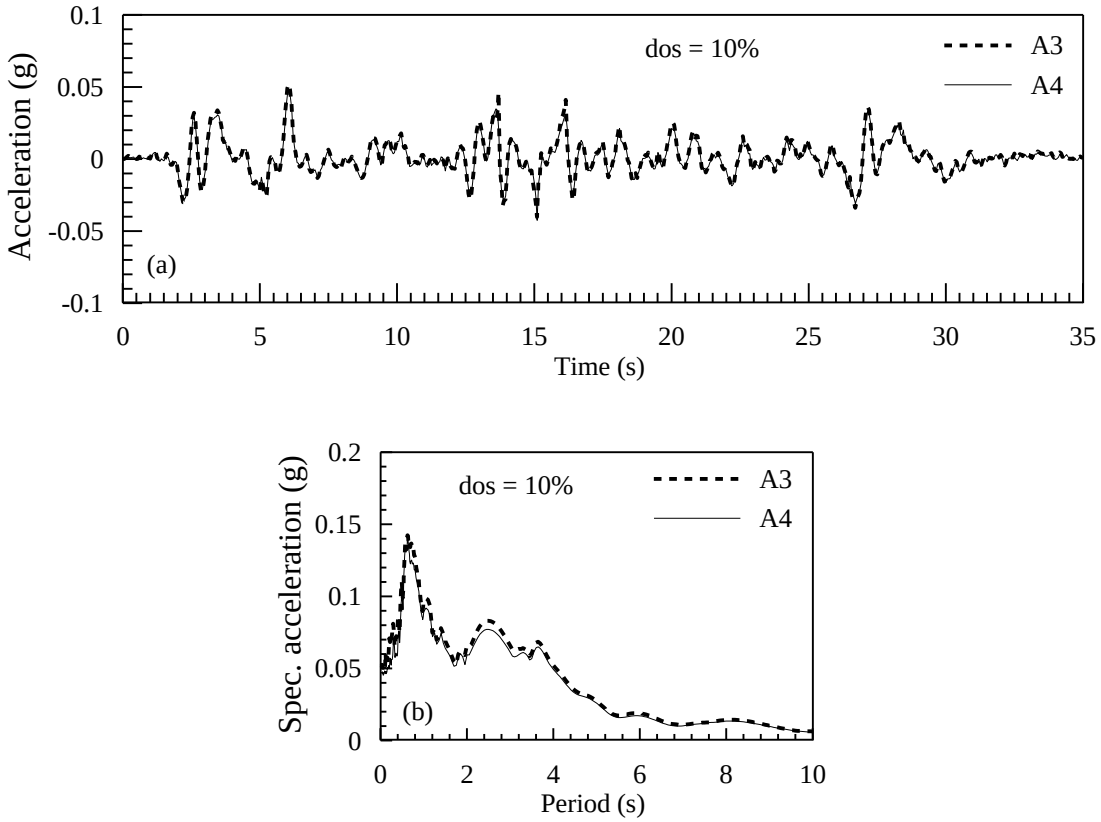

Figure 10.26 Comparison of results measured (at pile tip level) with and without the SPI influence, at 10% degree of saturation

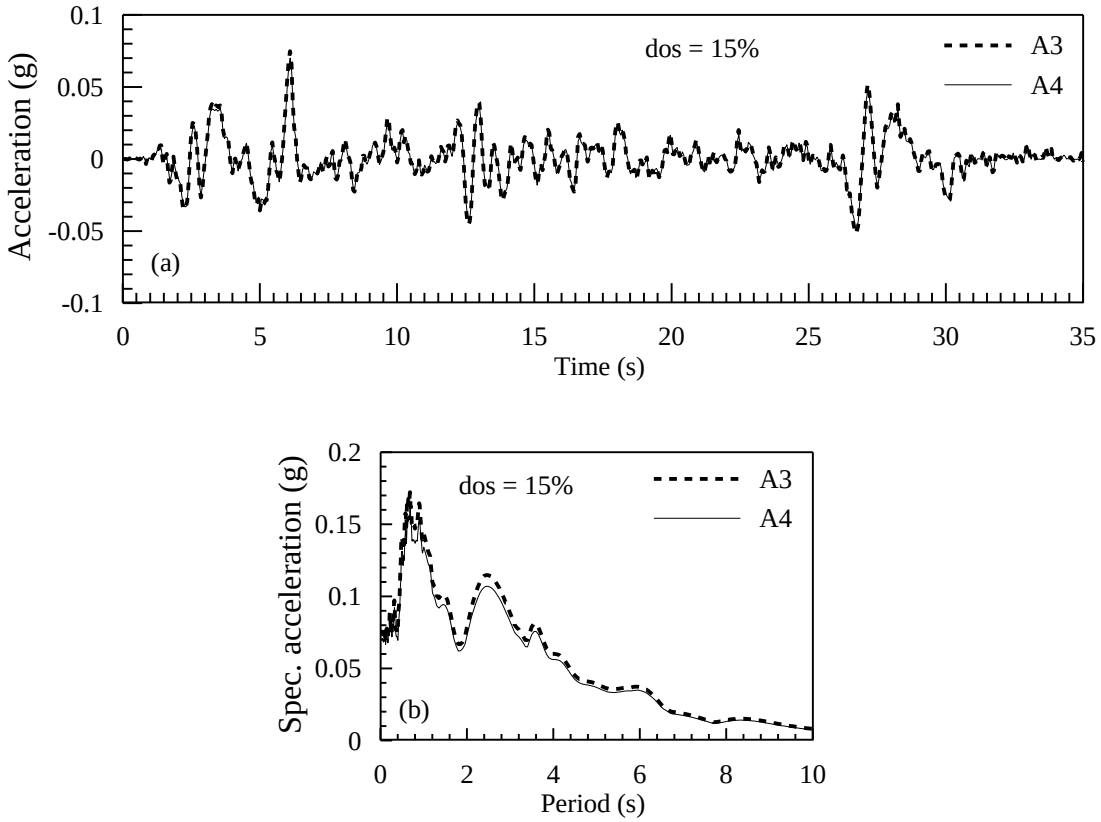

Figure 10.27 Comparison of results measured (at pile tip level) with and without the SPI influence, at 15% degree of saturation

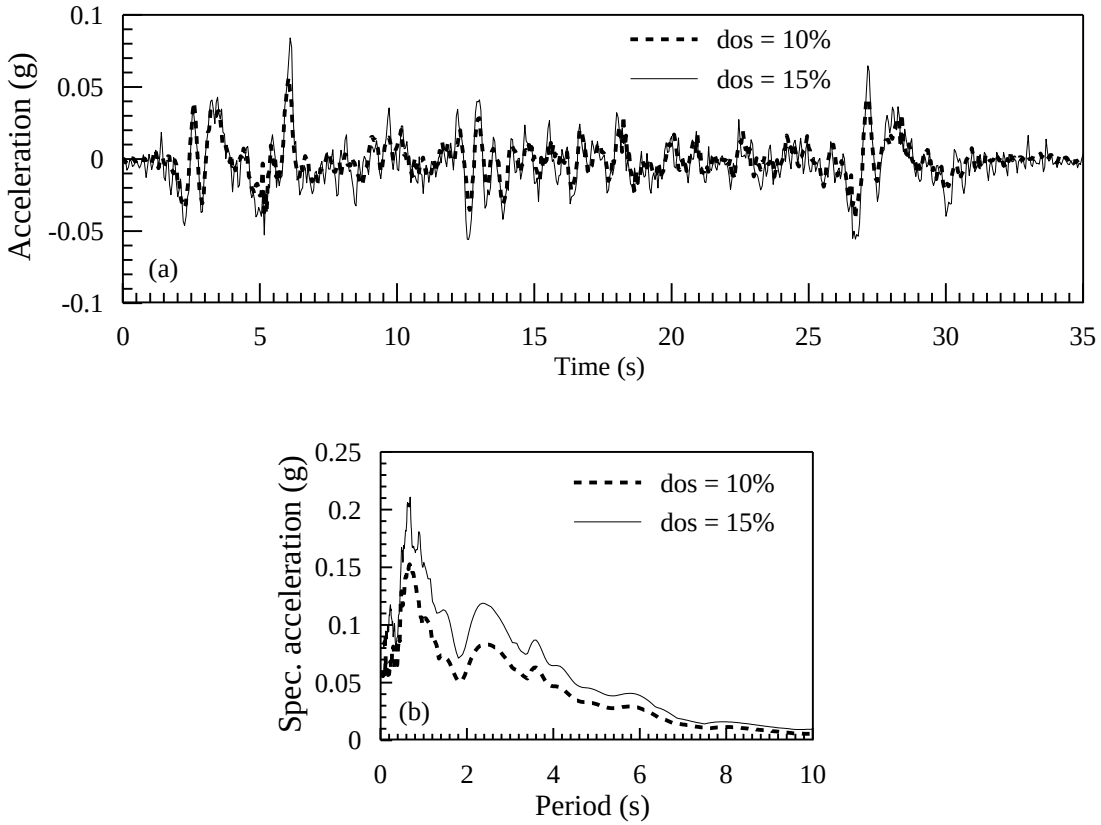

Figure 10.28 Comparison of results measured (at surface level) without SPI influence at 10% and 15% degrees of saturation

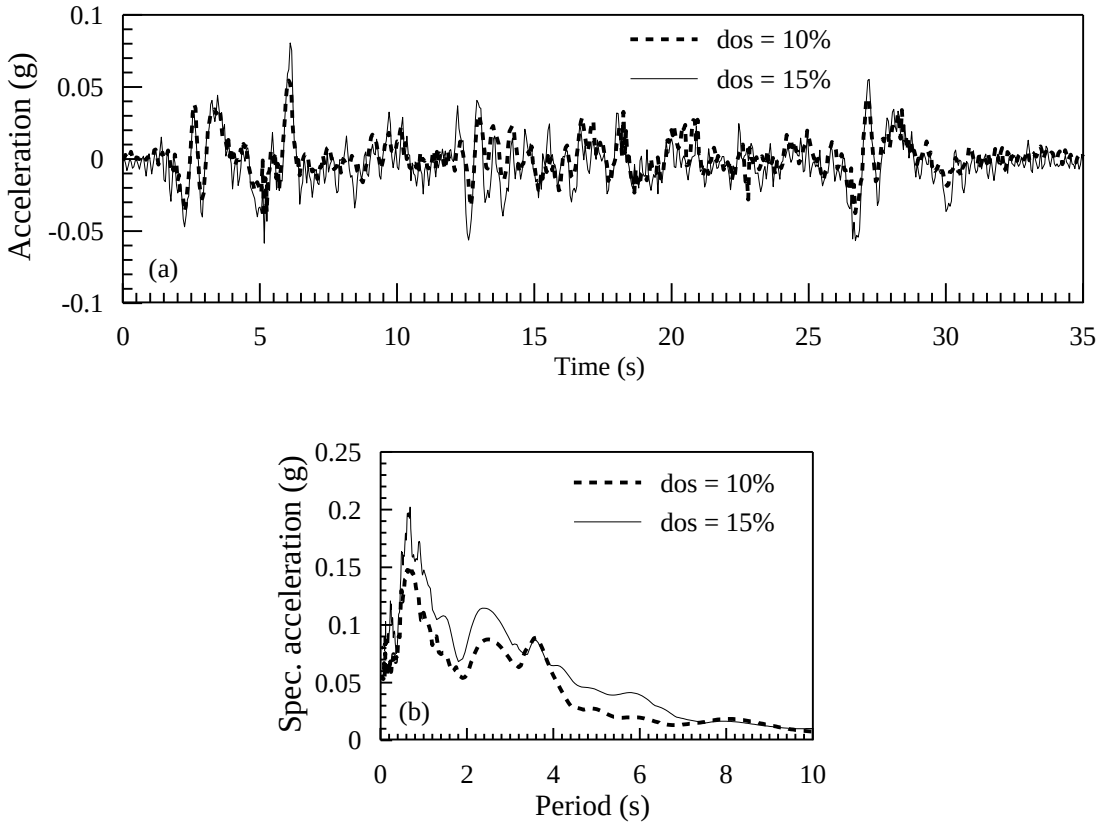

Figure 10.29 Comparison of results measured (at surface level) with SPI influence at 10% and 15% degrees of saturation

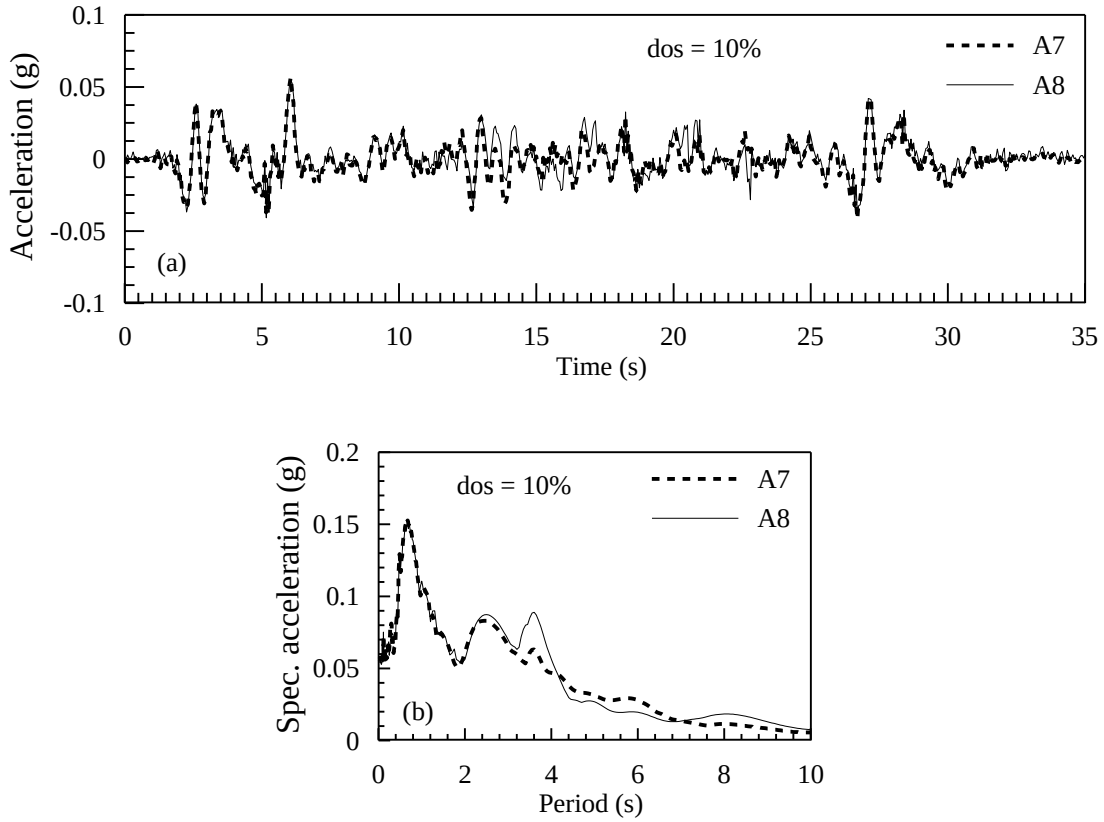

Figure 10. 30 Comparison of results measured (at surface level) with and without SPI influence, at 10% degree of saturation

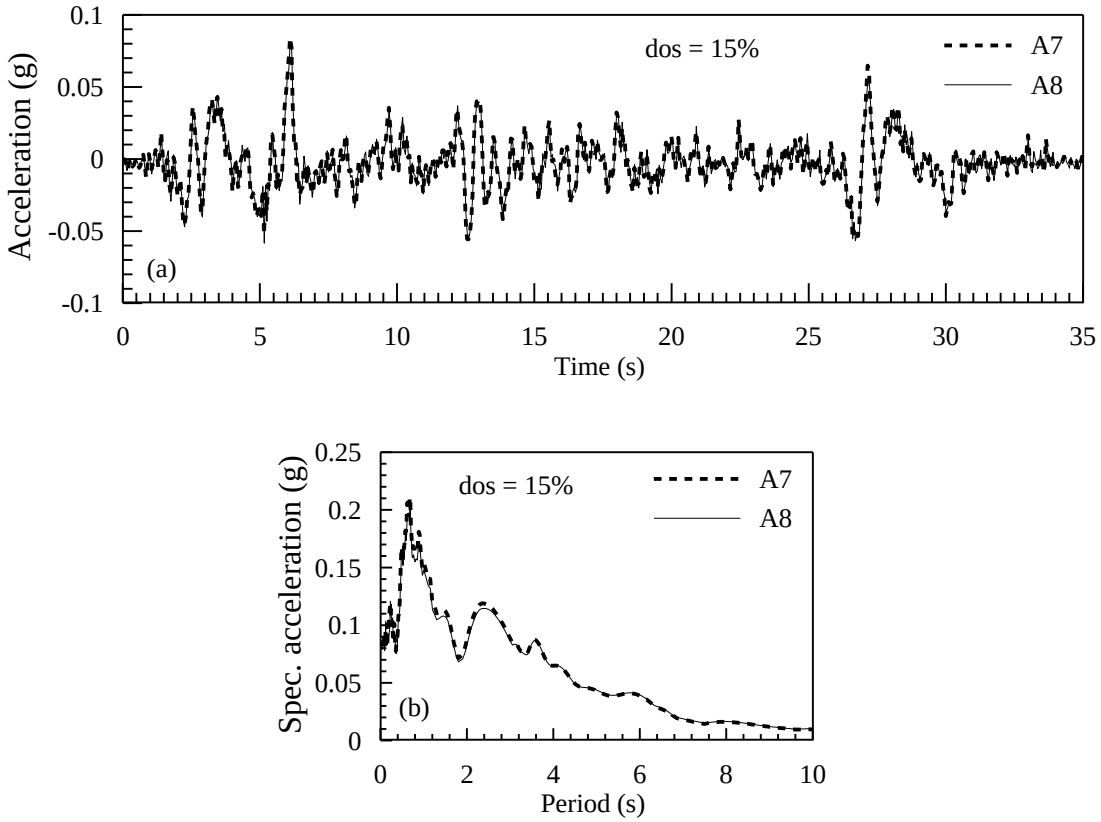

Figure 10. 31 Comparison of results measured (at surface level) with and without SPI influence, at 15% degree of saturation

Numerical Modeling and Comparison with Centrifuge Data

Based on the SPI problem used in the centrifuge modeling, a 2D finite element mesh is created for the numerical modeling with the coupled deformation-flow analysis finite element model. The finite element mesh, which is shown in Figure 10.32, is created with the dimensions of the prototype of the centrifuge model. To create the mesh with all the elements in the prototype, the pile #1 is also placed in the mesh; however this pile and its responses will not be referred in this discussion. The structural element is represented by Timoshenko beam theory. The structure consists of a single column with concentrated mass at the top, i.e., the superstructure is modeled using a single element at the top of the

pile with large density (represents the weight of the superstructure). The soil and the structural nodes are merged together at the interfaces. Since the model container used in the centrifuge modeling is a rigid-box, rigid box boundary condition is used in the simulation. I.e. the bottom of the mesh is fixed in all directions, and the left and right sides are fixed in horizontal direction, but free to deform in vertical direction.

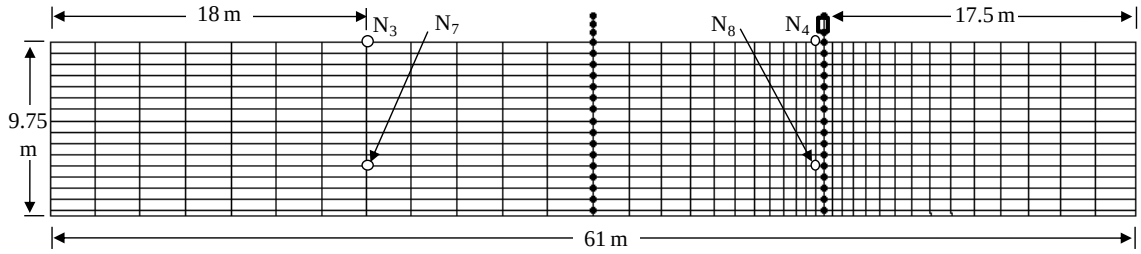

Figure 10.32 The finite element mesh used for the TeraDysac simulation

Elastoplastic Simulation and Comparison with Centrifuge Measurements

Material Model and Model Parameters

Using the centrifuge testing, the elastoplastic behavior of SPI in sandy soil is studied at dry and saturated conditions. Unfortunately, to simulate the elastoplastic behavior of sandy soil, an elastoplastic model of sandy soil is not available in TeraDysac. However, elastoplastic simulation is performed using a clay model with equivalent model parameters and compared with centrifuge data. This comparison analysis is not intended to examine the accuracy of predicted results; rather it is carried out to see the domain of the predicted results. The simulations were carried out with an initial degree of saturation of 50%. The engineering properties and equivalent elastoplastic model parameters of Ottawa sand (the soil used in the centrifuge modeling) are listed in Tables 10.6 and 10.7. Even though it is an elastoplastic modeling, the behavior of the structure is assumed to be

elastic and the corresponding model parameters used for the structural elements are given in Table 10.8.

Table 10.6 Bounding surface based elastoplastic model parameters for Ottawa sand

Parameter	Value
Slope of the isotropic consolidation line on $e - \ell n\ p'$ plot, λ	0.02
Slope of an elastic rebound line on $e - \ell n\ p'$ plot, κ	0.002
Slope of the critical state line in $q - p'$ space , M_c (compression)	1.00
Ratio of extension to compression value of M (M_e / M_c)	1.00
Value of parameter defining the ellipse1 in compression (R_C)	2.60
Value of parameter defining the hyperbola in compression (A_C)	0.10
Parameter defining the ellipse 2 (tension zone) (T)	0.05
Projection center parameter (C)	0.00
Elastic nucleus parameter (S)	1.00
Ratio of triaxial extension to compression value of R (R_e / R_c)	1.00
Ratio of triaxial extension to compression value of A (A_e / A_c)	1.00
Hardening parameter (m)	0.02
Shape hardening parameter in triaxial compression (h_c)	2.00
Ratio of triaxial extension to compression value of h (h_e/h_c)	1.00
Hardening parameter on I-Axis (h_o)	2.00

Table 10.7 Suction related elastoplastic model parameters

Parameter	dos = 50%
m	35
B	0.12
N	1.47
A	0.27
r	1.57
b	0.0133

Table 10.8 Linear elastic model parameters for the structural elements

Properties			Pile	Superstructure
Density		Mg/m^3	7.85	1495.92
Cross section area		m^2	0.0238	0.0238
2^{nd} moment of area	$x10^{-3}$	m^4	1.06	1.06
Young's Modulus	$x10^8$	kPa	2	2
Poisson's ratio			0.32	0.32

The moisture-suction relation of the Ottawa sand is modeled using the S-R-2 SWCC model. The model parameters were obtained by fitting the experimental SWCC data of Ottawa sand (Kim, 2001). The calibrated parameters are: ψ_{aev} = 1.5 kPa, a = 1.55, n = 7, m = 9, ψ_{max} = 1000 kPa, Nr = 1, and θ_r = 0. The fitted S-R-2 SWCC along with the model parameters are shown in Figure 10.33.

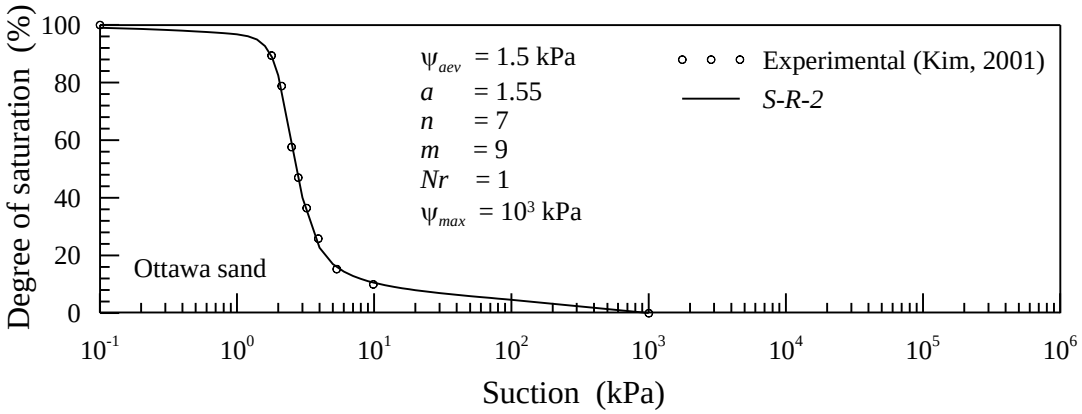

Figure 10.33 SWCC of Ottawa sand fitted with S-R-2 SWCC model

The acceleration-time history presented in Figure 10.34 is used as a base motion in this simulation. This acceleration-time history is measured at the bottom of the centrifuge model for the centrifuge modeling with dry sand.

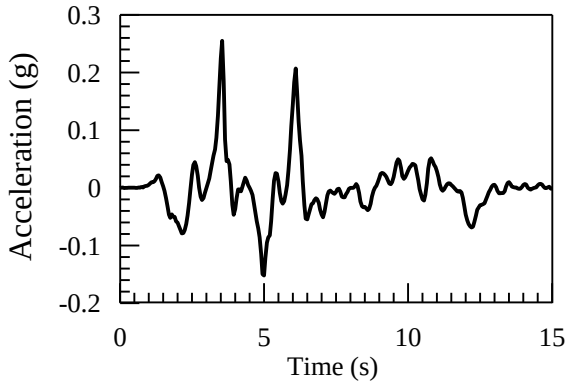

Figure 10.34 Time history of applied base motion

Results and Discussion

Comparison of Spectral Acceleration

The spectral accelerations, which are calculated, based on the measured (centrifuge) and predicted (simulation) horizontal accelerations are presented in Figures 10.35a through 10.35d. The Figure 10.35a shows the spectral acceleration, which is calculated using the measurement of Accelerometer A3 and the numerical prediction at a node, which represents the A3. Similarly the Figures 10.35b, 10.35c, and 10.35d show the predicted results corresponding to Accelerometers A4, A7, and A8, respectively. As shown in these figures, the prediction of the coupled deformation-flow finite element model reasonably matches with the experimental measurements. The results predicted with the influence of SPI shows better match (see Figures 10.35b and 10.35d) compared to the free-field predictions. Especially, the spectral acceleration predicted with SPI influence at surface level i.e. at a point corresponding to Accelerometers A8 is exactly a response expected (based on data of dry and saturated tests) for an unsaturated condition. When the degree of saturation increases, i.e. when the stiffness of the soil decreases, the peak spectral acceleration will decrease and the corresponding period will increase, and it

can be seen in Figure 10.35d. Even though 50% degree of saturation is used in the simulation, Figure 10.35d shows that the simulation result is rather close to the centrifuge measurement of the dry test. It is actually expected, because, the suction or the influence of suction makes the soil to behave in a stiffer manner. Therefore the accuracy of the elastoplastic simulation using the coupled deformation-flow analysis finite element model can be considered to be adequate.

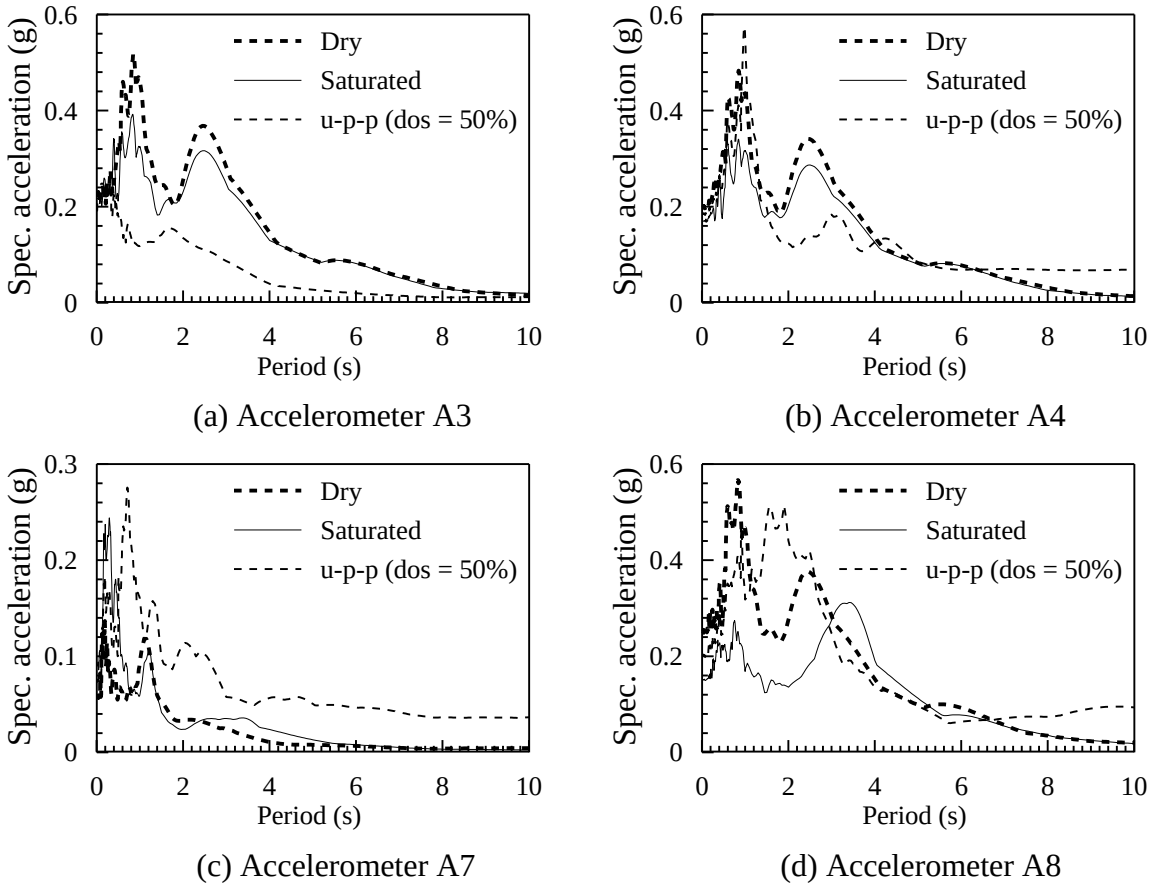

(a) Accelerometer A3 (b) Accelerometer A4

(c) Accelerometer A7 (d) Accelerometer A8

Figure 10.35 Comparison of elastoplastic simulation and experimental results (spectral accelerations)

Comparison of Settlement and Horizontal Displacement

As discussed previously, simulation with 50% degree of saturation is expected to behave between the response measured for dry and saturated conditions. However, because of the influence of the suction, the result of a simulation with 50% degree of saturation is rather expected to be comparable to the response of dry test compared to the response of saturated test.

The horizontal displacement measured (in centrifuge modeling) using LVDT2 and predicted (in numerical modeling) at a node, which represents the location of LVDT2 are compared and presented in Figure 10.36a. Similarly the Figure 10.36b, 10.36c, and 10.36d show the results corresponding to LVDT3, LVDT4, and LVDT5, respectively. As shown in these figures, the prediction of the coupled deformation-flow finite element formulation reasonably matches with the expected response for 50% degree of saturation. Therefore, the accuracy of the elastoplastic simulation can be considered to be sufficient and it can be concluded that the coupled deformation-flow finite element model can be effectively used for unsaturated SPI analysis.

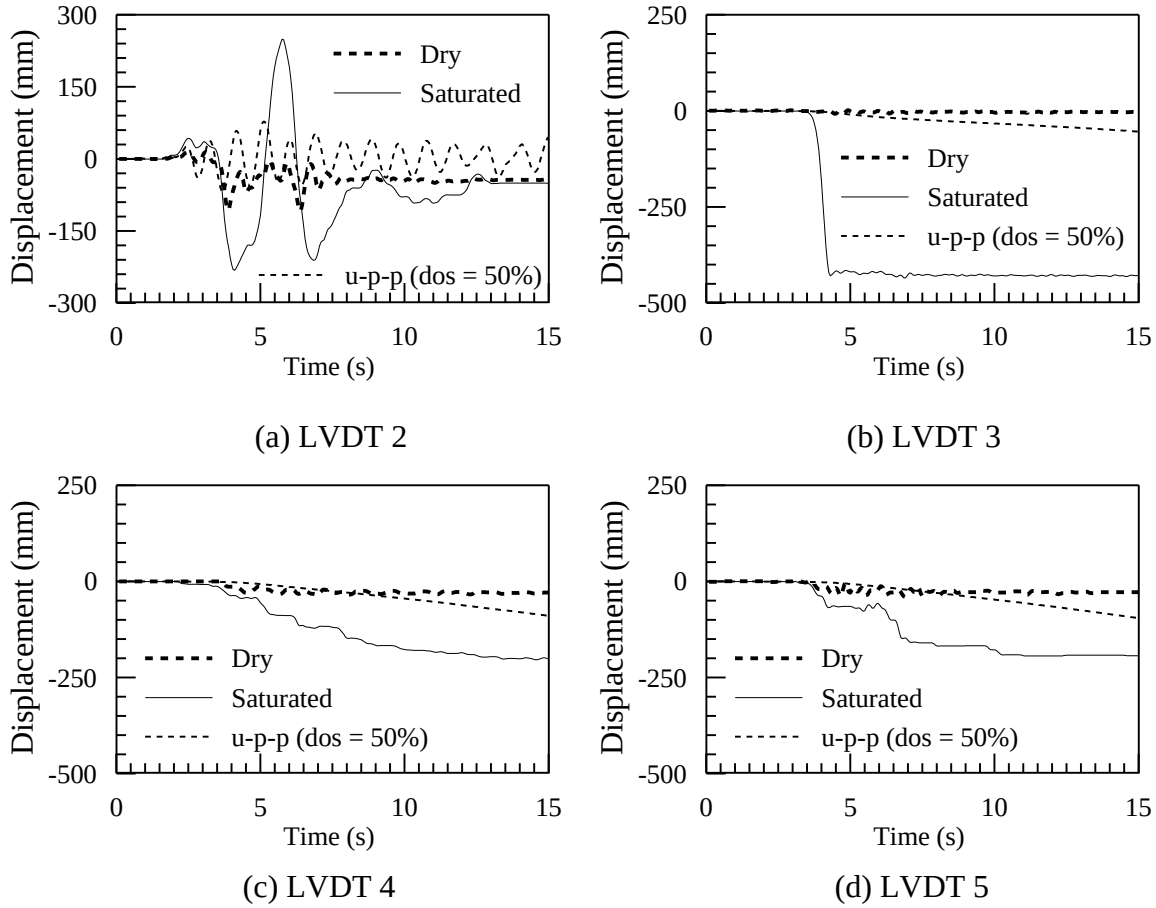

Figure 10.36 Comparison of elastoplastic simulation and experimental results (displacement)

Elastic Simulation and Comparison with Centrifuge Measurements

Material Model and Model Parameters

In the unsaturated centrifuge modeling, i.e. in the centrifuge tests with 10% and 15% degree of saturation, a base motion with a relatively smaller amplitude (about 0.07g) is applied. Therefore it can be assumed that the system behaved within the elastic range for this low amplitude loading. The results obtained from these tests can be compared with the finite element simulation results obtained using elastic material properties. Such comparison can serve as the verification of the code and validation of the elastic

response. The finite element mesh used for the previous elastoplastic simulation (shown in Figure 10.32) is used in this study. The elastic model parameters of Ottawa sand are listed in Table 10.9. The elastic model parameters used for the structural elements are given in Table 10.8.

Table 10.9 Linear elastic model parameters and properties for Ottawa sand

Properties			Value
Solid grain density		Mg/m^3	2.65
Young's Modulus	$x10^5$	kPa	1.5
Poisson's ratio			0.3

The moisture-suction relation of the Ottawa sand is modeled using the S-R-2 SWCC model. The calibrated S-R-2 SWCC along with the model parameters (ψ_{aev} = 1.5 kPa, $\boldsymbol{a}$ = 1.55, $\boldsymbol{n}$ = 7, $\boldsymbol{m}$ = 9, ψ_{max} = 1000 kPa, $\boldsymbol{Nr}$ = 1, and θ_r = 0) are shown in Figure 10.33.

The acceleration-time history presented in Figure 10.37 is used in the simulation as a base motion. This acceleration-time history is measured at the bottom of the centrifuge model (at the shake table) for the unsaturated centrifuge modeling with 10% degree of saturation.

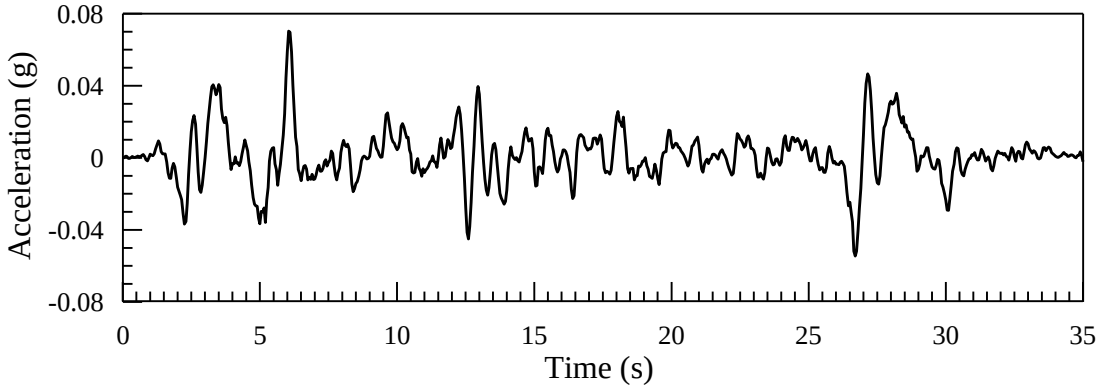

Figure 10.37 The time history of applied base motion

Results and Discussion

The spectral accelerations, which are calculated, based on the measured (centrifuge) and predicted (simulation) horizontal accelerations are presented in Figures 10.38a through 10.38d. The Figure 10.38a shows the spectral accelerations, which are calculated using the measurement of Accelerometer A3 and the numerical prediction at a node, which represents the A3. Similarly the Figures 10.38b, 10.38c, and 10.38d show the results corresponding to Accelerometers A4, A7, and A8, respectively. As shown in these figures, the prediction of the coupled deformation-flow finite element model reasonably matches with the experimental measurements, when the frequency is high or the period is low. The results predicted with the influence of SPI shows better match (see Figures 10.38b and 10.38d) compared to the free-field predictions. However, as shown in these figures, the *maximum spectral acceleration* of the predicted and measured spectral acceleration shows adequate fit in all four cases. Geotechnical structures are designed or their performance for dynamic loads is being analyzed using the maximum spectral acceleration values. Therefore, the accuracy of the elastic simulation with the coupled deformation-flow finite element model can be considered to be adequate and this model can be effectively used for both elastic and elastoplastic analysis of unsaturated SPI.

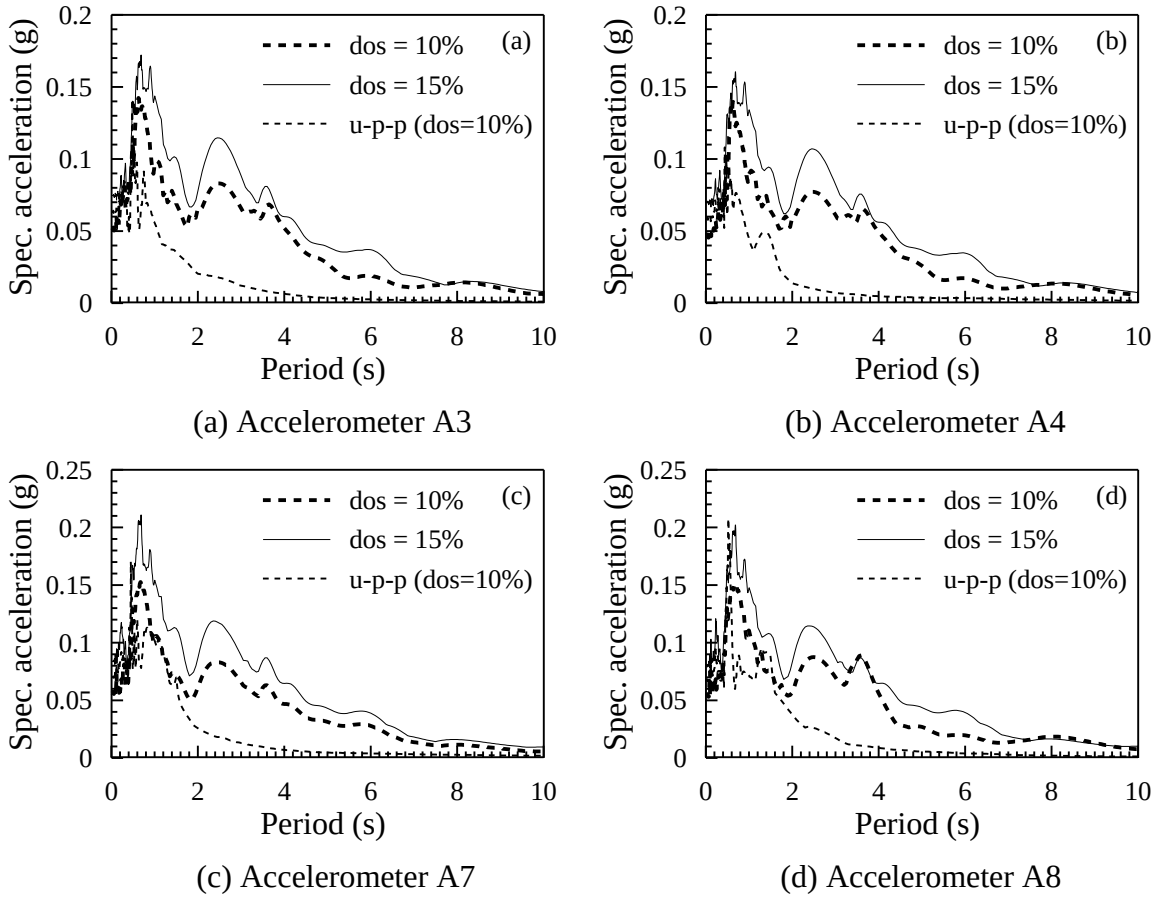

(a) Accelerometer A3 (b) Accelerometer A4

(c) Accelerometer A7 (d) Accelerometer A8

Figure 10.38 Comparison of elastic simulation results and centrifuge measurements

Summary of the Study

A new centrifuge scheme to study the behavior of unsaturated soil-pile systems is proposed and successfully used for a series of centrifuge tests. This scheme can also be used to increase the accuracy of saturated centrifuge modeling. The comparison of the numerical simulation results and the centrifuge measurements shows that the accuracy of the coupled deformation-flow analysis finite element model can be considered to be adequate for both elastoplastic and elastic simulations. Therefore it can be concluded that the coupled deformation-flow analysis finite element model can be effectively used to analyze the elastic and elastoplastic behavior of unsaturated soil-structure systems.

CHAPTER ELEVEN

SUMMARY, CONCLUSIONS, AND RECOMMENDATIONS

Summary and Conclusions

In this study, a coupled finite element model is developed for coupled deformation-flow analysis of dynamics of unsaturated soil and unsaturated soil-pile systems. The finite element formulation of the finite element model is called the *partially reduced formulation.* In addition, new equations for *soil-water characteristic curves* that represent the moisture-suction relationship of unsaturated soils and *relative permeability functions* that represent the permeability-suction relationship of unsaturated soils are developed. The existing simulation capability of TeraDysac is enhanced by implementing nodal pore liquid pressure boundary condition. The numerical model is validated against limited centrifuge test results. It should be noted that the experimental results used for validating the finite element model was an experiment with low amplitude loading. It is assumed that the soil did not experience plastic deformation under this low amplitude loading. Therefore, the finite element modeling was done with linear elastic model. The centrifuge experiments were conducted at the University of Colorado at Boulder centrifuge facility. Although the centrifuge data is preliminary, this is the first set of data obtained on the dynamics of unsaturated soil-pile interaction. The comparison of numerical simulation and centrifuge measurements shows that the accuracy of the elements of the coupled deformation-flow analysis finite element model can be considered to be adequate. Therefore, this finite element model can be effectively used to study the behavior of

unsaturated soils and unsaturated soil-structure systems. In addition, a new centrifuge scheme to study the behavior of unsaturated soil-pile systems is proposed in this research.

The new finite element model seems capable of simulating real world problems related to flow through unsaturated soils and coupled deformation-flow behavior of unsaturated soil-structure systems. The nodal pore pressure boundary condition implemented as part of this research significantly improves the simulation capability of the proposed model and TeraDysac software.

An in-depth analysis on the deformation behavior of unsaturated soils is performed using a simplified finite element formulation available in TeraDysac. The predicted responses of unsaturated clayey and silty soils show that the influence of suction is insignificant in unsaturated silty soils for the problem analyzed. However, when the silt is relatively soft, the suction considerably influences the overall response. In the case of unsaturated clayey soils, the suction or the degree of saturation significantly influences the overall responses. The influence of suction in unsaturated clayey soils is relatively large compared to the influence in unsaturated silty soils. From these results it can also be concluded that for an unsaturated silty soils, a numerical tool which does not incorporate the suction would give reasonable results. However, such numerical tool cannot be used for unsaturated clayey soils.

Effect of degree of saturation on soil-pile interaction response is investigated using TeraDysac simulations with the simplified finite element formulation. The results show that the initial degree of saturation influences the free-field responses and the response of coupled soil-pile systems. For a given base motion, soil-pile system with higher initial

degree of saturation produces larger amplification compared to the system with lower initial degree of saturation. In addition, for a given degree of saturation, the free field response shows lower amplification factor compared to the response of coupled soil-pile system. Therefore, the standard practice of using free-field soil motion to design or analyze the pile/structure with a fixed base assumption should be utilized with caution.

The performance of the simplified finite element formulation is improved by modifying the governing equation by incorporating external damping in the form of Rayleigh damping. The results of the unsaturated soil-pile interaction analyses performed using the improved simplified formulation show that the standard practice of using free-field ground motion to design the pile with a fixed base assumption should be utilized with caution or must take into account the effect of soil-pile interaction. In addition, the parametric studies show that the target damping coefficient in the Rayleigh damping model has significant influence on the overall response of the soil-pile system.

New mathematical models for the moisture-suction relation of unsaturated soils are developed and their capability to fit experimental data and performance in finite element simulation is examined. The limitations/ identified issues of currently available popular SWCC models are solved with the new models. These models can also be effectively used in finite element simulations with low range of degree of saturation. The newly developed models are flexible enough to fit with experimental data in entire range of degree of saturation. The new models can be used either with a residual water content or a maximum suction value. If the maximum suction and air entry suctions are available for a soil, this data can be directly used in the proposed model. The performance of the new

models is verified by fitting the experimental data of various types of soils. The calibration results show that the new models can be successfully used to model various types of soils over the entire range of degree of saturation without any numerical difficulties.

The popular Brooks and Corey, van Genuchten, and Fredlund and Xing SWCC models are also revised to improve their predictive capabilities. The modified SWCC models have the features to specify a residual water content and maximum suction values. The performance of the improved models is verified by fitting with the prediction of original models and experimental data for four different soils. The comparison study shows that the improved model can be successfully used to model the SWCC of various types of soils over the entire range of degree of saturation.

A new relative permeability function for water in unsaturated soil was developed using the model parameters of S-R SWCC models. The capability and the accuracy of the new permeability function were verified by comparing the predictions of the new permeability function with both experimental values and predictions of F-All permeability model for eight different soils. The comparisons show that the new model predicts the experimental data well over a wide range of suction (0 - 1,000,000 kPa) and the accuracy of the new model in higher suction range is better than the F-All model.

The proposed relative permeability model must be used with the corresponding parameters of S-R SWCC models. Therefore, the relative permeability model parameters can be obtained by calibrating the S-R SWCC model parameters against the experimental SWCC data. Based on the results of other simulation studies it can also summarized that

the new relative permeability model can be effectively used to calculate the permeability of water in unsaturated soils in finite element simulations.

Recommendations for Future Research

Based on the outcomes of this research, the followings are recommended for future research.

1. The partially reduced and simplified finite element formulations need to be validated against suitable experimental results. Geotechnical centrifuge experiment is suggested as the experimental method.
2. The capability of the mechanical-flow model was verified using only the elastic material model. An elastoplastic constitute model for sandy soil needs to be developed and implemented into TeraDysac for making use of the mechanical-flow model developed in this study.
3. The interface behavior has significant influence on the overall soil-pile behavior. Therefore, a suitable interface element needs to be implemented for accurately predicting the soil-pile interaction.
4. Another valuable task for future research would be to mathematically relate the fitting parameters of SWCC models with soil properties. This study will help to calculate the moisture-suction relationship, permeability-suction relationship of unsaturated soils, without experimental data.

REFERENCES

Abdoun T., Dobry R., and O'Rourke T. D. "Centrifuge and numerical modeling of soil-pile interaction during earthquake induced soil liquefaction and lateral spreading, Observation and Modeling in Numerical Analysis and Model Tests in Dynamic Soil-Structure Interaction Problems", *T. Nogami Ed., Geotechnical Special Publication*, ASCE, New York, 1997; 64: 76-90.

Aitchison, G. D. "Moisture Equilibria and Moisture Changes in Soils Beneath Covered Areas". Australia: Butterworths 1965; 278.

Aitchison, G. D., Peter, P., and Martin, R. "The Instability Indices Ipm and Ips in Expansive Soils". *Proceedings of 3rd International Conference in Expansive Soils*, Haifa, Istrail 1973; 2: 101-104.

Alonso E. E., Gens A., Josa A., "Aconstitutivemodelforpartiallysaturatedsoils", *Geotechnique*, 1990; 40(3): 405-30.

Amin J. A., Joshi J. R., and Bhatt J. J., "Structure Soil Structure Interaction Effects: Seismic Analysis of Safety Related Collocated Concrete Structures". *4th International Conference on Recent Advances in Geotechnical Earthquake Engineering and Soil Dynamics and symposium in honor of professor W.D Liam Finn*, San Diego, CA, March 26-31, 2001.

Ananthanathan P., "Laboratory testing of unsaturated Minco silt". *M.S. Thesis*, University of Oklahoma, Norman 2002.

ANATECH Corp. (formerly TeraScale LLC). "The TeraScale Framework. Version 1.0, Cedar Crest, NM 2001.

Barden, L., Madedor, A. O., and Sides, G. R. "Volume Change Characteristics of Unsaturated Soils". *Journal of Soil Mechanics and Foundation Division*, 1969; 95: 33-52.

Biot, M. A., "General Theory of Three-Dimensional Consolidation". *Journal of Applied Physics*, 1941; 12: 155-164.

Bishop, A. W., "The Principle of Effective Stress". Teknisk Ukeblad 1959; 106(39): 859-863.

Brooks R, Corey A., "Hydraulic properties of porous media". *Hydrology Paper*, Colorado State University 1964; 3.

Burdine N. T., "Relative permeability calculation size distribution data". *Transactions of the American Institute of Mining*. Metallurgical, and Petroleum Engineers. 1953; 198: 71-78.

Campbell J. D., "Pore pressures and volume changes in unsaturated soils". *Ph.D. thesis*, University of Illinois at Urbana- Champaign, Urbana-Champaign, ILL. 1973.

Chapuis R. P., "Predicting the saturated hydraulic conductivity of sand and gravel using effective diameter and void ratio". *Canadian Geotechnical Journal*. 2004; 41(5): 787-795.

Croney D., and Coleman J., "Pore pressure and suction in soils." *Proceedings of the Conference on Pore Pressure and Suction in Soils*, Butterworths, London, 1961, 31-37.

Dafalias Y. F., Herrmann L. R., "Bounding surface plasticity II: Application to Isotropic cohesive soils". *Journal of Engineering Mechanics*, 1986; 112(2):1260-1291.

Davidson J. M., Stone L. R., Nielsen D. R., and Larue M. E., "Field measurement and use of soil-water properties". *Water Resources Research,* 1969; 5: 1312-1321.

Dowrick D. J., "Earthquake resistant design: a manual for engineers and architects". New York: John Wiley and Sons Ltd; 1977.

Elrick D. E., Bowman D. H., "Note on an improved apparatus for soil moisture flow measurements". *Soil Science Society of America Proceedings*. 1964; 28: 450-453.

Elzeftawy A., Cartwright K., "Evaluating the saturated and unsaturated hydraulic conductivity of soils". *Permeability and Groundwater Contaminant Transport, ASTM STP 746,* Zimmie T. F., Riggs C. O., ASTM., PA. 1981; 168-181.

Escario V., and Juca J., "Shear strength and deformation of partly saturated soils." *Proceedings of the 12th International Conference on Soil Mechanics and Foundation Engineering*, Rio de Janerio, 1989, 2: 43-46.

Fredlund D. G., "Comparison of soil suction and one-dimensional consolidation characteristics of highly plastic clay." *MSc thesis*, Univ. of Alberta, Canada, 1964.

Fredlund D. G., Fredlund M. D., and Zakerzadeh N., "Predicting the permeability function for unsaturated soils". *International Conference on Clays and Clay Minerology*, Japan, 2001.

Fredlund D. G., and Morgenstern N. R., "Stress State Variables for Unsaturated Soil". *ASCE Journal of Geotechnical Engineering Division,* 1977; 103: 447-466.

Fredlund D. G., Rahardjo H., "Soil Mechanics for Unsaturated Soils". A Wiley-Interscience Publication, John Wiley and Sons inc., New York, 1993; ISBN 0-471-85008-X, 517 pages.

Fredlund D. G., and Xing A., "Equations for the soil-water characteristic curve." *Canadian Geotechnical Journal*, 1994, 31: 521-532.

Fredlund D. G., Xing A., Huang S., "Predicting the permeability function for unsaturated soils using the soil-water characteristic curve." *Canadian Geotechnical Journal*. 1994; 31: 533-546.

Gardner W. R., "Some steady state solutions of the unsaturated moisture flow equation with application to evaporation from a water table". *Soil Science*. 1958; 85: 228-232.

Gardner W., "Mathematics of isothermal water conduction in unsaturated soils." *Highway Research Board Special Report 40, International Symposuim on Physico-Chemical Phenomenon in Soils.* Washington D.C., 1956, 78-87.

Georgiadis K., Potts D. M., Zdravkovic L., "The influence of partial soil saturation on pile behavior" Geotechnique, 2003, 53(1), 11-25.

Han Y.C., "Dynamic Soil-Pile-Structure Interaction". *4th International Conference on Recent Advances in Geotechnical Earthquake Engineering and Soil Dynamics and symposium in honor of professor W.D Liam Finn*, San Diego, CA, 2001.

Hassanizadeh S. M., and Gray W. G., "General Conservation Equation for Multi-Phase System: 1. Averaging Procedure". *Advances in Water Resources*, 1979; 2: 131-144.

Hazen A., "Water supply". *American Civil Engineers Handbook*. Wiley, New York, 1930.

Herrmann L. R., Mish K. D., "Finite element analysis for cohesive soil, stress and consolidation problems using bounding surface plasticity theory". *Technical Report*, University of California, Davis, 1983.

Hilber H. M., Hughes J. R., Taylor R. L., "Improved numerical dissipation for time integration algorithms in structural dynamics". *Earthquake Engineering and Structural Dynamics*, 1977; 5: 283-292.

Hogarth W. L., Hopmans J., Parlange J. Y., and Haverkamp R., "Application of a Simple Soil-Water Hysteresis Model." *Journal of Hydrology*, 1988, 98: 21-29.

Hudson M., Idriss I. M., and Beikae M., "QUAD4M - A computer program to evaluate the seismic response of soil structures using finite element procedures and incorporating a compliant base", *Center for Geotechnical Modeling*, University of California, Davis, CA, 1994.

Hughes T. J. R., Pister K. S., "Consistent linearization in mechanics of solids". *Computers and Structures*, 1978; 8: 391-397.

Hughes T. J. R., "Analysis of transient algorithms with particular reference to stability". *In Computational Methods for Transient Analysis*, North-Holland, Amsterdam 1983.

Jaynes D. B., "Comparison of soil-water hysteresis models." *Journal of Hydrology*, 1985, 75: 287–299.

Kawai K., Karube D., and Kato S., "The Model of Water Retention Curve Considering Effects of Void Ratio." *In*: Rahardjo, H., Toll, D.G., Leong, E.C.(Eds.), *Unsaturated Soils for Asia*. Balkema, Rotterdam, 2000, 329-334.

Koorevaar P., MeaeIiIt G., and Dirksen C., "*Elements of soil physics".* E1sevier Science Publishers B.V. (North-Holland), Amsterdam, the Netherlands, 1983.

Kosugi K., "The parameter lognormal distribution model for soil water retention." *Water Resource Research,* 1994, 30: 891-901.

Kwok A. O. L., Stewart J. P., Hashash Y. M. A., Matasovic N., Pyke R., Wang Z., Yang Z., "Use of exact solutions of wave propagation problems to guide implementation of nonlinear, time-domain ground response analysis routines". *ASCE Journal of Geotechnical and Geoenvironmental Engineering,* 2007; 133(11): 1337–1481.

Leong E. C., and Rahardjo H., "Review of soil-water characteristic curve equations." *Journal of Geotechnical and Geoenvironmental Engineering,* 1997, 123:1106-1117.

Li J., Sun D. A., Sheng D. C., Sloan S., and Fredlund D. G., "Preliminary Study on Soil-water Characteristics of Maryland Clay" *The 3rd Asian Conference on Unsaturated Soil*, NanJing, China, 2007, 569-574.

Lloret A., and Alonso E. E., "Consolidation of unsaturated soils including swelling and collapse behavior". *Géotechnique*. 1980; 30(4): 449-477.

Lobbezoo J. P. and Vanapalli S. K., "A simple technique for estimating the coefficient of permeability of unsaturated soils". *55th Canadian Geotechnical Conference*. Niagara, Canada, 2002.

Martel R. R., "Effect of foundation on earthquake motion". *Civ Eng,* 1940; 10(1):7–10.

Matasovic N., “Seismic response of composite horizontally-layered soil deposits”. *PhD Thesis*, University of California, Los Angeles, California. 1993.

Matyas E. L., and Radhakrishna H. S. “Volume Change Characteristics of Partly Saturated Soils.” *Geotechnique*, 1968, 18(4), 432-448.

McKee C., and Bumb A., “Flow-testing coalbed methane production wells in the presence of water and gas”. *SPE Formation Evaluation*, 1987, 599-608.

Miller G. A., Muraleetharan K. K., and Lim Y. Y., “Wetting-Induced Settlement of Compacted-Fill Embankment”, *Transportation Research Record-Journal of the Transportation Research Board*, 2001; 1755:111-118.

Moore R. E., “Water conduction from shallow water tables”. Hilgardia. 1939; 12: 383-426.

Mualem Y., “Extension of the similarity hypothesis used for modeling the soil water characteristics”. *Water Resources Research*, 1977, 13(4): 773–780.

Mualem Y., “Prediction of the soil boundary wetting curve”. *Journal of Soil Science*, 1984, 137(6): 379–390.

Muraleetharan K. K., Liu C., Wei C., Tohren C. G., Kibbey, and Lixia Chen., “A Coupled Elastoplastic Model for Capillary Hysteresis and Stress-Strain Behavior of Unsaturated Soils”. *International Journal of Plasticity*, 2009; 25: 473-490.

Muraleetharan K. K., Mish K. D., Arulanandan K., “A fully coupled nonlinear dynamic analysis procedure and its verification using centrifuge test results”. *International Journal for Numerical and Analytical Methods in Geomechanics*, 1994; 18: 305-325.

Muraleetharan K. K., Ravichandran N., Taylor L. M., "TeraDysac: TeraScale Dynamic Soil Analysis Code". *Computer Code*, School of Civil Engineering and Environmental Science, University of Oklahoma, Norman, Oklahoma, 2003.

Muraleetharan K. K., and Wei C., "U_DYSAC2: Unsaturated Dynamic Soil Analysis Code for 2-dimensional Problems". *Computer Code*, University of Oklahoma, Norman, 1999b.

Newmark N. M., "A method for computation of structural dynamics". *ASCE Proceedings,* 1959; EM3, 85: 67-94.

Ng C. W. W., and Pang Y. W., "Influence of stress state on soil-water characteristics and slope stability". *Journal of Geotechnical and Geoenvironmental Engineering*, 2000, 126(2), 157-166.

Nimmo J. R., "Semi-empirical model of soil water hysteresis". *Soil Science Society of America Journal*, 1992, 56, 1723–1730.

Parlange J. Y., "Capillary hysteresis and the relationship between drying and wetting curves". *Water Resources Research*, 1976, 12(4), 224–228.

Park D., Hashash Y. M. A., "Soil damping formulation in nonlinear time domain site response analysis". *Journal of Earthquake Engineering*, 2004; 8(2): 249–74.

Peroni N., Fratalocchi E., Tarantino A., "Water permeability of unsaturated compacted kaolin". *Proceedings of the International Conference "From Experimental Evidence towards Numerical Modeling of Unsaturated Soils*," Weimar, Germany, 2003.

Pham Q. H., Fredlund D. G., and Barbour S. L., "A practical hysteresis model for the soil-water characteristic curve for soils with negligible volume change". *Géotechnique*, 2003, 53(2): 293–298.

Phillips C., Hashash Y. M. A., "Damping formulation for 1D site response analyses". *Soil Dynamics and Earthquake Engineering*, 2009; 29:1143-1158.

Puppala A. J., Punthutaecha K., Vanapalli S. K., "Soil Water Characteristic Curves of Stabilized Expansive Soils." *ASCE, Journal of Geotechnical and Geoenvironmental Engineering*, 132(6): 736-751.

Rayleigh J. W. S., Lindsay R. B., "The theory of sound". *Dover Publications*; New York, 1945; 2(1).

Rathje E. M., Bray J. D., "One- and two-dimensional seismic analysis of solid waste landfills", *Canadian Geotechnical Journal*, 2001; 38(4), 850-862.

Ravichandran N., Muraleetharan K. K., "Dynamics of Unsaturated Soils Using Various Finite Element Formulations". *International Journal for Numerical and Analytical Methods in Geomechanics*, 2009; 33(5): 611-631

Ravichandran N., "A framework-based finite element approach to solving large deformation problems in multiphase porous media". *Ph.D. dissertation*, School of Civil Engineering and Environmental Science, University of Oklahoma, Norman, Oklahoma 2005.

Reisenauer A. E., "Methods for solving problems of multi-dimensional partially saturated steady flow in soils". *Journal of Geophysical Research*, 1963; 68:5725-5733.

Richards L. A., “Capillary conduction of liquids through porous medium”. *Physics.* 1931; 1: 318-333.

Richards L. A., “Water conducting and retaining properties of soils in relation to irrigation”. *Proceedings, International Symposium on Desert Research*, Jerusalem. 1952; 523-546.

Richards, S. J., “Soil suction measurements with tensiometers. In: Methods of soil analysis.” *American Society of Agronomy*. Monograph 9. ASA, CSSA, and SSSA, Madison, WI, 1965, 153-163.

Rijtema P. E., “An analysis of actual evapotranspiration”. *Agricultural Research Reports* (Wageningen). 1965; 659.

Russam K., and Coleman J. D., “The effect of climatic factors on subgrade moisture condition.” *Geotechnique,* 1961, 3: 22–28.

Schrefler B. A., Simoni L., Li Xikui and Zienkiwicz O. C., “Mechanics of Partially Saturated Porous Media”. in Desai, C. S. and Gioda, G. (eds), Numerical Methods and Constitutive Modelling In Geomechanics, CISM Lecture Notes, Springer-Verlag, Wein, 1990; 169-209.

Sillers W.S., Fredlund D.G., and Zakerzadeh N., “Mathematical attributes of some soil-water characteristic curve models.” *Geotechnical and Geological Engineering.* 2001, 19: 243-283.

Sivakumar V. A., “Critical state framework for unsaturated soil.” *PhD thesis*, University of Sheffield, UK, 1993.

Tanabashi R., Ishizaki H., “Earthquake damages and elastic properties of the ground”. *Bulletin No.4,* Disaster Prevention Research Institute, Koyoto University. 1953.

Vanapalli S. K., Pufahl D. E., and Fredlund D. G., “The influence of soil structure and stress history on the soil-water characteristic of a compacted till.” *Geotechnique*, 1999, 49(2), 143-159.

van Genuchten, M.Th. “A closed-form equation for predicting the hydraulic conductivity of unsaturated soils.” *Soil Science Society of America Journal,* 1980, 44, 892–898.

Varatharaj S., "A fully coupled analysis procedure for dynamic soil-structure interaction during seismic events.” *M.S. Thesis,* University of Oklahoma, Norman 2001.

Wei C. F., “Static and dynamic behavior of multi-phase porous media: Governing equations and finite element implementation”. *PhD Dissertation,* University of Oklahoma, Norman 2001.

Wheeler S. J., “Inclusion of specific water volume within an elasto-plastic model for unsaturated soil”. *Canadian Geotechnical Journal,* 1996; 33(1): 42-57.

Wheeler S. J., Sivakumar V., “An elasto-plastic critical state framework for unsaturated soil”. *Geotechnique,* 1995; 45(1): 35-53.

Wilson D.W., “Soil-pile-superstructure interaction in liquefying sand and soft clay”, *Ph.D. dissertation,* University of California, Davis, 1998.

Wind G.P., “Field experiment concerning capillary rise of moisture in heavy clay soil”. *Netherlands Journal of Agricultural Science*. 1955; 3: 60-69.

Xikui L, Zienkiewicz O. C., “Multiphase flow in deforming porous media and finite element solution”. *Computers and Structures,* 1992; 45(2): 211-227.

Yang H., Rahardjo H., Leong E. C., and Fredlund D. G., "Factors affecting drying and wetting soil-water characteristic curves of sandy soils." *NRC Research Press*, 2004.

Zienkiewicz O. C, Shiomi T., "Dynamic behavior of saturated porous media; The generalized Biot formulation and its numerical solution". *International Journal for Numerical and Analytical Methods in Geomechanics*, 1984; 8: 71-96.

Zienkiewicz O. C., Humpheson C., and Lewis R. W., "A Unified Approach to Soil Mechanics Problems (Including Plasticity and Viscoplasticity)". G. Gudehus, (Ed.) in Finite Elements in Geomechanics, Wiley 1977; 151-178.